Universitat Ramon Llull

DOCTORAL THESIS

Title: **Micro-Nano-Bio Systems for on-line monitoring of in vitro biofilm responses**

Presented by Oscar Estrada Leypón

Centre Institut Químic de Sarrià

Department Bioengineering

Directed by Dr Salvador Borrós Gómez

C. Claravall, 1-3
08022 Barcelona
Tel. 936 022 200
Fax 936 022 249
E-mail: urlsc@sec.url.es
www.url.es

To my Family

A mi Familia

“You know more than you think you know, just as you know less than you want to know”

Oscar Wilde (1854-1900)

“Sabe usted más de lo que cree saber, pero menos de lo que desea saber”

Oscar Wilde (1854-1900)

ACKNOWLEGMENTS

Esta tesis doctoral realizada durante 4 años ha sido posible gracias inicialmente a la confianza del Profesor Salvador Borrós que desde el término del Máster de Bioingeniería me dio la oportunidad de poder conocer el mundo de la investigación en todos los ámbitos de ciencia fundamental a aplicación de un sinfín de metodologías para llevar a cabo proyectos de todo tipo.

El trabajo multidisciplinar llevado a cabo durante estos años no habría sido posible sin la ayuda de figuras como los Profesores Guillermo Reyes, Andrés García del departamento de Ingeniería Industrial apoyados en todo momento por César en su taller de mecánica de IQS. Todos ellos ayudaron en gran medida al diseño y fabricación del dispositivo gracias al asesoramiento de detalles frente a los distintos desafíos que iban surgiendo. También al Doctor Jordi Abellà por el análisis de muestras mediante SEM y la Doctora Montse Agut por dejarme la usar el laboratorio de microbiología para la puesta a punto de la plataforma diseñada en esta tesis.

A mi familia también quiero agradecer en general el apoyo incondicional durante estos años tanto en el día a día, como en las decisiones importantes como el hecho de irme a otro país a continuar con la investigación y ampliar mi formación. Además de cuidar también durante mi ausencia a Tere, quien me ha acompañado durante esta doble etapa de convivencia + doctorado el cual pasaremos página tras la defensa de esta Tesis para empezar un nuevo camino.

Muy importantes han sido también las buenas compañías del Biosotano, conformada por muchas personas que he visto pasar y que por más que mencione aquí seguro meteré la pata dejándome a alguien. Víctor Ramos el mejor asesor capaz de sacarte de dudas ante cualquier situación, acompañado Laura-Anna-María con poderes otorgados en el monte del destino. Robert el Gamer nº1 capaz de secretar hormonas contra el sueño, Ana Mas “the new sheriff” o “the organizer” capaz de leer más que Albus Dumbledore en Howgarts. Pere Dosta *el paciente* aún; no se sabe que ungüento toma para tener paciencia contra las hordas de “toca-huevs” presentes en el Bunker biomateriales. Jordi Arbusà *bioemprenedor 1* y Joan Gilabert *bioemprenedor 2* ejemplo a seguir a las nuevas generaciones que están entrando con fuerza en el grupo (Alberto, Antonio, Marta, Saras…) Pau, Ingrid, Cascante, Irene, Miguel Angel que completan el Mega-grupo de biomateriales completado por Marina, Nuria, Isabel y Elena (“the jocker” por lo de comodín). Las chicas de teixits Mireia, Cris, Lourdes, Nuria, Vero que he podido compartir Master + Doctorado, además de Carlos Semino que las ha liderado perfectamente durante ese viaje.

En cuanto al periodo de Inglaterra creo que por respeto debe estar en inglés, por tanto apretaremos el interruptor multilingüe. As mentioned I have only excellent words for the English group of the University of Bath because from the first second there I felt comfortable and more amazingly happy to be there surrounded by nice people. Toby you were an excellent supervisor which an impressive knowledge of everything (not talking about only science) that helped me at any moment I spent there. Sunny, Jess, Serena the English ladies who helped me a lot in & out the lab, spending very funny and useful conversations (one day we will save the world). Daves both professional climbers out of the laboratory, wonderful evenings we had. Diana and Patricia my Spaintuguese mates who allowed regular scheduled nights for our countries. Then Maisem and the Bioteam + Parade celebrations after games. Those football games closed the weeks in the best way especially with the presence of Terrence-Wolf (the strange couple), and the Post-Doc Spanish Team conformed by Patri, David, Victoria, Juanjo, Silvia (one day we will finish the golden mile of the Bars in the city center.

Finalmente también doy las gracias a mis amigos de toda la vida a los cuales los he visto de manera racheada durante estos años, pero que siempre han estado allí y seguirán estándolo, ya que cada uno tiene estudios infinitamente diferentes y eso nos ayuda a realizar viajes al pasado que son un oasis para el transcurso del tiempo incansable.

Esta tesis ha sido posible gracias a la beca doctoral (BES-2010-033566) del ministerio nacional de ciencia e innovación, asociada al proyecto del plan nacional TEC2009-14779-C02-02 y la ayuda extraordinaria para la estancia durante 8 meses en la Universidad de Bath (Marzo – Octubre 2013) teniendo como mentor al Profesor A.T.A Jenkins. Además del presupuesto de IQS para el laboratorio de Biomateriales.

This Thesis has been possible thanks to the Doctoral Fellowship (BES-2010-033566) of the National Ministry of Science and Innovation, associated to a National Project (TEC2009-14779-C02-02) and the extraordinary grant for the 8 month internship at University of Bath (March – October 2013) having as a supervisor PhD A.T.A Jenkins. Besides the IQS internal founding of the biomaterials laboratory.

ABSTRACT

The work presented in this thesis has the main aim to contribute in the field of clinical microbiology to understand the biofilms and the possible of development through the use of methods with multidisciplinary approach. Biofilms are defined as communities of microorganisms that grow embedded in a matrix of exopolysaccharides and adhering to an inert surface or living tissue. The formation of bacterial biofilms has an interest in clinical microbiology with the development of infections that usually arise from either direct contact or the colonization of implanted medical devices and prostheses. Currently they are considered the cause of over 60% of bacterial infections. The problem of bacterial biofilms at clinical level is showing great resistance to antibiotics, so that the biofilm bacteria are 500 to 5000 times more resistant to antimicrobial agents that the same bacteria grown in planktonic cultures (bacteria in suspension). There have been attempts to adapt methods to clinical laboratories where they reproduce the conditions of biofilms, but have not yet adopted an optimal standard protocol for this purpose to follow-up the formation and toxicity in real-time. There has been a growing interest in design, development and utilization of microfluidic devices that can emulate biological phenomena that occur in different geometries, fluid dynamics and mass transport restrictions in physiological microenvironments.

The research described in this thesis deals with different label-free methods based on variation of acoustic and electric properties for biofilm monitoring. The work presented in this monograph describe a custom-made device for using electrochemical impedance spectroscopy (EIS) as useful tool to obtain information of adherence and formation of biofilms. The addition of nanoparticles as toxicity biomarker allows the correlation of biofilm formation with its toxicity in real-time for detention of the optimal point for biofilm treatment. Finally the design of this technology is used for testing the biofilm response to antibiotic as *in vitro* model of biofilm-related infection.

RESUMEN

El trabajo presentado en esta tesis doctoral tiene como principal objetivo la contribución en el campo de la microbiología para entender los biofilms y el posible control de desarrollo mediante el uso de métodos y enfoque multidisciplinar. Los biofilms están definidos como comunidades de microorganismos que crecen embebidos en una matriz exopolisacárida y se adhieren a una superficie inerte o tejido vivo. La formación de los biofilms bacterianos tiene un gran interés en microbiología clínica debido al desarrollo de infecciones que son causadas por contacto directo o por colonización de dispositivos médicos implantados y prótesis. Actualmente se consideran la causa de más del 60 % de las infecciones bacterianas. El problema de los biofilms bacterianos a nivel clínico es que muestran mejor resistencia a antibióticos llegando incluso a ser de 500 a 5000 veces más resistentes a agentes antimicrobianos comparado a la misma bacteria planctónica (bacteria en suspensión). Ha habido muchas tentativas de adaptar métodos a laboratorios clínicos donde se reproducen las condiciones para el desarrollo de biofilms, pero aún no se ha llegado a obtener óptimos protocolos estándar para este propósito de monitorizar la formación y toxicidad en tiempo real. Ha crecido el interés en diseño, desarrollo y utilización de dispositivos de microfluídica que puedan emular los fenómenos biológicos que ocurren con diferentes geometrías, dinámica de fluidos y restricciones de transporte de biomasa en microambientes fisiológicos.

La investigación descrita en esta tesis se lleva a cabo con diferentes métodos *"label-free"* basados en variación acústica y/o propiedades eléctricas para la monitorización de biofilms. El trabajo presentado en esta monografía describe un dispositivo *"custom-made"* para la utilización de Espectroscopia de impedancia electroquímica como herramienta útil para obtener información de adherencia y formación de biofilms. El hecho de añadir nanopartículas como segundo biosensor permite la correlación de biofilm con su toxicidad en tiempo real para la detección del punto óptimo del tratamiento de biofilms. Finalmente el diseño de esta tecnología es usada para el ensayo de la respuesta de biofilms a antibióticos como modelo *in vitro* de infecciones causadas por biofilms.

RESUM

El treball presentat en aquesta tesi doctoral te com objectiu principal la contribució en el camp de la microbiologia per entendre el biofilms i el possible control de desenvolupament mitjançant l'ús de mètodes i enfoc multidisciplinari. Els biofilms estan definits com comunitats de microorganismes que creixen envoltats en una matriu exopolisacárida i s'adhereixen a una superfície inert o teixit viu. La formació dels biofilms bacterians tenen un gran interès en microbiologia clínica degut al desenvolupament d'infeccions que son causades pel contacte directe o per colonització de dispositius mèdics implantats i pròtesis. Actualment es consideren causa de més del 60 % de les infeccions bacterianes. El problema dels biofilms bacterians a nivell clínic es que mostren millor resistència a antibiòtics arribant inclús a ser de 500 a 5000 cops més resistents a agents antimicrobians comparant amb la mateixa bactèria planctònica (bactèria en suspensió). Hi ha hagut moltes temptatives d'adaptar mètodes a laboratoris clínics on es reprodueixen les condicions pel desenvolupament de biofilms, però encara no s'ha arribat a obtenir òptims protocols estàndard per a aquest propòsit de monitoritzar la formació i toxicitat a temps real. Ha crescut l'interès en disseny, desenvolupament i utilització de dispositius de microfluídica que poden emular els fenòmens biològics que ocorren amb diferents geometries, dinàmica de fluids i restriccions de transport de biomassa en microambients fisiològics.

La recerca descrita en aquesta tesis s'ha dut a terme amb diferents mètodes *"label-free"* basats en la variació acústica y/o propietats elèctriques per a la monitorització de biofilms. El treball presentat en la monografia descriu un dispositiu *"custom-made"* per a la utilització d'Espectroscòpia de impedància electroquímica com a eina útil per a l'obtenció d'informació d'adherència i formació de biofilms. El fet d'afegir nanopartícules com a segon biosensor permet la correlació de biofilm amb la seva toxicitat a temps real per a la detecció del punt òptim de tractament de biofilms. Finalment el disseny d'aquesta tecnologia s'utilitza per l'assaig de la resposta de biofilms a antibiòtics com a model *in vitro* d'infeccions causades per biofilms.

TABLE OF CONTENTS

LIST OF FIGURES

LIST OF TABLES

LIST OF ABBREVIATIONS

5(6)-CF: 5(6)-Carboxyfluorescein

AGR: Accessory gene regulator

AI-2: Autoinducer-2

AIP: Autoinducing peptide

BS: Biological sample

CAD: Computer Aided Design

CE: Counter electrode

CFD: Computational fluid dynamic

CFU: Colony Forming Unit

CHO: Cholesterol

CLSM: Confocal laser scanning microscopy

DIC: Differential interference microscopy

DLS: Dynamic light scattering

DNA: Deoxyribonucleic acid

DO: Dissolved oxygen

DPPC: 1,2-dipalmitoyil-sn-glycero-3-phosphocoline

DPPE: 1,2-dipalmitoyl-sn-glycero-3-phosphoethanolamine

ECM: Extracellular matrix

EDTA: Ethylenediaminetetraacetic acid

EIS: Electrochemical Impedance Spectroscopy

EPS: Extracellular polymeric substances

FDM: Fused Deposition Modelling

FEM: Finite element model

GPC: Gas-phase Chromatography

HAIs: Healthcare-associated infections

HEMA: Hydroxyethylene methacrylate

HEPES: 2-[4-(2-hydroxyethyl)piperazin-1-yl]ethanesulfonic acid

HPLC: High-pressure liquid chromatography

IDuE: Interdigitated microelectrode

LB: Luria Broth

LPN: Lipid nanoparticle

MALDI-TOF: Matrix assisted laser desorption ionization - Time-of-flight

MS: Mass spectroscopy

NTA: nanoparticle tracking analysis

OD: Optical density

PBS: Phosphate buffered saline

PC: Polycarbonate

PCB: Printed Circuit Board

PDMS: Polydimethylsiloxane

PE: Punctual electrode

PFM: Pentafluorophenyl methacrylate

PSM: Phenol-soluble modulin

QCM-D: Quartz Crystal Microbalance with Dissipation

QS: Quorum sensing

RE: Reference electrode

RF: Radiofrequency

RNA: Ribonucleic acid

RTCA: Real time cell analyzer

SEM: Scanning electrode microscopy

TCDA: 10,12-Tricosadiynoic acid

TSA: Tryptic soy agar

TSB: Tryptic soy broth

WE: working electrode

LIST OF PUBLICATIONS

O. Estrada-Leypón, A. Mas, J. Gilbert, A. Moya, A. Guimerà, G. Gabriel, M. Agut, S. Borrós. Microfluidic devices for real-time studies of bacterial biofilms quantified with label-free technologies tuned with antibacterial coatings. (In preparation).

O. Estrada-Leypón, M. Laabei, W. D. Jamieson, A. Moya, R. Villa, A. T. A. Jenkins, S. Borrós. Correlation between biofilm evolution and secreted virulence factors of Staphylococcus aureus using a customized microfluidic platform. (Submitted).

O. Estrada-Leypón, a. Moya, a. Guimerà, G. Gabriel, M. Agut, B. Sánchez, S. Borrós. Simultaneous monitoring of Staphylococcus aureus growth in a multi-parametric microfluidic platform using microscopy and impedance spectroscopy, *Bioelectrochemistry*. 105 (2015) 56–64. doi:10.1016/j.bioelechem.2015.05.006.

L. Montero, **O. Estrada,** J. Gilabert, R. Villa, S. Borrós. Following the Mechanism of Biofilm Formation Tailoring Surface Modification on Impedance Sensors. *Eur. Cells Mater*. 2011, 21, 14779.

PRESENTATIONS

Oral Presentation, Conferences at Bioengineering Department, Institut Químic de Sarrià (IQS), School of engineering **2015**, Barcelona, Spain.

Poster Presentation, 24th European Congress of Clinical Microbiology and Infectious Diseases (ECCMID) **2014**, Barcelona, Spain.

Poster Presentation, 25th European Conference on Biomaterials (Organized by the European Society for Biomaterials – ESB) **2013**, Madrid, Spain.

Oral Presentation, Bio-Nano Summer School **2013**, Hirschegg, Austria.

Poster Presentation, European Cells and Materials (eCM) XII Conference: Implant Infection **2011**, Davos, Switzerland.

Chapter 1 Introduction

1.1 Bacterial Biofilms and its impact

1.1.1 Background of biofilms

During the millions of years when only existed bacteria as a form of life on Earth, the prevailing aquatic environment was extremely oligotrophic. The niches allowed for life were limited by extreme environmental factors like UV radiation, heat and acidity[1]. At that time the purpose of the planktonic, free-living mode of bacterial growth enabled them to move from one habitat to another until an optimal location for growth was found. These first sessile organism began to form more complex structures named biofilms that allowed them to remain in place, and to trap and utilize the organic compounds of the environment. The next episode of the bacterial evolution was the development of co-operation among bacterial groups, permitting the use of more complex or more refractory nutrients. This complex behaviour also changed the environment of the colonized surface and made it more suitable for the bacteria growing there.

Although the existence of biofilms began a long time ago, the early observation of this structure took place at 1674, when Antonie van Leuwenhoek used a primitive microscope to describe aggregates of ‘‘animalcules” that he scraped from human tooth surfaces[2]. Since then, many advances in technology allowed more accurate descriptions of biofilms, although even today there is still ambiguity.

Biofilm formation has therefore been a mean of survival for bacteria, and it is the main reason why bacterial biofilms are the characteristic life form that can be found in extreme environments like stone surfaces in hot springs or even cold stones of mountain streams. Nowadays this survival strategy is successfully used by bacteria in industrial systems causing equipment damage, product contamination and energy loss[3,4]. This damaging impact can be found in various industrial applications such as drinking water distribution networks being a health risk. Despite the frequent problems caused by biofilms, there are industrial systems where biofilm growth is a beneficial phenomenon. The usefulness of biofilms is well known, especially in the field of bioremediation functioning as anaerobic digesters to remove contaminants, e.g. metals and radio nuclides[5], oil spills[6] and for the purification of industrial waste water, which have been studied lately by several researches[7,8]. Indeed, the adhesive characteristics of natural human flora was considered as a tool for preventing the adhesion of pathogenic bacteria to avert infection[9].

However, major problems due to the inappropriate formation of biofilms exist and these problems have a high economic impact in medicine[10]. Healthcare-associated infections

(HAIs) continue to be a tremendous issue today. It is estimated 1.7 million HAIs occur per year, and it cost the healthcare system up to $45 billion annually. Surgical site infections (SSIs) alone account for 290,000 of total HAIs and approximately 8,000 deaths[11]. This infections associated with surgical implants are generally more difficult to manage because they require a longer period of antibiotic therapy and repeated surgical procedures, which increase a lot the final cost of the treatment. In this thesis a development of new approaches that were required to understand undesirable biofilms are going to be addressed solve the actual diagnostic challenges. Furthermore this approaches permits the study of novel medical treatments against biofilms.

1.1.2 Understanding the mechanism of bacterial adhesion and development

As already mentioned biofilm is governed by a number of physical, chemical and biological processes. Attachment of bacteria to a substrate, also known as adhesion, is followed by cell-to-cell attachment, which is also known as cohesion. If the mechanisms behind these forms of attachment are optimal, a biofilm formation will exhibit with success. This biofilm formation has been described in the literature as a three-step process: first starting with an initial adsorption, or the accumulation of an organism in the substrate. Secondly the attachment of the bacteria to the material surface becomes stronger by the action of physical forces involving the formation of polymer bridges between the organism and the surface. Once the early biofilm has consolidated onto the surface, the third step leads to the formation and maturation of a strong bacterial layer by secreting extracellular polymeric substances (EPS)[12] that provides to the biofilm a high resistance to antibiotics[13,14]. Although this stepwise is very useful as snap shot of biofilm growth, and for running laboratory experiments with biofilms, the profile is very limited when considering chemical processes and genetic changes governing the biofilm communication with environment and itself. In order to understand the whole process with more accurate conditions, other different works described the molecular mechanisms and implications with more complexity.

A more complex biofilm cycle formation on biomaterials and the signal factors intervening in their control is well described by Arciola and coworkers[15] and shown in Figure 1.1. Hence the final process of biofilm development begins with a rapid accumulation of organic molecules and inorganic ions to form a layer called conditioning film[16]. Therefore planktonic bacteria adheres to the surface film that may

have different chemical properties than the non-living surface[17]. The initial attachment of this bacteria frequently involves a portion of the cell, a flagellum or EPS, while the bacterial cell continues to revolve. During so-called reversible attachment, the bacteria use its motility to sustain contact with the surface while searching for a suitable location there[18]. Such a search is also called chemo-sensoring if the bacteria prefer specific substrates present on the surface or produced by other bacteria[19]. After that the initially reversible attachment may transform into an irreversible one supported by the idea that physical appendages[20] (i.e. flagella, fimbriae or pili) make contact with the bulk lattice of the conditioning film stimulating chemical reactions such as oxidation and hydration[21] and consolidating the bacteria-surface bond. Some evidence has shown that microbial adhesion strongly depends also on the hydrophobic-hydrophilic properties of interacting surfaces[22]. The final step consists in the detachment of cells from the biofilm into a planktonic state to initiate a new cycle of biofilm formation elsewhere.

The illustration of biofilm cycle describes the early events involving expression of adhesins, exopolysaccharide and proteins implicated in cell aggregation and biofilm formation, which are orchestrated by the couple σ^B and SarA. Once biofilm reaches its final phase of maturation, the excess of autoinducing peptide (AIP) triggers the onset of the dispersal phase, characterized by the increase of expression of RNAIII with consequent production of extracellular proteases and phenol-soluble modulins. This molecules leads the toxin activation of the biofilms favouring the pathogenesis of them.

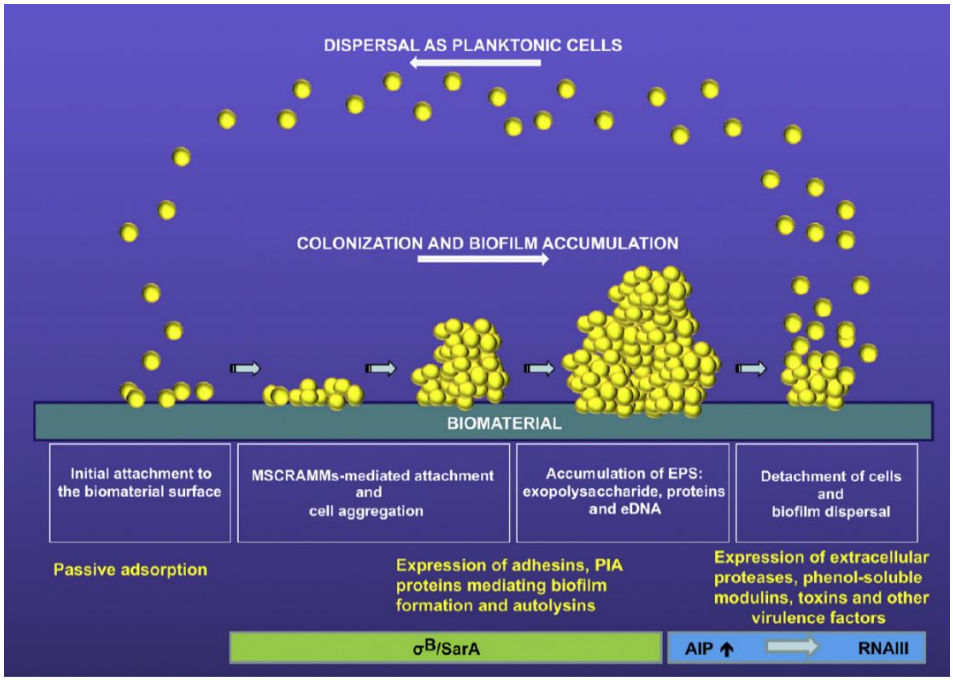

Figure 1.1. Schematic cycle of biofilm summarizing some features generally involved in biofilm formation and its dispersal[15].

1.2 Interactions of biofilms that influences development and pathogenesis

This section is going to analyse the biofilm virulence that triggers the toxicity and its clinical relevancies. The complex mechanisms required to form functional, mature biofilms are still under investigation. Only after the chemistry and the genetics of the slimy substance produced by microorganism were established, an association between the exopolysaccharide production and virulence began to be investigated. Following the summarized cycle of biofilm described in the previous section, many theoretical models tried to explain bacterial adhesion with the degree of hydrophobicity of the cell and the biomaterial surface[23]. Despite these models, specific proteins have been identified that mediate the binding to abiotic surfaces.

In the extensive amount of works related to orthopaedics, periprosthetic infections have been observed to occur with a frequency of 1.5-2.5% in primary hip and knee arthroplasties and with a frequency of 3.2-5.6% in the revision surgery[24]. Among the staphylococcal species that appear in the list of the leading etiologic agents, Staphylococcus aureus and Staphylococcus epidermidis are respectively at the first and the second positions. For this reason this thesis is focused on the proteins and molecules of this bacterial family. Figure 1.2 depicted many surface attached proteins produced during *Staphylococcus aureus* exponential growth. Alongside that proteins other host-damaging proteins like α-toxin can be secreted during its stationary phase of bacteria growth[25].

The synthesis of many of these proteins is dependent on the growth phase, as shown in Figure 1.2, and more importantly is controlled by Quorum-Sensing (QS) systems where regulatory genes play an important role such as AGR system. Thereupon QS system means cell-to-cell signalling, and it is an important phenomenon of microbial communities.

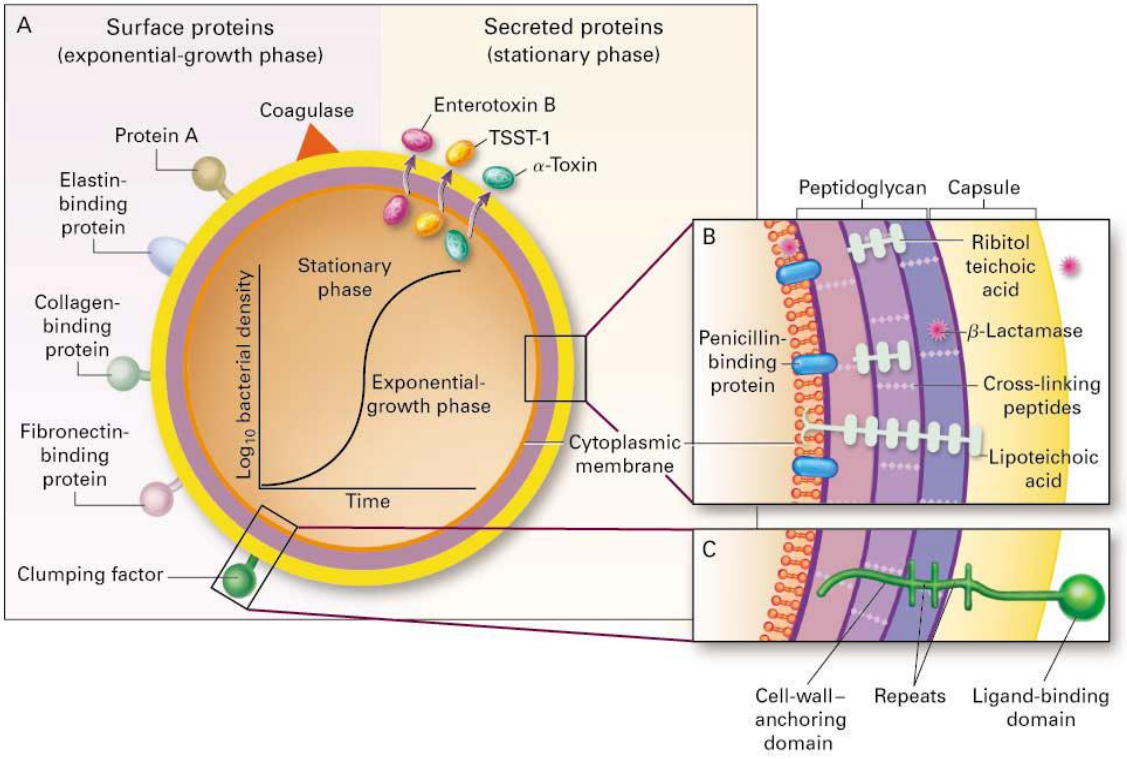

Figure 1.2. Structure of S. aureus membrane. (A) Shows the surface and secreted proteins.(B) and (C) show cross sections of the cell envelope. Many of the surface proteins have a structural organization similar to that of clumping factor, including repeated segments of amino acids[25].

The discovery of intercellular communication or “QS” among bacteria led to the realization that bacterial populations are capable of high-level coordinated behaviour that was once believed to be restricted to multicellular organisms. The capacity to behave collectively as a group (or population) endows bacteria with capabilities that cannot be achieved in solitude. Therefore cells located in the centre of a biofilm cluster, do not divide at all, or divide only slowly. However, they remain viable and cultivable once freed from the polymer encasement of the biofilm cluster. Bacterial products are constantly diffusing from one cell to another cell being responsible for intercellular communication. The reason why this metabolic communication (QS) is not efficient in the case of planktonic bacteria, is that the diffusing molecules will be diluted in the aqueous phase and only a small amount may reach the neighbouring bacteria.

The most intensely studied QS system was interestingly not related to pathogenic behaviour allowing the bioluminescent marine bacterium, *Vibrio fischeri*, to harmoniously live in symbiotic association with a number of eukaryotic hosts[26].

Although as mentioned before QS relationships are usually taking place on the adversarial role, nevertheless Raut *et al* in 2013 developed a method to detect QS molecules present in physiological samples for an early diagnosis of pathogenesis[27], by using *Vibrio harveyi*, which is a non-pathogenic bacteria. This bacteria emits bioluminescence in the presence of Autoinducer-2 (AI-2) molecules, which are present on a variety of disorders caused by pathogenic biofilms. The pathogenic molecules produced overwhelm the host defences, launching a successful infection to form an antibiotic-resistant biofilm, leading to disease[28,29], regulated by gene expression in response to fluctuations in cell-population density [30]. In the past decade, QS circuits have been identified in many bacterial species. The Regulatory circuit of *Staphylococcus aureus* depends mainly on two genetic locus very well explained by Arya and Princy [31] and depicted in Figure 1.3.

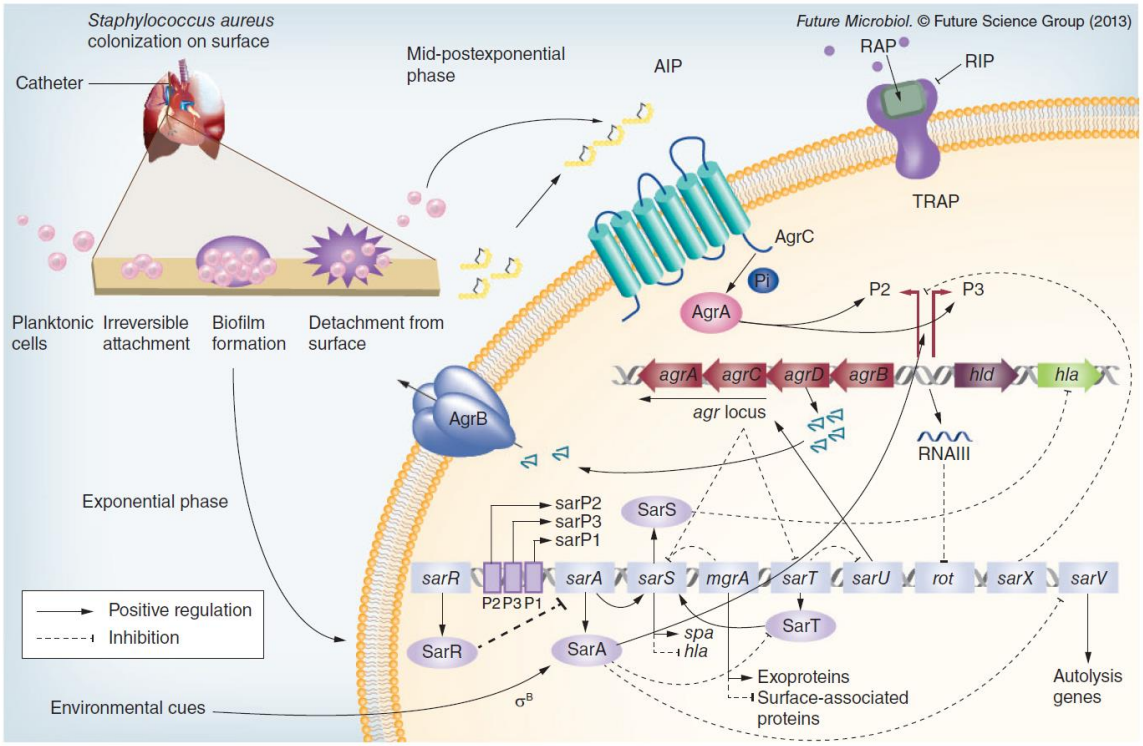

Figure 1.3. Network of factors that controls the virulence gene expression in Staphylococcus aureus**.**The expression of SarA leads to enhanced biofilm formation by triggering the cell wall-associated proteins during the exponential phase. σB plays a vital role to activate the sarA expression during stress conditions by binding to the P3 promoter. The expression of SarA is downregulated by binding to its own promoter through a feedback mechanism, which initiates the expression of the agr operon and, hence, the synthesis of extracellular proteins such as d-toxin and proteases. SarU acts as a positive regulator of agr and activation of agr locus would lead to repression of SarA homologs. AIP: Autoinducing peptide; RIP: RNAIII-inhibiting peptide; TRAP: Target of RNAIII-activating protein.

1.3 Bacterial growth detection and laboratory models for biofilm infection

Most of the current methods of bacterial detection employ conventional techniques such as fluorescence-activated cell sorting, counting colony forming units on petri-plates, optical density measurements, and fluorescence measurements of culture samples and colonies. Whereas these approaches yield useful and reliable information, they tend to be invasive, generally expensive, arduous, time consuming, and may require large amounts of sacrificial culture. Nowadays, the development of platforms for monitoring the biofilm growth is an important concern to understand the real behaviour of bacterial adhesion and to improve the efficacy of antibacterial treatments. Methods of continuous label-free monitoring techniques such as surface plasmon resonance[32,33] and quartz crystal microbalance [34] have gained attention, the latter able to calculate the amount of biomass attached on the surface. Also, the optical microscopy is a cheap and simple alternative method for characterizing biofilms but, at the same time, it is an end-point assay that involves labelling and destruction of bacteria. Combination of visualization techniques is deeply studied by Alhede *et al* in 2012 showing which techniques are more suitable for each application[35], and for adapting to predict the true architecture of biofilms.

Therefore, it is pertinent to develop tools that allow non-disruptive, continuous and label-free monitoring of the dynamic processes and mechanisms of biofilm formation under real conditions[36]. At this point the introduction of “microfluidics” is very appropriate to overcome the drawbacks described above. "Microfluidics" is the science and technology of systems that transport volumes of fluids that vary from microliters to femtoliters using micro-channels embossed in the surface of polymers or glass. The origins of microfluidics can be found in microanalytical methods such as high-pressure liquid chromatography (HPLC), gas-phase chromatography (GPC) and capillary electrophoresis. Due to the success of these technologies more compact and versatile formats were developed to enlarge the application sector[37–39]. Low requirement of sample volumes and reagents, low production of waste, short analysis times, cheap technology and reduced dimensions compared to commercial analysis systems[40] have attracted scientists in the fields of biology, chemistry, engineering and medicine from the last decade. These characteristics make microfluidics and microchip technology particularly useful for studying biomedicine and biology[41].

Although today many analytical methods for detecting DNA, pathogens, proteins and small organic molecules are conventionally available, miniaturization and integration into single microfabricated devices, i.e. microfluidic total analysis systems (*μTAS*),

provides higher detection sensitivity and signal-to-noise ratios. However, the resulting devices find essential application in the field of clinical diagnostics, proper analysis of pathogenic biofilms are still fundamental challenges. Numerous studies in the clinical diagnostic field are being achieved by the inclusion of integrated sensors that allows label-free detection of various biomolecules and reducing drastically the reagent volumes required for an experiment. Many of these studies used alternative methods for microorganism growth detection based on electrical impedance spectroscopy measurements[42]. There are many advantages using electrical signals to perform biological and chemical detection in microfluidic systems. The fabrication is inherently less complicated since these sensors typically only require patterned electrodes to operate. In addition, electrical signals can be directly interfaced with most measurement equipment while other signal modalities may require a transducer to convert the signal. Electrical sensors commonly measure changes in impedance[43,44], capacitance [45], or the redox activity of enzymes [46]. Some published examples of electrical sensing can be found in the literature based on the relative impedance changes induced after cell adhesion onto the electrodes [47,48], some of them using commercial interdigitated microelectrodes (IDuE) [49,50]. Despite offering a large sensitive area in a limited space, most of commercial IDuE do not offer the possibility to study cell growth under flow conditions, a variable already described, that affects biofilm structure and behaviour [51]. Moreover, the growth rate changes over time because of an ever-changing environment: as the organism grows it depletes the nutrients and dissolved oxygen while polluting its environment with waste products. These factors conspire to ultimately suppress the ability of the organism to divide.

The continuous flow experiments however, establishes an indefinitely long steady-state period of active growth, which enables long-term experimentation on microbes under essentially invariant conditions. Therefore, microfluidic devices have become an indispensable tool in the study of microbial metabolism, regulatory processes, adaptations and mutations. It provides constant environmental conditions for microbial growth and product formation[41] and facilitates characterization of microbial response to specific changes in the growth environment, one factor at a time. From such studies, it is possible to reconstruct the general behaviour of microorganisms in their native settings[52], allowing to understand biofilms during its formation. To address this issue label-free technologies and optimization of them were used along this monograph.

1.4 Objectives and organization of the work

As pointed out in the previous sections Biofilm lifeform is better than planktonic to understand the bacterial infections. To obtain this structure in a realistic model it has to be developed under flow conditions. The ability to continuously monitor bacterial biofilms using contactless impedance sensors promises to present new and innovative applications in healthcare. Consequently, the work of this thesis is chiefly the optimization of a custom-made device capable to detect biofilm formation into a controlled environment to accomplish the following objectives:

1. Design construction and validation of multi-parametric microfluidic device:
    a. Conception, design and manufacturing of the array of electrodes. The matrix of electrodes is the basic element for achieving Electrochemical Impedance Spectroscopy (EIS) data.
    b. Design and development of electronic instrumentation. The Instrumentation to develop will be responsible for generating the excitation signals, control and routing EIS data and control the multiplexation of the different devices working simultaneously.
    c. Integration of the platform
2. Data processing. Information obtained by EIS technology can give a lot of data that has to be processed to give the useful information to represent the more realistic data that is able to fit with equivalent circuits.
3. Inclusion of a second biosensor to monitor simultaneously toxicity. The increment of biomass monitored with label-free technologies has to be followed by toxin release studies in biofilm and planktonic modes of existence.
4. Setting up of surface modification techniques for bacterial treatment. The modification of the sensors can attract or inhibit the adherence of microorganisms on the surface modifying the signal of the bacteria growing inside.

The objectives detailed have been brought to a close along this thesis in the same order as they have been listed. Before going into the work a brief organization and description of the chapters is going to be carried out to summarize the accomplishments.

The core purpose of Chapter 2 is to provide a concise description of the material and the equipment used along the following chapters. It is described the canonical microbiological assays and the preparation of all the experiments related with bacteria. Then introduction of methods for characterization and visualization of the microbial growth was applied. Next, it was presented a brief description of the basis on Electrochemical Impedance Spectroscopy (EIS) methods for all the quantitative arguments made within this thesis. Furthermore, the methods used for surface modification to anchor antibacterial compounds, which are utilized in chapter 7 are described. Finally the synthesis of lipid vesicles that contain a biosensor for toxicity is described. This additional biosensor has been prepared at the Chemistry department of the University of Bath, in collaboration with Professor Toby Jenkins and his group.

Chapter 3 is a comprehensive description of the microfluidics by using an equipment available in our laboratory. This equipment is the Quartz Crystal Microbalance with Dissipation (QCM-D). This method is a high sensitive method able to detect protein attaching to the sensor surface. By using the equipment commercially available continuous flow conditions can be tested for growing bacterial biofilms. Furthermore, parameters like flow rate and temperature are tested with different bacterial strains. I describe the operation of the entire label-free equipment within the context of microfluidics, including data processing and data analysis. In addition Differential Interference Contrast (DIC) images are taken during the experiments. In summary, this chapter is the first contact to operate with micro-sized reactor volume to avoid the substrate-limited mode of operation. Finally, it was explored possible future directions and applications of the continuous flow approach developed in this thesis.

Chapter 4 firstly it was highlighted some of the recent published research involving microfluidic devices with integrated optical, mechanical and electrical sensors for the detection of biomolecules. The reason to analyse previous studies is to address some of the technological limitations faced by the conventional electrodes and current devices for bacterial biofilm growth, primarily based on cultivation within multi well platforms. In this direction we have designed and fabricated our own multi-parametric sensor and low-cost microfluidic platform. The roadmap for this part of the work is depicted in Figure 1.4 and applied for the two main parts of the platform, the device and the EIS sensor. This part of the work was coordinated and developed by *Institut Químic de Sarrià (IQS)* and the National Centre of Microelectronics (NCM), for the device and the sensor respectively. The design in both cases is followed by

computational modelling for quick test of the platform before its fabrication. Once the computational prototype becomes real, a functional test was finally ran for further redesign or fabrication until the final version of platform is ready. The final version of the device is dimensionally bounded to place a chip with interdigitated microelectrodes (IDuE) optimized for bacterial cultures and for working with two and four-electrode configuration. Besides the space of the sensing area depends on the space necessary to place a microscope objective to follow the bacterial growth in real-time as well. Finally the sterilization for reusability of the chip and the device is taken into account.

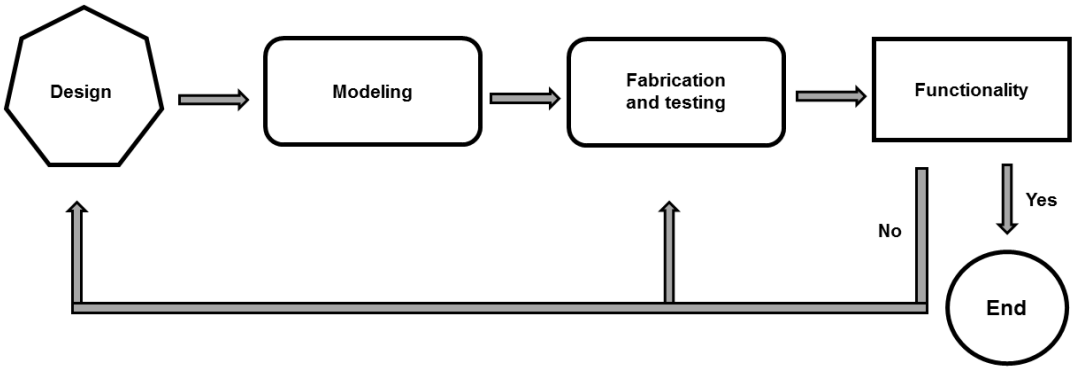

Figure 1.4. Schematic process for engineering the desired platform to accomplish the main goals of this monograph.

Chapter 5 describes how EIS data is applied to a microfluidic device to sense and detect bacterial growth. The detection mechanism due to biofilm development is explained along with the specific steady-state conditions already tested in chapter 3 with QCM-D methodology. The quantification of the bacterial growth on the IDuE geometry optimized in chapter 4 with a finite element model (FEM) is studied for confirming the increased resolution in detection while large electrode area was maintained. The designed platform designed allows the simultaneous and continuous monitoring of biofilm proliferation using optical microscopy and multiple read-outs, especially the comparison of two and four-electrode configuration impedance measurements that can be performed indistinctly on the same device, only performed before on eukaryotic cells[53]. In addition, relevant equations and models governing microbial growth in the device are studied for a comprehension of physiological behaviour of the biofilms.

Along the same lines as the fifth chapter, chapter 6 describes how the quorum-sensing systems triggers during the bacterial biofilm formation. The gene expression and regulatory circuits explained in section 1.2 is confirmed with the inclusion of the toxicity biosensor optimized by the group of Toby Jenkins (University of Bath, UK). The modified continuous flow experiment is described in this chapter to make multiple fluorescence readings. Previously many researchers predicted that biofilm becomes toxic when reaches the stationary phase as depicted in Figure 1.2. But no one developed a method to follow biofilm growth and detect the moment of the toxin secretion with certain accuracy by relating this release to its bacterial growth curve produced by EIS data. This achievement is carried out in Chapter 6 revealing results that confirm the relation of biofilm development with the virulence gene expression in *Staphylococcus aureus* by analysing toxin release studies.

The final Chapter 7 of the thesis explores the biofilm response to an antibiotic peptide called bacitracin that is well known by the efficient affection to the bacterial membrane. Moreover in the last 2 years new mechanism of action is being studied by Ciesio *et al* [54], and also patented for the affection to nucleic acids as well. The treatment is studied in static conditions and flow conditions by using both steady-state methods utilized before, in Chapter 3 and Chapter 5, with QCM-D and EIS technology respectively. The effect of the antibiotic peptide is analysed with the compound pumped into the devices and the antibiotic anchored onto the sensors with surface modification techniques.

1.5 References

(1) Costerton, J. W.; Lewandowski, Z.; Caldwell, D. E.; Korber, D. R.; Lappin-Scott, H. M. Microbial Biofilms. *Annu Rev Microbiol* **1995**, *49*, 711–45.

(2) Costerton, A. J. W.; Stewart, P. S.; Greenberg, E. P. Bacterial Bioflims: Common Cause of Persistent Infections. *Sci. Mag.* **1999**, *284*, 1318–1322.

(3) Hall-Stoodley, L.; Costerton, J. W.; Stoodley, P. Bacterial Biofilms: From the Natural Environment to Infectious Diseases. *Nat. Rev. Microbiol.* **2004**, *2*, 95–108.

(4) Yang, L.; Liu, Y.; Wu, H.; Song, Z.; Høiby, N.; Molin, S.; Givskov, M. Combating Biofilms. *FEMS Immunol. Med. Microbiol.* **2012**, *65*, 146–57.

(5) Barkay, T.; Schaefer, J. Metal and Radionuclide Bioremediation: Issues, Considerations and Potentials. *Curr. Opin. Microbiol.* **2001**, *4*, 318–323.

(6) Radwan, S. S.; Al-Hasan, R. H.; Salamah, S.; Al-Dabbous, S. Bioremediation of Oily Sea Water by Bacteria Immobilized in Biofilms Coating Macroalgae. *Int. Biodeterior. Biodegrad.* **2002**, *50*, 55–59.

(7) Duprey, A.; Chansavang, V.; Frémion, F.; Gonthier, C.; Louis, Y.; Lejeune, P.; Springer, F.; Desjardin, V.; Rodrigue, A.; Dorel, C. "NiCo Buster": Engineering E. Coli for Fast and Efficient Capture of Cobalt and Nickel. *J. Biol. Eng.* **2014**, *8*, 19.

(8) Vigueras-Cortés, J. M.; Villanueva-Fierro, I.; Garzón-Zúñiga, M. A.; De Jesús Návar-Cháidez, J.; Chaires-Hernández, I.; Hernández-Rodríguez, C. Performance of a Biofilter System with Agave Fiber Filter Media for Municipal Wastewater Treatment. *Water Sci. Technol.* **2013**, *68*, 599–607.

(9) Reid, G.; Howard, J.; Gan, B. S. Can Bacterial Interference Prevent Infection? *Trends Microbiol.* **2001**, *9*, 424–428.

(10) Mujagic, E.; Zwimpfer, T.; Marti, W. R.; Zwahlen, M.; Hoffmann, H.; Kindler, C.; Fux, C.; Misteli, H.; Iselin, L.; Lugli, A. K.; et al. Evaluating the Optimal Timing of Surgical Antimicrobial Prophylaxis: Study Protocol for a Randomized Controlled Trial. *Trials* **2014**, *15*, 188.

(11) Tsai, D. M.; Caterson, E. J. Current Preventive Measures for Health-Care Associated Surgical Site Infections: A Review. *Patient Saf. Surg.* **2014**, *8*, 42.

(12) An, Y. H.; Friedman, R. J. *Handbook of Bacterial Adhesion*; Humana Press: New Jersey, **2000**.

(13) Del Pozo, J. L.; Patel, R. The Challenge of Treating Biofilm-Associated Bacterial Infections. *Clin. Pharmacol. Ther.* **2007**, *82*, 204–9.

(14) Chandra, J.; Kuhn, D. M.; Mukherjee, P. K.; Hoyer, L. L.; Mccormick, T.; Mahmoud, A.; Cormick, T. M. C.; Ghannoum, M. A. Biofilm Formation by the Fungal Pathogen Candida Albicans : Development, Architecture, and Drug Resistance. *J. Bacteriol.* **2001**, *183*, 5385–5394.

(15) Arciola, C. R.; Campoccia, D.; Speziale, P.; Montanaro, L.; Costerton, J. W. Biofilm Formation in Staphylococcus Implant Infections. A Review of Molecular Mechanisms and Implications for Biofilm-Resistant Materials. *Biomaterials* **2012**, *33*, 5967–5982.

(16) Murga, R.; Miller, J. M. Biofilm Formation by Gram-Negative Bacteria on Central Venous Catheter Connectors : Effect of Conditioning Films in a Laboratory Model. *J. Clin. Microbiol.* **2001**, *39*, 2294–2297.

(17) Hall-Stoodley, L.; Costerton, J. W.; Stoodley, P. Bacterial Biofilms: From the Natural Environment to Infectious Diseases. *Nat. Rev. Microbiol.* **2004**, *2*, 95–108.

(18) Donlan, R. M. Biofilms: Microbial Life on Surfaces. *Emerg. Infect. Dis.* **2002**, *8*, 881–890.

(19) Nielsen, a. T.; Tolker-Nielsen, T.; Barken, K. B.; Molin, S. Role of Commensal Relationships on the Spatial Structure of a Surface-Attached Microbial Consortium. *Environ. Microbiol.* **2000**, *2*, 59–68.

(20) Olsson, A. L. J.; van der Mei, H. C.; Busscher, H. J.; Sharma, P. K. Novel Analysis of Bacterium-Substratum Bond Maturation Measured Using a Quartz Crystal Microbalance. *Langmuir* **2010**, *26*, 11113–7.

(21) Kumar, C. G.; Anand, S. . Significance of Microbial Biofilms in Food Industry: A Review. *Int. J. Food Microbiol.* **1998**, *42*, 9–27.

(22) Liu, Y.; Yang, S. F.; Li, Y.; Xu, H.; Qin, L.; Tay, J. H. The Influence of Cell and Substratum Surface Hydrophobicities on Microbial Attachment. *J. Biotechnol.* **2004**, *110*, 251–256.

(23) Legeay. G, Poncin-Epaillard. F, A. C. New Surfaces with Hydrophilic/hydrophobic Characteristics in Relation to (no)bioadhesion. *Int. J. Artif. Organs* **2006**, *4*, 453–461.

(24) Ravaioli, S.; Cangini, I.; Pietrocola, G. Scenery of Staphylococcus Implant Infections in Orthopedics. *Future Microbiol.* **2011**, *6*, 1329–1349.

(25) Lowy, F. D. Staphylococcus Aureus Infections. *N. Engl. J. Med.* **1998**, *339*, 520–532.

(26) Ruby, E. G.; Urbanowski, M.; Campbell, J.; Dunn, a; Faini, M.; Gunsalus, R.; Lostroh, P.; Lupp, C.; McCann, J.; Millikan, D.; et al. Complete Genome Sequence of Vibrio Fischeri: A Symbiotic Bacterium with Pathogenic Congeners. *Proc. Natl. Acad. Sci. U. S. A.* **2005**, *102*, 3004–3009.

(27) Raut, N.; Pasini, P.; Daunert, S. Deciphering Bacterial Universal Language by Detecting the Quorum Sensing Signal, Autoinducer-2, with a Whole-Cell Sensing System. *Anal. Chem.* **2013**, *85*, 9604–9.

(28) Yarwood, J. M.; Bartels, D. J.; Volper, E. M.; Greenberg, E. P. Quorum Sensing in Staphylococcus Aureus Biofilms. *Am. Soc. Microbiol.* **2004**, *186*, 1838–1850.

(29) Janakiraman, V.; Englert, D.; Jayaraman, A.; Baskaran, H. Modeling Growth and Quorum Sensing in Biofilms Grown in Microfluidic Chambers. *Ann. Biomed. Eng.* **2009**, *37*, 1206–16.

(30) Bassler, M. B. M. and B. L. Quorum Sensing in Bacteria. *Annu. Rev. Microbiol.* **2001**, *55*, 165–199.

(31) Arya, R.; Princy, S. A. An Insight into Pleiotropic Regulators Agr and Sar: Molecular Probes Paving the New Way for Antivirulent Therapy. *Future Microbiol.* **2013**, *8*, 1339–53.

(32) Jenkins, a T. a; Ffrench-Constant, R.; Buckling, A.; Clarke, D. J.; Jarvis, K. Study of the Attachment of Pseudomonas Aeruginosa on Gold and Modified Gold Surfaces Using Surface Plasmon Resonance. *Biotechnol. Prog.* **2004**, *20*, 1233–6.

(33) Tun, T. N.; Cameron, P. J.; Jenkins, a T. a Sensing of Pathogenic Bacteria Based on Their Interaction with Supported Bilayer Membranes Studied by Impedance Spectroscopy and Surface Plasmon Resonance. *Biosens. Bioelectron.* **2011**, *28*, 227–31.

(34) Schofield, A. L.; Rudd, T. R.; Martin, D. S.; Fernig, D. G.; Edwards, C. Real-Time Monitoring of the Development and Stability of Biofilms of Streptococcus Mutans Using the Quartz Crystal Microbalance with Dissipation Monitoring. *Biosens. Bioelectron.* **2007**, *23*, 407–13.

(35) Alhede, M.; Qvortrup, K.; Liebrechts, R.; Høiby, N.; Givskov, M.; Bjarnsholt, T. Combination of Microscopic Techniques Reveals a Comprehensive Visual Impression of Biofilm Structure and Composition. *FEMS Immunol. Med. Microbiol.* **2012**, *65*, 335–42.

(36) Stewart, P. S.; Costerton, J. W. Antibiotic Resistance of Bacteria in Biofilms. *Lancet* **2001**, *358*, 135–8.

(37) Whitesides, G. M. Poly (dimethylsiloxane) as a Material for Fabricating Microfluidic Devices. *Acc. Chem. Res.* **2002**, *35*.

(38) Whitesides, G. M. The Origins and the Future of Microfluidics. *Nature* **2006**, *442*, 368–73.

(39) Whitesides, G. M.; Ostuni, E.; Jiang, X.; Ingber, D. E. SOFT LITHOGRAPHY IN BIOLOGY AND BIOCHEMISTRY. *Biomed. Eng. (NY).* **2001**, *3*, 335–373.

(40) Manz, A.; Harrison, D. J.; Verpoorte, E. M. J.; Fettinger, J. C.; Paulus, A.; Lüdi, H.; Widmer, H. M. Planar Chips Technology for Miniaturization and Integration of Separation Techniques into Monitoring systemsCapillary Electrophoresis on a Chip. *J. Chromatogr. A* **1992**, *593*, 253–258.

(41) Balagaddé, F. K.; You, L.; Hansen, C. L.; Arnold, F. H.; Quake, S. R. Long-Term Monitoring of Bacteria Undergoing Programmed Population Control in a Microchemostat. *Science* **2005**, *309*, 137–140.

(42) Cady, P.; Dufour, S. W.; Lawless, P.; Nunke, B.; Kraeger, S. J. Impedimetric Screening for Bacteriuria. *J. Clin. Microbiol.* **1978**, *7*, 273–8.

(43) Varshney, M.; Li, Y. Interdigitated Array Microelectrodes Based Impedance Biosensors for Detection of Bacterial Cells. *Biosens. Bioelectron.* **2009**, *24*, 2951–60.

(44) Cai, H.; Lee, T. M. H.; Hsing, I. M. Label-Free Protein Recognition Using an Aptamer-Based Impedance Measurement Assay. *Sensors Actuators, B Chem.* **2006**, *114*, 433–437.

(45) Kim, T.; Kang, J.; Lee, J.-H.; Yoon, J. Influence of Attached Bacteria and Biofilm on Double-Layer Capacitance during Biofilm Monitoring by Electrochemical Impedance Spectroscopy. *Water Res.* **2011**, *45*, 4615–22.

(46) Lu, L.; Chee, G.; Yamada, K.; Jun, S. Electrochemical Impedance Spectroscopic Technique with a Functionalized Microwire Sensor for Rapid Detection of Foodborne Pathogens. *Biosens. Bioelectron.* **2013**, *42*, 492–5.

(47) Martins, S. B.; Selby, M. J. Evaluation of a Rapid Method for the Quantitative Estimation of Coliforms in Meat by Impedimetric Procedures. *Appl. Environ. Microbiol.* **1980**, *39*, 518–24.

(48) Kim, T.; Kang, J.; Lee, J.-H.; Yoon, J. Influence of Attached Bacteria and Biofilm on Double-Layer Capacitance during Biofilm Monitoring by Electrochemical Impedance Spectroscopy. *Water Res.* **2011**, *45*, 4615–22.

(49) Urcan, E.; Haertel, U.; Styllou, M.; Hickel, R.; Scherthan, H.; Reichl, F. X. Real-Time xCELLigence Impedance Analysis of the Cytotoxicity of Dental Composite Components on Human Gingival Fibroblasts. *Dent. Mater.* **2010**, *26*, 51–8.

(50) Rahim, S.; Üren, A. A Real-Time Electrical Impedance Based Technique to Measure Invasion of Endothelial Cell Monolayer by Cancer Cells. *J. Vis. Exp.* **2011**.

(51) Stoodley, P.; Lewandowski, Z.; Boyle, J. D.; Lappin-Scott, H. M. Oscillation Characteristics of Biofilm Streamers in Turbulent Flowing Water as Related to Drag and Pressure Drop. *Biotechnol. Bioeng.* **1998**, *57*, 536–44.

(52) Renslow, R. S.; Babauta, J. T.; Majors, P. D.; Mehta, H. S.; Ewing, R. J.; Ewing, T. W.; Mueller, K. T.; Beyenal, H. A Biofilm Microreactor System for Simultaneous Electrochemical and Nuclear Magnetic Resonance Techniques. *Water Sci. Technol.* **2014**, *69*, 966–73.

(53) Sarró, E.; Lecina, M.; Fontova, a; Solà, C.; Gòdia, F.; Cairó, J. J.; Bragós, R. Electrical Impedance Spectroscopy Measurements Using a Four-Electrode Configuration Improve on-Line Monitoring of Cell Concentration in Adherent Animal Cell Cultures. *Biosens. Bioelectron.* **2012**, *31*, 257–63.

(54) Ciesio, J.; Wrzesi, J.; Stokowa-so, K.; Nagaj, J.; Kasprowicz, A.; Leszek, B.; Szczepanik, W. Antibiotic Bacitracin Induces Hydrolytic Degradation of Nucleic Acids ☆. *Biochim. Biophys. Acta* **2014**, *1840*, 1782–1789.

Chapter 2 Experimental Methodology

2.1 Materials

TritonX-100 (#T8787), 10,12-Tricosadiynoic acid, TCDA (#91445), Cholesterol (#C8667), Ethylenediaminetetraacetic acid, EDTA (#EDS), sodium chloride, NaCl (#S7653), 5(6)-Carboxyfluorescein (#21877), were obtained from Sigma-Aldrich (UK). 1,2-dipalmitoyl-*sn*-glycero-3-phosphocholine (#850355), 1,2-dipalmitoyl-*sn*-glycero-3-phosphoethanolamine (#850705) were obtained from Avanti Polar Lipids (USA). Sephadex™ G25 columns were obtained from GE Healthcare (UK). FLUOstar Omega plate reader was purchased from BMG Labtech. UVP CL 1000 Crosslinker and the 96 well costar plates were purchased from Fischer Scientific (UK). Peristaltic pump and tubing were obtained from IsmaTec.

2.2 Microbiological assays

The experiments with the presence of living bacterial cells were carried out in aseptic conditions using a class II biosafety cabinet, sterilized with 70% ethanol and UV light for 15 minutes. These experiments with biological samples used bacterial medium obtained from Sigma-Aldrich. The bacteria strain manipulated for this work were four Gram-positive bacteria, *S.aureus* V329, *S. epidermidis* CH845, 448 and 617. This library of strains were cultured for the biofilm studies and/or toxin release studies.

2.2.1 Biosafety levels

A microbiological safety cabinet with class II biosafety level was utilised for the microbiological work (Figure 2.1) guaranteeing a sterile environment during the bacterial seeding growth and manipulation. The biosafety levels are widely used as the primary line of containment in laboratories that deal with dangerous pathogens with the purpose of protecting the safety of personnel by securing the materials safely in laboratories, and also in order to safeguard the environment against contamination[1]. In this work the performed platform for biofilm studies (refer to Chapter 4) was used in the incubator placed inside the cabinet. Also material as pipette tips, media bottles, tubing and connectors were decontaminated before using by autoclaving for 15 minutes at 121 ºC and 15 psi due the contact with microbes during the experiments.

Figure 2.1. Class II Microbiological safety cabinet that recirculates the 70 % of the air.

2.2.2 Bacterial preparation

The bacteria used in the biofilm and planktonic experiments were prepared from glycerol stock cultures stored at -80 °C and streaked onto tryptic soy agar (TSA) plates, in the case of Gram positive organism, and Luria Broth (LB), in the case of Gram negative organisms. The agar plates were placed into an incubator at 37 °C for 16 hours for colonies development. Following growth comes from picking an individual colony and transfers it from the plate to a falcon with 10 mL of TSB for 16 hours of agitation at 37 °C (Figure 2.2). After bacterial growth, the suspension have reached the stationary phase of the growth cycle (Figure 2.3), however log phase growth is required prior to dilution to have a final absorbance of 0.084 measured at a wavelength of 600nm. This dilution feeds the device and the static cultures in the wells.

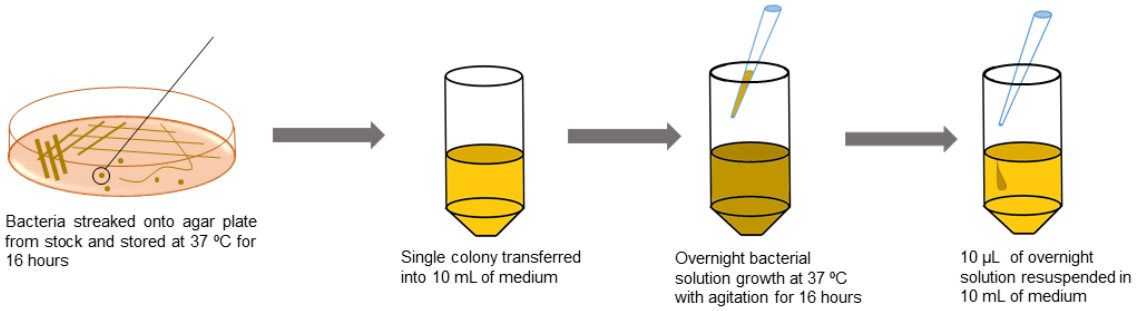

Figure 2.2. Preparation of an individual bacterial strain prior to dilution and seeding to the surface, sample or device of interest.

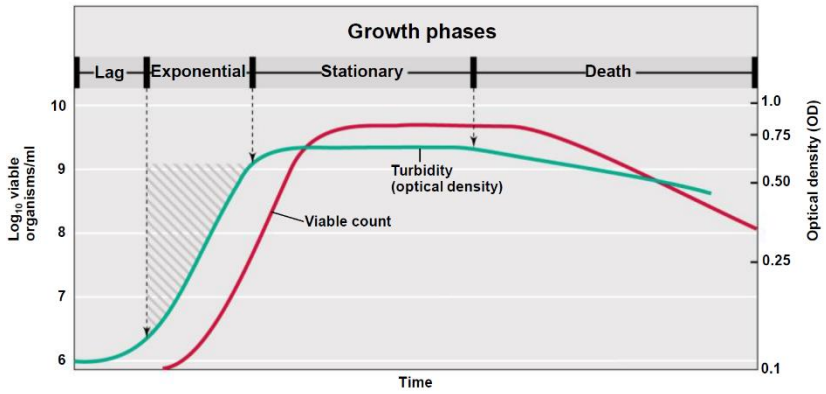

Figure 2.3. Typical growth curve of a bacterial population[2].

2.2.3 Bacterial growth in agar media

The Luria Agar (LA) and Tryptic Soy Agar (TSA), used for Gram-negative and Gram-positive bacterial growth respectively, were made at the concentration given on the container. The chemical was priory weighed with a HR120 A&D analytical balance and dissolved in ultra-pure deionised water obtained from Thermo scientific Barnstead easy pure II purification system. The mixture was autoclaved and poured the warm liquid into petri dishes. The presence of colonies prior to microbial seeding indicated contamination.

2.2.4 Bacterial growth in broth media

The Bacteria growth used in the experiments with living bacterial cells was a solution carried out with Luria Broth (LB) and Tryptic Soy Broth (TSB) for Gram-negative and Gram-positive bacteria, respectively. The dehydrated form of the media culture was weighed using a HR120 A&D analytical balance accordingly to the compositions given on the containers, and dissolved in ultra-pure deionised water from Thermo scientific Barnsted easy pure II purification system, autoclaved, and stored. The presence of precipitation cloudy compounds indicated contamination.

2.2.5 Bacterial supernatant preparation

Bacterial supernatant was used for toxicity analysis of the bacteria in biofilm and planktonic structure. The supernatant is the separable solution obtained from a bacteria culture by centrifugation process to discard the solution of the pellet where the whole bacterial cells are present. The overnight culture was centrifuged at 10.000 rpm for 10 minutes to form a pellet, and the solution was filtered by pressurisation through a 0.22 µm filter. The supernatant sample was tested against lipid vesicles in a 1:1 ratio and fluorescence was monitored for time periods of less than two hours.

2.3 Methods of characterization

2.3.1 Differential interference contrast microscopy (DIC)

This methodology was used for viewing bacterial attachment on surfaces, prior to more quantitative assessments. Differential interference contrast microscopy permits the visualization of bacteria by using visible light illuminating the sample. This image could be magnified up to 100 times by the objective lenses. The conventional bright field microscopy technique was firstly enhanced converting phase shift in the light passing through the sample, into brightness changes in the image, which means better contrast. A modification of this phase contrast microscopy was applied, with the differential interference contrast technique generating a pseudo 3D relief (Figure 2.4d) of the image separating a polarized light source into two orthogonally polarized mutually coherent parts which are spatially displaced at the sample plane, and recombined before observation.

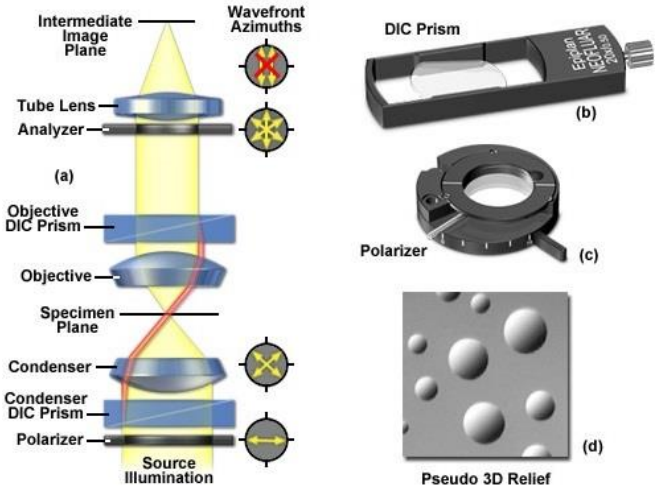

Figure 2.4. Schematic view of Differential Interference Contrast (DIC) technology: optical pathways and components.

Figure 2.4 illustrates the differential interference contrast beam path that is similar to that of polarized transmitted light. In DIC (as compared to polarized light), the two birefringent prisms (Figure 2.4b) are inserted into the optical train, one in the condenser and the second near the objective pupil. The condenser prism performs a vectorial decomposition of the previously linearly polarized light (Figure 2.4c) into two vibration directions that are perpendicularly polarized to each other, and laterally shifts these partial beams in such a way that a small lateral displacement of the wavefronts occurs where regions of thickness or refractive index vary.

2.3.2 Confocal Microscopy and bacteria staining

Confocal microscopy allows the use of a viability kit by staining the bacteria attached over the surfaces, and assess the impact of the surface modification treatment. The Figure 2.5 showed the light passing through an objective lens and directed onto the sample, emitted light than passes to the detector finally.

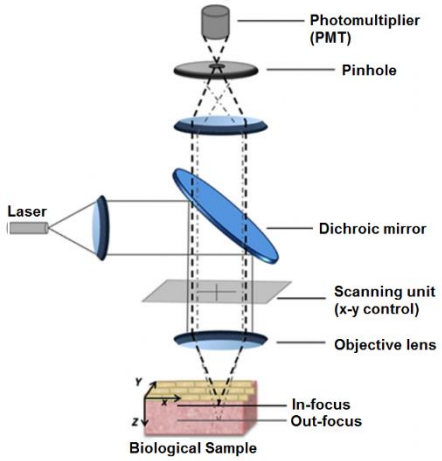

Figure 2.5. Schematic view of the Confocal Laser Scanning microscope (CLSM).

The bacterial culture was stained at the end of the experiment with Live/Dead Baclight ™ (Kit L13152) from Invitrogen detection technologies. An appropriate mixture of the SYTO 9 and propidium iodide stains to detect intact cell membranes with green fluorescence and bacteria with damaged membranes with red fluorescence, respectively. The confocal laser scanning microscopy (CLSM) LSM510 META from Zeiss was controlled by AIM software (version 3.2, Carl Zeiss MicroImaging GmbH, Jena, Germany) and equipped with lasers providing excitation wavelengths of 480nm (Syto 9) and 490nm (propidium iodide) that are employed. The staining was carried out for 15 minutes and the sample was washed 7 times before it was placed on a coverslip of 60 x 24 mm upside down to image the sample from the bottom. Biofilm image was acquired 15min after the end of the biofilm development.

2.3.3 Scanning Electron Microscopy

This methodology was used to visualize the biofilm formed in the sensor, placed into the impedance device, which is opened when all data is acquired and the experiment was finished. The sample was prepared for Scanning Electron Microscopy (SEM) as described previously by Sule and coworkers[3]. Briefly, the air-dried biofilms were fixed with 2 ml of 2.5% glutaraldehyde in 0.1 mol/L sodium phosphate buffer, rinsed once in the same buffer and then in deionized water followed by an overnight drying. The biosensor was attached to aluminium mounts and coated with gold using a Polaron Emitech SC7640 sputter coater (New haven, UK). Images were obtained with a JEOL JSM-5310 scanning electron microscope (JEOL Ltd., Tokyo, Japan) up to 80000X magnification.

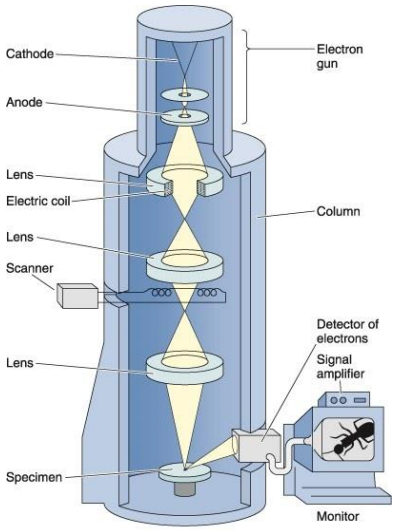

Figure 2.6. Schematic view of a scanning electron microscope (SEM). McGraw-Hill Companies, Inc.

2.3.4 Contact Angle

Contact angle measurement were used in the study of surface energy, wettability and adhesion of the modified surfaces. This technique was developed to provide a good understanding of the surface properties using relatively a very simple approach to probe different aspects of the physic and chemistry of the surfaces.

The contact angle measurements are based on the Young's equation that relates the contact angle θ, liquid surface tension γlv, solid surface energy γsv, solid-liquid surface tension γsl as represented in Figure 2.7[4]. The illustration shows that a small contact angle is observed when the liquid spreads on the surface, while a large contact angle is observed when the liquid beads on the surface, indicating hydrophilic and hydrophobic surfaces respectively.

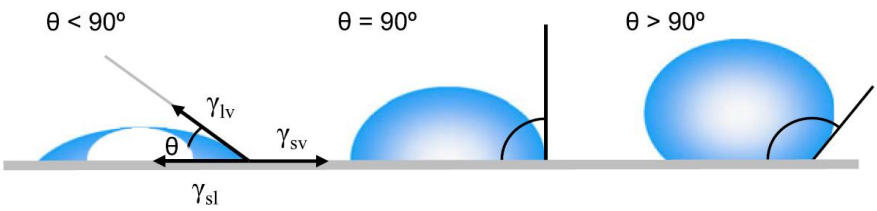

Figure 2.7. Illustration of contact angles formed by sessile liquid drops on a smooth homogeneous solid surface[4].

2.3.5 Fluorescence/Absorbance plate reader

The plate reader was used in the toxicity study of biofilms. The equipment allows a simultaneous measurement of optical density and fluorescence intensity at a wide range of wavelengths. The fluorescence excitation and emission filters of 485 ± 12 nm and 520 nm were used, with a gain of 650 to measure toxicity of the bacterial culture and/or bacterial supernatant. Optical density was measured at 600nm (OD_{600}) for monitoring bacterial growth of the experiments carried out using costar 96 well plates or the fluidic device. The continual or the endpoint measurements were obtained reading a triplicate of each time or condition, respectively. The equipment utilised was a FLUOstar Omega plate reader (Figure 2.8).

Figure 2.8. FLUOstar Omega Plate reader.

2.3.6 Nanoparticle tracking analysis

The vesicle used in section 6.2.2 were sized and visualized with nanoparticle tracking analysis (NTA). The technique is based on a particle-by-particle visualization in a liquid at real time with a minimal sample preparation. NTA provides size and concentration measurements of the particles undergoing Brownian motion. The technology comprises a laser light source, generated by focused 635 nm laser beam passing through a prism-edged optical flat, of which the refractive index is such that the beam refracts at the interface between the optical flat and the liquid sample layer placed above it. Due to the refraction, the beam compresses to a low profile, intense illumination region (Figure 2.9) that can be easily visualised by the microscope objective placed over the sample. The instrument tracks individual particles analysed by the software, which establishes mean square displacement and diffusion coefficient (D_t), then from Stokes Einstein equation the particle diameter (d_h) can be obtained. The nanoscale particles analysed by NTA are from approximately 10 nm to 1000 nm. Particle concentration and size measurements were obtained using a Nanosight LM14 (Malvern Instruments). Measurements were taken of a 1/100 diluted sample and multiple readings were taken to an average of these values.

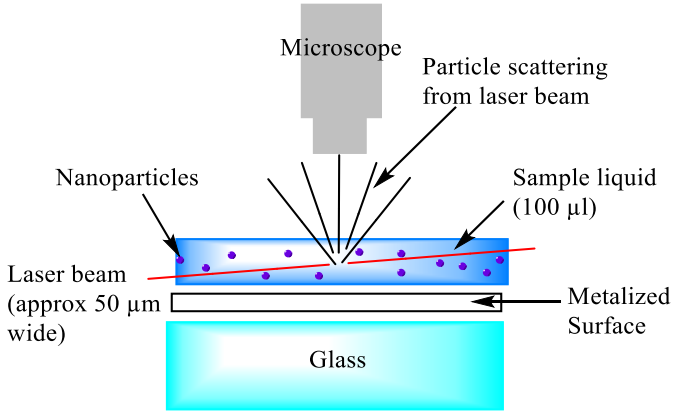

Figure 2.9. Schematic diagram of a Nanoparticle tracking analysis instrument.

2.3.7 Dynamic Light Scattering

The vesicles were also characterized with Dynamic light scattering (DLS), which is a technique that allows accurate measurement of the size of nanoparticles in solution. Scattering of a monochromatic light source by a particle, known as Rayleigh scattering if the particle size is smaller than the wavelength, allows detection and measurement. The detected particles are undergoing Brownian motion; the movement of particles resulting from bombardment of the solvent molecules around them, the smaller the particle size the faster the movement. Vesicle diameter was obtained using a Zetasizer Nanoscale Dynamic Light Scatterer, manufactured by Malvern instruments. Measurements were taken of multiple samples each with multiple readings and through the average of these values. 5-10 µl of sample was dispersed into 1 ml of buffer solution prior to measurement.

2.3.8 Quartz Crystal Microbalance with Dissipation (QCM-D)

QCM-D Technology was used to optimize the flow rate and the temperature for biofilm developing during 24 hours, with stainless steel and gold sensors. In order to obtain real time images of biofilm adhesion and subsequent formation we used the QCM-D window module (Figure 2.10). Thus, it was acquired a correspondence data between the QCM-D and optical microscope images, which will give us visual insight into the microscopic phenomena taking place during the measurement.

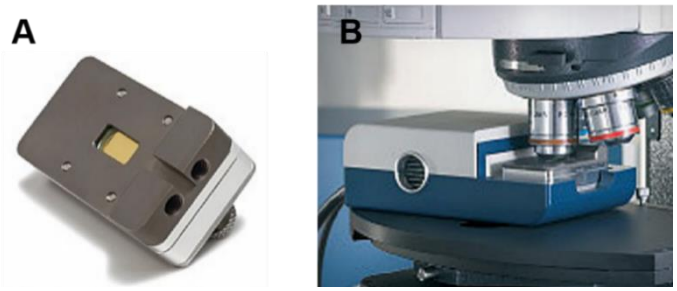

Figure 2.10. Schematic picture of Quartz Crystal Microbalance with Dissipation (QCM-D). (A) Window module that allows microscopic imaging. (B) Measurement of the bacterial attachment performed simultaneously with QCM-D data.

This technology monitors the frequency and energy dissipation response of a freely oscillating sensor, giving a faster and accurate information of the films attached and developed onto the sensors. The QCM-D methodology is based on quartz's inherent property of piezoelectricity[5]. This technique uses the changes in resonance frequency of the crystal to measure the mass attached on the surface, according to the Sauerbrey relation (Equation 2.1), where the resonance frequency shift (Δf) is highly dependent on any mass change (Δm) of the crystal. The constant C represents the mass sensitivity (17.7 ng/cm·Hz for a 5 MHz sensor) and n (1, 3, 5…) the overtone number.

$$\Delta \boldsymbol{m} = -\frac{\boldsymbol{C}}{\boldsymbol{n}}\Delta \boldsymbol{f} \qquad \text{(Equation 2.1)}$$

According to the Sauerbrey relation a decrease in frequency implies an increase of adsorbed mass over the sensor. The QCM-D technique is also able to monitor the dissipation parameter defined as the ratio between the energy dissipated and the energy stored by the oscillating sensor, and is given by the following equation:

$$\boldsymbol{D} = \frac{\boldsymbol{E_{Dissipated}}}{\boldsymbol{2\pi E_{Stored}}} \qquad \text{(Equation 2.2)}$$

QCM-D technique monitors changes in frequency (f) and dissipation (D) of an oscillating sensors. As mass adsorbs onto the sensor a frequency shift can be appreciated, besides the dissipation parameter gives information about the viscoelastic properties of the adsorbed layer. Softer coatings lead to an increase of the oscillation damping, which is traduced as an increase of dissipation. Figure 2.11 is an example that illustrates the behavioural differences between a rigid and a soft layer.

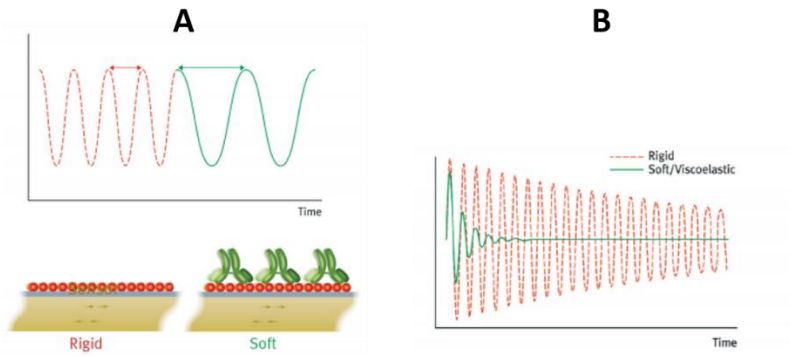

Figure 2.11. Differences in behaviour between soft and rigid adsorbed layers. (A) Frequency change due to an increase of the adsorbed mass by the addition of a molecular layer. This example shows the addition of an antibody (green) to a protein layer (red). (B) Difference in the dissipation signal generated by a rigid (red) and a soft (green) adsorbed layer.

Simultaneous measurement of multiple overtones is required to extract film thickness information. The different overtones give information about the homogeneity of the applied layers, as the detection range out from the crystal surface decreases with increasing overtone number (Figure 2.12). Thus, differences in frequency behaviour of the different overtones suggests vertical variations in film properties.

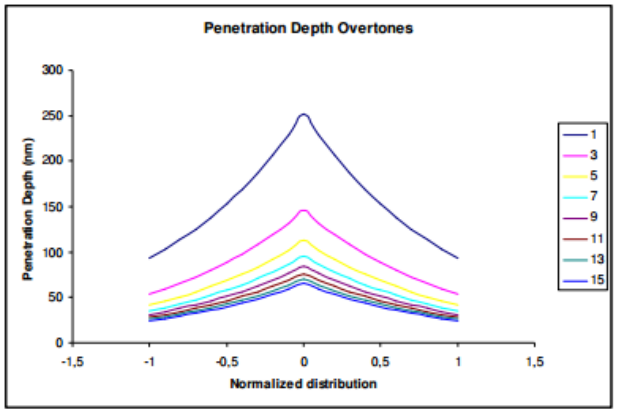

Figure 2.12. Viscous penetration depth as function of overtone (Q-Sense reported data).

2.4 Impedance Measurements methods

This section briefly introduces the electrochemical impedance methods applied in this work for biofilm detection, the two and four-electrode method. In the framework of this thesis work, both methods will be compared and optimized for biofilms. Here is also taken into account the injected current level for the measurement that had to be performed to use large currents to enlarge the voltage drop and, consequently, to

maximize the signal-to-noise ratio. However, two facts limit the allowable current intensity:

- Nonlinear behaviour of the living tissues. As most physical phenomena, electrical impedance reaches the nonlinear regime if the stimuli surpasses a certain value.
- Safety. The injected electrical energy can cause different sorts of damage to the living tissues.

In living tissues, the voltage/current relation is linear while the applied electrical fields do not reach the nonlinear threshold usually assigned to cell membranes and its polarization[6]. If an electric field is superimposed, the protein structures on the cellular membrane that are responsible for the transport of specific ions can change their conformation and alter the conductivity of the membrane.

The nonlinear impedance response of living tissues must not be confused with the nonlinear impedance response of the electrode-tissue interface, or electrode-electrolyte interface. This phenomenon has been studied experimentally[7] and theoretically[8].

In general, it seems that the criterion to select the current amplitude has been to use a current below 7 microA since the maximum allowable leakage current by the safety standards in the low-frequency range has a value of 10 microA[9].

2.4.1 Two-electrode method

The most evident way to perform electrical impedance measurements by using electrodes is to apply the two-electrode method, also referred as the bipolar method. That is, to inject a known current into the Biological Sample (BS) through two electrical contacts and to measure the resulting voltage drop between these two contacts (see Figure 2.13). This method only works properly if the impedance of the electrical contacts (Z_{C+} and Z_{C-}) is much lower than the impedance of the Biological Sample (Z_{BS}) since the measured impedance (Z') is the sum of Z_{BS}, Z_{C+} and Z_{C-} . As it has been seen here above, the electrode-electrolyte interface impedances can be higher than the impedance of the biological sample, especially at low frequencies, and are too instable and unpredictable to think of a mathematical correction of the measurement. Therefore, the repeatability and the reproducibility of the measurements will be seriously compromised.

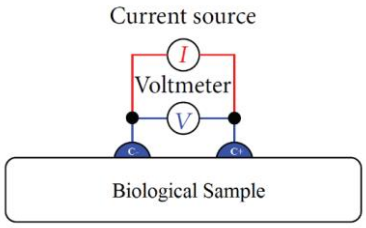

Figure 2.13. Schematic representation of the two-electrode method.

2.4.2 Four-electrode method

The four-electrode method, also referred as tetrapolar or Kelvin method, has been used in material science to measure the resistivity of materials since the late 1800's [10]. It uses a pair of electrodes to inject the current into the sample and another pair of electrodes to measure the resulting voltage drop (Figure 2.14). In principle, because no current flows through the voltage meter (V), the injected current completely flows through the biological sample and the voltage drop at this sample is the same that the meter 'sees'. Thus, in principle, the electrode-electrolyte interface impedance has no influence on the measurement, and the contact and wire impedance will be minimal on the meter.

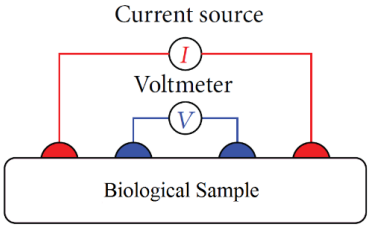

Figure 2.14. Schematic representation of the four-electrode method. The AC current is employed into the sample through current source (I) and the resulting potential is differentially measured across the inner electrodes with the Voltmeter (V).

This type of experimental setup is not very common in electrochemistry and usually it is used for measurements of junction potentials between two non-miscible phases or across a membrane, giving the possibility to calculate the resistance of the interface or the membrane conductivity. In this case the biofilms are considered a membrane or a tissue. In order to demonstrate the feasibility of the proposed methods for biofilm detection a multi-parametric platform was performed to carry on parallel measurements during the biofilm development. The results will be shown and analysed in chapter 5.

2.5 Lipid vesicle preparation method

The vesicles preparation was carried out and optimized for testing the toxicity of the biofilms (section 6.2.4.3), the planktonic and biofilm comparison structures of *Staphylococcus aureus* V329 (section 6.2.5).

2.5.1 Buffer preparation

The aqueous buffer solutions were made according to the compositions given below. The chemicals were weighed using a HR120 A&D analytical balance able to resolve to 0.1mg and dissolved in MiliQ water obtained from Thermo scientific Barnstead easy pure II purification system, sonicated as required, stored at 4°C and used for cleaning of equipment and in the purification step of vesicles. Self-quenched carboxyfluorescein solution was used as the signalling dye encapsulated inside the vesicles. The table below shows the components of the dye solution (Table 2.1).

Eluent HEPES buffer – pH 7.4

Chemical	Mass	Concentration
Deionised water	750 ml	
NaCl	4.680 g	112.55 mM
NaOH	0.168 g	6.58 mM
HEPES	1.7895 g	10 mM
EDTA	0.219 g	1mM

Table 2.1. The composition of the HEPES buffer solution for storage and purification of the vesicles.

50 mM 5(6)-carboxyfluorescein (5(6)-CF) solution

Chemical	Mass	Concentration
Deionised water	100 ml	
NaCl	0.0585 g	10 mM
NaOH	0.5405 g	160 mM
HEPES	0.2387 g	10 mM
EDTA	0.0285 g	10 mM
5(6)-CF	1.8789 g	50 mM

Table 2.2. The composition of the 5(6)-CF dye for encapsulation within the nanocapsules.

2.5.2 Stock Solution Preparation

Two different types of lipid stock solutions were prepared. Stock 1 solution consisted of each of the lipid components dissolved in 1mL of Chloroform at a concentration of 0.01mM. The lipid stock 2 solutions were then made using different percentage concentrations of each lipid stock 1 solutions.

Component	Mass (mg)
TCDA	35
DPPC	73
DPPE	69
CHO	39

Table 2.3. Stock 1 solution, in which each component was dissolved in 1mL of chloroform having a final concentration of 0.01 mM for all the components.

Component	Mole Percentage (%)	Mass (mg)	Amount taken from stock solution 1 for 100 µL of stock solution 2 (µL)
TCDA	25	8.75	25
DPPC	53	38.7	53
DPPE	2	1.38	2
CHO	20	7.80	20

Table 2.4. The components were all dissolved in 1mL of Chloroform.

2.5.3 Synthesis and Crosslinking of Lipid Vesicles

Vesicles were composed primarily of phosphocholine (PC) lipids, phosphoethanolamine (PE) lipids, and cholesterol. The vesicle components were stored at -20 °C, and dissolved individually in chloroform to a concentration of 0.1 $moldm^{-3}$, as explained above, and followed by combination together to enable synthesis. The vesicles were synthesized in a similar procedure to that carried out by Nayar, Hope and Cullis reported in 1993. The mixture of 100 µl of each stock 1 solution was added to 200µl of chloroform, followed by drying with nitrogen gas to remove the chloroform. After the mixture was dried the first step of the synthesis was the rehydration of the mixture with 5ml of 50mM [5,6]-carboxyfluorescein, that was heated

to 75 °C, cooled, and freeze-thawed three times. Next step was the extrusion that consisted in the pressurization of the vesicle preparation five times through two 100 nm polycarbonate membranes in the LiposoFast LF 50 extruder, at approximately 60 °C. After the vesicles were sized a purification step was carried on to separate unencapsulated dye vesicles using Sephadex NAP 25 column. The purified vesicles solution was then kept at 4 °C overnight, and crosslinked as last step the next morning using a commercial flood exposure UV source from Hamamatsu™, for cross linking of polymerisable components during 12 seconds at 254nm leading the chemical reaction shown in Figure 2.16. The steps of the synthesis process are depicted in Figure 2.15.

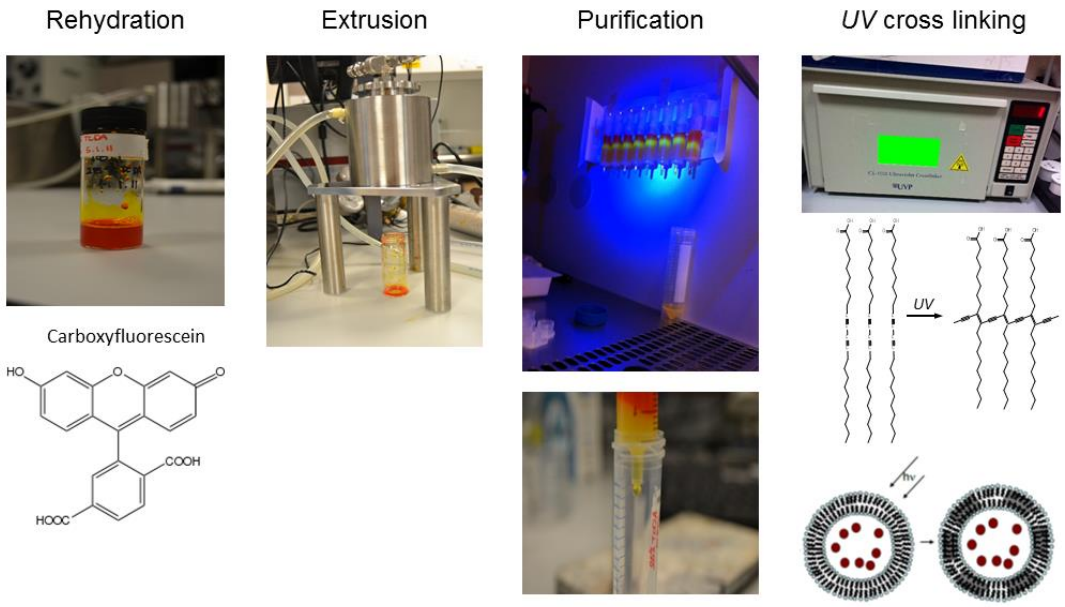

Figure 2.15. Lipid vesicle synthesis stepwise after mixing the components present in Table 2.4.

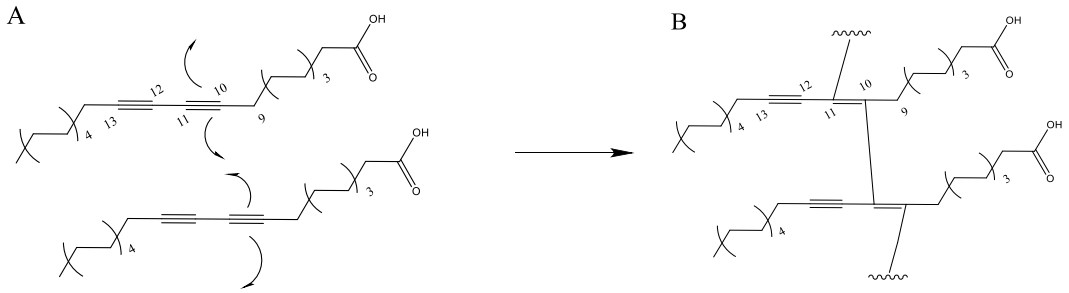

Figure 2.16. Cross linking of TCDA suggested by radical initiated mechanistic reaction. (A) TCDA cross-linking and (B) the cross-linked product found in the vesicle membrane.

2.6 Plasma polymerization

Surface modifications were performed using a cold plasma reactor at low pressure. The reactor is composed of a stainless steel cylindrical vertical chamber (Diameter of 25,5 cm and a height of 41,6 cm). Inside the chamber, there is an aluminium plate which serves as support for placing the chamber. A difference of potential is created inside the reactor chamber, which ionizes the gas and allows for plasma generation. The reactor chamber acts as ground electrode, while the aluminium plate acts as radiofrequency (RF) electrode. The latter is connected to a generator of radiofrequency pulses of 13,56 MHz with an integrated potentiometer. The system is in permanent vacuum (around $6 \cdot 10^{-4}$ mbar) except when the sample is introduced at the reaction chamber. The monomer is introduced inside the reactor at nearly constant pressure around 0,02-0,04 mbar.

Gases and monomers are introduced into the reaction chamber from its top, through stainless steel pipes. The flow can be regulated by a needle valve. The system's pressure can be monitored by a vacuum gauge controller (PDR900, MKS), which is connected to a Cold Cathode/MicroPirani™ vacuum transducer, which is placed inside the reactor.

As a safety measure, in order to avoid that the unreacted monomer reaches the vacuum pump (Trivac D 16BCS/PFPE Leybold, Germany), the reactor has an active carbon chemical trap and a liquid nitrogen or $CO_{2(S)}$/acetone cold trap.

2.7 Statistical analysis

The data was processed and analysed using GraphPad Prism 6. The statistical analysis was performed using a Student t-Test by comparing the means of each independent group (sample type) assuming that the variances of each group are equal. A *p* value of less than 0.05 (95 % confidence limit) was considered to be of significant difference, Equation;

$$S_E = \frac{\sigma\,(V_T)}{\sqrt{(V_c)}} \qquad \text{(Equation 2.3)}$$

Where S_E is the statistical error, σ is the standard deviation, V_T is the cumulative sum of the values, and V_c is the sum of the count of the values. The propagation of combined errors was achieved using, Equation;

$$P_E = \left(\sqrt{\left(\left(\frac{F_E}{F}\right)^2\right)} + \sqrt{\left(\left(\frac{I_E}{I}\right)^2\right)}\,N\right) \qquad \text{(Equation 2.4)}$$

Where P_E is the propagative error, F_E is the final value error, F is the final value, I_E is the initial value error, I is the initial value and N is the new value calculated.

2.8 References

(1) Hwang, S. H.; Lee, I. M.; Yoon, C. S. *Hum. Ecol. Risk Assess. An Int. J.* **2013**, *19*, 1576–1585.

(2) Michael T. Madigan, John M. Martinko, David A. Stahl, D. P. C. *Biology of Microorganism*; 13th editi.; Benjamin Cummings, **2010**; p. 1152.

(3) Sule, P.; Wadhawan, T.; Carr, N. J.; Horne, S. M.; Wolfe, a J.; Prüss, B. M. *Lett. Appl. Microbiol.* **2009**, *49*, 299–304.

(4) Bracco, G.; Holst, B. *Surface science techniques*; **2013**; Vol. 51.

(5) Dixon, M. C. *J. Biomol. Tech.* **2008**, *19*, 151–158.

(6) Gabriel, C.; Gabriel, S.; Corthout, E. *Phys. Med. Biol.* **1996**, *41*, 2231–2249.

(7) Bordi, F.; Cametti, C.; Gili, T. *Bioelectrochemistry* **2001**, *54*, 53–61.

(8) Mcadams, E. T.; Ireland, N. *IEEE Trans. Biomed. Eng.* **1994**, *41*, 498–500.

(9) Olson, W. H. In *Medical instrumentation, application and design*; New York, **1998**; pp. 623–658.

(10) Geddes, L. a. *IEEE Eng. Med. Biol. Mag.* **1996**, *15*, 133–134.

(11) Montero, L.; Baxamusa, S. H.; Borros, S.; Gleason, K. K. *Chem. Mater.* **2009**, *21*, 399–403.

Chapter 3 Quarzt Crystal Microbalance with Dissipation (QCM-D) as label-free technology for real time bacterial monitoring

3.1 Introduction

In the last years, there has been growing interest in the quartz crystal microbalance (QCM) technique, which has played a key role in elucidating various aspects of biological materials and their interactions. As mentioned in the introductory chapter 1, QCM technology is a nano-sensitive technique that utilizes acoustic waves generated by the oscillation of a piezoelectric single crystal quartz plate to measure mass. By applying alternating electric fields to quartz an alternating expansion and contraction of the crystal lattice is induced. QCMs became widely used as mass balances only when experiments were able to relate the frequency change of the oscillating crystal to the mass adsorbed on the surface. This relationship was demonstrated by Sauerbrey in 1959 [1], and explained in chapter 2 (section 2.3.9). There are three requirements that must be fulfilled for the Sauerbrey relationship to hold. First, the adsorbed mass must be small relative to the mass of the quartz crystal; second, the mass adsorbed is rigidly adsorbed; and third, the mass adsorbed is evenly distributed over the active area of the crystal [2]. This frequency/ mass relationship was, in the early days of QCM, almost exclusively used in vacuum or gas phase monitoring of metal plating in vacuum deposition systems. The widespread use of QCMs began when they were shown to be applicable in liquid environments around 1980[3]. Liquid application of QCM technology expanded the number of potential applications dramatically including biotechnology applications and in particular biosensor applications[4] (Figure 3.1A). The drawback of applying the QCM to many liquid applications was that the liquid phase often incorporated viscous and elastic contributions to the frequency change and thus violated the assumption of the Sauerbrey relation stating that the mass adsorbed must be rigidly adsorbed. This is a prompted new approach for characterizing mass deposits with frictional dissipative losses due to their viscoelastic character. Thereupon, the theory for interpreting this new data suffered a modification in the method including dissipation in the equation. Then, QCM with dissipation monitoring (QCM-D) fits the voltage of oscillatory decay after a driving power is switched off in such a way as to ensure that the quartz decays close to the series resonant mode[5,6] (Figure 3.1B). The amplitude decays over time depending on the properties of the oscillator and the contact medium.

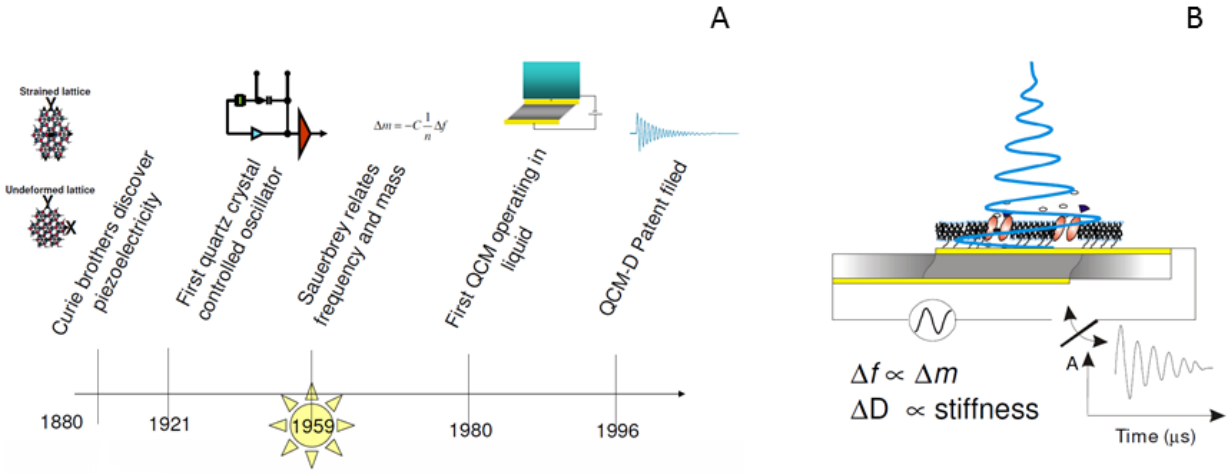

Figure 3.1. Quartz Crystal Microbalance (QCM) Scheme. (A) QCM time line where the evolution of the method conclude with introduction of dissipation and its patent for the commercial equipment from qsense. (B) Representation of the decay curve after the power is switched off, when monitoring dissipation over the sensor. Image acknowledgements to qsense.

The main feature and advantage of QCM-D, compared with the conventional QCM, is the fact that a part from measuring changes in resonant frequency (Δf), a simultaneous parameter related to the energy loss or dissipation (ΔD) of the system is also measured. Δf essentially measures changes in the mass attached to the sensor surface, while ΔD measures properties related to the viscoelastic properties of the layer added onto the sensor surface.

The QCM-D data (Δf and ΔD) allows for probing values at multiple harmonics also known as overtones (n = 3, 5, 7, 9, 11, 13) of a resonant frequency in succession on the millisecond time scale. The multiple harmonic data permits modelling the experimental data with theory to extract meaningful parameters such as mass, thickness, density, viscosity, or storage modulus[7–10]. All of this parameters analyse different depth that decreases when overtone number increases.

Viscoelastic data allows broader characterization of systems that fall outside of the scope of the linear Sauerbrey relationship between Δf and Δm and makes QCM-D more than a simple mass balance. Therefore, monitoring cell adsorption requires using the dissipation parameter to fully characterize the adsorption of a viscoelastic cellular structure.

The theoretical background can be related to a few studies that used QCM to study bacterial adhesion by using the shifts in the resonance frequency (Δf) reporting data for exponentially growing bacteria[11]. Moreover, differences in resonance frequency shifts (Δf) have been observed between bacteria with and without surface appendages[12] as well as differences due to substratum hydrophobicity[13]. However, in cases that exist positive frequency shifts it has been suggested that, dissipation is a better parameter for quantifying bacterial adhesion[14]. This complicates interpretation since positive frequency shifts indicate desorption according to the Sauerbrey equation. The difficult interpretation of QCM-D data on bacterial adhesion to a sensor surface is more confident with additional information on the exact number of bacteria adhering to the sensor surface. For this reason, in this chapter a combination of QCM-D with real-time image analysis of bacterial adhering on the sensor surface has been performed.

After analysing the previous studies that reported QCM-D data it could be established that the typical Frequency and Dissipation responses for protein, vesicle, or cell adsorption are on the order of tens to hundreds of Hz and single to tens ($\times 10^{-6}$) of dissipation units. For viscoelastic films greater than 100-nm thick, these responses are typically an order of magnitude higher.

The final issue that is really an advantage of the QCM-D technique over other methods commercially available for label-free bacterial detection, is the use of continuous flow cultivation of microbial populations in a steady state of constant active growth. By continually substituting a fraction of a bacterial culture with sterile nutrients, the continuous culture device, presents a near-constant environment ideal for controlled studies of microbes and microbial communities. It eliminates the artificial lag and stationary growth phase phenomena characteristic for static culture systems. As mentioned in chapter 1, the continuous flow devices serve as a model of a simple container where biofilms grow using the available nutrients constantly pumped in. The microfluidic devices ascertain the reproducibility of data and offer a possibility of studying one or a few environmental factors at a time with the aim of reconstructing more complex naturally occurring systems from known elements, being used as a laboratory model of the bacterial biofilm infection.

In summary this chapter presents a theoretical description of a commercial microfluidic device to prove the label-free detection of bacterial biofilm under flow conditions. For this reason different parameters are tested to find the optimal conditions of continuous flow experiments.

3.2 Results

As mentioned before, the optimization of the conditions applied to QCM-D technique are subjected to work in a steady state in a microfluidic device (see Figure 3.2) that only monitor biological changes caused by the bacterial activity. The attachment and development of biofilms on uncoated gold QCM-D sensors was tested at different flow rate, temperature, bacterial strain and glucose concentration on the Tryptic Soy Broth (TSB) medium. These parameters might also affect the relation between EPS development and the viscoelastic properties[8]. The viscoelasticity of the Extracellular polymeric substances (EPS) generated by the biofilm is caused by changes in porosity, density, water content, adsorption properties, charge, hydrophobicity, and mechanical stability[15].

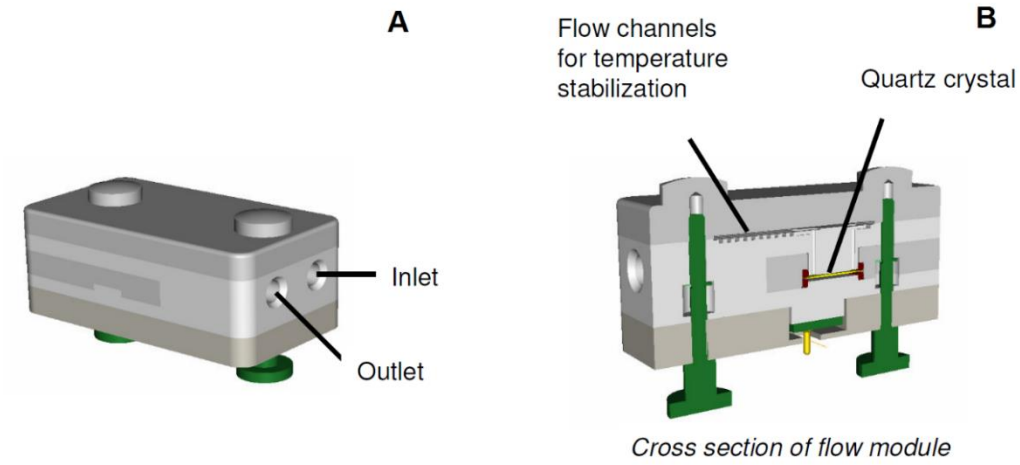

Figure 3.2. Flow module of the QCM-D. (A) The assembly of the flow chamber. (B) Cross section of flow module where the sensor is placed under the inlet and outlet channels.

To evaluate the influence of this parameters we have established a basic protocol depicted in Figure 3.3. First, a baseline is acquired by flowing through the chamber MiliQ water (A). Once both the frequency and dissipation remain constant the bacterial solution, with an optical density of 0.084, is introduced into the flow chamber provoking a decrease in frequency. This can be appreciated as the bacteria starts to interact with the sensor surface (B). As it can be seen, the interaction also leads to an increase of dissipation, as the biofilm layer being developed is softer than the sensor surface. After the process of biofilm formation was monitored for 22 hours, a wash with MiliQ water was achieved in order to eliminate the remaining unbound bacteria (C). This last step was expected to cause the detachment of bacteria not properly attached to the substrate, reflected by an increase in frequency and a decrease in dissipation signal.

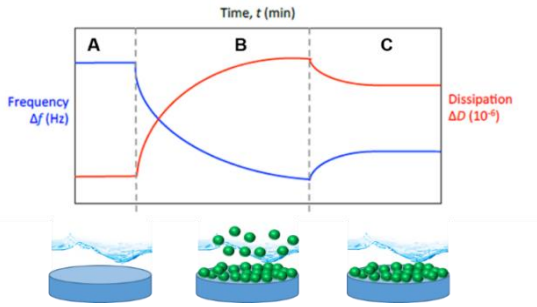

Figure 3.3. Frequency and dissipation profiles observed for the standard protocol used in this study[16]. Initial baseline of MiliQ water (A), followed by bacterial seeding and fresh TSB medium (B) for 2 and 20 hours, respectively (B), Finally MiliQ water was pumped in again to detach the non-adhering bacteria (C).

The experimental work carried out to evaluate the influence of temperature, flow rate, bacterial strain and glucose was applied in the order depicted in Figure 3.4. First a positive biofilm bacterial strain of *Staphylococcus* aureus was utilized to evaluate three different temperatures (20, 27 and 37 ºC). Then 27 ºC was the first temperature showing a substantial decrease in frequency shift and then a three flow rate test (50, 100, 200 µL/min) was carried out. After that, from the higher and physiological temperature (37 ºC) a third parameter was taken into account to evaluate a possible different profile between two different bacterial strains. This comparison studied two strains of *Staphylococcus aureus*, one of them was a non-infective (CETC 239) and the other one was the mentioned infective strain (V329), which provokes mastitis bovine[17] being associated to a biofilm formation. As long as *S. aureus* V329 is the bacterial strain that is going to be used in future chapters, also the final evaluation of glucose concentration (0, 0.25, 0.5 %) dissolved in TSB medium was performed with this strain at a flow rate of 50 µL/min and 37 ºC.

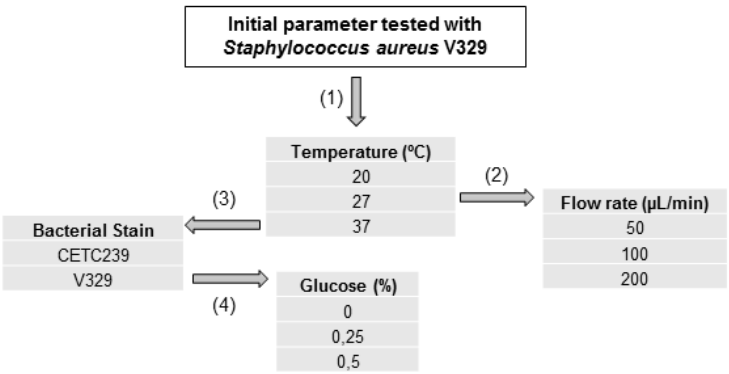

Figure 3.4. Routing slip scheme of the parameters tested with the QCMD equipment**.** The order of the different experimental conditions tested is shown from top to the bottom following the number next to the arrows.

The initial test with the QCM-D equipment was based on the protocol proposed by Schofield *et al* in 2007[18] for growing biofilm in the QCMD flow module. The conditions reported in that study were at 20 ºC and a flow rate of 50 µL/min.

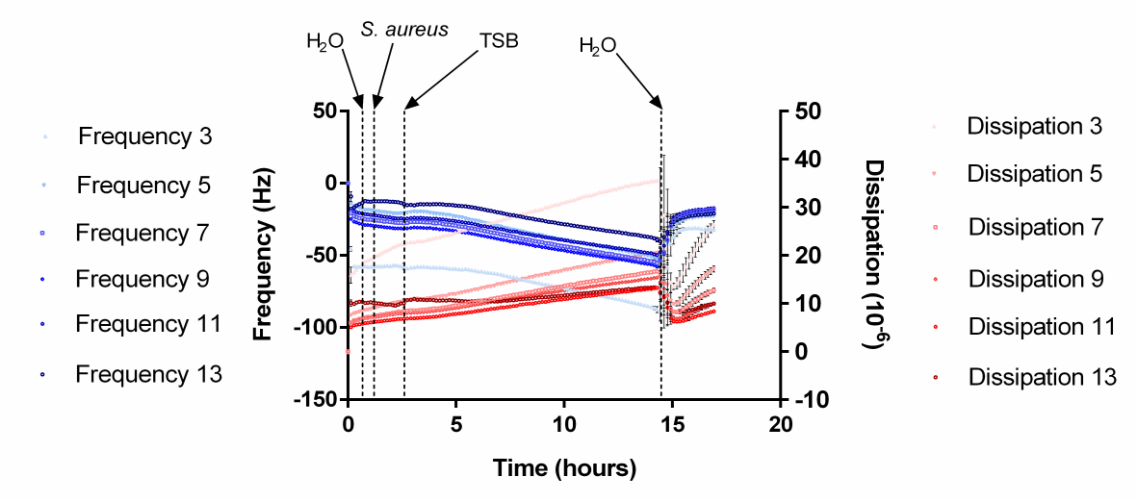

Figure 3.5. Time course of the Frequency and Dissipations shifts (mean±std, n=3) performed with QCM-D for detecting *Staphylococcus aureus* V329 biofilm development at 20ºC onto gold sensor.

The initial temperature proposed of 20 ºC was tested showing 50 Hz of Frequency shift and a very low increase of dissipation, except the third overtone, which is the lowest and represent the closest layer sensed on the sensor. It could be caused by a very thin layer of bacteria attached on the sensor but a poor growth of bacteria was observed subsequently. In parallel to the bacterial growth being monitored with QCM-D a continuous image of the attachment was captured with the microscopy technique described in section 2.3.1 and depicted in Figure 3.6.

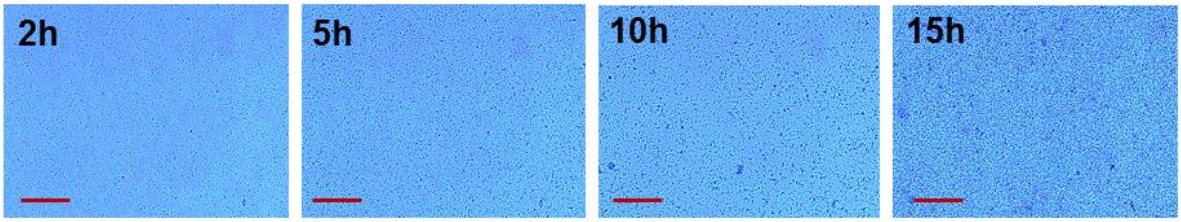

Figure 3.6. Optical microscope images showing bacterial growth on the surface of the QCM-D sensor. Continuous flow experiment at 20 ºC with *Staphylococcus aureus* V329. Images were taken at 2, 5, 10 15 hours during the bacterial growth in the flow module. Scale bar: 200 µm.

When the initial experiment was analysed, a subsequent experiment at 27 ºC was performed with the initial flow rate performed of 50 µL/min. With the temperature (27 ºC) fixed, the flow rate was the condition modified from 50 to 100 and 200 µL/min. This increment of flow rate with *Staphylococcus aureus* V329 was performed with these values because presumably they created a very similar laminar flow and no differences were going to be expected.

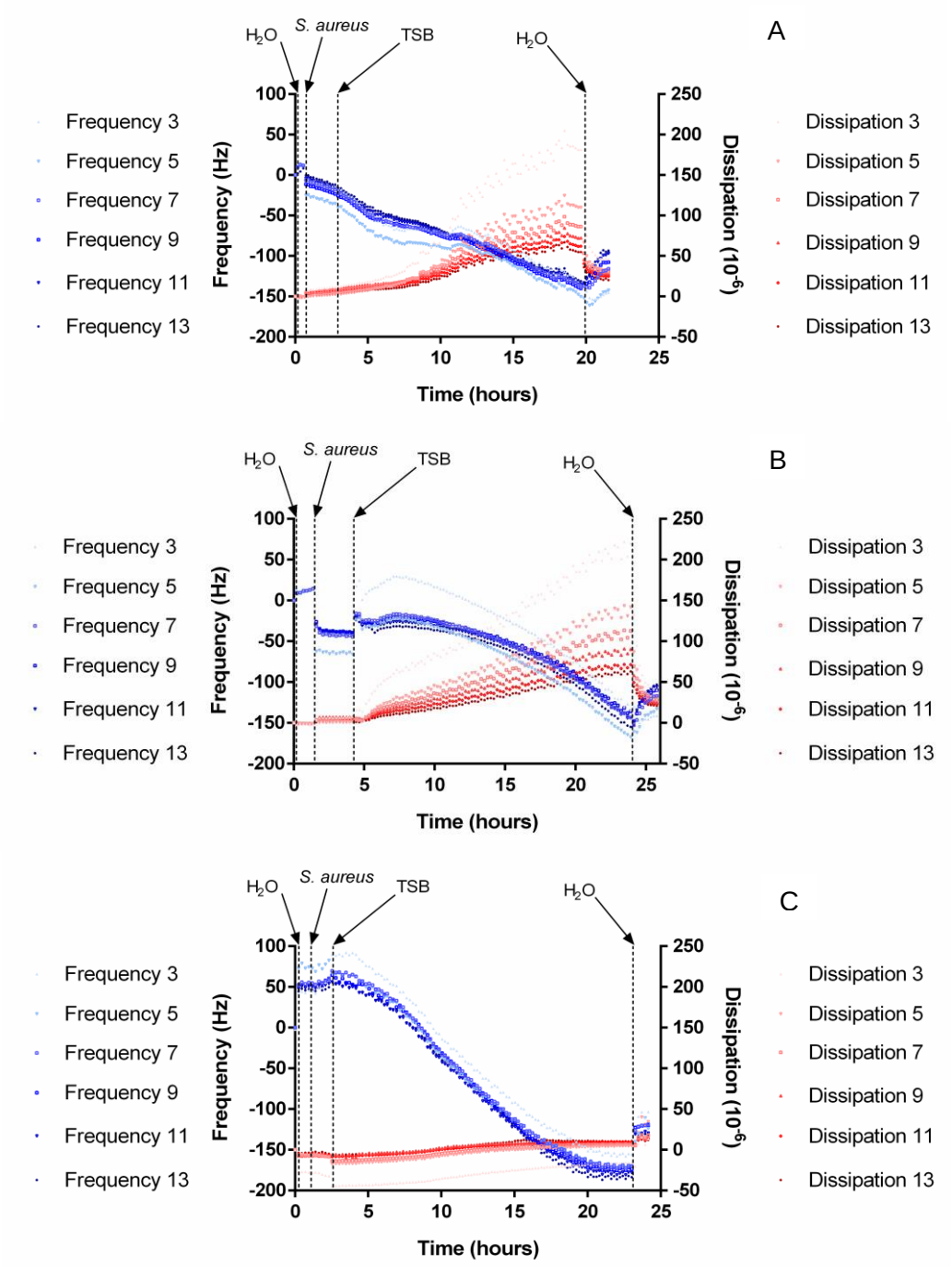

Figure 3.7. QCM-D measurement detecting *Staphylococcus aureus* V329 biofilm development at 27ºC. Three different flow rates were tested with values of 50 (A), 100 (B), 200 (C) µL/min.

As it can be observed in Figure 3.7 the increase of flow rate applied to independent continuous flow experiments, monitored in the flow module of the QCM-D (Figure 3.2), showed a shift in frequency with very similar values in all the overtones measured by the QCM-D equipment. This indicates an increase of mass over the sensor surface which is higher than the previous experiments which, can be associated with higher degree of bacterial attachment and development. The dissipation shifts observed in 50 and 100 µL/min were very similar with an almost equal profile, especially in the lowest overtone (number 3) that showed a higher increase. Although the profile of the 50 and 100 µL/min was very similar, the trend in the third flow rate only presented similarities only in the frequency shifts but no with dissipation. For this reason microscopic observations of all flow rates tested was necessary. The optical comparison between them was depicted in Figure 3.8 where almost no differences could be observed. The final MiliQ water wash altered slightly the frequency shift indicating that the amount of adsorbed bacteria almost remained intact, but not 100% attached. This fact reflected the existence of specific interactions between the bacterial monolayer with the substrate, the gold sensor in this case.

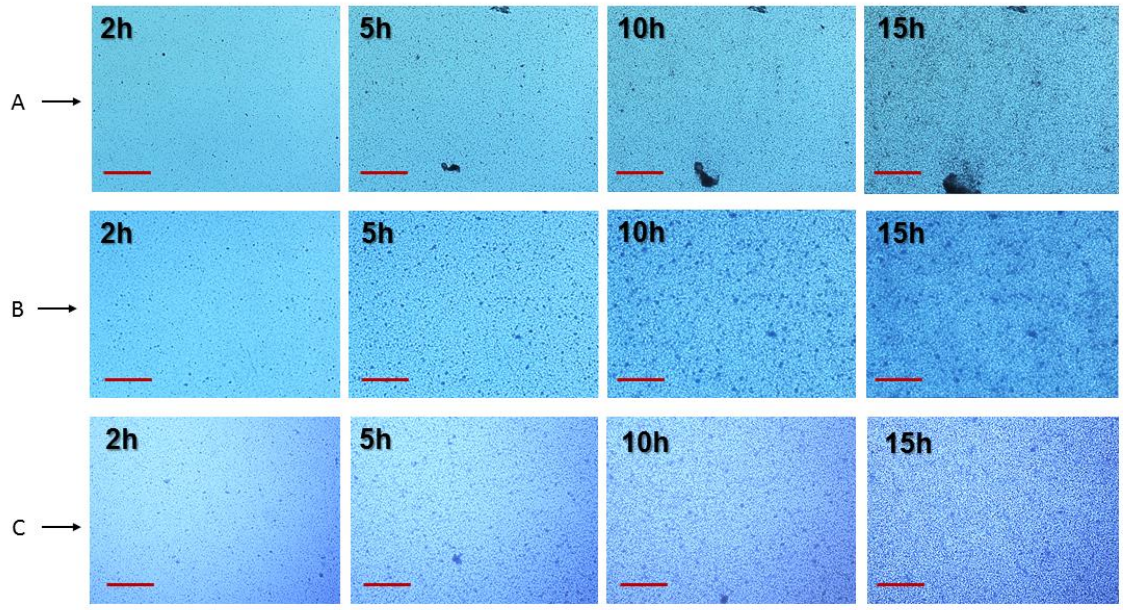

Figure 3.8. Optical microscope images showing bacterial growth on the surface of the QCM-D sensor during the continuous flow experiment at 27 ºC with *Staphylococcus aureus* V329. Three different flow rates were tested with values of 50 (A), 100 (B), 200 (C) µL/min. The times acquired during the real-time experiments for each different flow rate applied were 2, 5, 10, 15 hours. Scale bar: 200 µm.

The third evaluation with the QCM-D technology was the comparison of two different strains of *Staphylococcus aureus* in order to form biofilms. This evaluation compared a non-infective bacterial strain with an infective one to determine if the technique is sensitive to changes in their growth at the same conditions. This experiment was performed at physiological temperature (37 ºC), and the flow rate for this case was the lowest of the previous test (50 µL/min), chosen to minimize the amount of necessary TSB medium. The QCM-D data was acquired and shown in Figure 3.9.

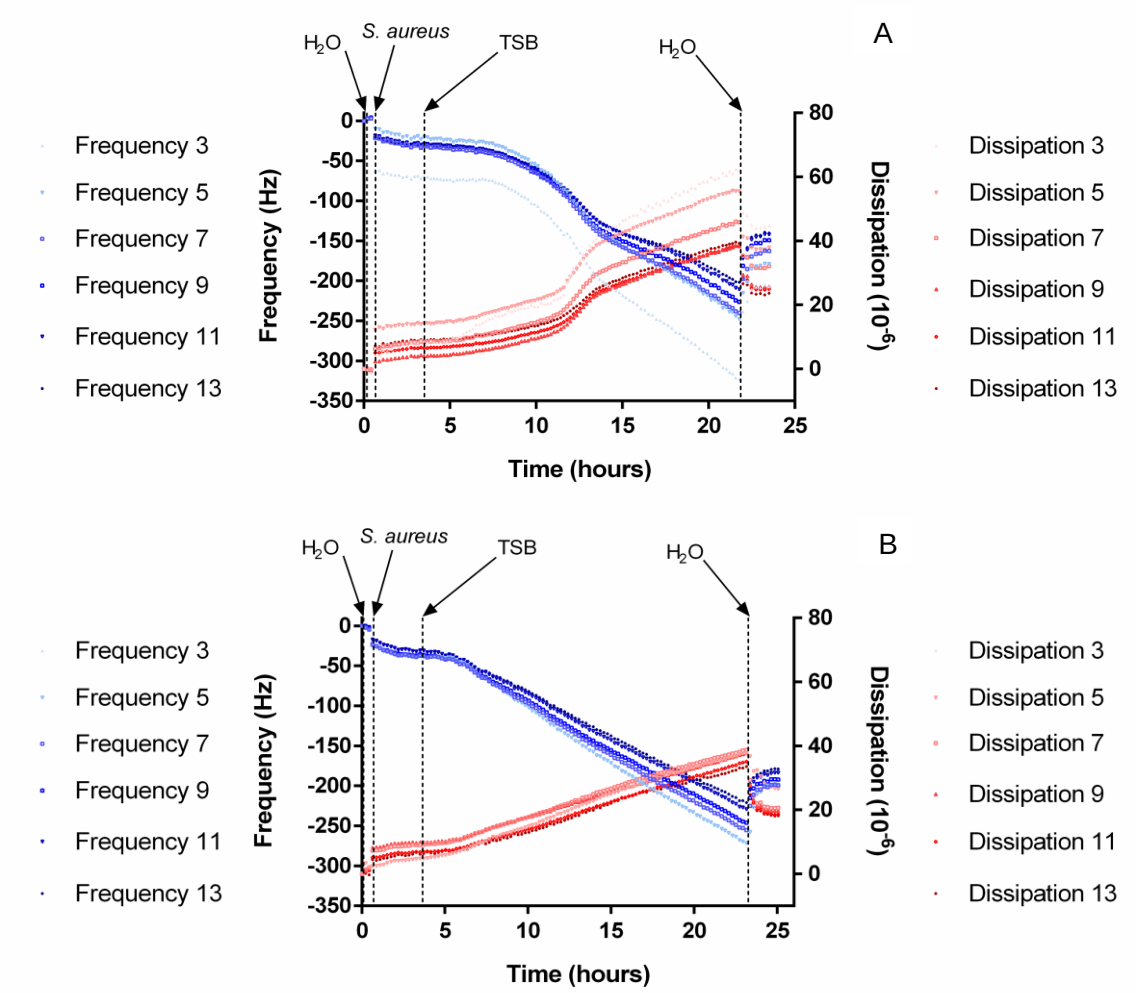

Figure 3.9. QCM-D measurement detecting *Staphylococcus aureus* V329 (A) and CETC239 (B). The biofilm development was monitored at 37ºC with a flow rate of 50 µL/min.

Interestingly, a similar tendencies was observed in both strains tested in this particular case. Furthermore slope and values of Frequency and Dissipations shifts for all the overtones analysed presented similar profile as well. In parallel microscopic observation was needed to point out some differences in the experiments.

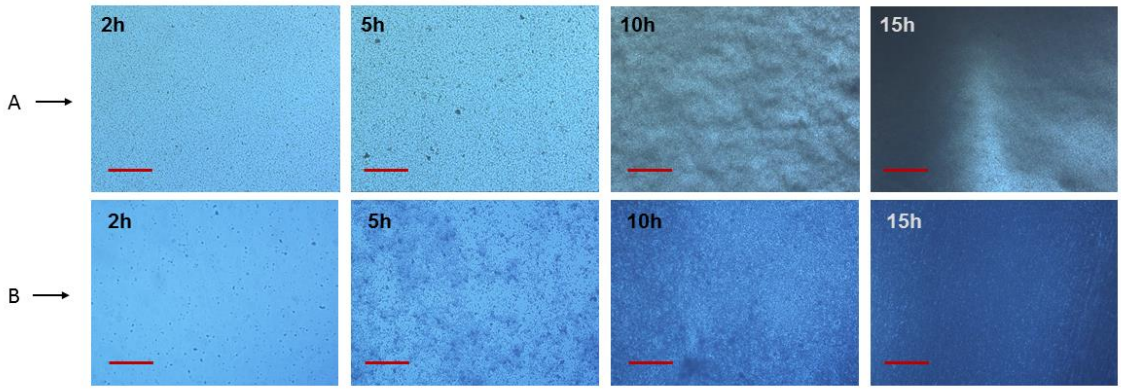

Figure 3.10. Optical microscope images showing bacterial growth on the surface of the QCM-D sensor. Continuous flow experiment at 37 ºC with *Staphylococcus aureus* V329 (A) and CETC239 (B). The times acquired during the real-time experiments were 2, 5, 10, 15 hours. Scale bar: 200 µm.

In accordance with further microscopic observations, the results indicated that bacterial biofilm formed over the QCM-D sensor was very similar for both bacterial strains, but slightly more attached for *Staphylococcus aureus* V329 that presented a more organized structure after 10 hours of constant feeding of TSB medium. Comparing Figure 3.10A (*S. aureus* V329) with the previous bacterial structures grown at 20 and 27 ºC it can be clearly appreciated how the variation in temperature induced changes in bacterial attachment, especially in later stages. Then, the variation in temperature changed not only the structure observed by microscopy but also both measured signals, frequency and dissipation.

The final parameter tested in this part of the thesis was the glucose concentration fixing the conditions already chosen up to this point (*Staphylococcus aureus* V329, 37 ºC and 50µL/min). In general, the presence of glucose represses the agr system, already described in the introductory chapter, through the generation of low pH[19]. However, biofilm development occurs in physiologic glucose-supplemented medium (1g/L), corresponding to normal blood glucose levels[20]. Glucose is a component that must be studied because biofilm formation often occurs on medical devices, like catheters and heart valves, which are in direct contact with normal (floating) blood. The QCM-D data and microscopy evaluation of the three glucose concentrations were shown in Figure 3.11 and Figure 3.12 respectively.

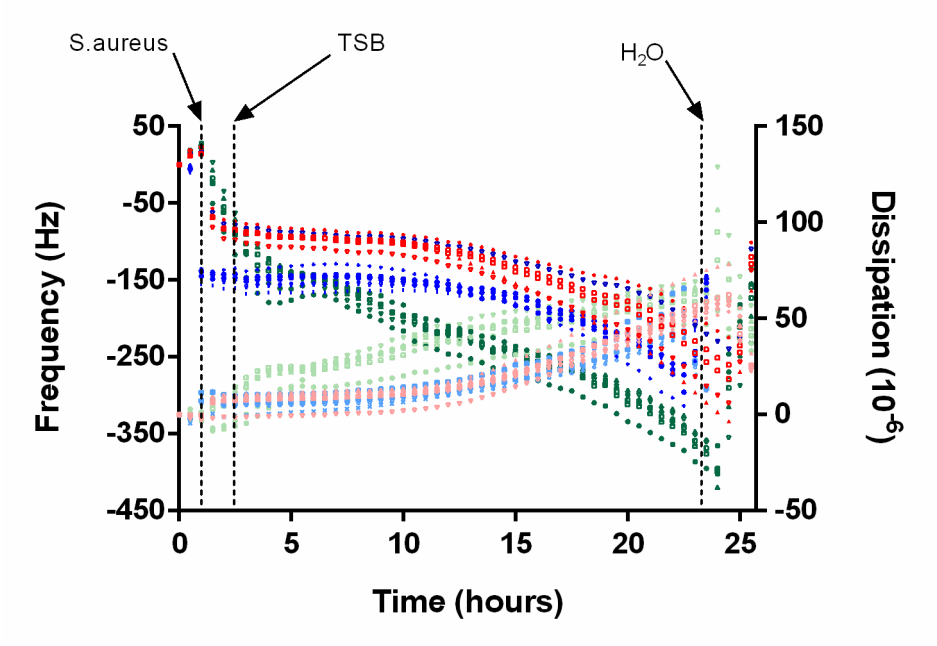

Figure 3.11. QCM-D measurement detecting *Staphylococcus aureus* V329 biofilm development at 37ºC. Three different glucose concentration were tested with values of 0 % (Red), 0.25 % (Blue), 0.5 % (Green).

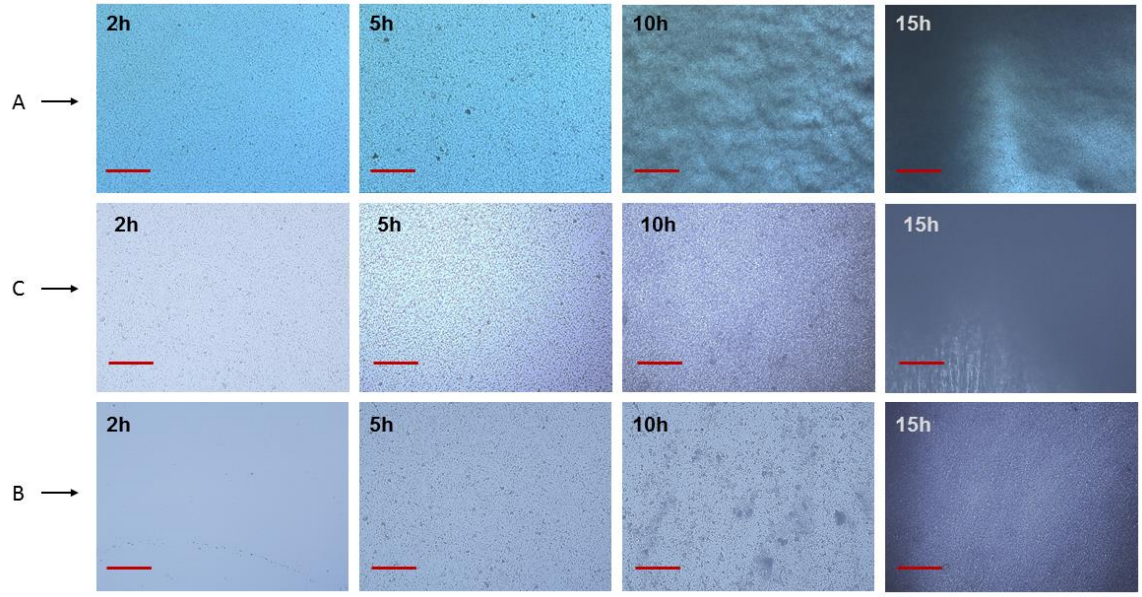

Figure 3.12. Optical microscope images showing bacterial growth on the surface of the QCM-D sensor. Continuous flow experiment at 37 ºC with *Staphylococcus aureus* V329. Three different glucose concentrations were tested with values of 0 (A), 0.25 (B), 0.5 (C) %. The times acquired during the real-time experiments for each different glucose concentration applied were 2, 5, 10, 15 hours. Scale bar: 200 µm.

The simultaneous measurements of the change in frequency (Δf) and dissipation (ΔD) were in this particular case of glucose concentration almost identical in the three cases. The biofilm development over the gold sensor described the decrease in frequency and increase in dissipation energy. The frequency shift values were very similar in these cases as the presented before in the bacterial strain comparison were no glucose was included. Moreover, the microscopy images showed a bacterial attachment and biofilm development along the vast majority of the surface imaged at late stages of the flow experiment (15h). Although the QCM-D data was very similar in all the cases, the microscopy showed an early attachment and structuration of the biofilm as long as glucose concentration was decreased, which made sense with the fact already mentioned of agr system repression in presence of glucose[19].

After analysing the QCM-D data in concordance with microscopy images, the change in viscoelastic properties of the adsorbed layer that takes place over the sensor must be also evaluated for each parameter studied in this chapter. A method to evaluate this viscoelastic properties of an attached bacterial layer consists in plotting the variation of the dissipation *versus* the frequency shift. The influence bacterial attachment on the viscoelastic damping of the crystals resonance can be appreciated, allowing to infer viscoelastic properties of the adsorbed layer[21]. In previous reported studies only frequency and dissipation was taken into account, and time was eliminated because it was considered an explicit parameter, therefore a direct comparison between the energy dissipation (ΔD) per unit mass attached to the surface (Δf) was represented[22]. Although, this ΔD over ΔF shows the induced energy dissipation per coupled unit mass, making it possible to analyse the effects of the extracellular polymeric substance (EPS) synthesis, and therefore the characterization of cell adhesion independently of position on the crystal surface[23], Fatisson *et all* in 2011[24] showed a more complex representation displaying Dissipation, Frequency and time, also known as Df-t plot. This representation of three parameter in a 3D plot is able to provide relevant insight regarding the specific signature of every condition analysed. The specific signature can be overlapped to a compared condition and assess the viscoelasticity. The results analysed with Df-t plot were organized according the evaluations carried out up to this point. Then, four Df-t plots represented the four conditions analysed (temperature, flow rate, strain and glucose concentration) and displayed in Table 3.1. This table showed the conditions fixed and the condition under evaluation organized in four columns, which represent the four Df-t plots depicted in Figure 3.13.

Fixed conditions →	V329	50 µL/min	V329	27 °C	50 µL/min	37 °C	V329	50 µL/min	37 °C
Variable condition →	**Temperature °C**		**Flow rate (µL/min)**		**Glucose concentration (%)**			**Bacterial Strain**	
	20		50		0			*S.aureus* V329	
	27		100		0.25			*S.aureus* CETC239	
	37		200		0.5			-	
	↑ **Df-t plot A**		↑ **Df-t plot B**		↑ **Df-t plot C**			↑ **Df-t plot D**	

Table 3.1. Parameters analysed in frequency and dissipation shifts, with fixed conditions to evaluate the influence of the variable condition. The viscoelastic evaluation of the variable condition was carried out by representing Df-t plots for each parameter in Figure 3.13.

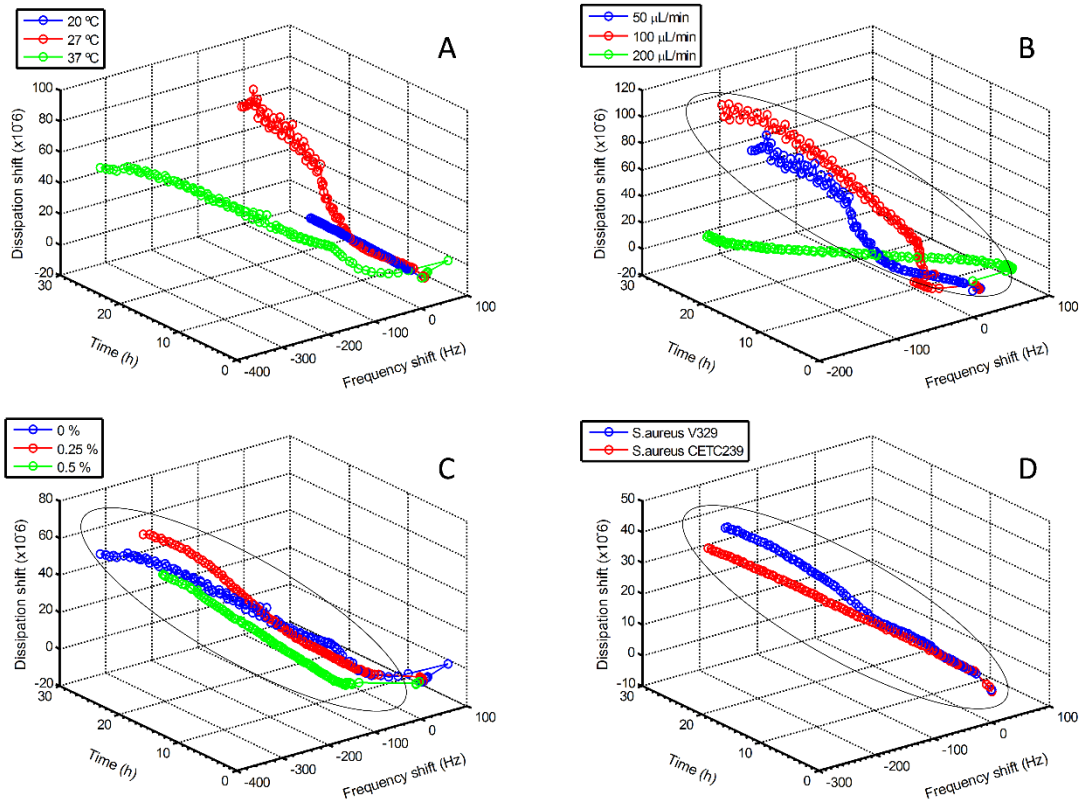

Figure 3.13. Plot of the seventh overtone dissipation, as a function of corresponding frequency and time, measured for bacterial layer developed on the QCM-D sensor. The parameters under evaluation were: Temperature (A), Flow rate (B), Glucose concentration (C) and Bacterial strain (D).

Before analysing Figure 3.13 was important to point out that in the previous QCM-D results analysed in this chapter all the overtones were showed to provide information about the homogeneity of the surface layer, as the detection range from the crystal surface decreases with increasing overtone number. Thus, differences in frequency behaviour of the different overtones suggest vertical variations in bacterial layer properties. However, in order to avoid excessive fluctuations due to environmental factors or the crystal sensor itself all the calculations shown with Df-t plots were performed using the seventh overtone, which correspond the one located in the middle of the overtone set.

As said before, the relation between the dissipation and the frequency signal can be used to analyse the viscoelastic properties of an adsorbed layer. Moreover, the representation of ΔD over Δf and time (Df-t plot) reflects qualitatively the amount of water trapped within the biofilm, which is an indicator of film viscoelasticity. This feature could be also attributed to cell spreading, caused by the formation of the EPS leading a progressive increase of viscoelastic mass (owing to high hydration state of cells) on the sensor surface.

The results obtained by this methodology involved plotting the variation of dissipation factor along with frequency as a function of time, showed reliable information about glucose concentration and bacterial strain, with no viscoelastic difference (Figure 3.13C and D). The Df–t plots obtained for different flow rates applied (Figure 3.13B) were performed to confirm that working in a streamline flow also known laminar flow, did not affect the bacterial attachment and subsequent biofilm development, however the highest value (200 µL/min) showed a different profile respect to lower flow rates. This different profile observed between 50 and 100 µL/min (ellipse Figure 3.13B) respect to 200 µL/min, interestingly showed no difference in frequency shift (biomass through Sauerbrey relationship) either microscopy images (Figure 3.8), that were similar in the three cases. Therefore the difference in this particular case could be owed to the effect of flow itself when the damping process begins, avoiding and optimal detection of dissipation shift when the flow is increased.

Finally, the method was shown to be applicable for sensing different temperatures that showed a displacement on the profile observed in Figure 3.13A. This suggests that the working temperature must be unaltered when ‘specific interactions’ with the surface are involved.

3.3 Discussion

Quartz crystal microbalance with dissipation (QCM-D) is an acoustic technique which measures both the amount and the viscoelastic properties of an adhering mass on an oscillating quartz-crystal sensor surface, in terms of shifts in the resonance frequency (Δf) and in dissipation (ΔD). The measurements analysed during this chapter showed an increase in dissipation along with a decrease in frequency indicating an enhancement of viscoelastic mass at the sensor interface. The increase in viscoelastic behaviour of the surface can be correlated with the interaction of bacteria with the surface of sensor as a result of surface protein interaction (see Figure 1.2). More specifically the EPS that are the components that play the major role in the cohesion of the biofilm layers developing on the QCMD sensors. Furthermore EPS are also in charge of biofilms viscoelastic properties which in turn, can strongly affect the microbial clusters and external biofilm layer that increase resistance to shear (refer to Chapter1).

In this study, it was observed and monitored how biofilm formation is strongly influenced by EPS cohesion and viscoelastic properties. The change of this properties produced differences of the EPS that could be also observed in the QCMD window module (Figure 2.10). Different EPS originated from biofilms at different flow rates with at constant temperature of 27 ºC showed similar adherence and viscoelastic properties that were correlated to the EPS composition and to adherence rate of the biofilm, also observed by real-time microscopy monitoring. After that it was intriguing to see if the platform could be sensitive to see if EPS adherence and viscoelasticity changed in correlation to different bacterial strains, promoting differences in biofilm development. As it was observed in the results no substantial differences were found. Temperature was also tested to detect changes of biofilms grown under constant flow conditions. This parameter exhibited some difference in the QCM-D data, showing a higher decrease of frequency shifts indicating more biopolymer layers created on the surface. Finally the addition of glucose was tested at 27 ºC in the presence of *Staphylococcus aureus* V329, the strain tested with the platform designed and optimized in the following chapters, did not show a significant difference in the biofilm development profile.

As mentioned before, an important issue of this technology applied to biological applications is that dissipation can extract viscoelastic parameters that are critical, to avoid underestimated calculations of adsorbed mass of cells. The shear wave of the oscillating quartz is dampened out before even reaching the middle of the cell in the simple QCM frequency[2]. Furthermore, the spatial distribution of cells on the quartz

sensor surface might affect the reproducibility between measurements[22]. However, the lateral sensitivity of Δf and ΔD is the same[5], for this reason plotting the *Df-t* plots represented at the end of the chapter were useful for giving a qualitatively independent information of the cell spatial distribution, therefore the effect of irreproducibility between each measurement was attenuated. The 3D plots representing frequency, dissipation and time, showed the similarities (ellipses of Figure 3.13) and differences of the parameters studied estimating the viscoelasticity, and these differences could be attributed to an increase EPS production of the bacterial culture.

3.4 Final Remarks

The technology has reached a point where commercially available instruments exist as well as associated theoretical models required for interpreting data in terms of meaningful physical parameters such as mass, thickness, density, viscosity, or storage modulus.

These achievements, plus the various publications using QCM-D, of which only a small number are described in the chapter, help to lay the groundwork for the QCM-D technology transitioning into a standardized approach for addressing questions about biological materials and their interactions, which are going to be more studied in chapter 7.

Since it would be hard to point out how a combination of the parameters tested may influence the properties of the attachment and accumulation of biofilm on the surface, the analysis of viscoelasticity represented in the *Df-t* plots helped to relate between EPS properties and biofilm development.

In summary in this chapter it is demonstrated the ability of QCM-D technique to monitor the bacterial growth onto gold surface, aiming to gain a little insight about label-free technique combined with microfluidics. Furthermore the working conditions stablished in this chapter are going to be useful to apply on the custom-made platform designed and tested in the following chapters. These conditions were 50 µL/min of flow rate, 37 ºC, no glucose concentration on *Staphylococcus aureus* V329.

3.5 References

(1) Sauerbrey, G. Verwendung von Schwingquarzen Zur Wagungdiinner Schichten Und Zur Mikrowagung. *Zeitschrift fur Phys.* **1959**, *155*, 206–222.

(2) Dixon, M. C. Quartz Crystal Microbalance with Dissipation Monitoring: Enabling Real-Time Characterization of Biological Materials and Their Interactions. *J. Biomol. Tech.* **2008**, *19*, 151–8.

(3) Konash, P. L.; Bastiaans, G. J. Piezoelectric Crystals as Detectors in Liquid Chromatography. *Anal. Chem.* **1980**, *52*, 1929–1931.

(4) Janshoff, A.; Galla, H. J.; Steinem, C. Piezoelectric Mass-Sensing Devices as Biosensors - An Alternative to Optical Biosensors? *Angew. Chemie - Int. Ed.* **2000**, *39*, 4004–4032.

(5) Rodahl, M.; Kasemo, B. A Simple Setup to Simultaneously Measure the Resonant Frequency and the Absolute Dissipation Factor of a Quartz Crystal Microbalance. *Rev. Sci. Instrum.* **1996**, *67*, 3238.

(6) Vogt, B. D.; Lin, E. K.; Wu, W.; White, C. C. Effect of Film Thickness on the Validity of the Sauerbrey Equation for Hydrated Polyelectrolyte Films. *J. Phys. Chem.* **2004**, *108*, 12685–12690.

(7) Rodahl, M.; Höök, F.; Fredriksson, C.; Keller, C. a; Krozer, a; Brzezinski, P.; Voinova, M.; Kasemo, B. Simultaneous Frequency and Dissipation Factor QCM Measurements of Biomolecular Adsorption and Cell Adhesion. *Faraday Discuss.* **1997**, 229–246.

(8) Sweity, A.; Ying, W.; Ali-Shtayeh, M. S.; Yang, F.; Bick, A.; Oron, G.; Herzberg, M. Relation between EPS Adherence, Viscoelastic Properties, and MBR Operation: Biofouling Study with QCM-D. *Water Res.* **2011**, *45*, 6430–6440.

(9) Ying, W.; Yang, F. E. I.; Bick, A.; Oron, G. Extracellular Polymeric Substances (EPS) in a Hybrid Growth Membrane Bioreactor (HG-MBR): Viscoelastic and Adherence Characteristics. *Environ. Sci. Technol.* **2010**, *44*, 8636–8643.

(10) Höök, F.; Kasemo, B.; Nylander, T.; Fant, C.; Sott, K.; Elwing, H. Variations in Coupled Water, Viscoelastic Properties, and Film Thickness of a Mefp-1 Protein Film during Adsorption and Cross-Linking: A Quartz Crystal Microbalance with Dissipation Monitoring, Ellipsometry, and Surface Plasmon Resonance Study. *Anal. Chem.* **2001**, *73*, 5796–804.

(11) Olofsson, A.; Hermansson, M.; Elwing, H. Use of a Quartz Crystal Microbalance To Investigate the Antiadhesive Potential of N Use of a Quartz Crystal Microbalance To Investigate the Antiadhesive Potential of N-Acetyl- L -Cysteine. *Appl. Environ. Microbiol.* **2005**, *71*, 2705–2712.

(12) Olsson, A. L. J.; Van Der Mei, H. C.; Busscher, H. J.; Sharma, P. K. Influence of Cell Surface Appendages on the Bacterium-Substratum Interface Measured Real-Time Using QCM-D. *Langmuir* **2009**, *25*, 1627–1632.

(13) Otto, K.; Hermansson, M. Inactivation of ompX Causes Increased Interactions of Type 1 Fimbriated Escherichia Coli with Abiotic Surfaces. *J. Bacteriol.* **2004**, *186*, 226–234.

(14) Poitras, C.; Tufenkji, N. A QCM-D-Based Biosensor for E. Coli O157:H7 Highlighting the Relevance of the Dissipation Slope as a Transduction Signal. *Biosens. Bioelectron.* **2009**, *24*, 2137–2142.

(15) Jiao, Y.; Cody, G. D.; Harding, A. K.; Wilmes, P.; Schrenk, M.; Wheeler, K. E.; Banfield, J. F.; Thelen, M. P. Characterization of Extracellular Polymeric Substances from Acidophilic Microbial Biofilms. *Appl. Environ. Microbiol.* **2010**, *76*, 2916–2922.

(16) Cifuentes, Anna., de Pablo, Ana., Ramos-Pérez, Victor., Borrós, S. Tailoring Carbon Nanotubes Properties for Gene Delivery Applications. *Plasma Process. Polym.* **2013**, *11*, 704–713.

(17) Tormo, M. A.; Ubeda, C.; Martí, M.; Maiques, E.; Cucarella, C.; Valle, J.; Foster, T. J.; Lasa, I.; Penadés, J. R. Phase-Variable Expression of the Biofilm-Associated Protein (Bap) in Staphylococcus Aureus. *Microbiology* **2007**, *153*, 1702–10.

(18) Schofield, A. L.; Rudd, T. R.; Martin, D. S.; Fernig, D. G.; Edwards, C. Real-Time Monitoring of the Development and Stability of Biofilms of Streptococcus Mutans Using the Quartz Crystal Microbalance with Dissipation Monitoring. *Biosens. Bioelectron.* **2007**, *23*, 407–13.

(19) Regassa, L. B.; Novick, R. P.; Betley, M. J. Expression of the Accessory Gene Regulator Glucose and Nonmaintained pH Decrease Expression of the Accessory Gene Regulator (agr) in Staphylococcus Aureus. *Infect. Immun.* **1992**, *60*, 3381–3388.

(20) Croes, S.; Deurenberg, R. H.; Boumans, M.-L. L.; Beisser, P. S.; Neef, C.; Stobberingh, E. E. Staphylococcus Aureus Biofilm Formation at the Physiologic Glucose Concentration Depends on the S. Aureus Lineage. *BMC Microbiol.* **2009**, *9*, 229.

(21) Feiler, A. a.; Sahlholm, A.; Sandberg, T.; Caldwell, K. D. Adsorption and Viscoelastic Properties of Fractionated Mucin (BSM) and Bovine Serum Albumin (BSA) Studied with Quartz Crystal Microbalance (QCM-D). *J. Colloid Interface Sci.* **2007**, *315*, 475–481.

(22) Fredriksson, C.; Khilman, S.; Kasemo, B.; Steel, D. M. In Vitro Real-Time Characterization of Cell Attachment and Spreading. *J. Mater. Sci. Mater. Med.* **1998**, *9*, 785–788.

(23) Fredriksson, C.; Kihlman, S.; Rodahl, M.; Kasemo, B. The Piezoelectric Quartz Crystal Mass and Dissipation Sensor: A Means of Studying Cell Adhesion. *Langmuir* **1998**, *14*, 248–251.

(24) Fatisson, J.; Mansouri, S.; Yacoub, D.; Merhi, Y.; Tabrizian, M. Determination of Surface-Induced Platelet Activation by Applying Time-Dependency Dissipation Factor versus Frequency Using Quartz Crystal Microbalance with Dissipation. *J. R. Soc. Interface* **2011**, *8*, 988–997.

Chapter 4 Platform Design and Fabrication

4.1 Introduction

In the previous chapter it was described the validation of flow conditions for biofilm formation and development. Once the flow was validated with the QCMD, as described in chapter 3, we propose a device with Electrical Impedance Spectroscopy (EIS) as different label-free technology, with continuous flow of culture media during the biofilm development. The design of this platform is described in this chapter to carry out the desired dimensions, and for an optimal fabrication of the EIS device. For this reason a brief explanation of microfluidics devices is necessary before design and fabrication of the real platform utilized.

In the last two decades there has been a growing interest in design, development and utilization of microfluidic devices for many applications[1,2] (Table 4.1). These devices can emulate biological phenomena that occur in different geometries, fluid dynamics and temperatures closed to physiological microenvironments. While most research efforts in microfluidics to date have focused on eukaryotic cells, they are expected to play an important role in advanced microbiology, due to local control of microenvironments around the microbial cultures and for providing reproducible and identical conditions for biofilms[3,4] found *in vivo*. The creation of these tailor-made microfluidic devices for research applications have been a reality since in 1998 a set of manufacturing techniques were developed to allow the creation of micro-structures in a simple and highly reproducible manner[1,2]. Moreover, there has been even more potential with the introduction of Computer-Aided Design (CAD) software to feed manufacturing techniques such as soft lithography. The conjunction of both methods permits not only possibility to create a micro-reactor for specific applications, but also design iterations, that can be easily done to achieve, in a not very expensive way, systems that are perfectly suited to the needs of research[1,5–7]. The final design of the device is based in different considerations like the size of the channel that will have a constant fluid flow of fresh Tryptic Soy Broth (TSB) during the biofilm formation. The width of the channel is an important dimension of the device because it should be dimensionally similar to a standard implant infection as the hip joint[8]. The free zone region of the hip joint can exhibit bacterial infection after the surgery like the study reported by WN. Ueng, CH. Shih[9], in 1995 that showed an early and late infection by *Mycobacterium tuberculosis* biofilm after hip arthroplasties. Approximately 50% of nosocomial infections per year in the US are associated with IMDs[10] so the understanding of bacterial infections should be done with similar dimensions of its cause and more importantly with a laboratory model priory to practice novel treatments in human to prevent and/or avoid biofilm development.

AREA	APPLICATION
Miniaturized analytical systems	
Genomic and proteomics	Rapid, high density sequencing, DNA fingerprinting, combinatorial analysis, forensics, gene expression assays, integration of fluidics with DNA arrays
Chemical/biological warfare defense	Early detection and identification of pathogens and toxins; early diagnosis; Triage
Clinical analysis	Rapid analysis of blood and body fluids, point of care diagnostics based on immunological or enzymatic assays, electrochemical detection, and cell counting
High throughput screening	Combinatorial synthesis and assaying for drugs. Toxicological assays
Environmental testing	*In situ* analysis of environmental contamination
Biomedical devices	
Implantable devices	Devices for *in vivo* drug delivery, *in vivo* monitoring for disease and conditions
Tools for chemistry and biochemistry	
Small-scale organic synthesis	Combinatorial synthesis
Sample preparation	Purification of biological samples for further analysis
Amplification of nucleic acids/sequences	PCR, RT-PCR
Systems for fundamental research	
Systems with which to study the flow of fluids	Studies of EOF and laminar flow in small channels, studies of diffusion
Studies of chemical reactions	Enzyme-substrate
Biomimetic systems	Development of machines that mimic biological functions
Systems to study small amounts of sample	Detection of single molecules

Table 4.1. Potential applications for microfluidics devices Cooper & Whitesides *et al* [2].

4.2 Platform design

The design of the platform is based on previous work with fluidic devices optimized for biofilm growth with continuous flow[11] and commercial impedance data analysis named Real Time Cell Analyzer (RTCA) which was invented by ACEA Biosciences and co-developed by Roche[12–14] (Figure 4.1). This commercial system is also known as xCELLigence and is a labelling-free cell based assay system integrating microelectronics and cell biology, suitable for uninterrupted monitoring of living cells. This system relies on a micro-electronic biosensor built to measure the electrical impedance of the cell population in every single well (Figure 4.1D). Although the data provided by RTCA is very valuable, the implementation of continuous flow for biofilm formation is necessary parameter for understanding the biofilm detachment[15]. For this reason the design of the platform consist in a flow channel to incorporate gold electrodes with different configurations and compare their sensitivity to monitor the attachment of the biofilm and the subsequent development over these electrodes.

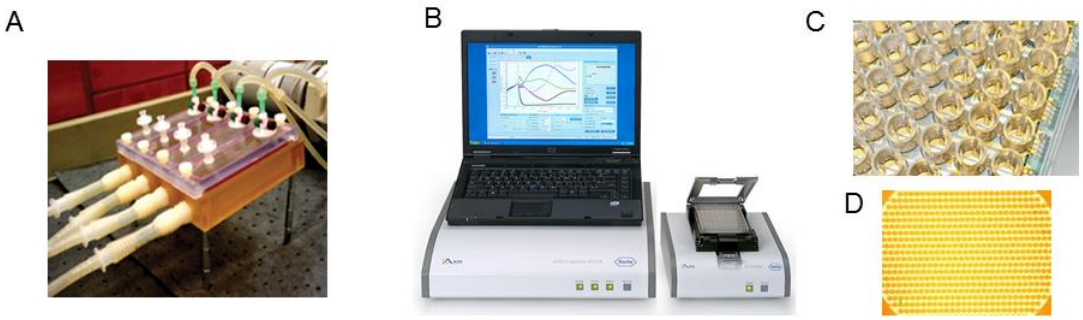

Figure 4.1. Conceptual platform: Electrochemical impedance spectroscopy. (A) Drip Flow Biofilm Reactor designed by Goeres *et al* [11]. (B) Commercial platform for Impedance analyses known as Real-Time Cell Analysis (RTCA) from Roche Instruments. (C) 96well plate with impedance electrode at the bottom of the each well. (D) Zoom of the interdigitated microelectrode (IDuE) of an individual well of the commercial platform.

4.2.1 Sensor design and Finite Element Modelling (FEM) analysis

The sensor is designed to limit the size of the entire platform. This sensor have punctual electrodes (WE) to measure dissolved oxygen (DO) [16], K+, Na+ and pH. Above an interdigitated microelectrode 1 (IDuE 1) was placed to perform indistinctly two and four-electrode configuration impedance measurements on the same device. Also a two-electrode configuration system (IDuE 2) is present to emulate the disposition in the space and the electrode dimensions used in the commercial XCelligence® equipment of Roche.

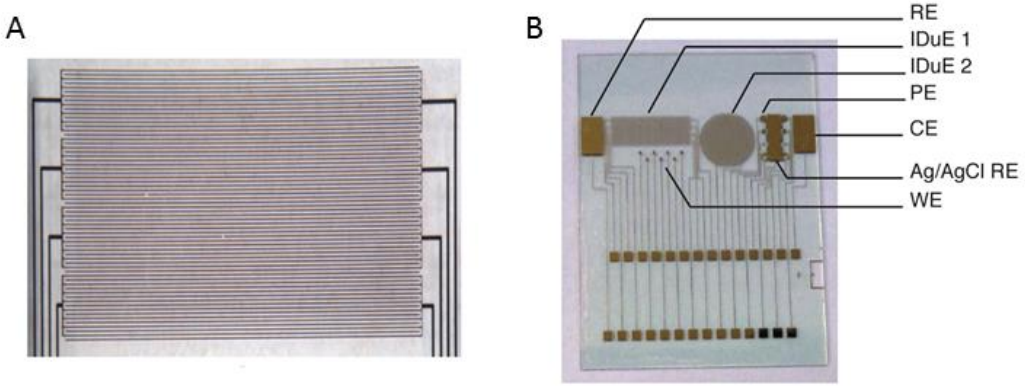

Figure 4.2. Impedance gold sensor. (A) Zoom of the rectangular IDuE fabricated on pyrex substrate. (B) Chip module containing the different sensors. The chip contains two IDuE, rectangular (IDuE 1) and circular (IDuE 2). The electrodes for the measurement of dissolved oxygen are the reference electrode (RE), the working electrode (WE) and the counter electrode (CE). The punctual electrodes (PE) for the potentiometric

measures are prepared to be selective for Na+ and K+. For the pH measurement, an additional iridium oxide layer is electrodeposited on the electrode selected. For robustness purposes, the PE are replicated. The reference electrode for potentiometric measures of Na+, K+ and pH is the silver/silver chloride electrode (Ag/AgCl RE).

This section details the overall design of the multi-parametric sensor, focusing in this section only on the performance of the impedance characteristics. To optimize the physical dimensions and geometry of the IDuE (Figure 4.4A), we simulated with COMSOL Multiphysics® 4.4 (Burlington, MA, USA) a 2D cross-section FEM model of the electrode geometry with a mesh of 20,000 elements (Figure 4.4B). The impedance sensitivity, which depends on the electrode dimensions, was calculated according to Grimnes and Martinsen[17]

$$S = \frac{\vec{J}_1 \vec{J}_2}{I^2}, \qquad \text{(Equation 4.1)}$$

where S is the sensitivity to the conductivity changes as a function of the position, J_1 is the current density vector when the current is injected between I+ and I- electrodes, and J_2 is the current density vector when the same current is injected between the voltage sensing electrodes V+ and V-. The results in Figure 4.4B reveal that the area where the IDuE sensitivity is higher corresponds to gap area between the IDuE groups denoted in the figure as W_{INT}. The FEM results (Figure 4.3) reveal that the optimal geometry is a trade-off between minimizing W_{INT} while also keeping minimal W_D and n_D, and maximal L_D. In all, the dimensions of the IDuE are W_{INT} = 21 µm the interdigitated group space, W_D = 21 µm the digit width, n_D = 32 the number of digit pairs and L_D = 7.11 mm the digit length (detail shown in Figure 4.2A). The chip dimensions are 23 mm x 18 mm.

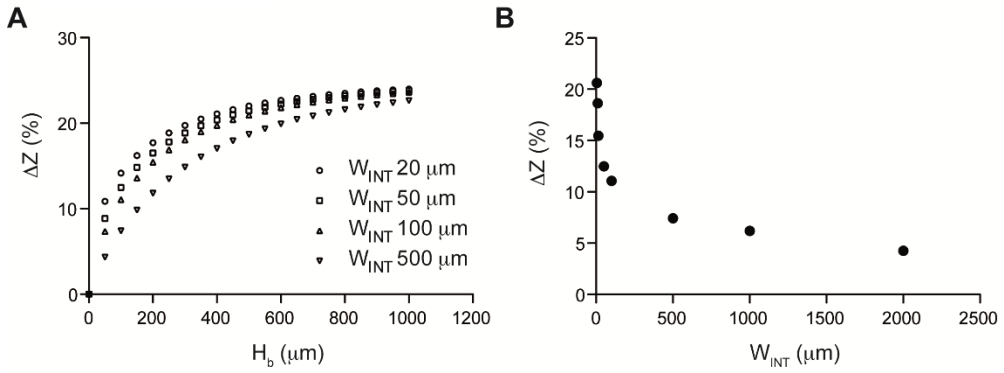

Figure 4.3. Internal parameters of the IDuE dimensions. (A) Relative increase in the impedance magnitude according to the height of biofilm H_b for different separations W_{INT}. The percentage of impedance variation decreases accordingly to the decrease of W_{INT} when considering small thickness biofilm H_b. (B) Relative decrease in the magnitude of the impedance as a function of the separation W_{INT} considering a given H_b.

The chip also incorporates additional sensors (Figure 4.2B) described elsewhere[16,18] for measuring different biofilm parameters of interest. The punctual electrodes allow to make electrochemical measurements of DO, K+, Na+ and pH. The amperometric measurement of DO is achieved using a working electrode (WE), a reference electrode (RE) and a counter electrode (CE)[16]. The measurement of Na+ and K+ ions is performed with a potentiometric ion-selective technique using the WE for each ion measurement and the RE. Finally, the pH sensor consists of a punctual electrode with an iridium oxide layer using the WE and the RE [18].

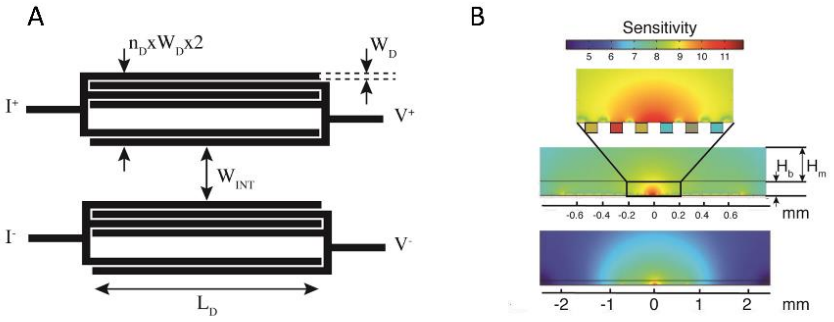

Figure 4.4. Dimensions of the electrodes and its sensitivity. (A) Schematic design of the interdigitated microelectrode (IDuE) optimized. The IDuE fingers are connected to the outer and inner current and voltage electrodes denoted in the Figure as I+ and I- and V+ and V- respectively. (B) Sensitivity map obtained from a 2D cross-section finite element model (FEM) considering the height of the biofilm and the flow channel, H_b and H_m respectively. Abbreviations: W_{INT}, interdigitated group space; W_D, digit width; n_D, number of digit pairs; L_D, digit length.

In Table 4.2 are summarized the main parameters of the developed FEM model, which is schematically depicted in Figure 4.4. It consists of two domains, one to model the culture medium (H_m) and another one to model the biofilm structure (H_b). From an electrical point of view, both domains are considered as a saline solution, and the electrical conductivity of the biofilm structure is modelled with a lower value than the culture medium conductivity in order to model the decrease in ion mobility due to the presence of EPS[19]. Moreover, the model also implements a four-electrode measurement setup. Thus, to simulate impedance measurements, a constant AC current has been injected through the outer electrodes (I+ and I-) and the inner electrodes (V+ and V-) used to sense the voltage drop (Figure 4.4). Then, the impedance has been calculated using Ohm's law, Z=V/I.

	Symbol	*Value*	*Units*
Culture medium			
Electrical conductivity	σ_m	1.5	S/m
Dielectric permittivity	ε_m	80	
Height	Hm	10	mm
Biofilm			
Electrical conductivity	σ_b	1.3	S/m
Dielectric permittivity	ε_b	80	
Height	Hb	0 ─ 1	mm
Electrodes			
Digit length	L_D	7.11	mm
Digit width	W_D	20	µm
Number of digit pairs	n_D	32	
IDEs separation	W_{INT}	20	µm

Table 4.2. Electrical and geometrical properties of FEM model.

4.2.2 Device design and Computational Fluid Dynamics (CFD) analysis

The different designs of the platform were performed with Catia V5R19 and the internal volume of them were computationally modeled with finite elements to simulate the flow range to work. The computational fluid dynamic (CFD) was projected through this internal channel of the microfluidic device and exported to IGES extension file (Initial Graphics Exchange Specification) shown in Figure 4.5. This file allows the simulation to run with the initial conditions required as input of the software (Table 4.3). With this conditions a Reynolds number was calculated to confirm the laminar flow along the channel supposing a parabolic profile of the flow following Poiseuille model. This model generates a distribution of the inlet speeds of the system used as input conditions.

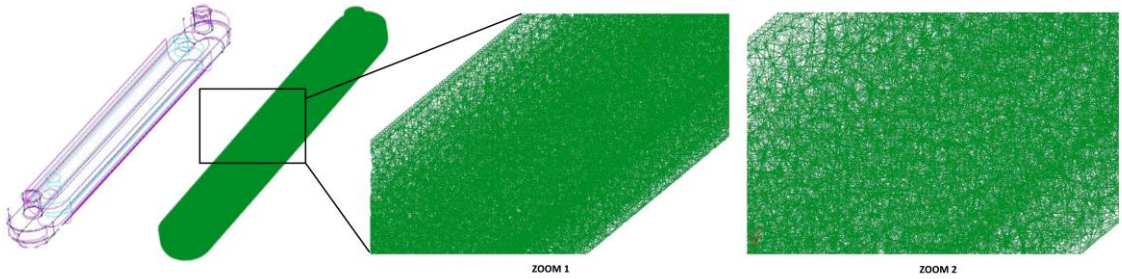

Figure 4.5. Suitable computational fluid dynamic simulation requires an internal volume of the flow chamber represented in 3D with final high density mesh engineered only appreciable in ZOOM 2.

This simulation was performed once the internal dimensions of the chamber were determined and the software used is Progis®, developed by the international center of numerical method on engineering (CIMNE). The 3D volume of the flow chamber was meshed (Figure 4.5) with a number of nodes of 183.543 with a maximum distance between them of 0.15 mm defining a correct geometry of the system for an optimal resolution. Simulations of the internal volume of the platform were based on previous work with microbalance experiments growing microbial cultures over the QCMD sensors[20–22] and carried out in chapter 3. These experiments strongly demonstrated that the range of flow conditions were optimal for biofilm development in relative short time (24 hour experiment). The flow chosen for the experiment is defined at 50 µL/min because is the lowest value for a correct behaviour of the peristaltic pump and also is low enough to avoid the use of high amounts of TSB medium for each experiment, leading a cost reduction.

Geometry data	
Inlet diameter / mm	2,5
Physical properties [water at 25ºC]	
ρ / kg·m^{-3}	996
μ / kg·m^{-1}·s^{-1}	0,86
Input conditions	
Inlet flow/ nL·min^{-1}	50000,00
Inlet mean speed/ mm·s^{-1}	0,1698
Inlet max speed/ mm·s^{-1}	0,3395
Outlet pressure / Pa	0,00
Calculation	
Reynolds	0,0004915

Table 4.3. Initial conditions of the Computational Fluid Dynamics (CFD) of the flow system.

Finally, the calculations were carried using the fluid dynamic model of Navier-Stokes with an increment of the time of 0.1 seconds, and a maximum number of iterations of 3 delimiting number of steps at 68.000 to obtain a convergent calculation of the internal flow of the system in steady state, taking into account that the physical properties of the liquid were ideally water at 25 ºC.

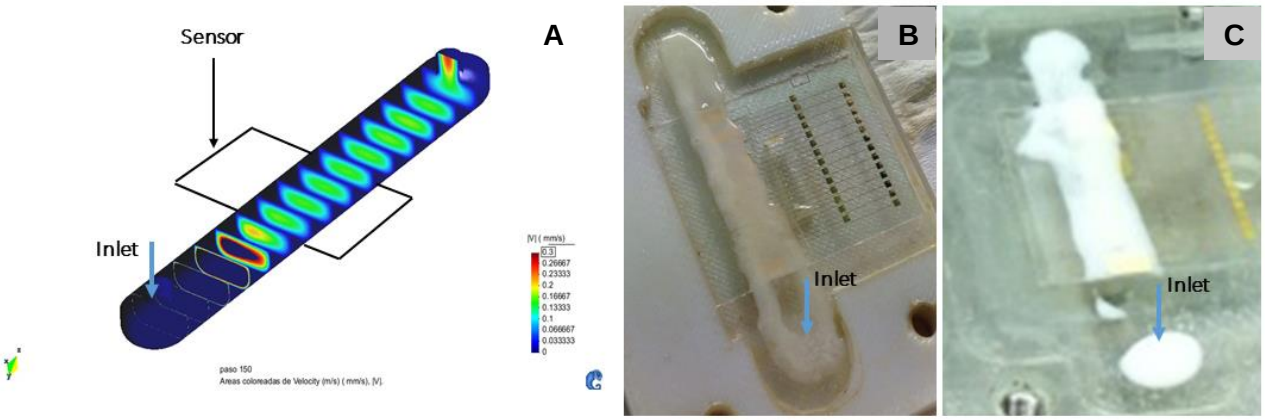

Figure 4.6. Simulation of the internal volume of the platform (A) and confirmed when biofilm was grown and developed in the experiments of chapter 5. The confirmation showed low bacterial attachment near the inlet where the shear-force was higher than the rest of the channel (B and C).

Once a convergent calculation of the internal flow channel was generated, the results were depicted performing serial longitudinal cuts shown in Figure 4.6. At the flow rate simulated here for the designed microfluidic device it was observed a laminar flow over the electrode that remained constant being representative from the beginning of the sensing area to the outlet. The higher shear stress at the inlet compared with the rest of the internal channel was confirmed when the device was open after biofilm growth (experiments from chapter 5) exhibiting no attachment of bacteria during its seeding and a consequent absence of biofilm in this location.

4.3 Platform fabrication and assembly

4.3.1 Sensor fabrication

This work shows an easy way to design an online monitoring biofilm with EIS electrodes coupled in a flow channel dimensioned to place a window for microscopy. The continuous observation of the bacterial growth over the electrodes with different electrode configurations is suitable to compare them and get the best signal to understand biofilms. The sensor was optimized before its fabrication modelling the EIS signal, dimension of the sensing area and size of the IDE (refer to section 4.2.1). The biofilm thickness modelled over the electrode will be confirmed by a real biofilm cultured over the IDE and imaged by Scanning Electron Microscopy (SEM) in the next chapter.

The sensor is an independent part of the device that can be sonicated, autoclaved and treated with plasma to reuse the device many times reducing the final cost of the experimentation. In addition this property permits the introduction of the sensor i.e. inside a plasma reactor for further modification of the surface which performs homogeneous thin films of different active molecules[23,24], making the system appropriate for real attachment studies with EIS and observational monitoring.

This sensor was fabricated in the clean room facilities at the Barcelona Microelectronics Institute, Spain, through standard photolithography techniques [25–27]. Three metal layers were deposited by sputtering over a 500 µm thick pyrex wafer. First, a 15 nm titanium layer was deposited to improve the adhesion of subsequent metals. Then, a second 15 nm nickel layer was deposited on top to provide a diffusional barrier and to prevent the formation of intermetallic titanium-gold compounds. Finally, a 150 nm gold layer was deposited. Thereupon, the electrodes and the metal tracks were patterned using selective wet etching baths following a standard lithographic process. To define the electrode active area and the connection pads, the final photolitographic step was the deposition of the passivation layer, which consisted of a double layer of 400 nm of silicon oxide and 400 nm of silicon nitrite, using plasma enhanced chemical vapour deposition. After the clean room process, a disk saw was used to dice the wafer into individual chips (8 per wafer). Finally, each chip was characterized by a cyclic voltammetry using saline solution (0.9% sodium chloride) to verify there was no shortcut between the IDuE fingers.

4.3.2 Device fabrication

Once the size of the platform is limited by the sensor three different system of additive manufacturing were tested to evaluate which is the best way to work with static and dynamic culture. Two technologies are based on fotocuring agents from important companies as Objet and EnvisionTEC, and the third one is based on extrusion technology (Fused Deposition Modelling, FDM) of polycarbonate and is available in our facility (IQS) with Fortus 400mc 3D printer. The different evolution of the platform designs and the material tested is shown in Annex IV.

Polycarbonate is a versatile, tough plastic used for a variety of applications, from bulletproof windows to compact disks (CDs). The main advantage of polycarbonate over other types of plastic is unbeatable strength combined with light weight. While acrylic is 17% stronger than glass, polycarbonate is nearly unbreakable. For this reason polycarbonate was used for iterative experiments with microorganism due to sterilization property that is a crucial factor to guarantee experiments with pure microbiological cultures. The sterilization of this material could be done using all major methods: ethylene oxide (EtO), irradiation (both gamma and electron-beam), and steam autoclaving. Polycarbonate could also be disinfected with common clinical disinfectants, such as isopropyl alcohol. This range of techniques offers the device designer broad flexibility in determining a cost-effective method to develop the needed platform.

Figure 4.7. Fortus 400mc 3D printer uses Fused Deposition Modelling (FMD) technology to print the principal lids of the EIS device. The parts printed in the 3D printer machine have material support with different mechanical properties to separate easily (see below).

The fabrication process of the device required an additional material for placing the EIS sensor and fit this correctly with the flow channel and the spring-loads, which are necessary to connect the sensor to the electronics (see Assembly section 4.3.3). This additional material was Polydimethylsiloxane (PDMS) used for the channel and the support of the EIS sensor and components shown in Figure 4.9. This PDMS channel with the connectors and the base was patterned via replica moulding technique applying different master structures that act as negative piece (Figure 4.8). The master structures were also printed in 3D with FDM technology that can be appreciated in Figure 4.8 A, D and F that are the points where PDMS is applied for its reticulation for 5 hours at 60 ºC.

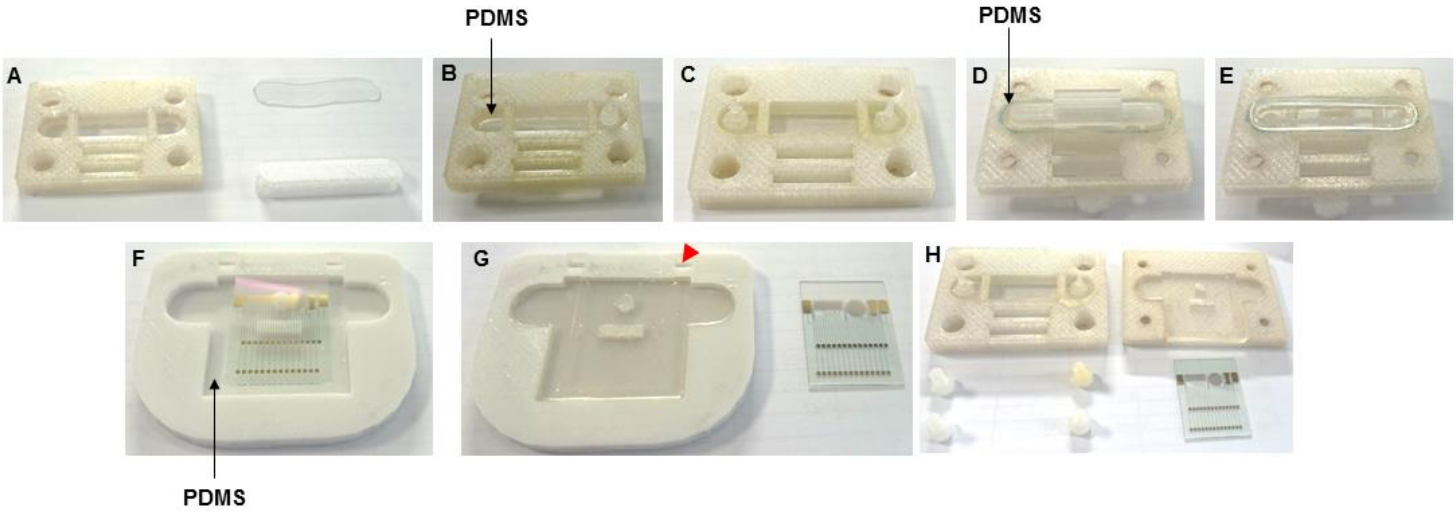

Figure 4.8. Stepwise fabrication process of the device to place Electrochemical Impedance Spectroscopy (EIS) gold sensors. (A) Top lid and master support. (B) Top lid with master support and connector to introduce PDMS in the window and around the connectors. (C) Top lid with cured PDMS fixing the connectors. (D) Top lid upside down with the second master allowing the formation of PDMS O-ring. (E) Top lid finished for its use. (F) Master moulding for PDMS support formation. (G) PDMS cured in the master with sensor space formed with the reference (red arrow). (H) Top and Bottom lids with sensors plastic screws, PDMS window and support.

4.3.3 Platform assembly

When the fabrication process of the device and sensor finished the platform was assembled to accomplish two main objectives: the impedance and the microscope monitoring at the same time. In terms of material, we know that biofilm attaches to biological or non-biological surfaces[28] so as described above, the device was fabricated with two non-biological materials with biocompatibility. The first one is Polycarbonate (PC) used for the construction of the two main lids of the device (Figure 4.9A) that mainly had the function of holding the channel, connectors, screws and sensor all together and close the device in a single piece. The technology used to fabricate the parts previously designed in the computer is a 3D printing technique known as Fused Deposition Modelling (FDM) which is very cheap and quick for device fabrication[29]. The second material is Polydimethylsiloxane (PDMS) which is well known for its biocompatibility[30], gas permeability, mechanical flexibility and optical transparency[31]. This material is used to generate the channel and the sensor support (Figure 4.11) having in contact only PDMS and the biosensor with the bacterial culture once the device is closed (Figure 4.9B). The mentioned properties are very important for the setup because the culture needs biocompatibility to grow the biofilm correctly, gas permeability to supplement oxygen constantly in the device while the nutrients are pumped through the channel, mechanical flexibility for the base of the sensor that avoids the sensor fracture when the two parts are closed, and finally the optical transparency for the microscope window over the sensing area.

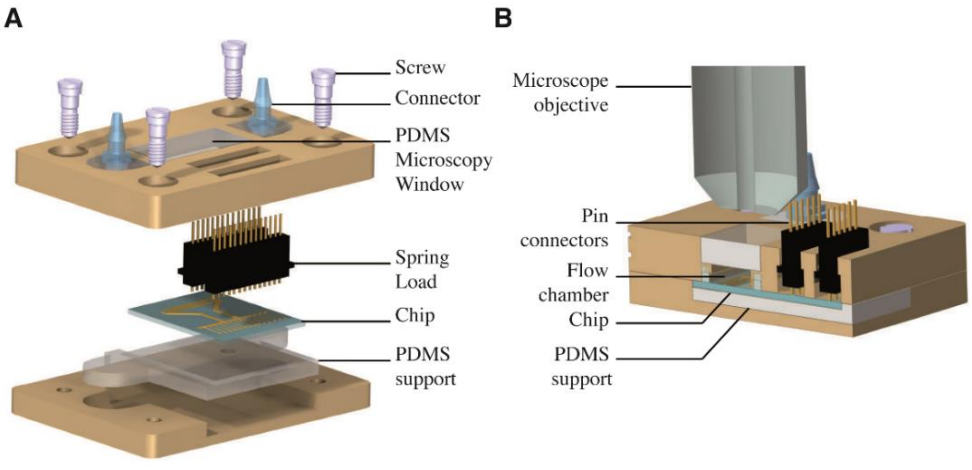

Figure 4.9. Prototyped device with Catia V5R19. (A) Computed aided design and components of microfluidic device designed. (B) Cross-section of the device under the microscope.

The perfect assembly of the device and closing process by using four screws in the corners of it, guarantees no fluid scape in the microfluidic device (see lasts version of Table 4.5) and as seen in Figure 4.9. This device used spring-load for the EIS connections instead of Printed Circuit Board (PCB) connected to the sensor and protected with black epoxy resin (Figure 4.10A) which is used very often in electronics. This feature complicates the use of flow channels with sensors connected to EIS equipment due to the poor homogeneity of the thickness. Thanks to the spring-load the sensor is connected to the cables only during the assembly having the sensor as a single part when the device is open (Figure 4.9). This setup avoids soldered parts for connections allowing a proper sterilization by autoclaving before the experiment giving to the user the capacity to reuse the sensor. Besides, the biofilm formed can be imaged easily with confocal microscope because the sensor, as independent part, is completely flat and fits perfectly with cover slip to perform end-point assays.

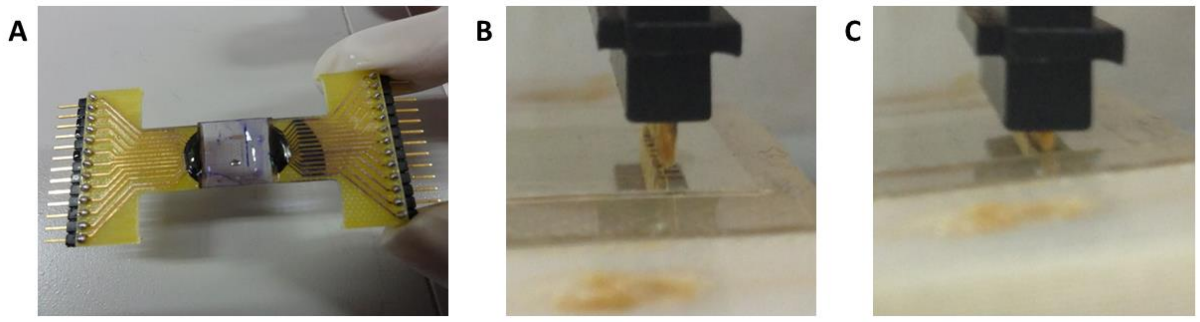

Figure 4.10. Printed Circuit Board commonly used in electronics (A). Spring-load in low stroke force (B) and maximum stroke Force (C).

As mentioned above, the electronics of the system performed in the device were designed to hold the spring-load that has a stoke range over the pad contact zone of the sensor. This design has to guarantee a perfect spring pin application to operate in the Mid-Stroke range when the platform is assembled. Operating at the Minimum Stroke Force range may produce a short-circuit for the lack of contact (Figure 4.10B) and operating at the Maximum Stroke Force may over-compress and damage the spring pin or even break the electrode when this press the lower zone of the sensor (Figure 4.10C).

The final design allows a proof of concept with the different components of the platform and its validation to compare in the laboratory of microbiology the computational design with the real prototype (Figure 4.11). The flow channel is suitable for flow experiments feeding the biofilms with Tryptic Soy Broth (TSB) and this flow channel fitted onto the electrodes of interest has a PDMS window allow a microscopy monitorization.

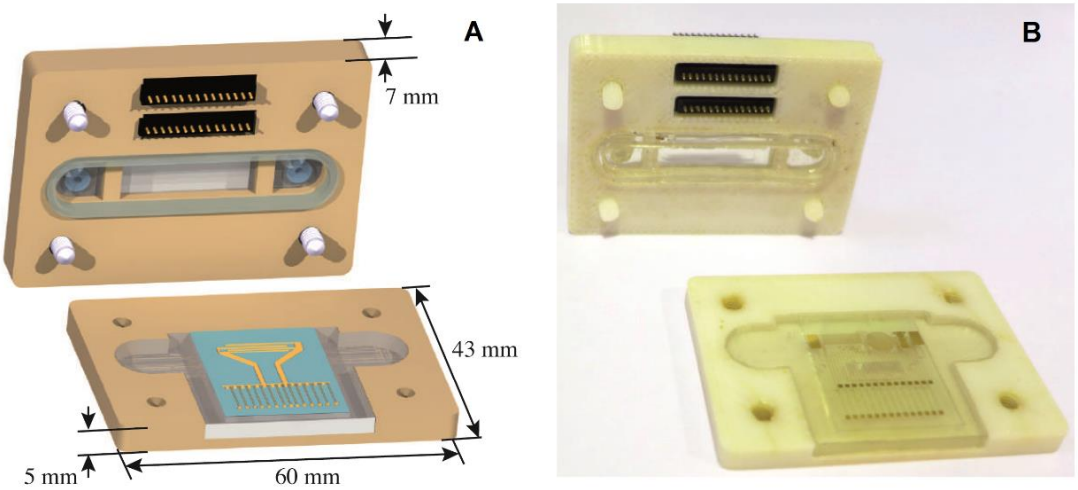

Figure 4.11. Open view of the microfluidic platform. (A) Designed with Catia V5R19 and (B) Zenithal view of the platform fabricated with rapid prototyping technique.

4.4 Final Remarks

It was observed that there is no fluid loss during the process and the final version is consistent enough to carry out the biofilm studies with reusability by autoclaving the sensors and platform before each experiment. Also, the geometry simulation of the interdigitated microelectrode (IDuE) with a finite element model allowed the optimization of the sensitivity of our sensor for the detection of *Staphylococcus aureus* biofilm proliferation. The suitability of the microfluidic platform design is going to be validated in the next chapter to perform a selective label-free monitoring of *S. aureus* under constant flow conditions combining simultaneously microscopy and impedance measurements with two- and four-electrode methods.

Contrary to other state-of-the-art approaches based on commercial multi-well plates used today for biofilm assays, our multi-parametric microfluidic platform could be integrated in multiple environments and offers the advantage to account for the effect of shear stress on the formation of bacterial biofilm, a variable that affects biofilm structure and behaviour[32]. Furthermore, the system presented also offers the possibility to measure multiple read-outs configurations to detect other analytes of interest such as dissolved oxygen, K+, Na+ and pH.

In summary it can be said that up to this moment there was no other platforms optimized to: grow a biofilm under flow conditions with a microfluidic device designed to use IDuE integrated, and electrodes performed for an optimal sensitivity. From this point the real applications of this platform will be developed in the next chapters.

4.5 References

(1) Mcdonald, J. C.; Duffy, D. C.; Anderson, J. R.; Chiu, D. T. Review General Fabrication of Microfluidic Systems in Poly (Dimethylsiloxane). *Electrophoresis* **2000**, *21*, 27–40.

(2) Whitesides, G. M. Poly (dimethylsiloxane) as a Material for Fabricating Microfluidic Devices. *Acc. Chem. Res.* **2002**, *35*.

(3) Lee, J.-H.; Kaplan, J. B.; Lee, W. Y. Microfluidic Devices for Studying Growth and Detachment of Staphylococcus Epidermidis Biofilms. *Biomed. Microdevices* **2008**, *10*, 489–98.

(4) Figallo, E.; Cannizzaro, C.; Gerecht, S.; Burdick, J. a; Langer, R.; Elvassore, N.; Vunjak-Novakovic, G. Micro-Bioreactor Array for Controlling Cellular Microenvironments. *Lab Chip* **2007**, *7*, 710–9.

(5) Mcdonald, J. C.; Chabinyc, M. L.; Metallo, S. J.; Anderson, J. R.; Stroock, A. D.; Whitesides, G. M. Prototyping of Microfluidic Devices in Poly(dimethylsiloxane) Using Solid-Object Printing. *Anal. Chem.* **2002**, *74*, 1537–1545.

(6) Printing, I. New Advances in Rapid Prototyping Using Answering the Requirements of Form , Fit and Function. **2011**.

(7) Parts, R. For Conceptual Modeling, Functional Prototyping, Manufacturing Tools, and End-Use-Parts.

(8) BR Rawal, Rahul Ribeiro, Rajesh Malhotra, N. B. Anthropometric Measurements to Design Best-Fit Femoral Stem for the Indian Population. *Indian J. Orthop.* **2012**, *46*, 46–53.

(9) WN. Ueng, CH. Shih, S. H. Pulmonary Tuberculosis as a Source of Infection after Total Hip Arthroplasty. *Int. Orthop.* **1995**, *19*, 55–59.

(10) Harris, L. G.; Richards, R. G. Staphylococci and Implant Surfaces: A Review. *Injury* **2006**, *37 Suppl 2*, S3–14.

(11) Goeres, D. M.; Hamilton, M. a; Beck, N. a; Buckingham-Meyer, K.; Hilyard, J. D.; Loetterle, L. R.; Lorenz, L. a; Walker, D. K.; Stewart, P. S. A Method for Growing a Biofilm under Low Shear at the Air-Liquid Interface Using the Drip Flow Biofilm Reactor. *Nat. Protoc.* **2009**, *4*, 783–8.

(12) Limame, R.; Wouters, A.; Pauwels, B.; Fransen, E.; Peeters, M.; Lardon, F.; De Wever, O.; Pauwels, P. Comparative Analysis of Dynamic Cell Viability, Migration and Invasion Assessments by Novel Real-Time Technology and Classic Endpoint Assays. *PLoS One* **2012**, *7*, e46536.

(13) Teng, Z.; Kuang, X.; Wang, J.; Zhang, X. Real-Time Cell Analysis--a New Method for Dynamic, Quantitative Measurement of Infectious Viruses and Antiserum Neutralizing Activity. *J. Virol. Methods* **2013**, *193*, 364–70.

(14) Kustermann, S.; Boess, F.; Buness, a; Schmitz, M.; Watzele, M.; Weiser, T.; Singer, T.; Suter, L.; Roth, a B. A Label-Free, Impedance-Based Real Time Assay to Identify Drug-Induced Toxicities and Differentiate Cytostatic from Cytotoxic Effects. *Toxicol. In Vitro* **2012**.

(15) Manz, B.; Volke, F.; Goll, D.; Horn, H. Measuring Local Flow Velocities and Biofilm Structure in Biofilm Systems With Magnetic Resonance Imaging (MRI). *Biotechnol. Bioeng.* **2003**, *84*, 424–432.

(16) Moya, A.; Guimera, X.; del Campo, F. J.; Prats-Alfonso, E.; Dorado, A. D.; Baeza, M.; Villa, R.; Gabriel, D.; Gamisans, X.; Gabriel, G. Profiling of Oxygen in Biofilms Using Individually Addressable Disk Microelectrodes on a Microfabricated Needle. *Microchim. Acta* **2014**, Accepted.

(17) Martinsen, S. G. and Ø. G. Sources of Error in Tetrapolar Impedance Measurements on Biomaterials and Other Ionic Conductors. *J. Phys. D. Appl. Phys.* **2006**, *40*.

(18) Prats-Alfonso, E.; Abad, L.; Casañ-Pastor, N.; Gonzalo-Ruiz, J.; Baldrich, E. Iridium Oxide pH Sensor for Biomedical Applications. Case Urea-Urease in Real Urine Samples. *Biosens. Bioelectron.* **2013**, *39*, 163–9.

(19) Martinsen, S. G. and O. G. *Bioimpedance & Bioelectricity Basics*; second.; Academic Press: New York, 2008.

(20) Schofield, A. L.; Rudd, T. R.; Martin, D. S.; Fernig, D. G.; Edwards, C. Real-Time Monitoring of the Development and Stability of Biofilms of Streptococcus Mutans Using the Quartz Crystal Microbalance with Dissipation Monitoring. *Biosens. Bioelectron.* **2007**, *23*, 407–13.

(21) Olsson, A. L. J.; van der Mei, H. C.; Busscher, H. J.; Sharma, P. K. Novel Analysis of Bacterium-Substratum Bond Maturation Measured Using a Quartz Crystal Microbalance. *Langmuir* **2010**, *26*, 11113–7.

(22) Tam, K.; Kinsinger, N.; Ayala, P.; Qi, F.; Shi, W.; Myung, N. V Real-Time Monitoring of Streptococcus Mutans Biofilm Formation Using a Quartz Crystal Microbalance. *Caries Res.* **2007**, *41*, 474–83.

(23) Marí-Buyé, N.; O'Shaughnessy, S.; Colominas, C.; Semino, C. E.; Gleason, K. K.; Borrós, S. Functionalized, Swellable Hydrogel Layers as a Platform for Cell Studies. *Adv. Funct. Mater.* **2009**, *19*, 1276–1286.

(24) Montero, L.; Baxamusa, S. H.; Borros, S.; Gleason, K. K. Thin Hydrogel Films With Nanoconfined Surface Reactivity by Photoinitiated Chemical Vapor Deposition. *Chem. Mater.* **2009**, *21*, 399–403.

(25) Gabriel, G.; Erill, I.; Caro, J.; Gómez, R.; Riera, D.; Villa, R.; Godignon, P. Manufacturing and Full Characterization of Silicon Carbide-Based Multi-Sensor Micro-Probes for Biomedical Applications. *Microelectronics J.* **2007**, *38*, 406–415.

(26) Guimera, A.; Gabriel, G.; Plata-Cordero, M.; Montero, L.; Maldonado, M. J.; Villa, R. A Non-Invasive Method for an in Vivo Assessment of Corneal Epithelium Permeability through Tetrapolar Impedance Measurements. *Biosens. Bioelectron.* **2012**, *31*, 55–61.

(27) Bonilla, D.; Mallén, M.; de la Rica, R.; Fernández-Sánchez, C.; Baldi, A. Electrical Readout of Protein Microarrays on Regular Glass Slides. *Anal. Chem.* **2011**, *83*, 1726–1731.

(28) Hall-Stoodley, L.; Costerton, J. W.; Stoodley, P. Bacterial Biofilms: From the Natural Environment to Infectious Diseases. *Nat. Rev. Microbiol.* **2004**, *2*, 95–108.

(29) Murugesan, K.; Anandapandian, P. A.; Sharma, S. K.; Vasantha Kumar, M. Comparative Evaluation of Dimension and Surface Detail Accuracy of Models Produced by Three Different Rapid Prototype Techniques. *J. Indian Prosthodont. Soc.* **2012**, *12*, 16–20.

(30) Sethu, P.; Moldawer, L. L.; Mindrinos, M. N.; Scumpia, P. O.; Tannahill, C. L.; Wilhelmy, J.; Efron, P. A.; Brownstein, B. H.; Tompkins, R. G.; Toner, M. Microfluidic Isolation of Leukocytes from Whole Blood for Phenotype and Gene Expression Analysis. *Anal. Chem.* **2006**, *78*, 5453–5461.

(31) Minteer, S. D. *Microfluidic Techniques*; Humana Press Inc.: Totowa, New Jersey 07512, **2006**.

(32) Stoodley, P.; Lewandowski, Z.; Boyle, J. D.; Lappin-Scott, H. M. Oscillation Characteristics of Biofilm Streamers in Turbulent Flowing Water as Related to Drag and Pressure Drop. *Biotechnol. Bioeng.* **1998**, *57*, 536–44.

Chapter 5 Online monitoring of biofilm development with Electrochemistry Impedance Spectroscopy (EIS) platform

5.1 Introduction

The previous chapter was focused in the optimization of the multi-parametric microfluidic platform with computational tools and fabrication with additive manufacturing techniques of both principal components: the device and the sensor. Once the assembly of all the components was tested to evaluate possible fluid scape, the biofilm detection method (EIS technology) is going to be deeply studied along this chapter.

As explained in the introductory chapter, the bacterial attachment and the development of microbial communities commonly known as biofilms have a relevant impact in medicine being prominent source of infection[1], mainly indwelling medical devices, such as the catheters and heart stents that often requires a complete removal of the device from the patient[2]. For this reason, the bacterial infection needs to be studied at laboratories as biofilm instead of planktonic.

Briefly, the biofilm formation has been described in the literature as a three-step process, first starting with an initial attachment of the bacteria to the material surface followed by the formation of a strong bacterial layer and finally the maturation/activation of the biofilm by secreting extracellular polymeric substances (EPS)[3] that provides to the bacterial community a high resistance to antibiotics[4,5] and mechanical stress.

As commented before it was pertinent to develop tools that allow non-disruptive, continuous and label-free monitoring for studying the dynamic process of biofilm formation[6]. The method utilised in this chapter for microorganism growth detection is based on electrical impedance spectroscopy (EIS) measurements[7] used under flow conditions, a parameter that highly affects biofilm structure and behaviour[8].

Monitoring biofilm formation combining label-free biosensors and impedance spectroscopy measurements on the surface of electrodes is an alternative approach that has gained increasing interest, previously described using IDuEs[9–14] which combine both impedimetric and amperometric measurements[15]. In particular, much of the existing studies are based on two- or three-electrode measurements[16–20] because it is simplicity and ability to detect and track the biofilm formation by the changes occurring at the surface electrode. These features are of great interest by themselves but introduce a source of indetermination if the interest is to obtain a quantitative measurement of the biofilm growing in the layers above the electrode surface. On top of that, the fact that the two-electrode configuration includes the impedance and polarization of the counter and the working electrodes can jeopardize the data analysis

if the contribution of each electrode is not the same. Furthermore, when the electrode surface is fully covered by bacteria or EPS, the inherent sensibility of this technique is significantly reduced as compared to the four-electrode configuration technique [21]. With the four-electrode method [22], the effect of the electrode-electrolyte is excluded from the impedance measurement offering an increased sensitivity to monitor cell concentration and the possibility to extract morphological and structural information from the impedance (refer to Section 5.2.3). Despite the aforementioned advantages, we are not aware of any previous work where four-electrode electrode measurements were performed in a microfluidic device to monitor biofilm, so this technology will be further studied and refined in this chapter to confirm the optimization of the sensor carried out in chapter 4.

The culture area of the proposed platform was fabricated using transparent material over the electrodes to enable the comparison with microscopy evaluation techniques. In this work real-time monitoring of a Gram positive pathogen, *Staphylococcus aureus* V329, was carried out. This strain is a very pathogenic bacteria and good biofilm former[23,24] that provokes mastitis bovine affecting the alimentary field, nevertheless it requires lower biosafety level thanks to be an animal infective strain that forms biofilm only in the cow udder. However as described before all the experiments were prepared in a class II safety cabinet (Figure 5.1A and B) and took place inside an incubator (Thermo scientific) at 37 ºC (Figure 5.1C).

Figure 5.1. Continuous flow experiment preparation. (A) Connection of all the components inside a biosafety cabinet. (B) Assembly of the platform, bottles and peristaltic pump on the incubator tray. (C) Perform the software to connect by Bluetooth the impedance analyser with the laptop and record the data wireless.

5.2 Results

5.2.1 Continuous flow experiment for biofilm formation

In order to prepare the continuous flow experiment the bacteria were prepared as explained in section 2.2.2 from glycerol stock cultures stored at -80 °C and streaked onto tryptic soy agar (TSA) plates[24]. The agar plate was placed into an incubator at 37 °C for 16 hours to grow the colonies and for picking up a single colony to a falcon tube containing 10 mL of tryptic soy broth (TSB) medium agitated for 16 hours at 37 °C. Following, the culture was diluted to have a final absorbance of 0.084 at 600 nm wavelength. This dilution was used to feed the measurement device in the Phase 2 (Seeding) of the flow experiment to generate the biofilm (Figure 5.2).

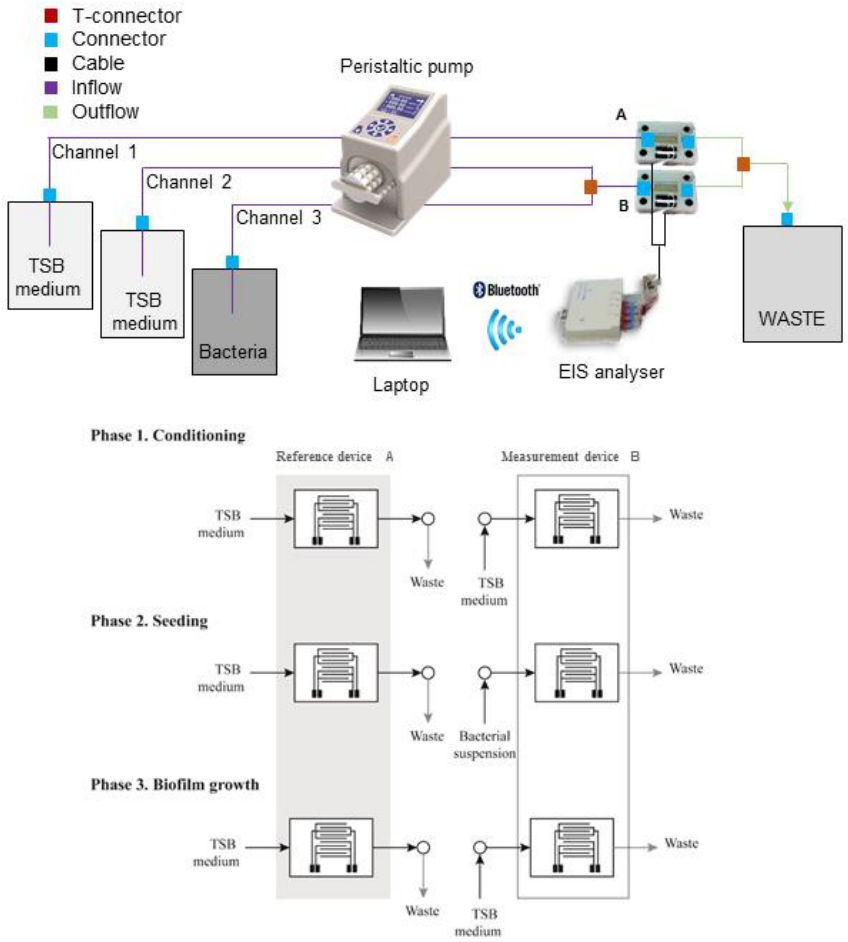

Figure 5.2. Flow diagram of the measurement setup. The system is divided in: (A) reference device and (B) measurement device. The experiment is divided in three phases. The Phase 1 (conditioning) is pumping TSB to the reference and the measurement devices for 2 hours. The Phase 2 (seeding) pumps bacteria into the measurement device for 2 hours. The Phase 3 (biofilm growth) pumps TSB medium for 16 hours. During the phase 2 and 3 the reference device is pumped with TSB medium.

During the course of the experiments, the two independent channels of the peristaltic pump (Reglo ICC, Ismatec, Glattbrugg, Switzerland) were working simultaneously. Both channels were connected with PharMed® Ismaprene tubes (0.89 mm internal diameter) to the microfluidic platform. A third channel was used to introduce fresh TSB medium into a second microfluidic platform to have negative control of biofilm formation. Both devices were connected to the impedance analyser multiplexed front end and the impedance measurements were repeated every 10 minutes. The experiment consisted of three phases (Figure 5.2):

1. Conditioning phase. Constant feeding of TSB medium to stabilize the system forming the conditioning layer over the electrode and to prevent the formation of bubbles. Duration 2 hours, flow rate 50 µL/min.
2. Seeding phase. Introduction of the bacteria into the system. Duration 2 hours, flow rate 50 µL/min.
3. Biofilm growth phase. Constant feeding of sterile TSB media to establish the biofilm over the biosensor. Duration 22 hours, flow rate 50 µL/min.

5.2.2 Electrical Impedance Spectroscopy (EIS) for online Biofilm monitoring

The first result using the designed device and performing the experiment described above was carried out to compare the two and four electrode configuration systems with only the custom IDuE 1 with the measuring device and the reference device (Figure 5.2). Impedance evolution is showed in Figure 5.3 A and B for two-electrode configuration in a Bode representation for different times of the biofilm formation (5, 11, 17 and 23 hours), and Figure 5.3 D and E for four-electrode configuration. As commented, the two-electrode measurements behaviour is controlled by the electrode EDL for frequencies below 7 kHz, and at higher frequencies it is controlled by the solution resistance. Likewise, in the case of four-electrode measurements, the solution resistance only controls the measurement. Therefore, a resistive behaviour (flat modulus and 0º in phase shift) is expected, at least during the initial measurements. However, this behaviour is only observed at frequencies below 19 kHz. This deviation from the expected behaviour can be associated with capacitive couplings and current leakages due to the instrumentation and wires, for this reason in both cases to better analyse the obtained results and evaluate the ability of the proposed design to monitor the biofilm growth, the time evolution has been represented using a single frequency

with a value of 12 kHz. The Bode plot represented showed a higher difference in between the different times plotted (5, 11, 17, 23 hours) for four-electrode measurement (Figure 5.3D) compared with two-electrode measurement (Figure 5.3A) which means a higher sensitivity assuming a bigger detection window. Interestingly the relative change of impedance along the time for a single frequency showed the real difference of both configurations. An obvious artefact effect was observed especially during the Phase 2 (seeding) of the setup that corresponds to the green square of the Figures 5.3 C and F where the bacteria dilution was pumped into the measurement device. The increment of the signal during this stage is caused by the lower temperature of the TSB used for the bacterial dilution which was not pre-warmed at 37ºC. These results confirmed a high influence of the temperature in both electrode configuration measurements, especially during the Phase 2 of the experiment. Furthermore the surface covered area was more influenced in the two-electrode measurement compared with the four-electrode measurement, because this last suffer a recovery in short time (less than 1 hour) allowing the impedance signal to detect an increment caused by the biofilm formation.

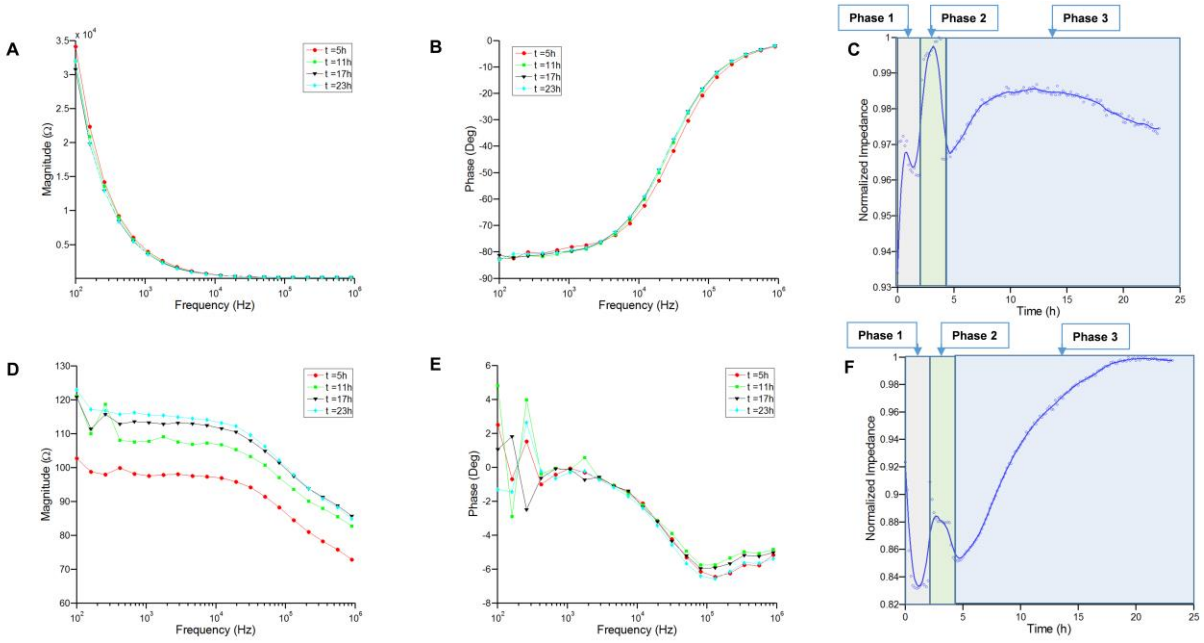

Figure 5.3. Comparison between two and four-electrode measurements of the measurement device. Bode plot of impedance module versus frequency at different times of two-electrode configuration (A) and four-electrode configuration (D). Bode plot of phase angle versus frequency at different times of two-electrode configuration (B) and four-electrode configuration (E). Relative change normalized of the magnitude of the electrical impedance versus time of two-electrode configuration (C) and four-electrode configuration (F) at a frequency of 12 kHz.

Comparing the reference device with the measurement device (both depicted in Figure 5.4A and B) the presence of bacteria and the biofilm development during the experiment is confirmed due to the signal increment of impedance for a single frequency, in the measurement device (Figure 5.4A) while the reference device (Figure 5.4B) remains almost flat during 17 hour, where presumably a contamination of the inlet bottle with TSB medium was present. Since the fresh TSB medium feeding both devices was independent a contamination of the reference device did not affect the measurement device. Only by visualising the bottles connected to channel 1 and channel 2 and represented in Figure 5.2 a contamination could be detected after the 24 hour experiment, discarding in this case a contamination in the measurement device, because there was no turbidity in the TSB medium feeding bottle connected to this device.

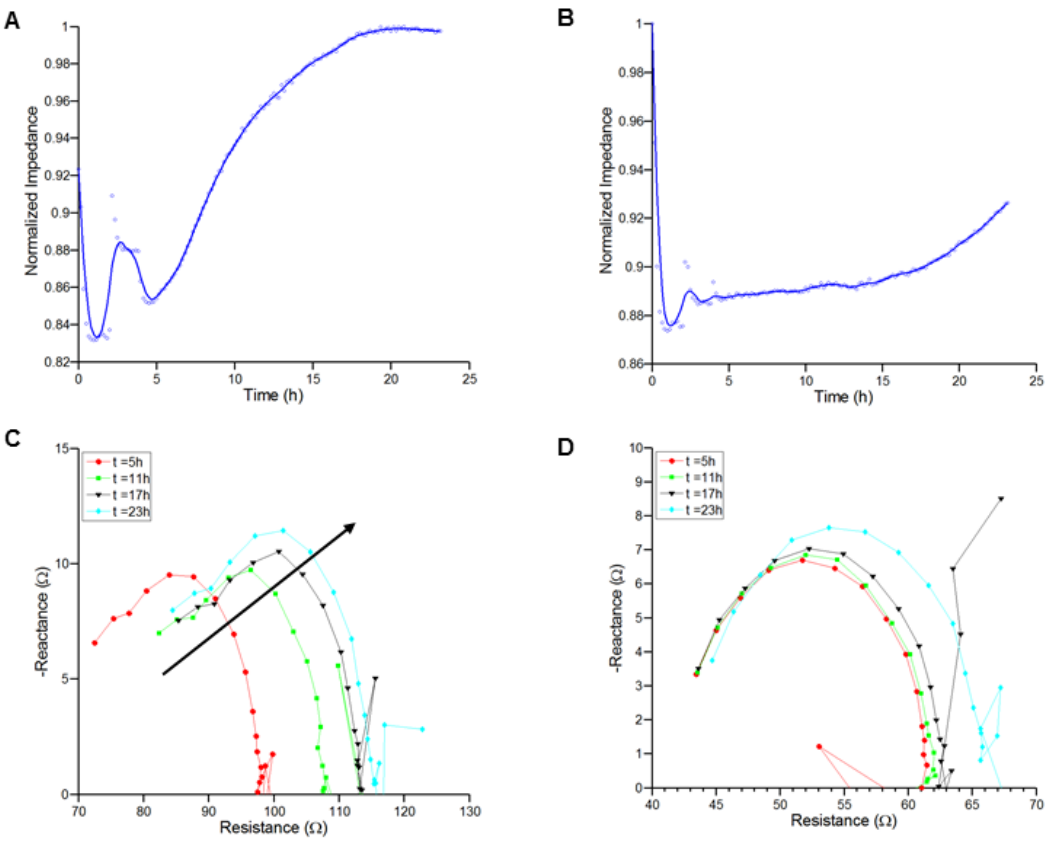

Figure 5.4. Four electrode Impedance Spectroscopy data. Relative change of the normalized electrical impedance versus time of the measurement device (A) and the reference device (B). Representation in the complex plane of the impedance measured with four-electrode configuration of the measurement device (C) and the reference device (D).

The representation in the complex plane, decomposing in real (resistance) and imaginary (reactance) data, of the impedance for both devices showed that the arc in the biofilm moved on the horizontal axis during the experiment due to the proliferation increasing the resistance, whereas the reference channel only increased at the last arc represented attributed to contamination detected after 17 hours. Once the platform was preliminary tested, the biofilm formation during 24-hour experiment was initiate to compare real-time data using the optimized IDuE with the circular IDuE electrode similar to that from Roche Applied Science (Basel, Switzerland) (see section 4.2). The EIS results were repeated n=3 and confirmed by scanning electrode microscopy and fluorescence microscopy after live/dead cell staining of the biofilm measured.

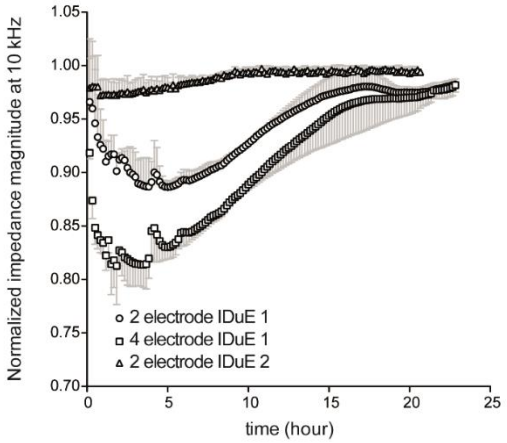

Figure 5.5. Time course of the normalized impedance magnitude (mean±std, n=3) detected with the rectangular and circular interdigitated microelectrodes (IDuEs), IDuE 1 and IDuE 2 respectively, in the measurement channel.

The results were shown in the time course of the impedance magnitude at 12 kHz where it is more sensitive to biofilm formation[25]. Impedance is normalized to its maximum value for comparison purposes (Figure 5.5). The unexpected increase at 2 hours is attributed to the transient phase before stabilization of the TSB containing bacteria that cooled down during its preparation. Similar to the results shown by Paredes *et al* in 2013[13], the ideal point to detect impedance changes due to biofilm growth is about 5 hours. In the initial phase where the concentration of biofilm is low, it can be seen that sensibility of the two-electrode technique to detect biofilm proliferation is decreased. Figure 5.5 shows also that the two-electrode circular IDuE has lower dynamic range to detect cell growth than the rectangular IDuE, and after 10 hours saturates to its maximum value. The ability to detect growth changes can be further

improved with the four-electrode method. The detected change is 15%, approximately 5% higher than two-electrode method measuring under the same experimental conditions. The level of impedance changes detected is similar to that 10% change detected for the same range of frequencies at 12 hours obtained by Zikmund *et al* [26] where the growth of *Echerechia coli* was monitored.

Despite the differences in the dimensions and geometry between pathogens, *E. coli* is a rod-shaped bacterium and measures approximately 0.5 μm in width by 2 μm in length while *Staphylococcus aureus* has a spherical shape and size of 0.5-1 μm, it was detected the same relative change at 10 hours after infection (2 hours after starting the experiment). Compared to the 5% impedance change detected by Paredes *et al* [13], we think this difference may be due to the electrode optimization through FEM simulations.

5.2.3 Impedance models for structural and morphological biofilm changes

Impedance data measured with the four-electrode configuration method was fitted to the empirical complex nonlinear model described by Cole approximation[27], to perform an approximation of biological changes occurring during the biofilm formation.

$$Z(f) = R_\infty + \frac{R_0 - R_\infty}{1 + \left(j\frac{f}{f_c} \right)^\alpha}. \qquad \text{(Equation 5.1)}$$

The acquired data was plotted in Matlab (Natick, MA, USA) using Marquardt-Levenberg iterative weighted complex nonlinear least square algorithm[28]. The maximum iterations and the fitting tolerance were set to 1e6 and 1e-12 respectively. From the optimal curve-fit parameters, the Jacobian was calculated numerically. The covariance matrix was estimated from the Jacobian using a diagonal matrix containing as weights the impedance data std. The asymptotic standard error for the optimal model parameters was finally obtained from the square root of the diagonal elements of the covariance matrix. The central relaxation frequency f_c corresponds to the frequency with the highest absolute value of the impedance imaginary part. The α parameter explains the dispersion in the cellular membrane capacitances measured thus is related to the dispersion of the shape and size distribution. The case when α =1 the ideal case when cells are perfectly homogenous with a spherical shape as proposed by Fricke and Morse [29]. The resistances R_0 and R_∞ are the resistances when $f \to 0$ and $f \to \infty$ respectively [30].

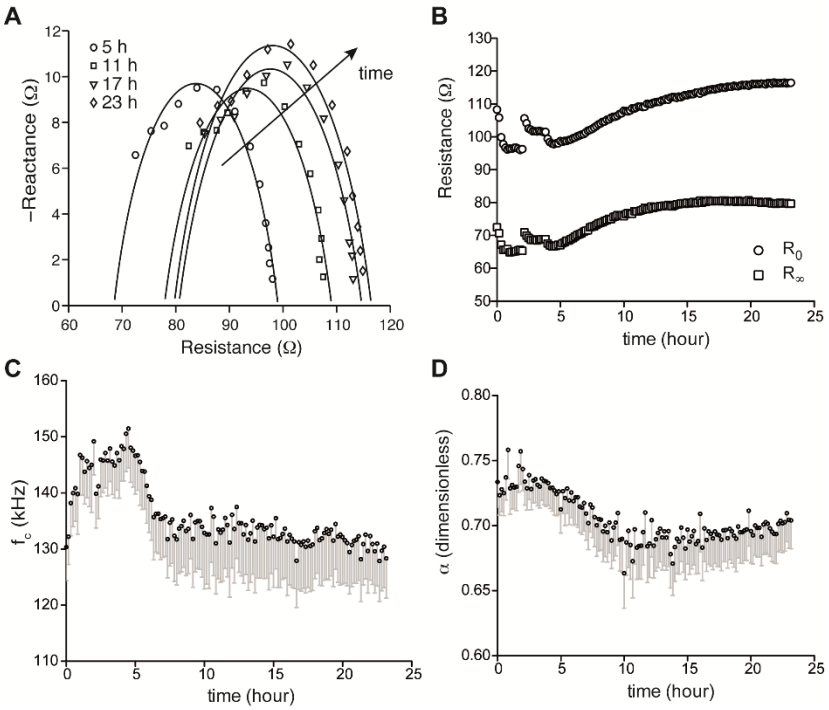

Figure 5.6. Equivalent circuit of the Biofilm Impedance spectroscopy. (A) Representation in the complex plane of the impedance measured with four-electrode method. The solid lines correspond to the Cole fitting. Time course of the impedance model parameters (mean±std); R_0 and R_∞ represent the impedance resistances when $f \to 0$ and $f \to \infty$ (B), f_c is the center frequency of the impedance relaxation (C) and α (dimensionless) the empirical parameter (D).

Figure 5.6A shows the fitting four-electrode impedance data to the Cole model for different time points. It is noted that as the experiment proceeds, the impedance arc moves on the horizontal axis due to an increased resistance caused by cell proliferation. The details of the time evolution of the parameters R_0 and R_∞ are illustrated in Figure 5.6B. The increase in R_0 and R_∞ at 2 hours is due to the same reasons mentioned in the previous section (cooling down of the bacterial preparation). Immediately after, both parameters R_0 and R_∞ started to increase during the first 15 hours. Thereafter, while R_0 continued to increase slightly over time, R_∞ experienced a slight decrease starting at 20 hours. We hypothesis that this decrease might be caused by the metabolic activity of the biofilm, which changes the intracellular ionic concentration of the medium affecting the high frequencies as reported Varshney and Li in 2008[9].

As for the value of the center frequency shown in Figure 5.6C, the high value at the beginning of the experiment (approximately 150 kHz) and the monotonously decreasing evolution from 5 hours reveal structural changes occurring during formation of the biofilm. The high value of the center frequency in the early hours reflects a lower cell dimension corresponding to a few scattered cells on top of the electrode surface. The increase in dimension when cells are clustered forming colonies leads to a reduction in the center frequency (about 130 kHz). Of note, the frequency range in which morphological changes can be detected is in the range of 100 kHz to 200 kHz, where the electrode impedance contribution measured with the two-electrode method might hinder the detection of such changes (Figure 5.7).

The observation in the change in biofilm structure is also supported analyzing the time dependence of the α parameter in Figure 5.6D. At the beginning of the experiment, the value of α is closer to one due to the homogeneity of the cells present on the electrode. The few sparse cells present on the electrode surface still maintain their spherical shape intact. The lower α value explains when cells group together to create colonies [8]. At first, clusters of cells and colonies are of a variety of sizes and therefore more heterogeneous than the initial phase. As the dimensions of the colonies are more homogenous, the alpha value increases towards 1.

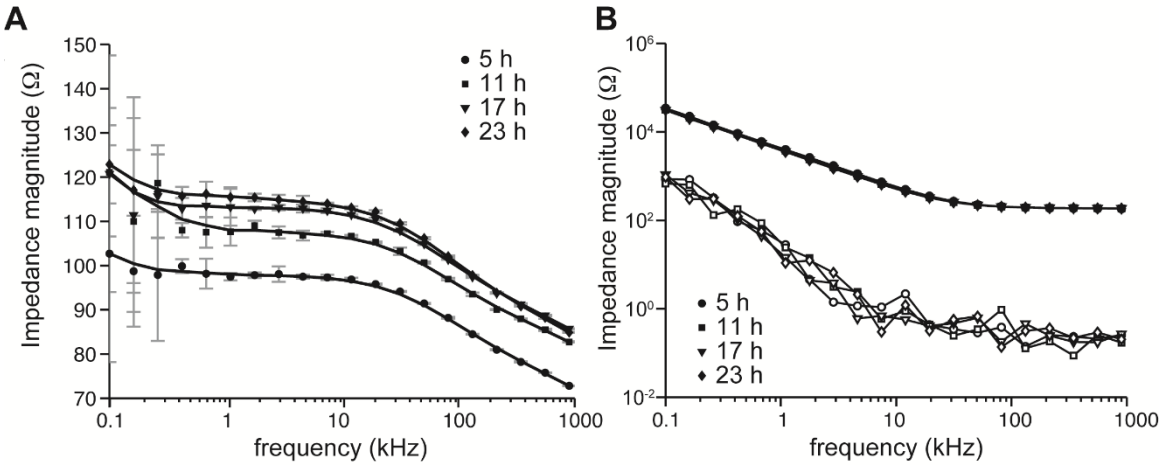

Figure 5.7. Impedance magnitude spectrum (mean±std, n=3) using the rectangular interdigitated microelectrode (IDuE 1) switching between two-electrode (A) and four-electrode (B) methods.

In order to prevent the interpretation of the four-electrode impedance measurements could be influenced by ion concentration changes due to the biofilm metabolic activity [9] or temperature variation effects, it is proposed the use of a ratiometric biofilm estimator *E* following the same reasoning as Soley *et al* in 2005 and Sarró *et al* in 2012[21,31]. The estimator allows obtaining a quantitative measurement of biofilm considering cells above the electrode surface. The estimator is based on the relative variation of the Cole resistances R_0 and R_∞ and it is proportional to the biofilm volume fraction. We use the full expression for the calculation of the propagation of uncertainty σ_E based on the parameters covariance matrix calculated in the fitting procedure, herein

$$E(\%) = 100 \cdot \left(1 - \frac{R_\infty}{R_0}\right)$$
$$\sigma_E(\%) = 100 \cdot \sqrt{\left(\frac{1}{R_0}\right)^2 \sigma_{R_\infty}^2 + \left(\frac{R_\infty}{R_0^2}\right)^2 \sigma_{R_0}^2 - 2\left(\frac{R_\infty}{R_0^3}\right)\mathrm{Cov}(R_0, R_\infty)}. \qquad \text{(Equation 5.2)}$$

Figure 5.8 shows the *E* biofilm density estimator time course. It can be seen that during the first 5 hours, the estimated biofilm density decreased 5% until 7-10 hours, after which it increased progressively during the consecutive 15 hours. The fact that the estimator is far from being saturated at 24 hours value suggests that it is possible to quantify biofilm with four-electrode method performing an experiment that lasts more than 24 hours.

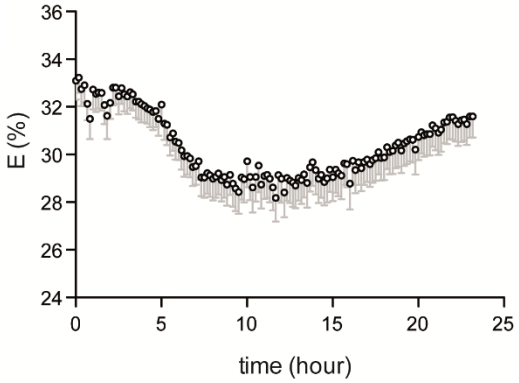

Figure 5.8. Time course of the Cole-based biofilm estimator *E* (mean ± std). Impedance has been shown previously in Figure 6 of impedance data.

5.3 Visualization of Biofilm

5.3.1 Real-time visualization with Differential Interference Microscopy

In order to evaluate the feasibility of the microfluidic platform to monitor biofilm formation on the IDuE, it was performed real-time image recording and impedance measurements simultaneously. Figure 5.9 shows a time-lapse microscopy images indicating the two main steps of biofilm conditioning and formation [3]. In the initial absorption phase (Figure 5.9B-C), the IDuE surface is initially covered by the conditioning film [32,33], a mixture of small molecules (water and salt ions) followed by a single layer of small organic molecules or proteins that are present in the medium. Then, the second stage (Figure 5.9C-D), is characterized by the initially reversible adsorption of microorganisms to the conditioning film, which arrives by Brownian motion, gravitation, diffusion or intrinsic motility [3]. At the same time, bacteria also adhere to each other forming microbial aggregates before adsorbing the conditioning film (Figure 5.9E). Since the bacteria adhere to the conditioning film and not to the IDuE surface, the strength of the initial biofilm will depend on the structure of the conditioning film and/or the flow conditions of the system. The beginning of the third stage starts when the initial biofilm has the enough strength to support the constant flow of fresh TSB media for a long period of time (Figure 5.9G-H). At a certain point during the third stage, the initial reversible adsorption becomes irreversible, mainly through the secretion of EPS by the adsorbed bacteria in the second stage.

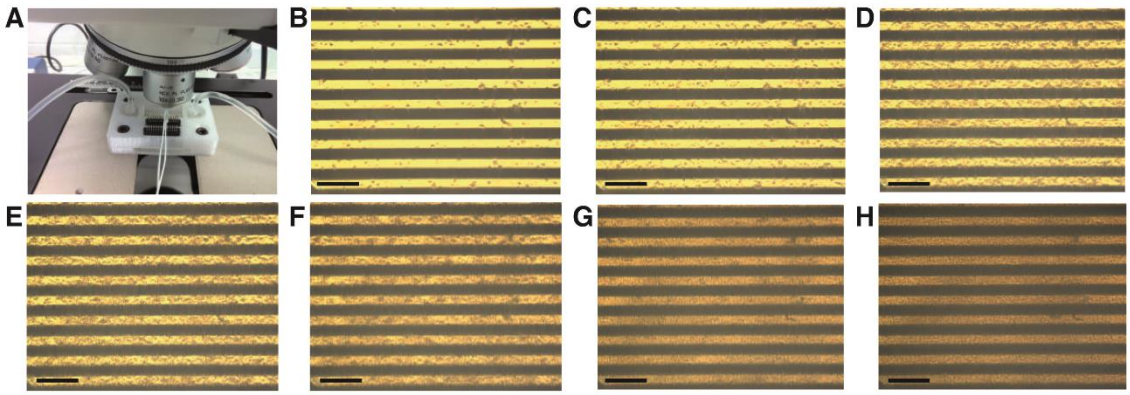

Figure 5.9. Time-lapse of the biofilm. (A) Time-lapse optical microscope (Leica DM2500) at the initial timing just before the bacterial infection; (B), 0 hours; (C), 3 hours; (D), 5 hours; (E), 8 hours; (F), 13 hours; (G), 16 hours; and (H), 21 hours. The time-lapse recording was performed with 1 min interval for 24 hours for editing a video at 25 fps (data available in Annex I). Scale bar: 200 µm.

5.3.2 End-point Scanning Electron microscopy

Biofilms were prepared for scanning electron microscopy (SEM) as described previously[34]. Briefly, the air-dried biofilms were fixed with 2 ml of 2.5% glutaraldehyde in 0.1 mol/L sodium phosphate buffer, rinsed once in the same buffer and then in deionized water followed by an overnight drying. The biosensor was attached to aluminum mounts and coated with gold using a Polaron Emitech SC7640 sputter coater (New haven, UK). Images were obtained with a JEOL JSM-5310 scanning electron microscope (JEOL Ltd., Tokyo, Japan) at 3000X magnification. The final result is the biofilm structure (Figure 5.10), a community of cells which together are medically important as they are highly resistant to both the cells of the immune system and antibiotics and provide a reservoir for future infection[4]. The thickness of the dehydrated biofilm was estimated to be around 100 µm approximately using SEM.

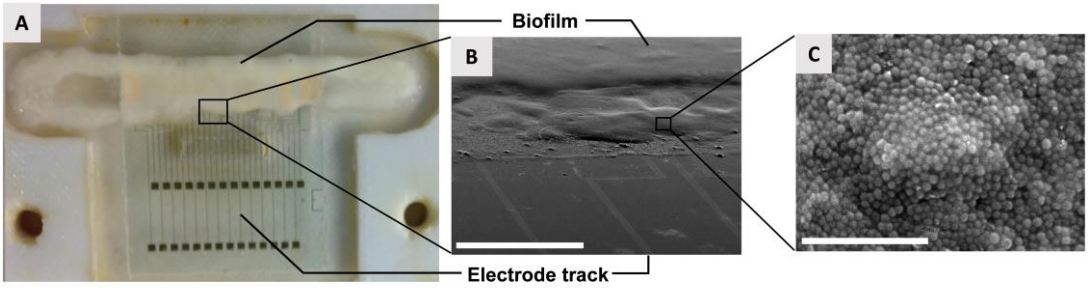

Figure 5.10. No staining microscopy of the biofilm. (A) Presence of biofilm in the flow chamber after the end of a 24 hours experiment. (B) Scanning electron microscopy images showing the biofilm growth on top of the interdigitated microelectrode. (C) Detail of Staphylococcal bacteria attached on IDuE surface. Scale bars: (B), 700 µm; (C), 10 µm.

5.3.3 Confocal Laser Scanning microscopy (CLSM)

The end-point assay was performed immediately after the completion of a 24 hours experiment opening the microfluidic device and staining the IDuE with fluorescence. We used a confocal laser scanning microscope (LSM510 META, Zeiss), controlled with AIM software (version 3.2, Carl Zeiss MicroImaging GmbH, Jena, Germany). The microscope is equipped with two lasers (480 nm syto9 and 490 nm propidium iodide wavelengths) that are used to determine the presence of biofilm alive with Live/Dead Baclight™ Bacterial Viability Kit L13152 from Invitrogen. The staining was carried out for 15 minutes inmediatly after the 24 hour experiment finished and the sensor was washed seven times before it was placed on a coverslip of 60 mm x 24 mm upside down to image the sample.

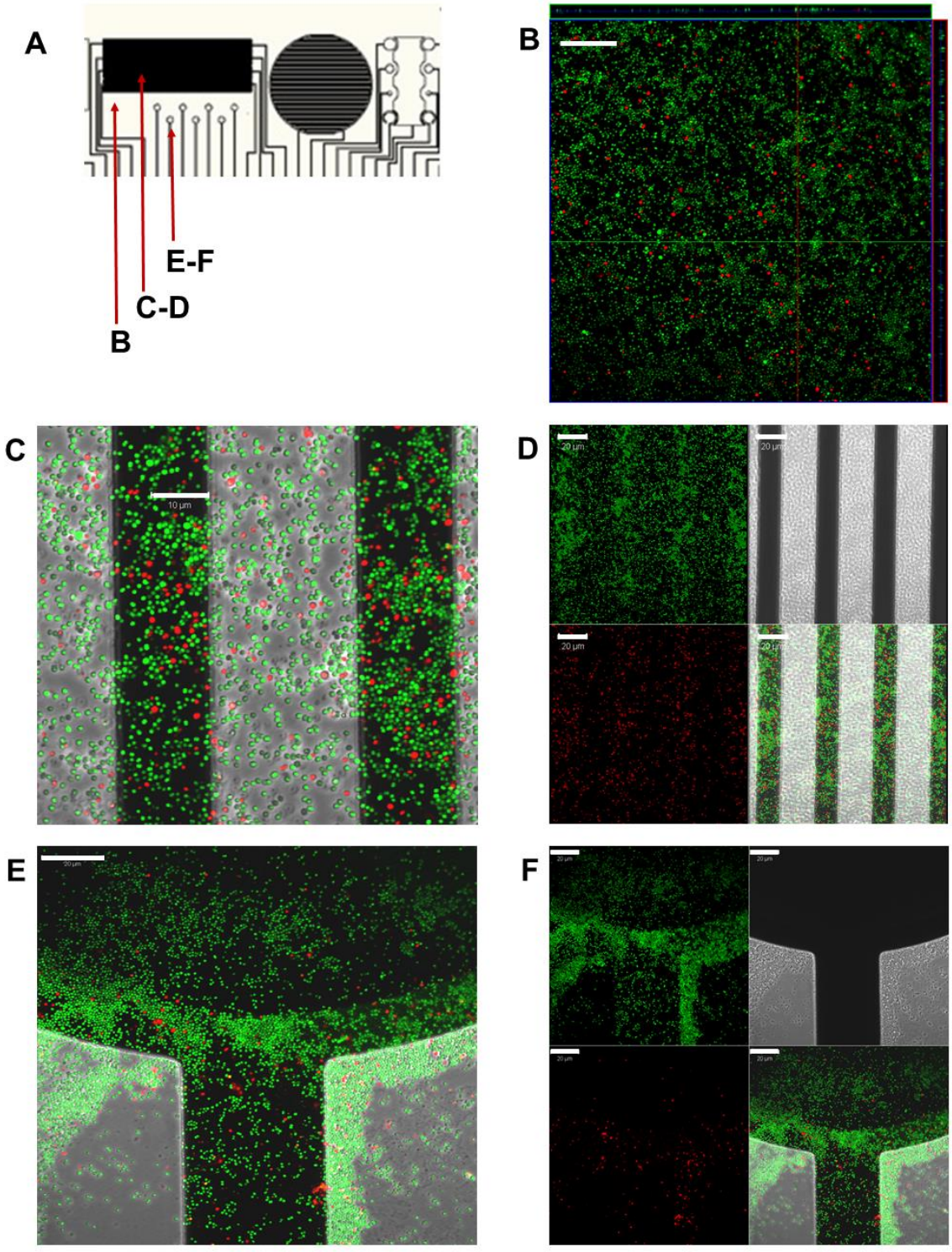

Figure 5.11. Live/dead cell staining in the completion of a 24-hour experiment. Representation of the sensing area of the EIS sensor (A). The non-electrode surface stained (B). In grey, the fingers of the IDuE 1 showing a zoom of the merge (C) and a separated non-zoomed image (D). Punctual rounded electrode in a maximum intensity projection (E) and separation of the two channels (F). Scale bars: (B, D, E, F), 20 µm; (C), 10 µm.

Although most of the bacteria were still alive after 24 hours (Figure 5.11), the number of cells on the electrode was less than expected considering the thickness shown in Figure 5.10B. Even it could be quantified the number of cells by means of colony-forming unit or spectrophotometry, we preferred no to do so to prevent altering the course of the experiment. The disagreement in the estimated biofilm thickness between the SEM experiment and the live and dead experiment was caused by the dry cleaning cycles performed on the stained sample. On the other hand, this result serves to prove the point that biofilm is capable of withstanding high shear forces due to the washing process as compared to the low shear stress of media flowing and SEM preparation.

5.4 Discussion

As it was described above there was a lack of studies performing simultaneous measurements with two and four-electrode configuration, performed in parallel in the same device, for bacterial biofilm studies under flow conditions of culture media. In addition, the impedance coupled to microscopy images conveyed the same results and were in good agreement with the timings and relative changes published in the literature [15]. The novel four-electrode based measurements confirmed an improvement in detecting biofilm formation compared to two-electrode technique as shown by the 5% increased sensitivity, in part because the effect of the electrode-electrolyte was excluded from the measurement and the IDuE was optimized. Perhaps more importantly, we could detect and track biofilm morphological and structural changes by fitting impedance to the Cole model. Unlike the two-electrode method approach based on equivalent electrical circuits, the four-electrode technique along with the Cole-based fitting approach allowed to obtain a quantitative estimate of biofilm estimator free of temperature variations and changes in ionic concentrations. The detected changes by the estimator confirm that it is possible to detect biofilm growth performing experiments that lasts more than 24 hours.

From an application perspective, this method could be employed as a monitoring sensor to health and clinical equipment integrated in a waterline in medical devices or a water purifier. Despite this equipment is in general under clean conditions, every system has possibility to experience a contamination by bacteria and subsequent development of biofilm. Therefore, periodic monitoring by EIS could provide useful information when to react against contamination.

5.5 Final Remarks

The previous studies with EIS for bacterial detection were usually carried out with two-electrode measurements only[35,36]. This chapter have demonstrated that only using this method in its simplest method (two-electrode system) has significant drawbacks, such as low sensitivity of bacterial thickness once the surface is covered, and the masking effects such as temperature changes. This results exhibit the real differences between both configurations measuring a bacterial biofilm formed in the most realistic way, with continuous feeding of nutrients. Also this complex method (four-electrode) allows to interpret the morphological impedance spectrum and structural information regarding the biofilm (Figure 5.8).

In summary this chapter described how the biofilm development has to be monitored to obtain the typical bacterial growth curve (refer to section 2.2.2), however to understand correctly biofilms we need to take into an account that this typical bacterial growth profile has the same shape on any bacterial mode of existence (Planktonic or Biofilm) but the necessary time to complete all the phases of the growth profile suffer changes subjected to a different genetic activation. As long as we need to know what provokes the differences in time to become active compared with planktonic structure, a deeper study has to be performed to understand the biofilm toxicity, which is the real concern about biofilm infections. This study is going to be described in the next chapter with real-time comparison between planktonic and biofilm.

5.6 References

(1) Yang, L.; Liu, Y.; Wu, H.; Song, Z.; Høiby, N.; Molin, S.; Givskov, M. Combating Biofilms. *FEMS Immunol. Med. Microbiol.* **2012**, *65*, 146–57.

(2) Richards, J. J.; Melander, C. Controlling Bacterial Biofilms. *Chembiochem* **2009**, *10*, 2287–94.

(3) An, Y. H.; Friedman, R. J. *Handbook of Bacterial Adhesion*; Humana Press: New Jersey, **2000**.

(4) Del Pozo, J. L.; Patel, R. The Challenge of Treating Biofilm-Associated Bacterial Infections. *Clin. Pharmacol. Ther.* **2007**, *82*, 204–9.

(5) Chandra, J.; Kuhn, D. M.; Mukherjee, P. K.; Hoyer, L. L.; Mccormick, T.; Mahmoud, A.; Cormick, T. M. C.; Ghannoum, M. A. Biofilm Formation by the Fungal Pathogen Candida Albicans : Development, Architecture, and Drug Resistance. *J. Bacteriol.* **2001**, *183*, 5385–5394.

(6) Stewart, P. S.; Costerton, J. W. Antibiotic Resistance of Bacteria in Biofilms. *Lancet* **2001**, *358*, 135–8.

(7) Cady, P.; Dufour, S. W.; Lawless, P.; Nunke, B.; Kraeger, S. J. Impedimetric Screening for Bacteriuria. *J. Clin. Microbiol.* **1978**, *7*, 273–8.

(8) Stoodley, P.; Lewandowski, Z.; Boyle, J. D.; Lappin-Scott, H. M. Oscillation Characteristics of Biofilm Streamers in Turbulent Flowing Water as Related to Drag and Pressure Drop. *Biotechnol. Bioeng.* **1998**, *57*, 536–44.

(9) Varshney, M.; Li, Y. Double Interdigitated Array Microelectrode-Based Impedance Biosensor for Detection of Viable Escherichia Coli O157:H7 in Growth Medium. *Talanta* **2008**, *74*, 518–25.

(10) Yang, L. Electrical Impedance Spectroscopy for Detection of Bacterial Cells in Suspensions Using Interdigitated Microelectrodes. *Talanta* **2008**, *74*, 1621–9.

(11) Gomez, R.; Bashir, R.; Sarikaya, A.; Ladisch, M. R.; Sturgis, J.; Robinson, J. P.; Geng, T.; Bhunia, A. K.; Apple, H. L.; Wereley, S. Microfluidic Biochip for Impedance Spectroscopy of Biological Species. *Biomed. Microdevices* **2001**, *3*, 201–209.

(12) Gomez-Sjoberg, R.; Morisette, D. T.; Bashir, R. Impedance Microbiology-on-a-Chip: Microfluidic Bioprocessor for Rapid Detection of Bacterial Metabolism. *J. Microelectromechanical Syst.* **2005**, *14*, 829–838.

(13) Paredes, J.; Becerro, S.; Arizti, F.; Aguinaga, A.; Del Pozo, J. L.; Arana, S. Interdigitated Microelectrode Biosensor for Bacterial Biofilm Growth Monitoring by Impedance Spectroscopy Technique in 96-Well Microtiter Plates. *Sensors Actuators B Chem.* **2013**, *178*, 663–670.

(14) Paredes, J.; Becerro, S.; Arana, S. Label-Free Interdigitated Microelectrode Based Biosensors for Bacterial Biofilm Growth Monitoring Using Petri Dishes. *J. Microbiol. Methods* **2014**, *100*, 77–83.

(15) Pires, L.; Sachsenheimer, K.; Kleintschek, T.; Waldbaur, A.; Schwartz, T.; Rapp, B. E. Online Monitoring of Biofilm Growth and Activity Using a Combined Multi-Channel Impedimetric and Amperometric Sensor. *Biosens. Bioelectron.* **2013**, *47*, 157–63.

(16) Ehret, R.; Baumann, W.; Brischwein, M.; Schwinde, A.; Stegbauer, K.; Wolf, B. Monitoring of Cellular Behaviour by Impedance Measurements on Interdigitated Electrode Structures. *Biosens. Bioelectron.* **1997**, *12*, 29–41.

(17) Faure, M.; Pallandre, A.; Chebil, S.; Le Potier, I.; Taverna, M.; Tribollet, B.; Deslouis, C.; Haghiri-Gosnet, A.-M.; Gamby, J. Improved Electrochemical Detection of a Transthyretin Synthetic Peptide in the Nanomolar Range with a Two-Electrode System Integrated in a glass/PDMS Microchip. *Lab Chip* **2014**, *14*, 2800–5.

(18) Varshney, M.; Li, Y. Interdigitated Array Microelectrodes Based Impedance Biosensors for Detection of Bacterial Cells. *Biosens. Bioelectron.* **2009**, *24*, 2951–60.

(19) Radke, S. M.; Alocilja, E. C. A High Density Microelectrode Array Biosensor for Detection of E. Coli O157:H7. *Biosens. Bioelectron.* **2005**, *20*, 1662–7.

(20) Paredes, J.; Becerro, S.; Arizti, F.; Aguinaga, A.; Del Pozo, J. L.; Arana, S. Real Time Monitoring of the Impedance Characteristics of Staphylococcal Bacterial Biofilm Cultures with a Modified CDC Reactor System. *Biosens. Bioelectron.* **2012**, *38*, 226–32.

(21) Sarro, E.; Lecina, M.; Fontova, A.; Sola, C.; Godia, F.; Cairo, J. J.; Bragos, R. Electrical Impedance Spectroscopy Measurements Using a Four-Electrode Configuration Improve on-Line Monitoring of Cell Concentration in Adherent Animal Cell Cultures. *Biosens. Bioelectron.* **2012**, *31*, 257–63.

(22) Schwan, H. P. Four-Electrode Null Techniques for Impedance Measurement with High Resolution. *Rev. Sci. Instrum.* **1968**, *39*, 481.

(23) Toledo-arana, A.; Merino, N.; Vergara-irigaray, M.; De, M.; Penade, R. Staphylococcus Aureus Develops an Alternative , Ica-Independent Biofilm in the Absence of the arlRS Two-Component System. *Am. Soc. Microbiol.* **2005**, *187*, 5318–5329.

(24) Tormo, M. A.; Ubeda, C.; Martí, M.; Maiques, E.; Cucarella, C.; Valle, J.; Foster, T. J.; Lasa, I.; Penadés, J. R. Phase-Variable Expression of the Biofilm-Associated Protein (Bap) in Staphylococcus Aureus. *Microbiology* **2007**, *153*, 1702–10.

(25) Yang, L.; Li, Y.; Griffis, C. L.; Johnson, M. G. Interdigitated Microelectrode (IME) Impedance Sensor for the Detection of Viable Salmonella Typhimurium. *Biosens. Bioelectron.* **2004**, *19*, 1139–47.

(26) Zikmund, A.; Ripka, P.; Krasny, L.; Judl, T.; Jahoda, D. Biofilm Detection by the Impedance Method. In *2010 3rd International Conference on Biomedical Engineering and Informatics*; IEEE, **2010**; Vol. 4, pp. 1432–1434.

(27) Cole, K. S. Permeability and Impermeability of Cell Membranes for Ions. *Cold Spring Harb. Symp. Quant. Biol.* **1940**, *8*, 110–122.

(28) Marquardt, D. W. An Algorithm for Least-Squares Estimation of Nonlinear Parameters. *J. Soc. Ind. Appl. Math.* **1963**, *11*, 431–441.

(29) Fricke, H.; Morse, S. The Electric Resistance and Capacity of Blood for Frequencies between 800 and 4(1/2) Million Cycles. *J. Gen. Physiol.* **1925**, *9*, 153–67.

(30) Martinsen, O. G.; Grimnes, S. *Bioimpedance and Bioelectricity Basics, Second Edition*; Academic Press, **2008**; p. 488.

(31) Soley, A.; Lecina, M.; Gámez, X.; Cairó, J. J.; Riu, P.; Rosell, X.; Bragos, R.; Gòdia, F. On-Line Monitoring of Yeast Cell Growth by Impedance Spectroscopy. *J. Biotechnol.* **2005**, *118*, 398–405.

(32) Palmer, R. J.; Kazmerzak, K.; Hansen, M. C. Mutualism versus Independence : Strategies of Mixed-Species Oral Biofilms In Vitro Using Saliva as the Sole Nutrient Source. *Infect. Immun.* **2001**, *69*, 5794–5804.

(33) Murga, R.; Miller, J. M. Biofilm Formation by Gram-Negative Bacteria on Central Venous Catheter Connectors : Effect of Conditioning Films in a Laboratory Model. *J. Clin. Microbiol.* **2001**, *39*, 2294–2297.

(34) Sule, P.; Wadhawan, T.; Carr, N. J.; Horne, S. M.; Wolfe, a J.; Prüss, B. M. A Combination of Assays Reveals Biomass Differences in Biofilms Formed by Escherichia Coli Mutants. *Lett. Appl. Microbiol.* **2009**, *49*, 299–304.

(35) Rafael Gómez, Rashid Bashir, A. K. B. Microscale Electronic Detection of Bacterial Metabolism. *Sensors Actuators B* **2002**, *86*, 198–208.

(36) Radke, S. M.; Alocilja, E. C. A High Density Microelectrode Array Biosensor for Detection of E. Coli O157:H7. *Biosens. Bioelectron.* **2005**, *20*, 1662–7.

Chapter 6 Real-time monitoring of bacterial toxicity using lipid nano-vesicles as biomarker

6.1 Introduction

Once the Electrochemical Impedance Spectroscopy (EIS) platform for on-line monitoring of biofilm has been optimized, there is an additional issue that involves the study of the activation of this biofilm while it is forming. This chapter will study in real time the moment of this activation by introducing a toxicity biosensor as an additional and complementary method to EIS technology described in chapter 5. In order to achieve the additional measurement of the biofilm activation in real-time a toxicity biomarker was required. This biosensor was developed by the group of A. Toby Jenkins from the chemistry department of the University of Bath, and was added to the platform designed thanks to the continuous flow inlet into the EIS device.

As it was described in the general introduction (Chapter 1) the bacterial biofilms are the most common representation of prevalent microbial mode of existence in nature, with estimates suggesting that more than 90% of bacteria exist within biofilms[1]. This mode of existence affords bacteria many advantages over a planktonic existence, including improved adaptation to nutrient deficiency and increased resistance to predation and antimicrobial agents, characteristics that provide biofilms with an extremely difficult control in medical, industrial, and agricultural settings[2]. Biofilm-associated microorganisms have been shown to colonize a wide variety of medical devices, and have been implicated in over 80% of chronic inflammatory and infectious diseases of soft tissues and chronic infections of humans with underlying predispositions[3].

Bacterial biofilm formation proceeds in three main steps described in the introductory chapter: initial adhesion, proliferation, and detachment. A briefly summarize of the stages begins with the adhesion that occur onto any biotic or abiotic surface. Staphylococci bacteria, in this case has an extraordinary capacity to attach to indwelling medical devices through direct interaction with the device surface or by establishing connections to human matrix proteins after those proteins have covered the device. Then, proliferation proceeds through the production of an Extracellular matrix (ECM) that contributes to intercellular aggregation. The creation of a viable biofilm requires channels through which nutrients can penetrate into deeper biofilm layers and also can precede the disruption of cell-cell interactions leading the last step, the detachment of cells and cell clusters from the biofilm. Biofilm detachment plays a critical role during biofilm-associated infection, because it enables cells to spread through the blood and other body fluids to new infection sites[4]. The most important infections are caused by the Gram positive bacteria *Staphylococcus aureus* having an extreme clinical significance based on both their frequency and severity[5].

The structural and developmental complexity of biofilms, and its significance in natural and human-made environments, has been increasingly appreciated over the few years owing to the concomitant development of sophisticated imaging and molecular techniques that have identified the mechanisms that are involved in biofilm development. *In situ* observations of biofilm structure using confocal laser microscopy showed mushroom-like bacteria developed in heterogeneous matrix-enclosed microcolonies interspersed with open water channels[6]. This complex architecture was one of the first indications that biofilm development was not simple and uniform, but rather more complex and differentiated[7], suggesting that secreted molecules can module this architecture. With only one technique is not possible to understand the real behaviour of biofilms itself, nevertheless the conceptualization of dual sensor platform could be the best way to detect the activation of biofilm while development is being monitored.

It has been published that *Staphylococcus aureus* biofilm detachment is controlled by the quorum-sensing system Agr[8]. The enzymes that degrade essential biofilm polymers and contribute to biofilm detachment are surfactant-like molecules, which include *Bacillus subtilis* surfactin, *Pseudomonas aeruginosa* rhamnolipid, and the phenol-soluble modulin (PSM) in *Staphylococcus aureus*. PSMs are staphylococcal peptides with an α-helical, amphipathic structure, which gives them surfactant-like characteristics. *S. aureus* produces four PSMα peptides, which are encoded in the psmα operon, two PSMβ peptides encoded in the psmβ operon, and the RNAIII-encoded δ-toxin[9,10] (Figure 6.1). All of this molecules are also known as bacterial toxins.

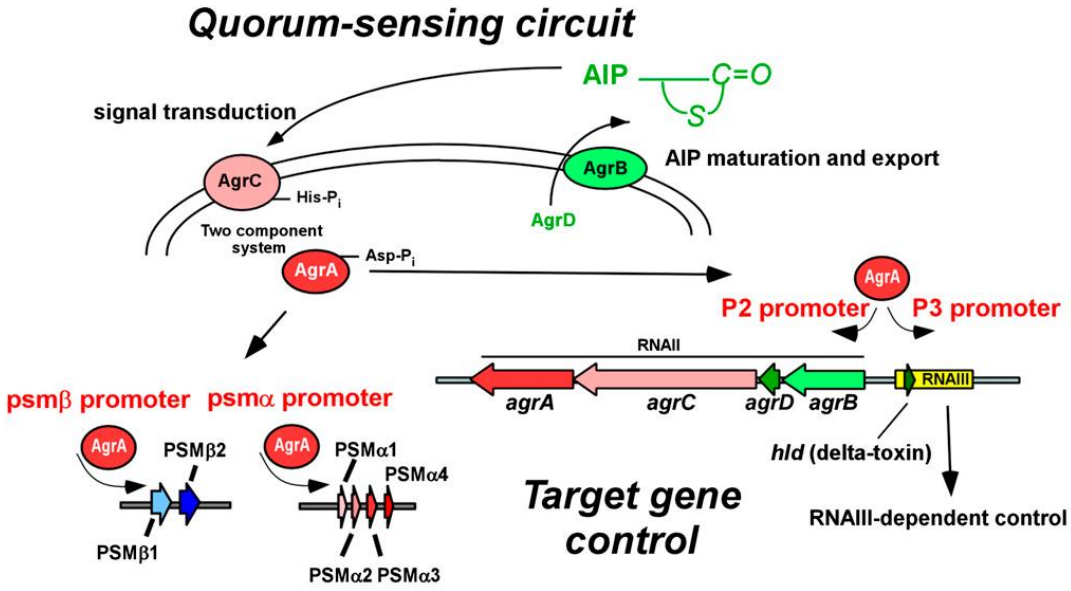

Figure 6.1. Expression of psm and agr promoters in static and dynamic *S. aureus* biofilms and more specifically Agr quorum-sensing control circuit and regulation of target genes. The quorum-sensing circuit is shown at the top. AgrB modifies and exports the AgrD Agr autoinducing peptide precursor, which activates the histidine kinase AgrC. Activated (phosphorylated) AgrA binds to the P2, P3, psmα, and psmβ promoters. The P2 promoter controls expression of RNAII, comprising the agrB, agrD, agrC, and agrA transcripts, which form the basis of the Agr quorum sensing autofeedback mechanism. Most Agr targets other than the psm genes are regulated by the P3-controlled RNAIII, which also encodes the PSM δ-toxin (hld gene).[9]

All the toxins mentioned have recently attracted much attention because they have been found to have a key impact on the pathogenesis of *S. aureus* infections[11]. The multiple roles in staphylococcal pathogenesis, as the lysis of red and white blood cells[12], and the capacity to kill human neutrophils after phagocytosis might explain failures in the development of anti-staphylococcal vaccines[13]. There are many diseases caused by the toxicity in general of *Staphylococus aureus* like bacteraemia, endocarditis, metastatic infections, sepsis or toxic shock syndrome[14], moreover there are also detailed studies focusing only in one type of molecule like δ-toxin, also known as δ-hemolysin, showing the critical role in dermatitis caused by activation of mast cells, which induces allergic skin disease[15]. The export system of the δ-toxin and the other PSM is deeply explained by Chatterjee and coworkers[16], and the pore formation on the lipid membranes was studied by Huyet and coworkers[17] showing the action mechanism of cytotoxicity through molecular modelling, validated with electron micrographs of liposomes affected by δ-toxin. Verdon and coworkers[18] also proposed a putative model that explains deeper the interaction of δ-toxin with membranes (Figure 6.2).

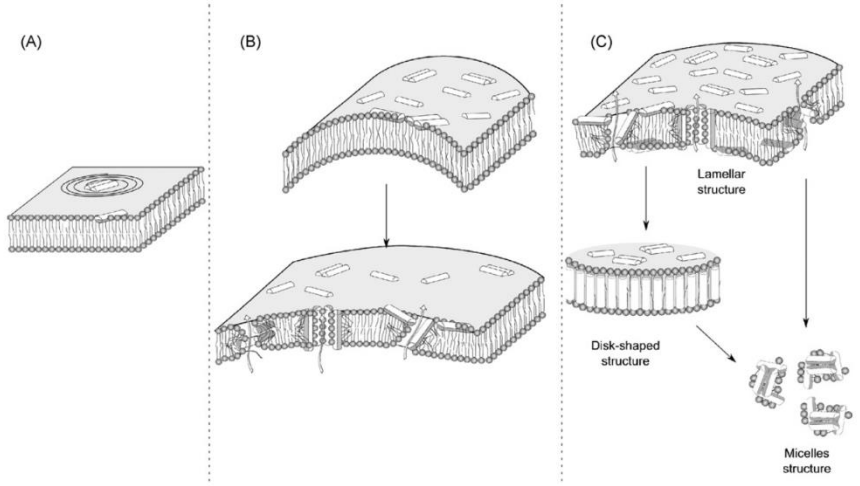

Figure 6.2. Putative model proposed for δ-hemolysin membrane activity describing the sequence of events in function of peptide concentration. The α-helices are shown as cross sections, the lighter parts representing the polar faces and the darker parts the hydrophobic faces. (A) At low concentrations δ-hemolysin adsorbs on the surface of the membrane in a parallel manner, perturbing the bilayer (circles). (B) Membrane-bounded peptides (monomers and dimers) may induce a local curvature strain of the membrane (top). Some peptides self-associate in transient structures across the membrane. They likely form aggregates of peptides that disturb the membrane inducing cytoplasmic efflux. (C) In higher peptide concentration above a threshold results in a detergent-like solubilisation of the membrane. Three populations of lipid particles are shown, representing the gradual membrane disintegration: lamellar structure, disk-shaped structure and micelle structure[18].

The toxicity of the biofilm explained can be detected with Matrix Assisted Laser Desorption Ionization - Time-of-Flight (MALDI-TOF) mass spectrometry (MS)[19], but it is an expensive technique, which is not allowing either the real-time detection. Alternatively detection with lipid vesicles sensitive to δ-toxin was proposed as cheaper methodology previously reported in an elegant work done by Marshall and coworkers[20]. Lipid nanoparticles (LPN) are very useful for carrying molecules internally[21] like carboxyfluorescein, which has a fluorescence property detectable when the lipid membrane of the vesicle is lysed as mentioned before. The synthesis of the vesicles as toxicity biomarker and the stability were carried out based on previous optimization works carried out by Szleifer and Marshall and coworkers, respectively[20,22]. This toxicity takes place during the bacterial growth either planktonic or biofilm structure that should be monitored with a robust and convenient biosensing platform to provide a tool for rapid detection of the pathogenic infection. The technology for this issue could be done with Fibre optical device, however this is not appropriate for thick biofilm[23], but the platform optimized in chapter 5 is able to monitor by Electrochemical Impedance Spectroscopy (EIS) technology thicker biofilms. As described before the platform uses tetrapolar impedance system, instead of bipolar impedance system used more often for

bacterial monitoring in planktonic structure or biofilm with less than 200 µm [24,25]. The platform proposed demonstrates for the first time a fast, highly sensitive, and non-invasive assay for the detection of *Staphylococcus aureus* in a portable, customizable, and reusable biotechnological device. The studies with EIS for bacteria mostly were carried out in static conditions or shaking conditions without media renewal in the bacterial culture, believing that the introduction of flow conditions are fundamental for more detailed understanding of biofilm, which also permits the introduction of sensitive toxicity biomarkers, mentioned above, in the media culture pumped into the designed device (refer chapter 4). In this study the strain *Staphylococcus aureus* V329 isolated from bovine mastitis [26] was used as a model, knowing that it has a common toxicity with human infections differing in some virulence genes among cow, goat, and human isolates[27].

In summary the aim of this chapter was the real-time measurement of biofilm toxicity and compare this toxicity with planktonic structure of the same bacterial isolate. The parameter for measuring the amount of cytolitic virulence factors released by the biofilm is fluorescence intensity which is increased when the vesicles, with carboxyfluorescein inside, are lysed (Figure 6.3). Furthermore the differential activity of both structures was confirmed studying the supernatant activity after 24 hours growth of the same initial concentration of bacteria for planktonic and biofilm development.

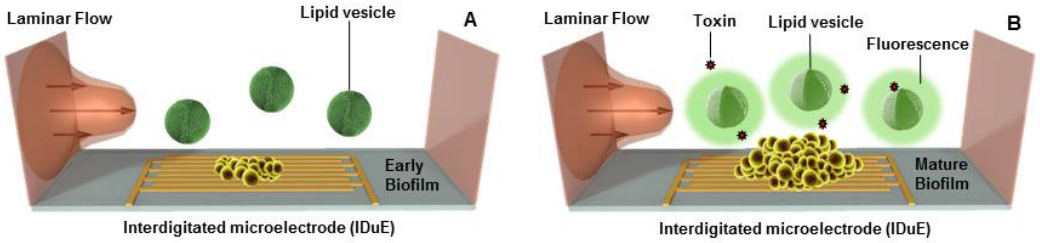

Figure 6.3. Mode of action of the vesicles. (A) Early Biofilm developed in the flow channel feeding TSB with lipid vesicles in solution. (B) Late Biofilm developed in the flow channel feeding TSB with lipid vesicles in solution lysed by the toxin released from the bacterial biofilm, once it occurs inside the flow channel the fluorescence can be observed under UV light and/or detected with florescence plate reader.

The bacterial toxin release studies carried out in the literature required a real-time signal to be observed during its growth. This is an important parameter within the scope of investigation, however detachment and real-time growth development was not ever monitored in parallel. The difficulties associated with obtaining the multiple signal monitored will be also discussed further in this chapter.

6.2 Results

6.2.1 Modification of the buffer solution for bacterial growth

The buffer where the vesicles were dissolved had stablished composition defined by Marshall and co-workers [20] at University of Bath. The composition was optimized for using the bacterial supernatant after certain period of time as described in section 2.2.5. However, in this work further study and refinement of the buffer solution composition was required due to the use of living cells instead of only supernatant, which is used only as end-point assay. After the analysis of the components used for vesicle preparation it was found that Ethylenediaminetetraacetic acid (EDTA) was the only in the literature with certain bacterial adherence inhibition in Gram positive bacteria as *Staphylococcus aureus* V329, and more specifically of *Listeria monocytogenes*[28], evidencing that EDTA affected the bacterial biofilm growth and suggesting that the buffer solution (refer to 2.6) used in this work, required an optimization. For this reason an initial test was carried out using Hepes with and without EDTA, leading a change in buffer composition for living cells studies.

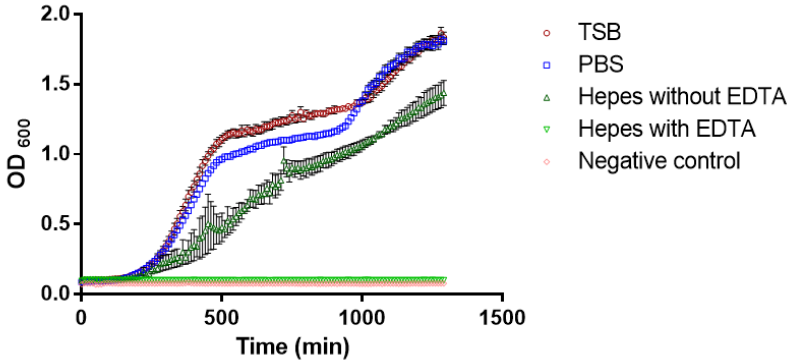

Figure 6.4. Initial test of bacterial biofilm development in static conditions in a 96well. Test at 25% of TSB or PBS or Hepes with and without EDTA. As negative control only TSB was seeded.

6.2.2 Characterization of the lipid vesicles

The vesicle characterization was carried out using two techniques described in chapter 2, Dynamic Light Scattering (DLS)[29] and nanosight tracking analysis (NTA) for size distribution and concentration. The size distribution of 90-120nm was measured by both methods resulting in a very consistent size around 100nm (Figure 6.5A and E).

The concentration was 4,52x10^{12} particles/µl measured by NTA that analyse the Brownian motion of the particle suspension in a certain volume cell, generating the approximation of nanoparticle concentration. A single capture of the nanoparticle suspension was shown in Figure 6.5B. Phospholipids and CHO ordered from Avanti Polar Lipids, TCDA and 5(6)-carboxyfluorescein ordered from sigma were the components that form the cross-linked vesicles in the percentage shown in Figure 6.5C, which is the chosen to satisfy the two biophysical parameters of stability and sensitivity. When the lipid vesicles are stable in aqueous media they are self-quenched whereas a toxin activity that lyses them show a higher fluorescence excitation (Figure 6.5D).

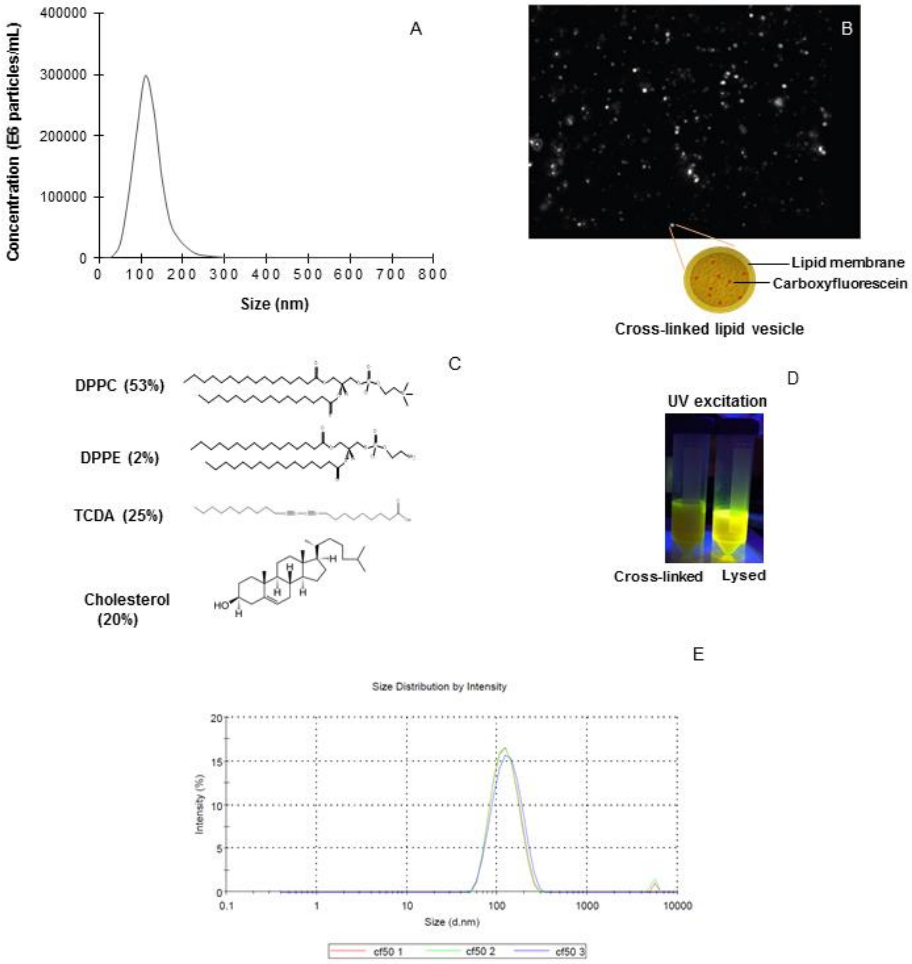

Figure 6.5. Characterization of lipid vesicles. (A) Nanosight sizing of the vesicles gave a mean radius of 114 nm. (B) Video frame of the vesicles in suspension during the Nanosight measurement and the structure of the cross-linked vesicle. (C) Vesicle composition of phosphatidylcholine (PC) lipids, phosphatidylethanolamine (PE) lipids, 10,12-tricosadiynoic acid (TCDA), and cholesterol. (D) Vesicle solution of the self-quenched preparation when is Cross-linked (left) and vesicles are lysed with Triton x-100 detergent (right). (E) Size distribution by intensity measured by Dynamic Light Scattering (DLS).

Another parameter to take into account was the time left before the cross-linking step, which is the last vesicle synthesis step (refer to section 2.6.3). Briefly, when the lipid vesicle with TCDA within the membrane was almost finished, except for the crosslinking step, the vesicles were stored at 4 ºC for certain period of time. The variation of this time could be critical for fluorescence sensitivity and for this reason different storage times were tested with *Staphylococcus aureus* V329 (Figure 6.6A) and *Staphylococcus epidermidis* Ch845 (Figure 6.6B), and compared to the lytic response with the positive control: the surfactant triton x-100, and the non-lytic negative response with HEPES buffer. This incubation was carried out with bacteria supernatant; the separated solution obtained from a bacteria culture following centrifugation and discarding of the pellet (whole bacterial cells). Interestingly in both cases an early crosslinking after 10 hours of storage was the best option to finish the lipid vesicle synthesis and obtain an optimal fluorescence sensitivity. The lipid vesicle test was quantified with the plate reader measurements but the excitation with *UV* lamp was enough to visualize a better signal with less storage time (Figure 6.6D). Despite all different storage times had higher signal than the negative control.

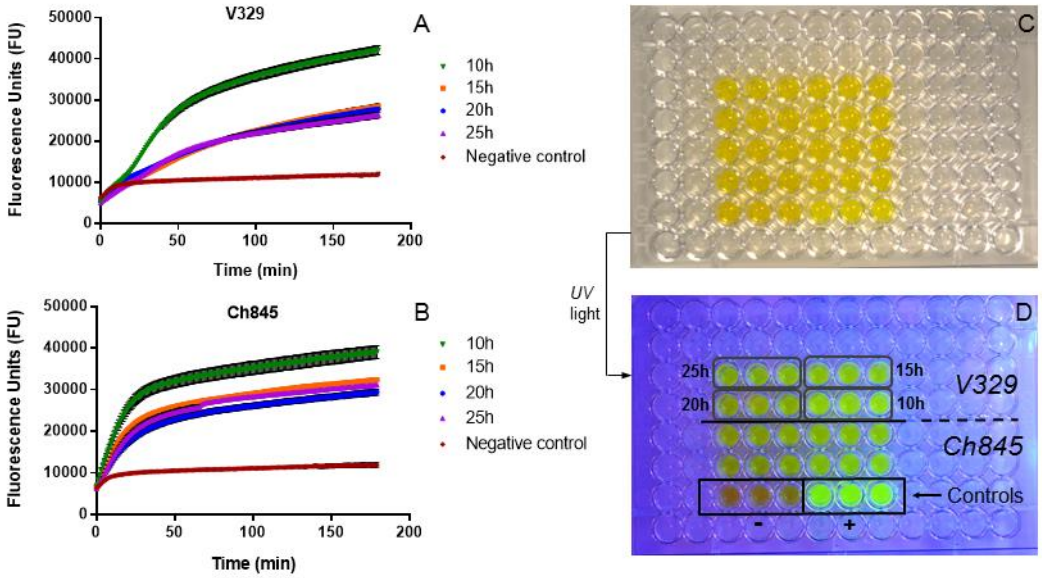

Figure 6.6. Different storage times tested before final crosslinking step in the lipid vesicle synthesis. Different times of 10, 15, 20 and 25 hours were tested with supernatant debris of an overnight growth of planktonic bacterial culture of *Staphylococcus aureus* V329 (A), and *Staphylococcus epidermidis* Ch845 (B). All the conditions were plated and incubated during 3 hours in a 96 well plate (C) and excited with *UV* lamp to visualize the difference between the different storage times (D).

6.2.3 Optimization of vesicle concentration for toxin analysis

The concentration of the lipid vesicles was a parameter to consider when they are used as continuous biomarker during bacterial growth. Three different concentrations were prepared and tested during a 24h with a bacterial biofilm developed in static conditions. The 24 hour plots of fluorescence intensity along the time were represented for 25, 12 and 6% of vesicle preparation as final volume (Figure 6.7). The bacterial growth was seeded with the vesicle preparation in the 96 well plate and the optical density (OD) and fluorescence were recorded for every well, but only the fluorescence signal was represented because the optical density of the three lipid vesicle concentration was no different (data not shown), evidencing that the previous optimization of the buffer solution (refer 6.2.1) was consistent enough to obtain a correct bacterial biofilm development.

Figure 6.7D showed the comparison of the different final concentration of lipid vesicles in the bacterial culture exhibiting the same signal saturation in 25 and 12%, but fluorescence dramatically decreased at a final concentration of 6%. Comparing only the higher concentrations we could determine that 25% provided an adequate signal window for toxin release studies with living bacteria.

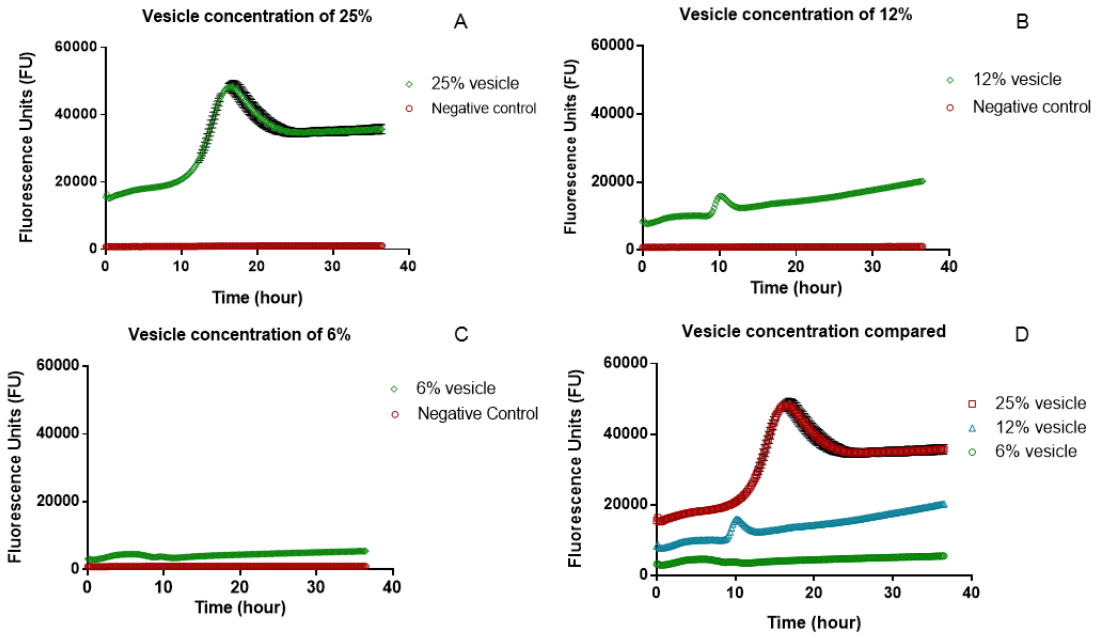

Figure 6.7. Activity for 24 hours of lipid vesicles at different concentrations: (A) 25% as final concentration, (B) 12 % as final concentration, (C) 6 % as final concentration. (D) The three lipid vesicle concentration are represented in a single plot without the controls.

Figure 6.8 showed the 96 well distribution of the different lipid vesicle concentrations, tested with three different microorganisms (quantitative representation only for *S. aureus* V329), with *UV* excitation to discern qualitatively the difference between fluorescence signals. The growth of bacteria in vesicles with Tryptic Soy Broth (TSB) and Triton X-100 was included to ensure that contamination of controls was not occurring.

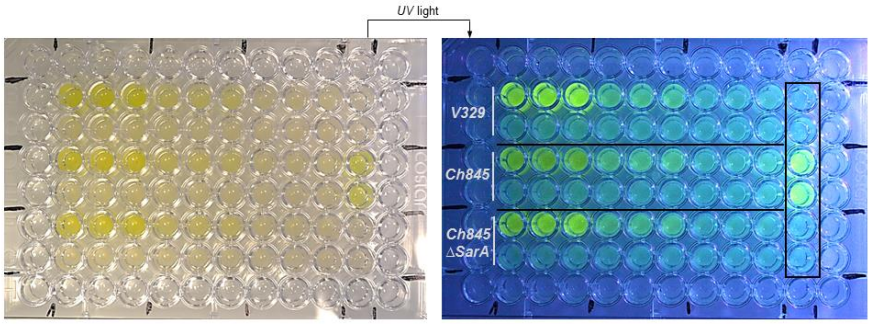

Figure 6.8. The photograph shows the three different vesicle concentrations tested with three different strains taken under visible light (left) and UV light (right).

6.2.4 Online monitoring of Bacterial Biofilm

A schematic diagram of the biofilm growth process is depicted in Figure 6.9 before the analysis of the data provided by the multi-parametric platform. This scheme shows the platform assembled during the biofilm formation, which is monitored by the impedance analyser and the plate reader loaded with samples downstream every hour. The sample loaded in the plate reader was collected for 10 minutes at the outlet of the channel every hour during the experiment (bypassing the bottle WASTE 2 with the sterile Eppendorf). The internal volume of the device is 500 µL hence collecting 10 minutes at a flow rate of 50 µL/min allowed the analysis of the whole internal volume of the channel to monitor the fluorescence and optical density (as described above). During the process of biofilm development the impedance analyser is also multiplexing the reference and the measurement device (Figure 6.9A and B respectively) by switching the measures between devices. The EIS analysis was recorded every 15 minutes and it took 2 minutes to run and overwrite a new file immediately after every measurement. The toxin release study coupled to EIS technology already optimized for biofilms was carried on exactly in the same way of the previous chapter experiments (refer to section 5.2.1) except for the presence of vesicles diluted in the TSB medium.

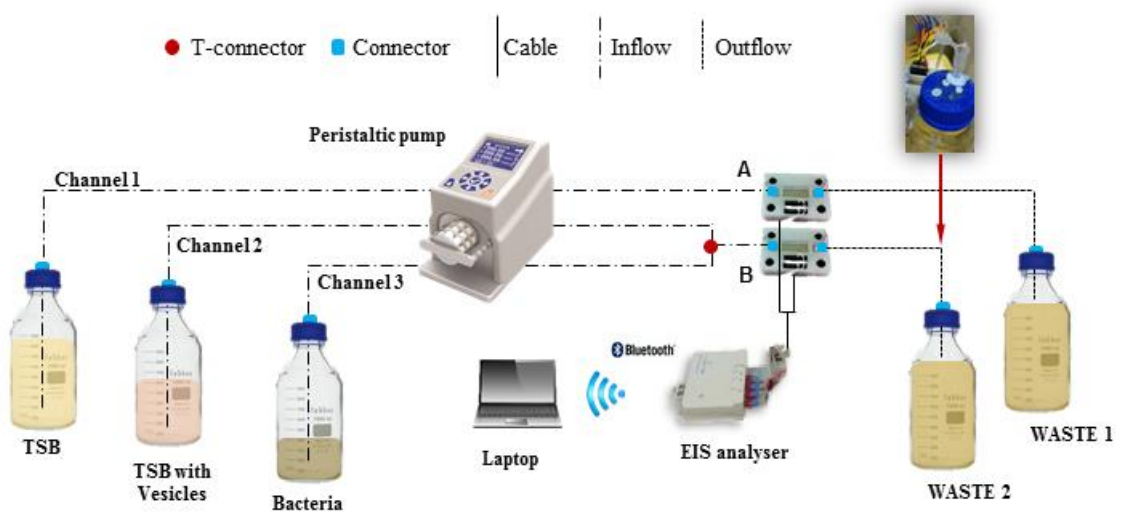

Figure 6.9. Flow diagram of the measurement setup. The system is divided in: (A) reference device and (B) measurement device. The experiment is divided in three stages. The phase 1 (conditioning) is pumping TSB to the reference and the measurement devices with the channel 1 and 2 respectively for 2 hours. The phase 2 (seeding) stops the channel 2 for the measurement device and starts channel 3 for bacteria pumping for 2 hours. The phase 3 (biofilm growth) stops the channel 3 to starts the channel 2 for 16 hours. During the phases two and three the channel 1 is pumping fresh TSB to the reference device during all the experiment.

6.2.4.1 Growth

The initial measurement analysed from the multi-parametric platform was the impedance spectroscopy to visualize the whole process of biofilm formation and development. The impedance analyser multiplex measured the signal at two and four electrode configuration but only the four electrode configuration, of the 2 devices connected in parallel, was depicted (Figure 6.10). The impedance magnitude was obtained from a sweeping of frequencies in a range between 100 Hz to 1 MHz (Figure 6.10C). The attachment of bacterial cells and biofilm development on the IDuE was measured, with the single frequency 10 kHz response found to be most sensitive to the biofilm formation (Figure 6.10A). The representative response of the single frequency of the measurement device showed the beginning of the bacterial exponential phase at around 5 hours, and a levelling off of the signal after 18 hours suggesting that the biofilm has formed and large changes on the electrode dielectric are no longer taking place.

The actual assignment of the various components of the biofilm to different changes in the electrode / film dielectric was deeply analysed in chapter 5 ceasing to be the core purpose of this study. Therefore a pragmatic approach was used, whereby a measureable change in the dielectric that was sensitive to the biofilm formation was taken accepting that many different changes in the electrode – film dielectric will contribute to this value, without (in this study) actually deconvolution the signal to work out what these actually were. Finally the negative control represented (Figure 6.10B) from the four electrode signal at 10 kHz of the reference device, showed a flat profile ensuring that no contamination in the fresh TSB container occurred.

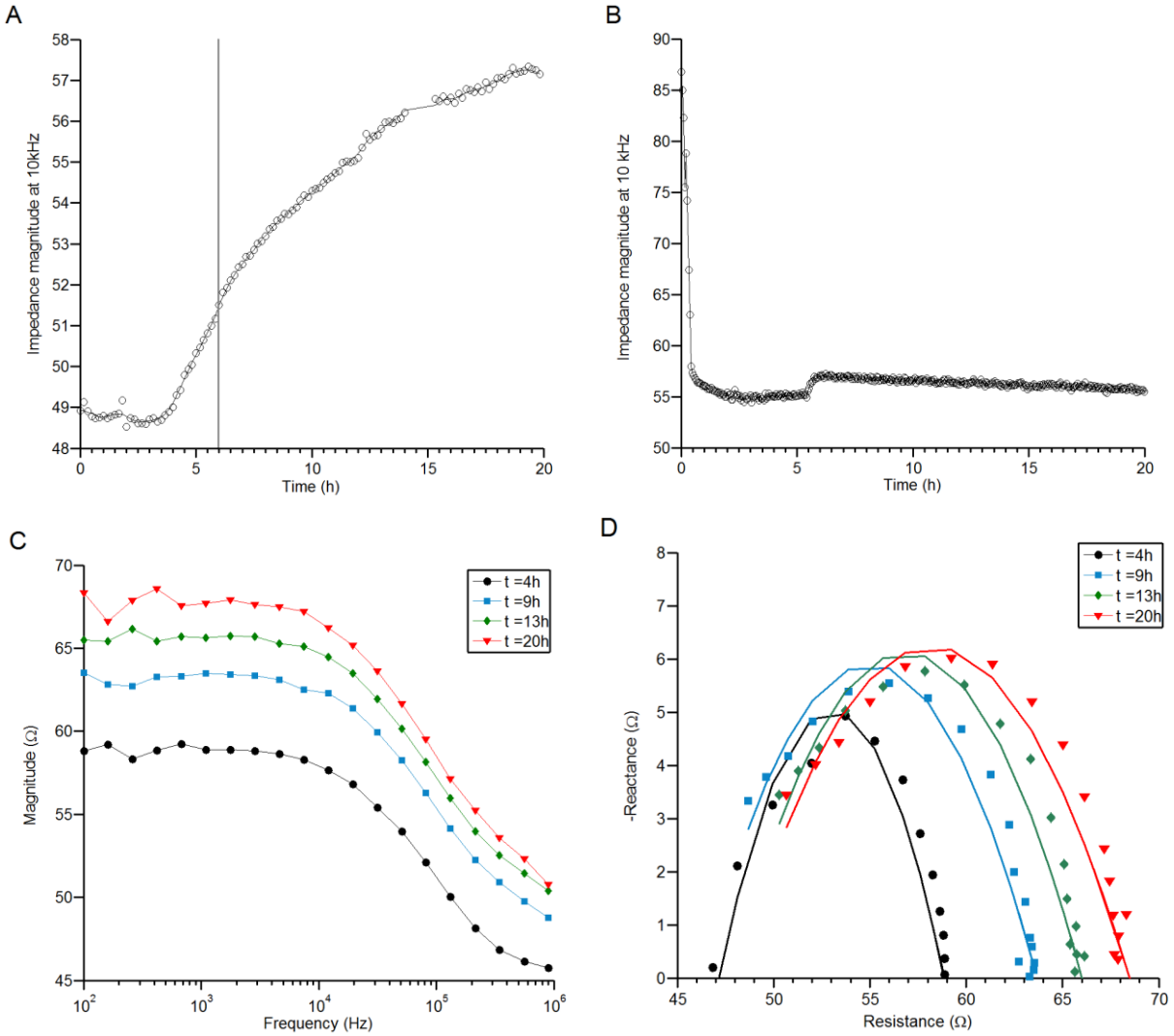

Figure 6.10. Tetrapolar impedance measurement of the devices connected in parallel. (A) Electrical impedance of the measurement device versus time at 10 kHz. (B) Electrical impedance of the reference device (negative control) versus time at 10 kHz. (C) Bode plot of the impedance magnitude at different times of the biofilm monitored. (D) Representation in the complex plane with quadratic fitting of the impedance at different times of the biofilm monitored.

After the biofilm development in the device the biosensor was imaged by Differential Interference Contrast (DIC) zooming into the area selected with a square (Figure 6.11). The biofilm formed on the surface of the electrode was well distinguished in the microscopic image where EPS and *Staphylococcus aureus* were visualized over the IDuE surface, which was the sensing area for EIS measurement.

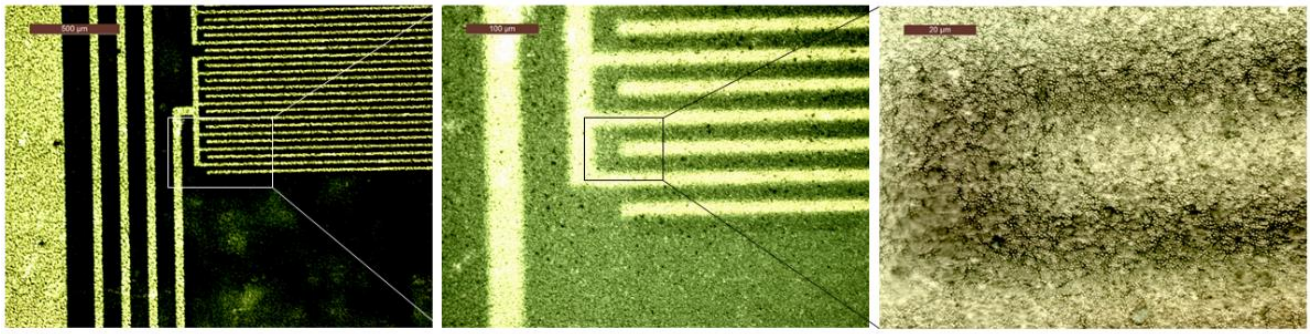

Figure 6.11. Presence of biofilm developed in the flow chamber at the end of the experiment. The image shows the bacterial structure over the interdigitated microelectrode (IDuE) in a detailed pseudo-3D image carried out with Differential Interference Contrast (DIC). Magnifications: (A) 5X; (B) 20X; (C) 100X.

6.2.4.2 Detachment

The optical density (OD) profile was carried out measuring the same sample collected in the outlet channel, in parallel. Figure 6.12 showed an initial increase after 3 hours that quickly reached its maximum level around 5 hours when the signal remained stable. The stability of the signal means that some clumps are detached constantly from the surface to colonize new surfaces, because what is pumped into the device is fresh media without bacteria. The negative control is TSB media measured over the time in parallel with the outlet sample collected from the device.

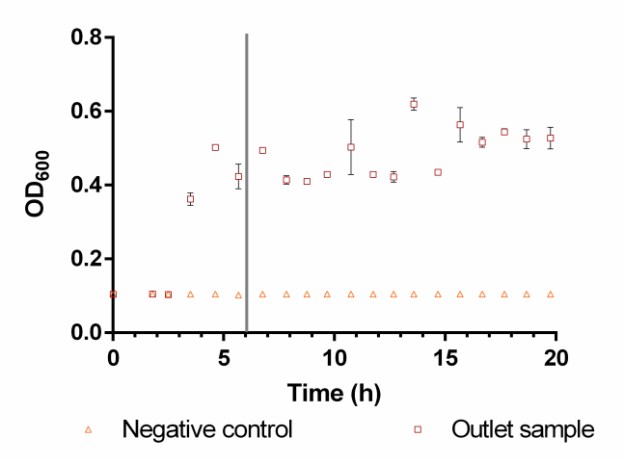

Figure 6.12. Optical Density (OD) measurement of the outlet sample collected during the constant flow experiment from the measurement device compared with negative control.

6.2.4.3 Toxicity

The toxicity of the bacterial biofilm has been monitored by fluorescence using lipid vesicles, which have an internal fluorescent dye only released when the vesicles are lysed by the delta toxin and phenol soluble modulins secreted, as described before. Positive and negative controls of vesicles were measured with Triton X-100 at 0.1% in Hepes and Hepes buffer, respectively, but only the negative control was represented because the values were too high and interpretation the fluorescence detected downstream was easier.

Figure 6.13 showed the fluorescence measured during the biofilm development by collecting the media from the outlet channel and compared with a negative of TSB with vesicles. An increase in fluorescence begins approximately after 6 hours of the experiment, which means that the bacterial culture becomes toxic 2 hours after the fresh media was pumped constantly into the device. The sample collected for 12min every hour was representative of the internal volume of the device because the time of residence of the media culture pumped is about 10 min. The fluorescence becomes stable at 8 hours, indicating that the bacterial culture had a constant expression, synthesis and secretion of toxin molecules to the media.

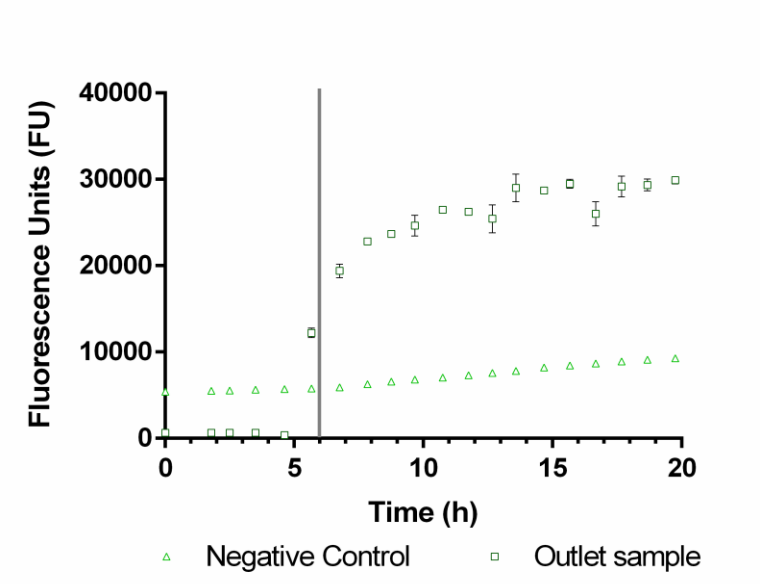

Figure 6.13. Fluorescence measurement of the outlet sample collected during the constant flow experiment from the measurement device compared with negative control.

In parallel with the biofilm toxin release study a different monitoring was setup to follow the vesicle lysis during bacterial growth in planktonic conditions. The analysis of this structure allowed the comparison of real-time monitoring toxicity in planktonic and biofilm structure using living cells instead of supernatant, which is used only for an end-point toxin analysis[20].

The vesicle lysis was monitored by optical density and fluorescence evidencing that vesicle lysis occurs at early stationary phase at OD > 1.0 (Figure 6.14). Downstream from biofilm in the device, the fluorescence was switched on at OD = 0.4 concluding the toxins of the biofilm were the responsible for switching on fluorescence in vesicles not the planktonic bacteria measured at OD 0.5 at the outlet i.e. it is not the detached cells lysing the vesicles, it is the biofilm toxins.

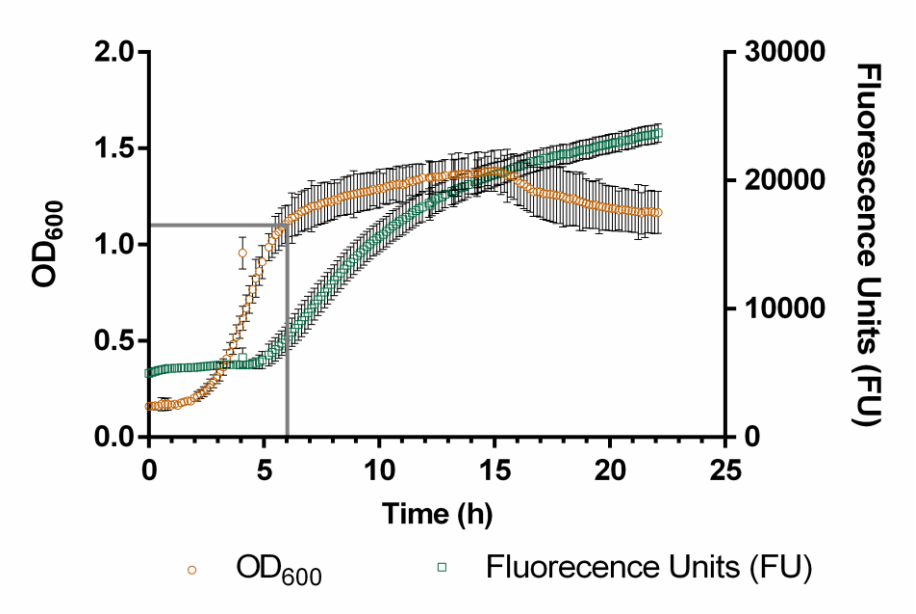

Figure 6.14. Bacteria were grown for 18 h with lipid vesicles monitoring optical density and fluorescence showing a vesicle an evident lysis at early stationary phase.

6.2.5 Comparison of planktonic and biofilm toxin activity

6.2.5.1 Planktonic vs Biofilm in Static conditions

Initially an overnight culture of six different bacterial strains were grown in parallel. Afterwards the bacterial growth of all the strains was optical density monitored in a 96 well plate. The Static Biofilm was grown in a falcon without shaking until the stationary phase (refer section 2.2.2). In parallel another falcon with constant shaking was also grown, which corresponded to Planktonic structure. Both bacterial structures were transferred to an Eppendorf to centrifuge for collecting and filtering the supernatant as

described in section 2.2.5. The toxicity of different strains comparing the two modes of existence (Planktonic and Biofilm) are plotted for 2 hours showing no difference in the fluorescence profiles (Figure 6.15A and B). The toxin activity in vesicles of Hepes and Triton X-100 was included as negative and positive controls, respectively. The difference of the toxin activity could also be visualized qualitatively by looking at the 96 well plate under *UV* lamp (Figure 6.15D), once the activity of the toxins secreted by each strain reached its maximum level.

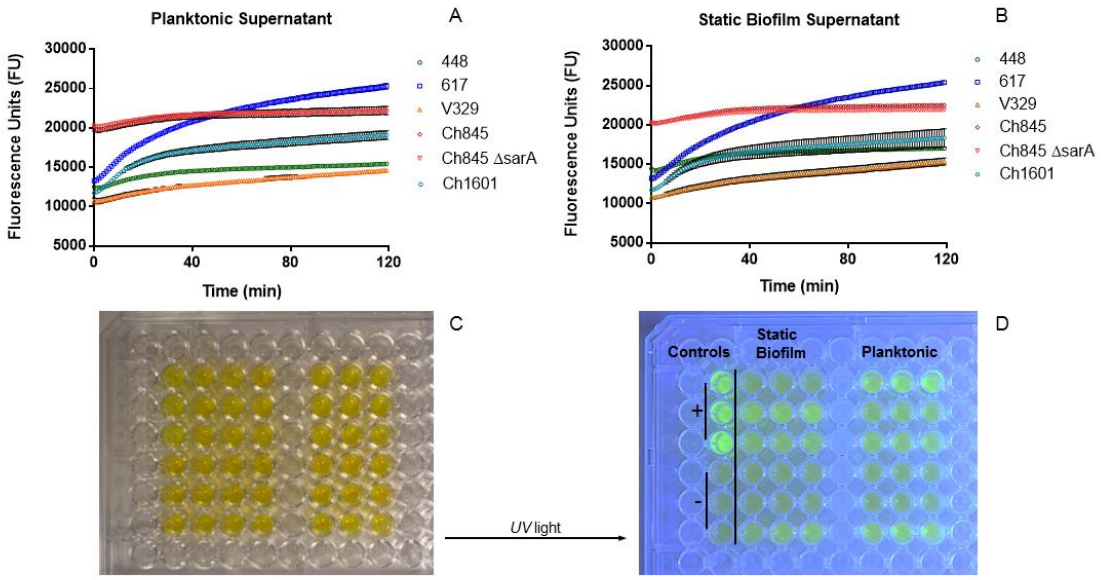

Figure 6.15. Bacterial activity for 2 hours of the supernatant after an overnight culture of six different strains. Vesicles are lysed by the supernatant collected from Planktonic (A) and Static Biofilm (B) cultures. The photos in (C) and (D) are the 96well plate taken under UV light after activity monitoring for 2 hours, and allow for observed differences in fluorescence monitoring planktonic, static biofilm and the controls activity that were placed in the left column.

6.2.5.2 Planktonic vs Biofilm in Flow conditions

The supernatant toxicity assay performed to compare the toxin activity of planktonic and biofilm bacteria grown in flow conditions was carried out running two experiments in parallel for 24 hours to obtain both morphologies supernatant of *Staphylococcus aureus* V329. Planktonic structure was grown in 21 ml of TSB (initial optical density of 0.084) with constant shaking for 24 h then 1 ml of this culture, spun for 10 min at 10,000 rpm using a bench top centrifuge and the supernatant removed and filtered through 0.2 µm filter membranes to ensure all cells were removed. The lytic effect of the supernatant: a mixture of secretion virulence factors and enzymes from the bacteria

on the carboxyfluorescein loaded lipid vesicles was measured on the plate reading fluorimeter (*vide supra*). The biofilm structure was grown inside the fluidic device with bacterial suspension pumped inside the fluidic device during the second stage (seeding) with an initial absorbance of 0.084. Following biofilm formation (after 24 h) the device was disassembled and the biofilm detached using sonication [30] with the bacteria being resuspended in the same volume of TSB as in the planktonic study. 1 ml of the bacteria culture was spun down and the supernatant removed and tested using the carboxyfluorescein assay to assess relative lytic effect of the bacteria primarily resident in the biofilm compared with the planktonic bacteria.

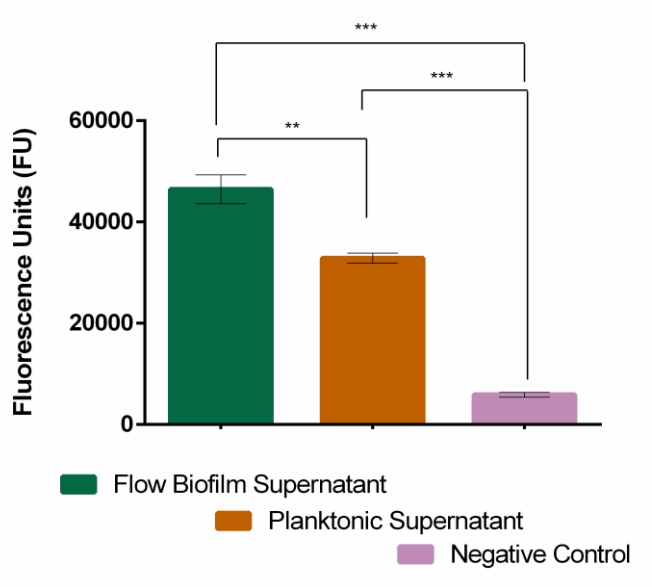

Figure 6.16. Toxicity assay of the supernatant extracted from 24 hour growth of *Staphylococcus aureus* V329 in planktonic compared with biofilm conditions. Both are compared with negative control. Statistical values were reported as means ± SD of triplicates. Differences between toxicity activity were calculated by unpaired t-test with values of **p= 0.0014 between morphologies and ****p<0.0001 comparing the toxicity of both morphologies with the negative control.

Figure 6.16 showed a higher activity in the biofilm morphology when it is well stablished than the planktonic bacteria. The amount of bacteria at of end the cultures was calculated indicating that Colony Forming Units (CFU) were 2.94 x 10^8 and 5.3 x 10^9, for planktonic and biofilm respectively. This last parameter revealed that the biofilm also grew 10 times more than planktonic bacteria. The statistical significance of the toxicity was achieved comparing both morphologies by using the Student t test with 95% confidence intervals, and 99% to compare both with the negative controls exhibiting p-values with statistical significance.

6.3 Discussion

In this chapter it has been demonstrated a two-pronged approach in order to monitor the biofilm formation and the toxicity activity of *Staphylococcus aureus* V329 during the adhesion, proliferation and detachment of the biofilm. First, the EIS sensor placed in the fluidic device (refer to chapter 4) detect the presence of a bacterial film on the electrode surface by measuring the surface impedance with tetrapolar configuration (refer to chapter 5). Second, the lipid vesicles suspended in the culture media, introduced in the inlet channel is used to monitor the toxicity activity of the biofilm when the fluorescence dye is detected due to the lysis activity of the toxin released by the biofilm (Figure 6.3). Both datasets were recorded during the biofilm formation by a custom-made impedance analyser, and a plate reader with sample collected from the outlet channel of the device. Furthermore the optical density of the outlet can also be monitored with the plate reader allowing relating the signal to a continuous detachment of the biofilm. Combining the three signals not only the overall of the biofilm process can be studied, but also its toxicity and detachment. To the best of our knowledge, this is the first work reporting such a combined approach targeting detailed and comprehensive characterization of biofilm formation.

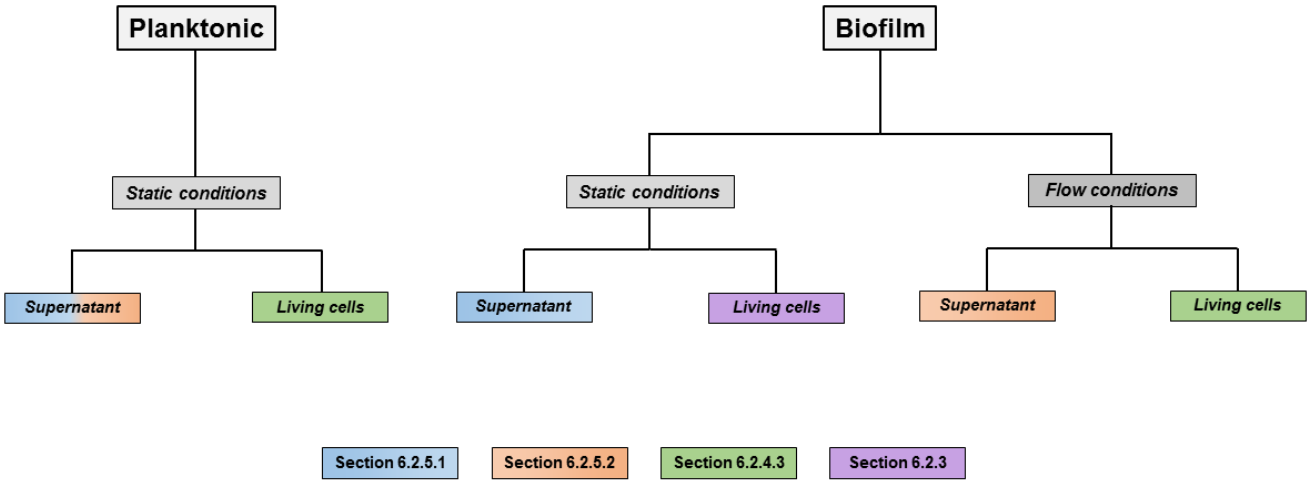

Figure 6.17. Scheme of toxicity tested with different structures. The coincident colours depict the toxicity comparison between Planktonic and Biofilm structure in similar conditions. The comparison test is described in the sections mentioned in the squares below.

Another important issue carried out on in this chapter was the comparison of toxicity between biofilm and planktonic structures. Both are complementary mode of existence and they were compared in similar conditions by studying the supernatant, living cells and the introduction of flow for developing a more realistic biofilm. The conditions compared are illustrated in Figure 6.17, where the coincident colours show the experiments carried on in parallel.

Analysing compared toxicity between planktonic and biofilm structures there is no difference if the biofilm is grown in static conditions (6.2.5.1), but interestingly we find significant difference when planktonic and biofilm structures were compared if this last is grown in flow conditions. It was found a difference in the compared supernatant activity (6.2.5.2), but comparing the signal of the living cells activity there was no significant difference (6.2.4.3), suggesting that this difference was caused by the methodology carried out for supernatant analysis. The supernatant analysis to compare both morphologies was performed to analyse the toxicity of the biofilm by disrupting the biofilm formed to resuspend it, whereas the living cell comparison never touched the biofilm suggesting that some toxic molecules remained embedded in the biofilm structure. However no different fluorescence values were found in the living cell comparison (6.2.4.3) but the moment when toxin activity begins is different being an important issue that gives the biofilm an advantage over the planktonic form because the Figure 6.14 (Planktonic) showed a toxin release when the bacteria is in the stationary phase, whereas an overlapping of Figure 6.10A and Figure 6.13 showed a toxin release as the biofilm forms, not when the biofilm is formed (around 6 hours in both data plots). As this is a real-time monitoring, in both cases the detection of the moment that provokes the toxin release was possible to be compared in both modes of bacterial existence, suggesting that biofilms are a reservoir of toxicity.

Comparing also the fluorescence signal between planktonic supernatant activity of sections 6.2.5.1 and 6.2.5.2 there was a significant difference in the signal when this should be apparently the same preparation of toxin extraction. However the preparation was slightly different due to the time of bacterial growth. The planktonic supernatant extracted to compare with the static biofilm (section 6.2.5.1) was limited only until the end of the exponential phase, whereas the extraction to compare against biofilm in flow conditions (section 6.2.5.2) was a long-term growth. This difference in the supernatant preparation suggest potentially that the higher toxin release activity is taking place at the postexponential phase, supporting the work published by Arya and Princy[12]. This work was precisely fuelling the idea that post-exponential phase was initiating the expression of agr operon and, hence the synthesis of extracellular proteins as δ-toxin

and proteases. The way this quorum sensing system, named accessory gene regulator (Agr), works and leads the regulation of toxin production primarily within *S.aureus* bacteria[31,32] is depicted in Figure 6.18. The complexity of the quorum sensing system, and its role in down-regulation of surface proteins and up-regulation of secreted proteins during *in-vitro* growth[33] is encoded in the Agr locus with a two component divergently transcribed signal systems; the P2 operon – which contains the AgrB, AgrD, AgrC and AgrA genes, and the P3 operon – which consists of the regulatory effector molecule: RNA III and the gene encoding δ-hemolysin (hld).

As future work the relevance and importance of this quorum sensing system could be demonstrated by incubating in the EIS device vesicles tested with *S.aureus* RN6390B, as Agr positive (Agr+) strain i.e. it contains the up-regulatory system gene, and with *S.aureus* RN6911, an Agr negative (Agr-) strain i.e. the gene that codes for the AGR system have been removed. The important point of these possible experiments would be finding an increase of toxicity in the case of Agr+ compared to Agr-, and thanks to the impedance monitoring we could also confirm if there is a reduction of adhesin production (Figure 6.18) resulting in a lower impedance increment during the biofilm development.

Finally, the variation of crosslinking time need further study and chemical analysis to confirm if the storage time before the final step of vesicle preparation (crosslinking) influences the TCDA activity in the membranes which affects the stability of the lipid vesicles.

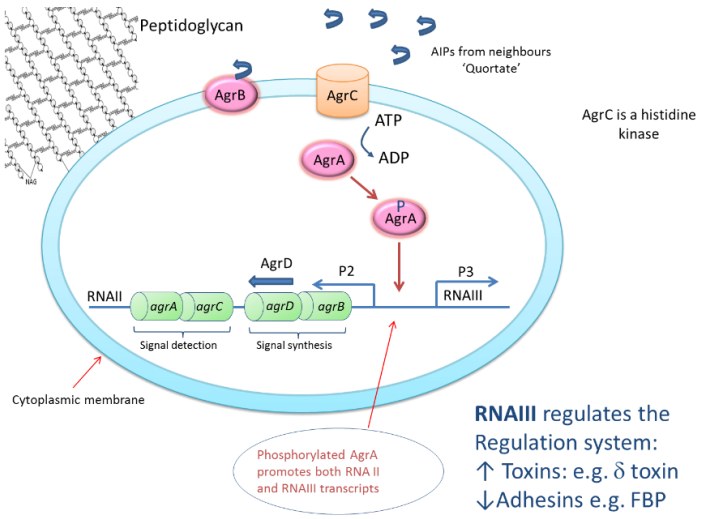

Figure 6.18. Representation of the up-regulated Agr system. Within the P2 operon, AgrA activity results in the secretion of the autoinduing pheromone, AgrD, which consequentially binds and activates the histidine kinase receptor, AgrC, which then subsequently activates the response regulator AgrA.[33] Image acknowledgements to A. T. A. Jenkins.

6.4 Final Remarks

The pathogenic bacteria strain used for investigating the sensitivity of vesicles to toxins released by a biofilm grown under flow conditions have proven effective at lysing the membranes, ensuring effective release of the carboxyfluorescein. The signalling aspect of this system is of large importance in the online monitoring bacterial toxicity, hence it is important with regard to vesicle response coupled to EIS monitoring measurements and optical density analysis, suggesting that biofilms act as reservoir of toxicity production having serious implications for understanding wound and medical device colonization and infection because the *in vivo* process can only be properly understood in terms of biofilm formation.

Furthermore, this methodology of bacterial growth monitoring and toxicity studies coupling could be a good point to use the device in the future as laboratory model for antibiofilm treatment studies. This conceptual studies could be carried out by measuring in real-time with EIS the attempt of bacterial growth onto the surface of the sensor modified with peptide antibiotics or anchored antimicrobial compounds. The methodology typically used for this application is plasma polymerization[34–36] that will be deeply studied in the next chapter for new conceptual methodologies for bioactive surfaces in the antimicrobial field.

6.5 References

(1) Chambers, J. R.; Sauer, K. *Trends Microbiol.* **2013**, *21*, 39–49.

(2) Stoodley, P.; Cargo, R.; Rupp, C. J.; Wilson, S.; Klapper, I. *J. Ind. Microbiol. Biotechnol.* **2002**, *29*, 361–367.

(3) Costerton, A. J. W.; Stewart, P. S.; Greenberg, E. P. *Sci. Mag.* **1999**, *284*, 1318–1322.

(4) Otto, M. *Curr. Top. Microbiol. Immunol.* **2008**, *322*.

(5) Otto, M. *Cell. Microbiol.* **2012**, *14*, 1513–1521.

(6) Wagner, M.; Ivleva, N. P.; Haisch, C.; Niessner, R.; Horn, H. *Water Res.* **2009**, *43*, 63–76.

(7) Hall-Stoodley, L.; Costerton, J. W.; Stoodley, P. *Nat. Rev. Microbiol.* **2004**, *2*, 95–108.

(8) Cheung, a L.; Koomey, J. M.; Butler, C. a; Projan, S. J.; Fischetti, V. a. *Proc. Natl. Acad. Sci. U. S. A.* **1992**, *89*, 6462–6466.

(9) Periasamy, S.; Joo, H.-S.; Duong, A. C.; Bach, T.-H. L.; Tan, V. Y.; Chatterjee, S. S.; Cheung, G. Y. C.; Otto, M. *Proc. Natl. Acad. Sci. U. S. A.* **2012**, *109*, 1281–1286.

(10) Laabei, M.; Jamieson, W. D.; Massey, R. C.; Jenkins, a T. a. *PLoS One* **2014**, *9*, e87270.

(11) Wang, R.; Braughton, K. R.; Kretschmer, D.; Bach, T.-H. L.; Queck, S. Y.; Li, M.; Kennedy, A. D.; Dorward, D. W.; Klebanoff, S. J.; Peschel, A.; DeLeo, F. R.; Otto, M. *Nat. Med.* **2007**, *13*, 1510–1514.

(12) Arya, R.; Princy, S. A. *Future Microbiol.* **2013**, *8*, 1339–1353.

(13) Peschel, A.; Otto, M. *Nat. Rev. Microbiol.* **2013**, *11*, 667–673.

(14) Lowy, F. D. *N. Engl. J. Med.* **1998**, *339*, 520–532.

(15) Nakamura, Y.; Oscherwitz, J.; Cease, K. B.; Chan, S. M.; Muñoz-Planillo, R.; Hasegawa, M.; Villaruz, A. E.; Cheung, G. Y. C.; McGavin, M. J.; Travers, J. B.; Otto, M.; Inohara, N.; Núñez, G. *Nature* **2013**, *503*, 397–401.

(16) Chatterjee, S. S.; Joo, H.; Duong, A. C.; Dieringer, T. D.; Vee, Y.; Song, Y.; Fischer, E. R.; Cheung, G. Y. C.; Li, M.; Otto, M. *Nat. Med.* **2013**, *19*, 364–367.

(17) Huyet, J.; Naylor, C. E.; Savva, C. G.; Gibert, M.; Popoff, M. R.; Basak, A. K. *PLoS One* **2013**, *8*, e66673.

(18) Verdon, J.; Girardin, N.; Lacombe, C.; Berjeaud, J.-M.; Héchard, Y. *Peptides* **2009**, *30*, 817–823.

(19) Gagnaire, J.; Dauwalder, O.; Boisset, S.; Khau, D.; Freydière, A.-M.; Ader, F.; Bes, M.; Lina, G.; Tristan, A.; Reverdy, M.-E.; Marchand, A.; Geissmann, T.; Benito, Y.; Durand, G.; Charrier, J.-P.; Etienne, J.; Welker, M.; Van Belkum, A.; Vandenesch, F. *PLoS One* **2012**, *7*, e40660.

(20) Marshall, S. E.; Hong, S.-H.; Thet, N. T.; Jenkins, a T. a. *Langmuir* **2013**, *29*, 6989–6995.

(21) Hadinoto, K.; Sundaresan, A.; Cheow, W. S. *Eur. J. Pharm. Biopharm.* **2013**, *85*, 427–443.

(22) Szleifer, M. J. U. and I. *Faraday Discuss.* **2013**, *161*, 177–303.

(23) Tamachkiarow, A and Flemming, H.-C. *Water Sci. Technol.* **2003**, *47*, 19–24.

(24) Mcgraw, S. K.; Alocilja, E.; Senecal, K.; Senecal, A. *J. Appl. Biosens.* **2012**, *1*, 36–43.

(25) Varshney, M.; Li, Y. *Biosens. Bioelectron.* **2009**, *24*, 2951–2960.

(26) Tormo, M. A.; Ubeda, C.; Martí, M.; Maiques, E.; Cucarella, C.; Valle, J.; Foster, T. J.; Lasa, I.; Penadés, J. R. *Microbiology* **2007**, *153*, 1702–1710.

(27) Chu, C.; Wei, Y.; Chuang, S.-T.; Yu, C.; Changchien, C.-H.; Su, Y. *Foodborne Pathog. Dis.* **2013**, *10*, 256–262.

(28) Chang, Y.; Gu, W.; McLandsborough, L. *Food Microbiol.* **2012**, *29*, 10–17.

(29) Enoki, T. a; Henriques, V. B.; Lamy, M. T. *Light scattering on the structural characterization of DMPG vesicles along the bilayer anomalous phase transition.*; Elsevier Ireland Ltd, 2012; Vol. 165.

(30) Monsen, T.; Lövgren, E.; Widerström, M.; Wallinder, L. *J. Clin. Microbiol.* **2009**, *47*, 2496–2501.

(31) Bunce, C.; Wheeler, L.; Reed, G.; Musser, J.; Barg, N. *Am. Soc. Microbiol.* **1992**, *60*, 2636–2640.

(32) Cheung, A. L.; Eberhardt, K. J.; Chung, E.; Yeaman, M. R.; Sullam, P. M.; Ramos, M.; Bayer, A. S. *J. Clin. Invest.* **1994**, *94*, 1815–1822.

(33) Novick, R. P.; Ross, H. F.; Projan, S. J.; Kornblum, J.; Kreiswirth, B.; Moghazeh, S. *EMBO J.* **1993**, *12*, 3967–3975.

(34) Khalilpour, P.; Lampe, K.; Wagener, M.; Stigler, B.; Heiss, C.; Ullrich, M. S.; Domann, E.; Schnettler, R.; Alt, V. *J. Biomed. Mater. Res. B. Appl. Biomater.* **2010**, *94*, 196–202.

(35) Duque, L.; Menges, B.; Borros, S.; Förch, R. *Biomacromolecules* **2010**, *11*, 2818–2823.

(36) Vasilev, K.; Sah, V.; Anselme, K.; Ndi, C.; Mateescu, M.; Dollmann, B.; Martinek, P.; Ys, H.; Ploux, L.; Griesser, H. J. *Nano Lett.* **2010**, *10*, 202–207.

Chapter 7 Surface Modification

7.1 Introduction to biofilm treatment

The previous chapters have shown an approach to monitor the growth, development and toxicity of bacterial biofilms in real-time. The techniques harnessed for the label-free bacterial detection were QCM-D (chapter 3) and EIS (chapter 5) technologies. Both methods have demonstrated a potential sensitivity for this issue working under continuous flow of sterile TSB medium. The versatility of the methods open up the possibility of using them as a tool for testing the bacterial response to antimicrobial treatments.

In recent years, a variety of new technologies have been proposed that allow more rapid microbiological analyses. The new microbiological testing technologies provide many benefits in comparison with conventional methods, in terms of precision, sensitivity, objectivity and quickness of response. In the previous chapter the optimization of a platform was performed to offer also real-time results. In the field of implant infections, these new technologies offer valuable support and promise real advancements toward possible solutions, in particular infection diagnosis.

As described in chapter 1 *Staphylococcus aureus* is the main agent in implant infection acting as opportunistic pathogen[1], for this reason is fundamental the development of new targeted strategies of treatment. With regard to the treatment of implant infections, biofilm infections give rise to major concerns about their ability to resist medical therapies and surgical explorations. Therefore, the search for strategies for controlling biofilm infections arouses lively interest in the microbiology field, together with full attention toward finding new means to eradicate them[2].

Given the resistance of biofilms to conventional antimicrobial compounds, most implant-associated infections have a chronic course. Frequently, surgical removal of the prosthesis, debridement of the site, and re-implantation of the prosthesis are the only recourse[3].

Alternatively, biofilm-detaching agents may represent a potentially useful clinical strategy for eradicating implant infections related to biofilm. Among many agents taken into consideration for staphylococcal biofilm disruption, enzymes able to attack biofilm components appear the most rational and promising. Besides the proposal of innovative enzymatic treatments promoting biofilm destruction, the use of antibiotics efficacious against bacterial biofilm is also under investigation[4].

Even though innovative treatments against implant infections are emerging, the total number of implant infections is destined to increase further, due to the increase of patients, surgeries and new antibiotic-resistant bacterial strains. Therefore control strategies must rely on prevention instead of post-infection treatment. There are many studies addressed to the development of infection-resistant biomaterials, such as material doped with effective antimicrobial drugs or resurfaced to repel bacterial adhesion[5]. However, there is a lack of studies for testing the effectivity of the antimicrobial compounds working under flow regime, which is more similar to *in vivo* condition in spite of working *in vitro*. As mentioned above, the design for screening biofilm response to some antibiotic agents have demonstrated a great potential tool for prediction of *in vitro* models of biofilm-related infections[6–8]. In consequence, this chapter is going to describe different approaches for testing bacterial response to different modified surfaces.

In a previous work Humblot *et al* in 2009[9] performed a study reporting the antimicrobial activity over thin gold surfaces (similar to QCM-D and EIS sensors) exposing grafted magainin I, a 23 amino acid-long linear peptide produced by an amphibian; magainin I interacts with lipids of bacteria and fungi cell membranes[10]. The modified surfaces showed to display an antimicrobial activity via a putative bacteriostatic mode of action[11]. Although magainin showed an effective interaction with the pathogen membrane, a different antibiotic peptide named Bacitracin was selected for this chapter.

The mode of action of this antibiotic provokes a bacterial inhibition by acting on three different points. The first one affects the biosynthesis of peptidoglycan, present in the bacterial wall. This synthesis involves the transfer of a sugar peptide unit from uridine nucleotide precursors of the cell wall to the C_{55} isoprenyl pyrophosphate, which facilitates the transfer of the cell wall building units across the cytoplasmic membrane. The lipid C_{55} isoprenyl pyrophosphate acts as a carrier through the dephosphorylation into a monophosphate form, which is required for the reaction with the UDP sugars.

Bacitracin is a cyclic peptide antibiotic that inhibits the dephosphorylation of the lipid carrier by forming a complex lipid-antibiotic, which is very strong and specific to this phospholipid. Due to the complex the lipid carrier cannot recycle in the cell wall biosynthesis, inhibiting this process ceasing the bacterial growth.

A part from the bacterial wall biosynthesis, Bacitracin in second term affects the permeability of the plasma membrane because this lipid is also an integral component of the membrane, and this binding provokes modifications in permeability [12,13].

The third point of bacterial inhibition has been recently described[14] and involves the degradation of nucleic acids. Such an ability of bacitracin was a surprising observation because no other antibiotic available showed similar capabilities. This ability to degrade nucleic acids is especially active against RNA molecules, but also has the capability of degrading single-stranded DNA, however it requires higher antibiotic concentrations. Furthermore, this antibiotic can affect the formation of biofilm when the treatment is at early or late stages, differentially to other antibacterial compound like mupirocin that only affects early stages[15]. For these reasons bacitracin is able to affect gram positive and gram negative bacteria either, being one of the polypeptide antibiotics with more potential for antimicrobial therapy[16], especially in *Staphylococcus aureus*.

The use of this antibiotic in both microfluidic devices (QCM-D and EIS platforms) is going to be studied along this chapter for guiding the development of novel anti-biofilm strategies in vitro that better address future anti-bacterial implants. To perform bacterial susceptibility the working conditions are going to be equal to chapter 5, keeping the flow rate and temperature fixed as long as the bacterial strain (*Staphylococcus aureus* V329), so the changes are associated to the antibacterial treatment applied.

The surface modification of the sensors was the key factor in this chapter to build an antimicrobial coating with the antibiotic described (bacitracin), with low thickness to increase the stability of the thin layer. To address this issue two different approaches of immobilization were described subsequently.

The first approach was performed to attach the antibiotic covalently onto the surface by using a method developed in our group[17,18]. Summarizing, this method begins with a Pentafluorophenyl methacrylate (PFM) coating, which contains a high number of reactive ester groups. These reactive groups could be used to bind biomolecules promoting active coatings for different biomaterials (Figure 7.1). In the present work, it was intended to take advantage of the high reactivity of PFM esters to attach the peptide antibiotic via covalent bonding onto both QCM-D sensors. As a preliminary study, it has been analysed the effect of a plasma polymerized PFM coating onto a QCM-D gold sensor with subsequent bacitracin adsorption. As the coating contains reactive groups towards the amino groups present in bacitracin (red circles – Figure 7.1), an adsorption on the modified surface was expected. Moreover, thanks to the PFM coating the vast majority of Bacitracin molecules are going to be attached on the substrate via covalent bonding instead of electrostatic interactions, therefore a lower antibiotic detachment was expected.

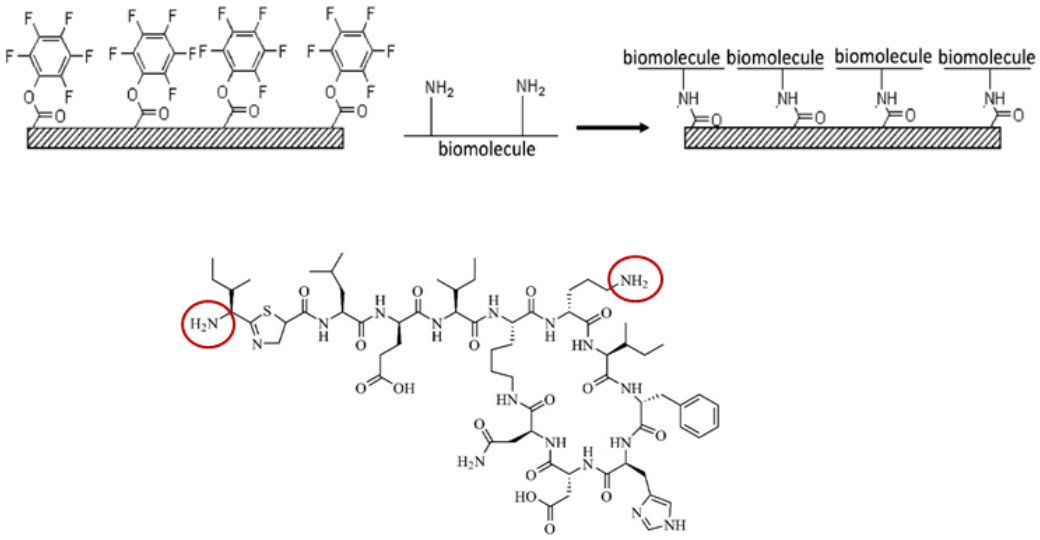

Figure 7.1. General description of biomolecules interacting with Pentafluorophenyl methacrylate (PFM)[19] coated previously with plasma polymerization (Top). The biomolecule utilized to interact with the modified surface through the amino groups highlighted with circles (Bottom).

The second methodology for antibiotic immobilization was performed by coating hydroxyethylene methacrylate (HEMA) onto the sensors[20,21]. The process performed for the pHEMA coating was plasma polymerization and allowed the deposition of geometries not limited to planar surfaces. Although the modification was performed over sensor and presumably one could think about possible interference in the signal, a previous study demonstrated the stability of the impedance signal using two electrode[22] and four electrode[23] impedance systems. These results showed identical impedance response signals for both coated and uncoated sensors. Therefore, the plasma polymerization process does not seem to damage the sensor functionality.

The polymer network was well described by Mary-Buyé *et al* in 2009 [24]. Then, taking advantage of the polymer conformation the antibiotic was trapped inside the pHEMA coating afterwards by placing a drop of bacitracin dissolved in milliQ water until evaporation. After that a second pHEMA thin layer was polymerized to immobilize the non-trapped antibiotic increasing even more the stability of the antimicrobial coating to constant flow. In order to check the potential of such techniques both QCM-D and EIS sensor were tested. The characterization of the double layer deposited with approximately 100 nm of pHEMA was carried out with SEM microscopy. It could be observed that the coating is continuous and the double polymerization was efficient indicating the two-step with arrows heads in Figure 7.2.

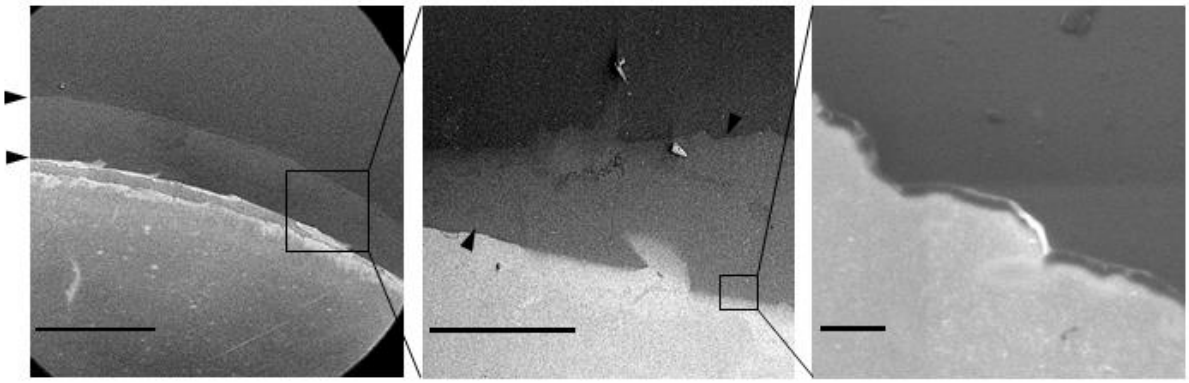

Figure 7.2. Characterization of double layer pHEMA polymerization. Cross-section imaged with Scanning Electron Microscopy (SEM) of the double layer polymer coating. Images taken from left to right at 80x, 200x and 80.000x magnification, with scale bars (black southwest corner): 1mm, 200 µm and 500 nm.

7.2 Biofilm response in static conditions

The first result analysed in this chapter was the evaluation of the bacitracin in static conditions with the bacterial *Staphylococcus aureus* V329. This evaluation was performed in real time for 5 hours, time enough to determine if the antibiotic was active or not in terms of antimicrobial activity. Different concentrations of bacitracin were dissolved in the TSB medium from absence of antibiotic to 5 mM as the highest concentration. The test took place in the plate reader by monitoring the optical density of the bacterial dilution seeded in a 96 well plate with triplicates to detect possible contamination. This experiment confirmed that all the different bacitracin concentration were active in suspension without peptide antibiotic attachment on the surface.

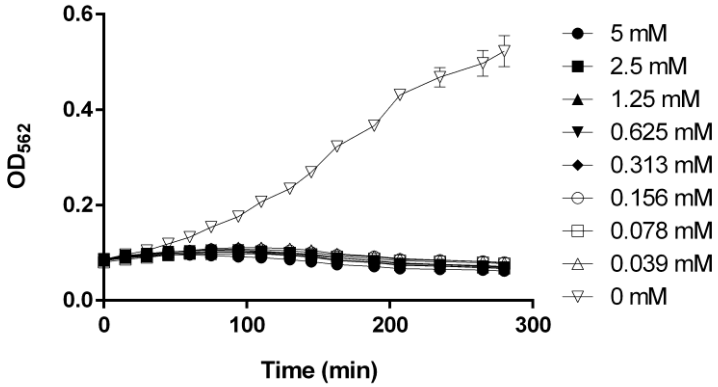

Figure 7.3. Effect of the peptide antibiotic tested with different concentrations for 5 hours.

When the antibiotic was tested in the 96 well exhibited an increase of the optical density at 600 nm (OD_{600}) only in the case of total absence of bacitracin (Figure 7.3 triangles). The next step to be analysed was the activity of the compound when it was linked to the reactive groups previously polymerized in the plasma reactor (Figure 7.1). This test was carried out by introducing an 8-well chamber slide in the plasma reactor. The 8-well chamber system is commercially available (nunc™) and consist in a regular glass slide with a silicon glued on the surface to fit the plastic wells to have a final piece depicted in Figure 7.4. The wells can be detached from the glass surface facilitating the plasma polymerization compared to the 96well that cannot be dissembled. When 6 of 8 wells were modified with PFM the chamber was mounted again to anchor the antibiotic, washed the non-attached molecules of bacitracin and cultured the bacteria for susceptibility analysis.

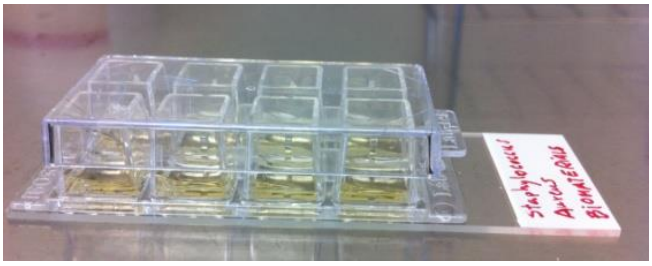

Figure 7.4. 8-well chamber slide with bacteria suspended in TSB medium for testing different concentrations of bacitracin attached on the modified surface.

As mentioned before, 2 wells of the chamber slide were covered with Teflon tape while the PFM was polymerized on the other 6 wells. After mounting back the 8 wells, different concentrations of bacitracin were introduced into the chamber including the 2 non-modified wells. The bacterial growth evaluation took place into the wells placing 200 µL of TSB medium during 16 hours at 37°C. After that the medium was aspirated from the corner of each chamber and 200 µL of PBS were dispensed along the wall of each chamber to wash the non-attached bacteria and avoid shear forces that could disrupt the biofilm. Then a live/dead bacterial staining was performed on the surfaces under study, to ensure the bacterial adhesion and survival. The staining and the observational procedure followed the protocol described in section 2.3.2.

The analysed superficial treatment with bacitracin could be observed in Figure 7.5 and Figure 7.6 that showed the non-modified and modified surface respectively. As it could be observed the modified surface lead to notably inhibition of the bacterial growth showing a vast majority of non-living bacterial cells (red), while the non-modified showed a high viability bacterial cells represented in green.

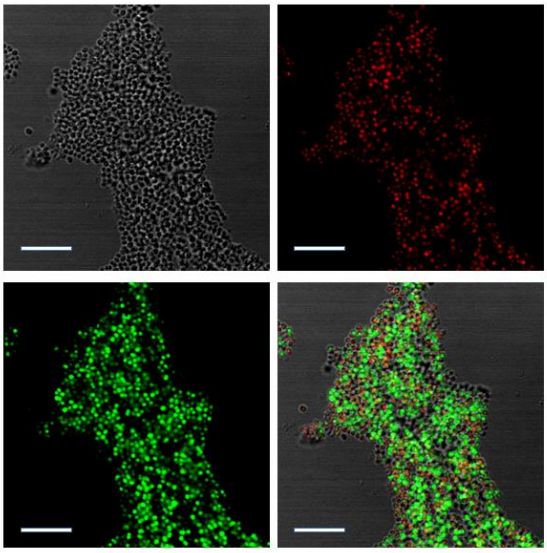

Figure 7.5. Live/dead cell staining of the non-modified surface for a bacterial growth during 24 hours. In grey, the phase contrast microscopy. Red and green images belongs to the independent excitation channels, which means negative and positive viability, respectively. Merge image of both channels placed in bottom-right. Scale bar: 10 µm.

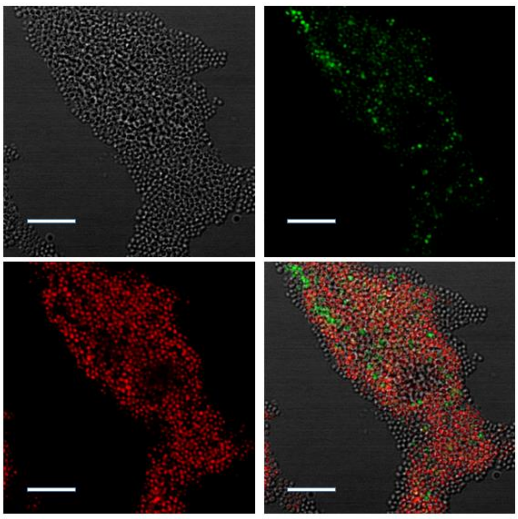

Figure 7.6. Live/dead cell staining of the modified surface for a bacterial growth during 24 hours. In grey, the phase contrast microscopy. Red and green images belongs to the independent excitation channels, which means negative and positive viability, respectively. Merge image of both channels placed in bottom-right. Scale bar: 10 µm.

7.3 Biofilm response in flow conditions

7.3.1 QCM-D monitoring

The biofilm response to bacitracin was monitored firstly under flow conditions by modifying the surface of the QCM-D gold sensors. This technique not only allows the measure of both mass and viscoelastic properties of the films formed with plasma polymerization is possible, but also the subsequent antibiotic adsorption of bacitracin can be additionally measured. This is one of the major advantages of QCM-D as an analytical technique. Essentially any material that can be evaporated or deposited within a sufficiently thin regime (~ nm to µm range) is capable of being coated on the QCM-D sensor surface. This means that specialized surfaces were modified and the stepwise monitored during antimicrobial layer preparation. These surfaces were used then as for studying further biomolecular interactions, and this provides a potential platform for biological-based studies. A non-treated gold sensor has been taken as reference (Figure 7.7) to evaluate the peptide antibiotic effect against biofilm formation. This reference experiment belongs to chapter 3 and it is shown at this point to compare the profile with the data of the following experiments performed with same conditions with presence of bacitracin as the only difference. The presence of bacitracin was tested with the antibiotic dissolved in the TSB medium and anchored onto sensor.

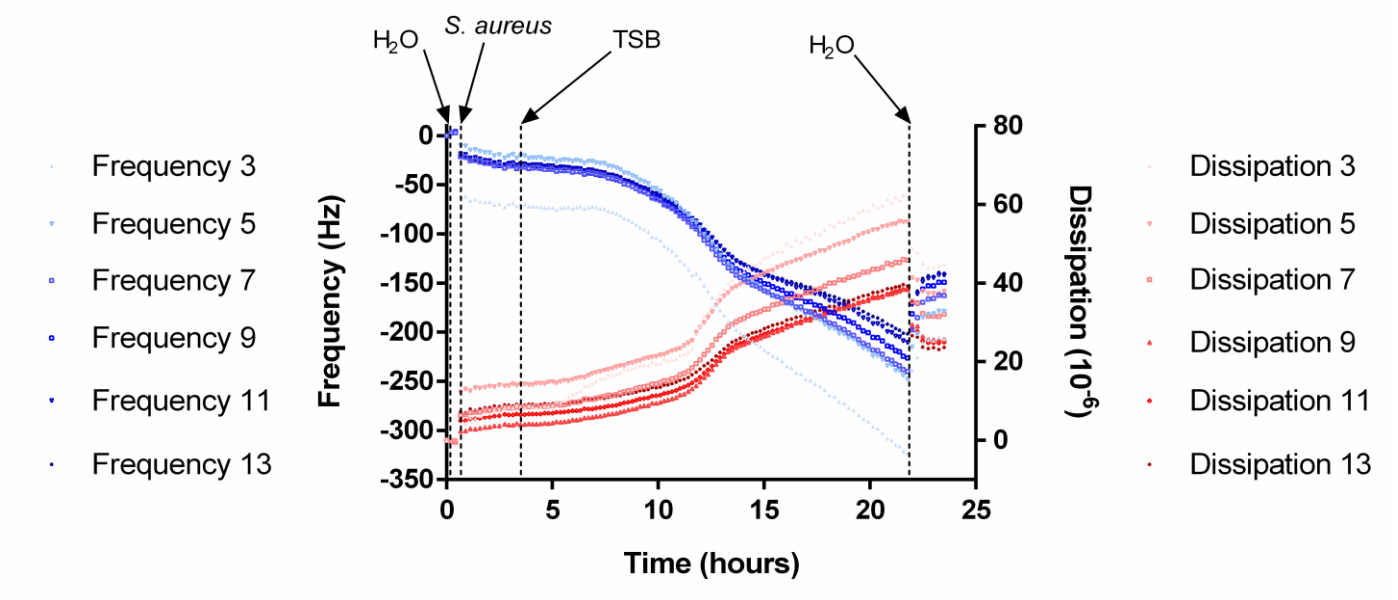

Figure 7.7. QCM-D measurement evolution profile bacterial growth at 37ºC onto gold QCM-D sensor. Data Acquired in Chapter 3.

7.3.1.1 Antibiotic in suspension

The antibiotic was dissolved in the TSB medium at 300 µM which is 10-times lower than the concentration that is going to be used in the next bacitracin anchoring experiment. The decrease of the concentration used for this experiment was caused by the high volume necessary to run the 24 hour experiment.

As it could be seen in Figure 7.8, in either case of frequency and dissipation did not show a characteristic profile of biofilm formation (Figure 7.7) indicating a poor bacterial adhesion and subsequent no biofilm development. Furthermore, as it was expected, the final H_2O wash lead to the detachment of the little amount of bacteria attached initially due to the absence of bacitracin during this initial seeding step.

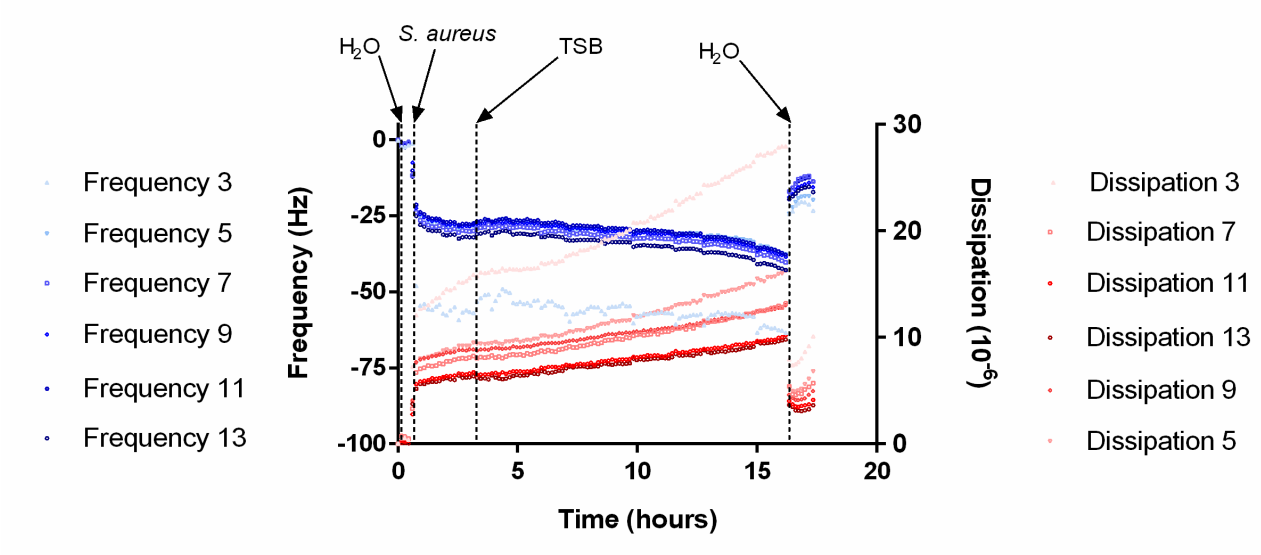

Figure 7.8. QCM-D measurement evolution profile bacterial growth at 37ºC onto gold QCM-D sensor. In presence of bacitracin dissolved with the TSB medium.

7.3.1.2 Antibiotic anchored

The evaluation of the antibiotic peptide adsorption and its subsequent effect against biofilm formation, were performed in a set of experiment with the flow fixed at 50 µL/min. The number of experiments to study the interaction between the PFM and the antibiotic, were six that consisted in two groups of three (Table 7.1). Each individual group contained an initial test (A and D) to confirm if the molecules present in TSB medium were more absorbed compared to phosphate buffered saline (PBS). Then bacitracin adsorption was tested in both solutions PBS and TSB.

Surface condition	# Experiment	Baseline	Adsorption process	Cleaning process
No Treatment	A	PBS	TSB	PBS
	B	PBS	PBS + Bacitracin	PBS
	C	TSB	TSB + Bacitracin	TSB
Treatment	D	PBS	TSB	PBS
	E	PBS	PBS + Bacitracin	PBS
	F	TSB	TSB + Bacitracin	TSB

Table 7.1. Biomolecules attachment onto PFM.

The first group of three were performed with no treatment of the sensor surface with PFM, while the second presented a PFM modification of the sensors. The time of the experiments was limited to its stabilization of the signal believing that bacitracin molecules saturate the active surface to link with. In addition the antibiotic concentration in this case was 2 mM for the four the cases that bacitracin was pumped into the QCM-D flow chamber (B, C, E, F). This preliminary experiments were plotted and depicted in Figure 7.9 that included lines in each profile that belonged to the three different steps: baseline, adsorption process and cleaning process that changed according to the experiment performed (see Table 7.1).

Analysing the adsorption experiments no interaction between bacitracin and the surface was observed in the experiments A, B, C and D. These results were expected due to the absence of PFM onto the surface for the A, B and C experiments, while the fourth one (D) did not have bacitracin inoculation, therefore no possible interaction could occur. When bacitracin was introduced into the flow chamber either dissolved in PSB or TSB a decrease in frequency shift was detected if the sensor surface was previously modified with PFM (E and F).

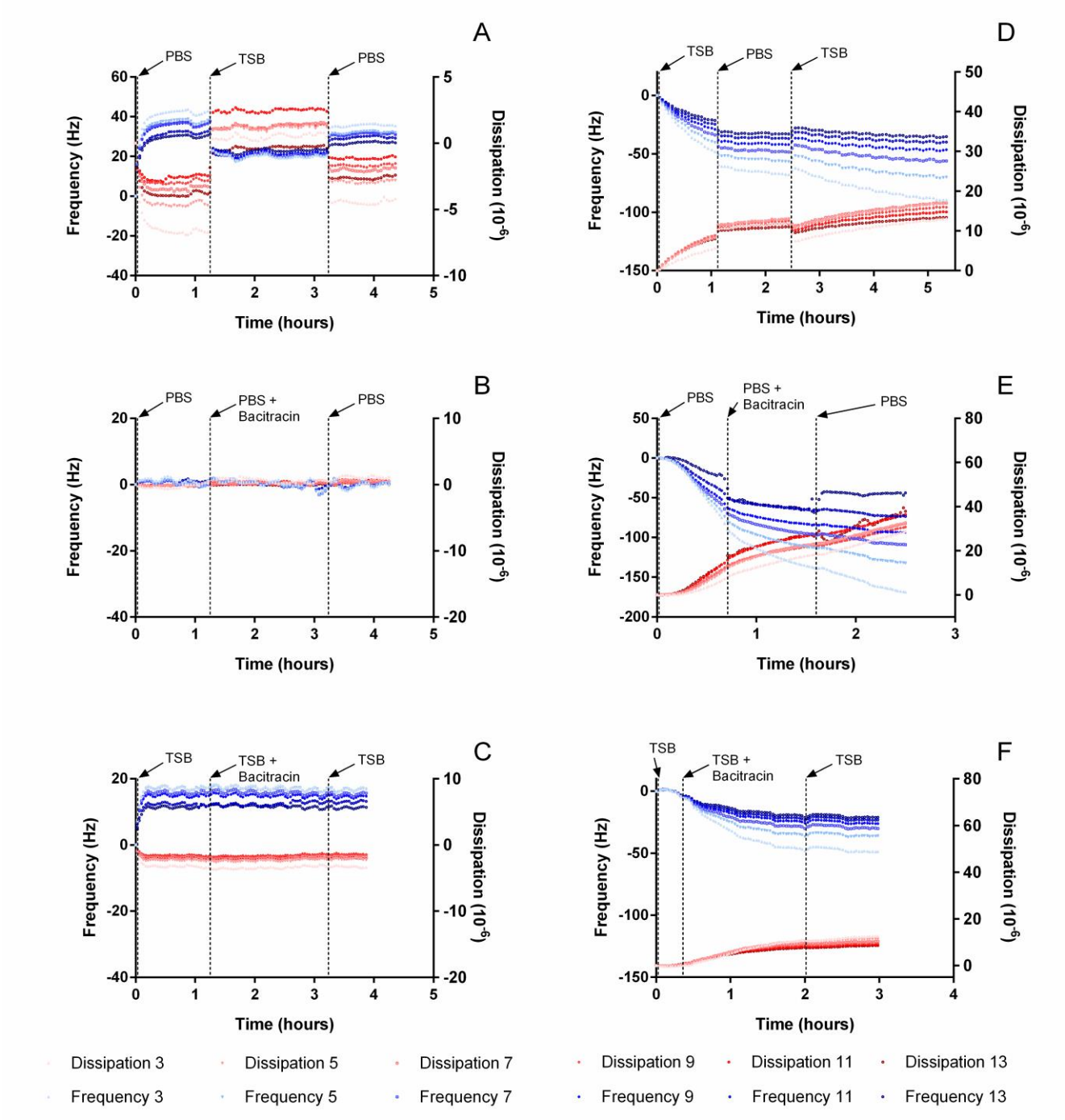

Figure 7.9. QCM-D measurements evolution profile bacterial growth at 37ºC onto gold QCM-D sensor. The conditions of surface and adsorption process specified in Table 7.1.

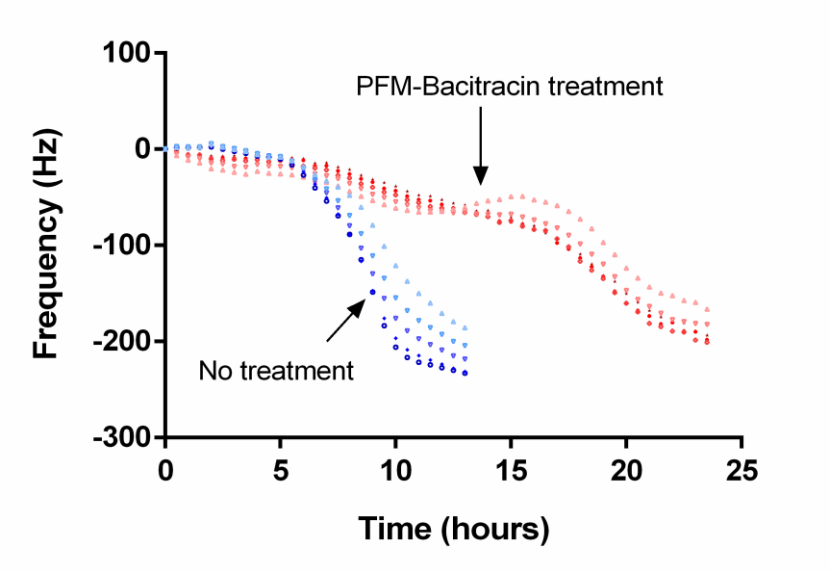

Figure 7.10. QCM-D measurements evolution profile bacterial growth at 37ºC onto gold QCM-D sensor.

Once Bacitracin adsorption was finished a bacterial growth test was performed into the flow QCM-D module. To relate the experiments with the susceptibility test it was necessary to take into account that experiment D was followed by the final test with bacteria shown in Figure 7.10 (blue) while experiment F was followed by the final test with bacteria shown in Figure 7.10 (red). Observing the comparison between the bacterial growths over the PFM-treated surfaces with presence and absence of bacitracin, a bacterial growth and biofilm development was present in both cases. Nevertheless the treated surface was more resistant for approximately 15 hours, where a frequency shift drop occurred indicating a possible wash or depletion of the antibiotic present in the QCM-D sensor surface.

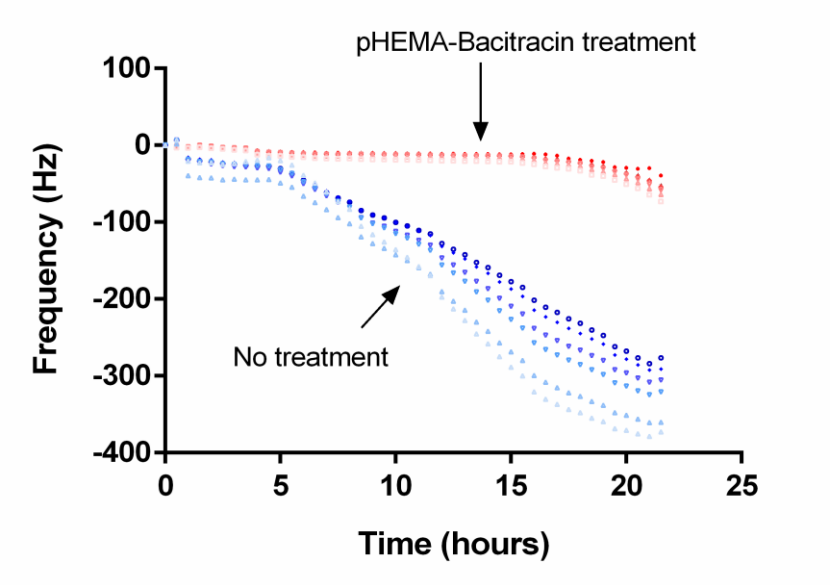

Figure 7.11. QCM-D measurements evolution profile bacterial growth at 37ºC onto gold QCM-D sensor.

Finally, the double layer of pHEMA described above and shown in Figure 7.2 was used to adsorb and trap the antimicrobial compound and test in real-time the anti-biofilm effect with QCM-D flow module. As for the previous methodology a comparison between presence and absence of bacitracin over the modified surfaces was carried out. In this case the modified surface almost stayed in the baseline values. It must be noticed that when TSB medium was flown through the chamber it might be releasing bacitracin from the network so a slow cleaning process could take place. The frequency shift of the treatment experiment was very low compared to the positive control meaning that bacitracin influenced the bacterial growth. The control with the treated surface in absence of bacitracin showed a higher decrease in frequency confirming that the double layer itself did not affect the biofilm development.

As the anchoring process of bacitracin within pHEMA network was not a covalent mechanism, the adsorption was performed without flow by depositing on the sensor a drop of the same Bacitracin concentration used with PFM (2 mM). For this reason the anchoring process was not able to be monitored with this method.

7.3.2 Impedance monitoring

The method applied in this section has been described in chapters 5 and 6. This final part of the work described the biofilm detection to evaluate bacitracin treatment in suspension and attached onto the sensor surface, as the previous section 7.3.1 where QCM-D was used. Although the custom device designed was used for this issue only pHEMA double layer modification was performed due to the results obtained with QCM-D equipment that exhibited a higher antibiofilm activity, together with this method does not require an a covalent bonding of the molecules.

7.3.2.1 Antibiotic in suspension

The effect of the antibiotic suspended in the TSB medium was depicted in Figure 7.12 that showed the normalized impedance at 10 kHz over the time using two and four electrode configuration. *S. aureus* bacteria was targeted with bacitracin confirming the inhibition of the complex lipid carrier in the cell wall biosynthesis ceasing bacterial growth. As described above bacitracin influences biofilm at any stage of the process, so the inhibition process was expected to be successful, although the bacteria was initially seeded without bacitracin. The bacterial proliferation in presence of dissolved bacitracin presented relative changes in impedance the first 10 hours which were not significant as they were in the same order of the standard deviation. The fact that there is no significant change from baseline to the end of the experiment indicated the inhibition effect of bacitracin effect onto the biofilm formation.

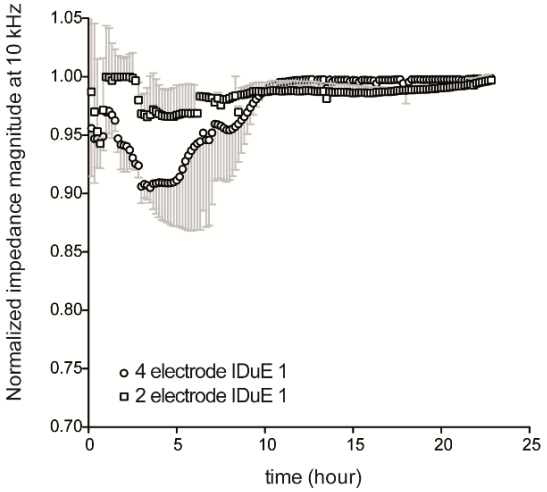

Figure 7.12. Time course of the normalized impedance magnitude (mean±std, n=3) detected with the rectangular IDuE 1 with bacitracin dissolved in the TSB medium using two and four electrode configuration.

This section studied not only the activity of the antimicrobial compound anchored over the impedance sensor presented and tested in chapter 5, but also its stability to continuous flow. The pHEMA coating is known that increase the hydrophilicity of the surface and several studies show how a higher hydrophilic surface enhances the interaction between the implant and the biologic surrounding[25]. Thus, surface wettability is a parameter that must be taken into account to evaluate this interaction with surfaces. Therefore, we measured the contact angle of non-treated and treated sensor with pHEMA double layer, in order to assess the influence of surface hydrophilicity. Figure 7.13 showed how the superficial modification decrease the contact angle when the surface was treated compared with non-treated sensor used as a control.

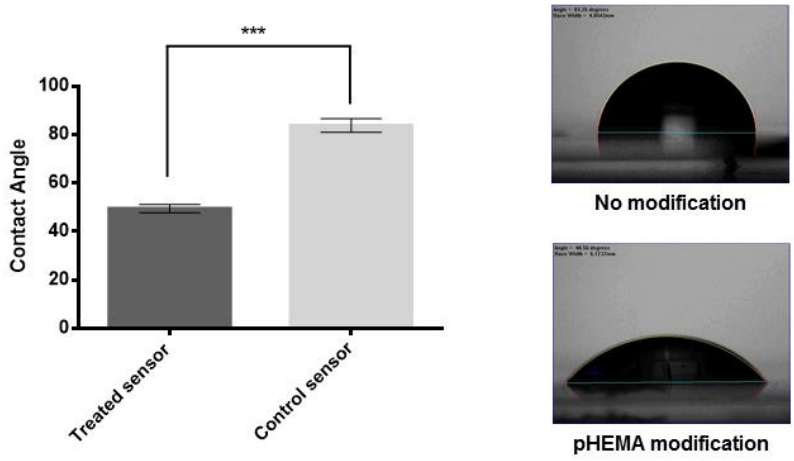

Figure 7.13. Contact angle measurements of non-modified and modified surface with pHEMA for antibiotic entrapment. Non-modified surface act as positive control. Data was represented as means ± SD of triplicates. The contact angle of the samples was compared using unpaired t-test with value of $p > 0.0001$.

As detailed before, it has been proved that pHEMA coating increased the cell attachment and proliferation onto the substrate according to the data obtained in previous studies, so one might think that an increase of cell attachment could lead a biofilm formation even containing bacitracin embedded. However, the result presented in Figure 7.14 showed a very opposite result where the lack of bacitracin in the double pHEMA layer exhibited a biofilm formation whereas the treated surface had a very similar profile to the antibiotic dissolved in TSB. Only four electrode configuration was used to represent the compared EIS data between treated and non-treated surfaces.

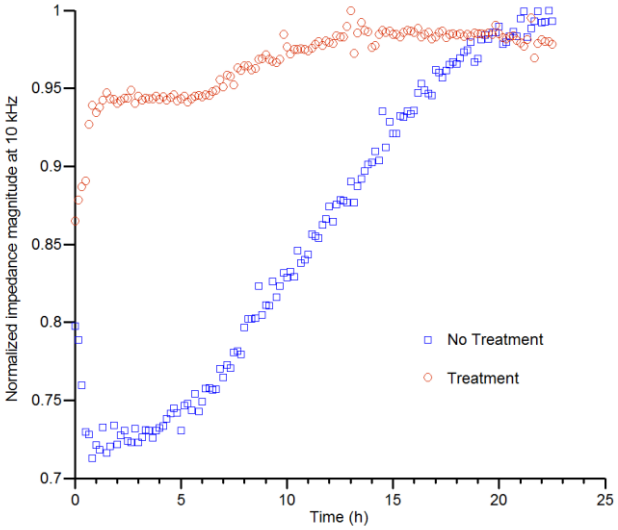

Figure 7.14. Time course of the normalized impedance magnitude (mean±std, n=3) detected with the rectangular IDuE 1 with bacitracin anchored on the surface using four electrode configuration systems.

7.4 Discussion

In implant infections, biofilm is still the major problem for bacterial persistence to antibiotic therapy. Among antimicrobial agents, bacitracin promises to be one of the greatest therapeutic possibilities, due to effect at different cellular points and biofilm stages. The continuous progress in the field could approach the creation of infection-resistant biomaterials able to inhibit biofilm development. Understanding the structure of the antimicrobial compounds and its adsorption onto modified polymer surfaces the influence to cellular adhesion can be measured by label-free technologies resulting in a powerful susceptibility diagnostic tool.

The improvements in diagnosis, together with the validation and adoption of more specific clinical control strategies able to be a disaggregating biofilm agent, could revolutionize the treatment of implant infections. Implant materials have garnered much attention recently and label-free technologies could help to test the biomaterial's response to certain continuous flow for longer periods of time.

The susceptibility to the antimicrobial peptide bacitracin has been investigated in this chapter, by using active immobilization of the antibiotic and the entrapment into polymer network, monitoring the bacterial response with QCM-D and EIS technologies as label-free methods.

The first method of antibiotic immobilization studied in this chapter was the coating of the surface with PFM that have been demonstrated to be a suitable linking interface method to link bacitracin. PFM coatings contain a highly reactive ester group, which could be used to bind biomolecules (Figure 7.1) considered as active coatings for different biomaterials[26]. This method was proved to be an effective antibacterial coating when there is total absence of flow, nevertheless the introduction of flow showed contrary results. The adsorption process of bacitracin was analysed with flow using QCM-D and the whole process (baseline, adsorption and cleaning) showed a lower recovery frequency shift signal in case of using TSB, which indicated that the cleaning process was less affected. However when the biofilm growth was monitored, the bacteria manage to survive, indicating that this method was not stable enough. This poor stability could be caused by a possible wash of bacitracin molecules plus a reduction of non-active molecules due to the linking process itself, which is not present in the case of pHEMA double layer methodology. This immobilization method did not require a specific targeted molecule to link, therefore it covers a wider range of antimicrobial compounds to immobilize. Furthermore pHEMA double layer results indicated that the antibiotic diffusion is not affected by the presence of the hydrogel thin film in either both cases the commercial QCM-D and the custom-made EIS platform.

7.5 Final Remarks

As mentioned before, the aims of this chapter were to study the bacterial viability and the growth monitoring by using different coated surfaces treated with plasma polymerization. The polymerized films had homogeneous spatial distribution of PFM groups within the polymer film. The incorporation of a functional molecule with amino groups like bacitracin facilitated the activation of the entire surface of the film. From this point of view, it seems a better option to keep the PFM on the surface to ensure its complete reaction. However, the possible blockage of the active site and the possibility to include a multi-component therapy demanded an entrapment method seems more useful than covalent attachment. Therefore, pHEMA deposited enhanced the surface resistance to non-specific protein adhesion, which is especially useful for *in vivo* applications of sensors. The mesh size of the resulting films, based on swelling properties, is small enough to allow small molecules like bacitracin to diffuse to the underlying substrate. The promising results achieved in this chapter so far encourage the further exploration of plasma polymerization as a potential technique to engineer multi-layer structures on different materials to obtain functional antibacterial implants.

7.6 References

(1) Ravaioli, S.; Cangini, I.; Pietrocola, G. Scenery of *Staphylococcus* Implant Infections in Orthopedics. *Future Microbiol.* **2011,** *6,* 1329–1349.

(2) Sato, H.; Feix, J. B. Peptide-Membrane Interactions and Mechanisms of Membrane Destruction by Amphipathic ??-Helical Antimicrobial Peptides. *Biochim. Biophys. Acta - Biomembr.* **2006,** *1758,* 1245–1256.

(3) Darouiche, R. O. Treatment of Infections Associated with Surgical Implants. *N. Engl. J. Med.* **2004,** *350,* 1422–1429.

(4) Arciola, C. R.; Montanaro, L.; Costerton, J. W. New Trends in Diagnosis and Control Strategies for Implant Infections. *Int. J. Artif. Organs* **2011,** *34,* 727–36.

(5) Davidson, C. A. B.; Lowe, C. R. Optimisation of Polymeric Surface Pre-Treatment to Prevent Bacterial Biofilm Formation for Use in Microfluidics Y. *J. Mol. Recognit.* **2004,** *17,* 180–185.

(6) Stoodley, P.; Cargo, R.; Rupp, C. J.; Wilson, S.; Klapper, I. Biofilm Material Properties as Related to Shear-Induced Deformation and Detachment Phenomena. *J. Ind. Microbiol. Biotechnol.* **2002,** *29,* 361–7.

(7) Goeres, D. M.; Hamilton, M. a; Beck, N. a; Buckingham-Meyer, K.; Hilyard, J. D.; Loetterle, L. R.; Lorenz, L. a; Walker, D. K.; Stewart, P. S. A Method for Growing a Biofilm under Low Shear at the Air-Liquid Interface Using the Drip Flow Biofilm Reactor. *Nat. Protoc.* **2009,** *4,* 783–8.

(8) Kim, J.; Park, H.-D.; Chung, S. Microfluidic Approaches to Bacterial Biofilm Formation. *Molecules* **2012,** *17,* 9818–34.

(9) Humblot, V.; Yala, J.-F.; Thebault, P.; Boukerma, K.; Héquet, A.; Berjeaud, J.-M.; Pradier, C.-M. The Antibacterial Activity of Magainin I Immobilized onto Mixed Thiols Self-Assembled Monolayers. *Biomaterials* **2009,** *30,* 3503–12.

(10) Huang, H. W. Molecular Mechanism of Antimicrobial Peptides: The Origin of Cooperativity. *Biochim. Biophys. Acta - Biomembr.* **2006,** *1758,* 1292–1302.

(11) Yala, J.; Thebault, P.; Héquet, A.; Humblot, V.; Pradier, C. Elaboration of Antibiofilm Materials by Chemical Grafting of an Antimicrobial Peptide. *Appl. Microbiol. Biotechnol.* **2010.**

(12) Storm, D. R. Mechanism of Bacitracin Action: A Specific Lipid-Peptide Interaction *. *Ann. New York Acad. Sci.* **1967,** 387–398.

(13) Stone, K. J.; Jack, L. Complexation Pyrophosphate. *Proc. Natl. Acad. Sci. U. S. A.* **1971,** *68,* 3223–3227.

(14) Ciesio, J.; Wrzesi, J.; Stokowa-so, K.; Nagaj, J.; Kasprowicz, A.; Leszek, B.; Szczepanik, W. Antibiotic Bacitracin Induces Hydrolytic Degradation of Nucleic Acids ☆. *Biochim. Biophys. Acta* **2014,** *1840,* 1782–1789.

(15) Roche, E. D.; Renick, P. J.; Tetens, S. P.; Carson, D. L. A Model for Evaluating Topical Antimicrobial Efficacy against Methicillin-Resistant Staphylococcus Aureus Biofilms in Superficial Murine Wounds. *Antimicrob. Agents Chemother.* **2012,** *56,* 4508–4510.

(16) Amato, M.; Pershing, S.; Do, M. W.; Tanaka, S. Trends in Ophthalmic Manifestations of Methicillin-Resistant Staphylococcus Aureus (MRSA) in a Northern California Pediatric Population. *J. AAPOS* **2009,** *17,* 243–247.

(17) Francesch, L.; Garreta, E.; Balcells, M.; Edelman, E. R.; Borrós, S. Fabrication of Bioactive Surfaces by Plasma Polymerization Techniques Using a Novel Acrylate-Derived Monomer. *Plasma Process. Polym.* **2005,** *2,* 605–611.

(18) Francesch, L.; Borros, S.; Knoll, W.; Förch, R. Surface Reactivity of Pulsed-Plasma Polymerized Pentafluorophenyl Methacrylate (PFM) toward Amines and Proteins in Solution. *Langmuir* **2007,** *23,* 3927–3931.

(19) Duque, L.; Menges, B.; Borros, S.; Förch, R. Immobilization of Biomolecules to Plasma Polymerized Pentafluorophenyl Methacrylate. *Biomacromolecules* **2010,** *11,* 2818–2823.

(20) Baxamusa, S. H.; Montero, L.; Dubach, J. M.; Clark, H. a; Borros, S.; Gleason, K. K. Protection of Sensors for Biological Applications by Photoinitiated Chemical Vapor Deposition of Hydrogel Thin Films. *Biomacromolecules* **2008,** *9,* 2857–62.

(21) Urcan, E.; Haertel, U.; Styllou, M.; Hickel, R.; Scherthan, H.; Reichl, F. X. Real-Time xCELLigence Impedance Analysis of the Cytotoxicity of Dental Composite Components on Human Gingival Fibroblasts. *Dent. Mater.* **2010,** *26,* 51–58.

(22) Linderholm, P.; Bertsch, A.; Renaud, P. Resistivity Probing of Multi-Layered Tissue Phantoms Using Microelectrodes. *Physiol. Meas.* **2004,** *25,* 645.

(23) Guimera, A.; Gabriel, G.; Plata-Cordero, M.; Montero, L.; Maldonado, M. J.; Villa, R. A Non-Invasive Method for an in Vivo Assessment of Corneal Epithelium Permeability through Tetrapolar Impedance Measurements. *Biosens. Bioelectron.* **2012,** *31,* 55–61.

(24) Marí-Buyé, N.; O'Shaughnessy, S.; Colominas, C.; Semino, C. E.; Gleason, K. K.; Borrós, S. Functionalized, Swellable Hydrogel Layers as a Platform for Cell Studies. *Adv. Funct. Mater.* **2009,** *19,* 1276–1286.

(25) Zhao, G.; Schwartz, Z.; Wieland, M.; Rupp, F.; Geis-Gerstorfer, J.; Cochran, D. L.; Boyan, B. D. High Surface Energy Enhances Cell Response to Titanium Substrate Microstructure. *J. Biomed. Mater. Res. A* **2005,** *74,* 49–58.

(26) Duque, L.; Queralto, N.; Francesch, L.; Bumbu, G. G.; Borros, S.; Berger, R.; Förch, R. Reactions of Plasma-Polymerised Pentafluorophenyl Methacrylate with Simple Amines. *Plasma Process. Polym.* **2010,** *7,* 915–925.

CONCLUSIONS

- It has been demonstrated that Quartz Crystal Microbalance with Dissipation (QCM-D) and Electrochemical Impedance Spectroscopy (EIS) are label-free techniques that have the ability to monitor biofilms onto gold sensors, aiming to gain a little insight about real-time detection combined with microfluidics.
- QCM-D results can be associated to theoretical models for interpreting meaningful physical parameters such as mass, thickness, density or viscoelasticity, therefore is an optimal approach for addressing questions about biological materials and their interactions to study the formation of antimicrobial coating.
- The promising results of antibacterial coatings so far encourage the further exploration of plasma polymerization as a potential technique to engineer multi-layer structures on different materials to obtain functional antimicrobial implants.
- The working conditions stablished by the commercially available equipment (QCM-D) are useful to apply on the custom-made platform to use Electrochemistry Impedance Spectroscopy (EIS).
- The geometry of the device designed using Computational Fluid Dynamics (CFD) and Finite Element Models (FEM) simulation was optimized for the detection of *Staphylococcus aureus* biofilm proliferation with interdigitated microelectrodes (IDuEs) that permits two- and four-electrode methods analysis.
- The compared results of two- and four-electrode configurations exhibited real differences of bacterial detection confirming that the common method used (two-electrode) presented significant drawbacks, such as low sensitivity of bacterial thickness once the surface is covered, and the masking effects i.e. temperature changes.
- The method with four-electrode allows to interpret morphological impedance spectrum and structural information regarding the biofilm by fitting to Cole model equivalent circuit.
- The system presented also offers the possibility to measure multiple read-outs to detect other analytes of interest such as dissolved oxygen, K+, Na+ and pH.
- The investigation of vesicles sensitivity to toxins released by a biofilm grown under flow conditions, have proven effective at lysing the membranes, ensuring effective release of the embedded carboxyfluorescein.
- The multi-parametric measurement of toxin activity coupled to EIS conclude that toxin activity occurs as the biofilm forms, not when the biofilm is formed contrary to planktonic behaviour that becomes toxic in the stationary phase.

- As the moment that toxin activity begins is different, comparing real-time measurements of both modes of existence (biofilm and planktonic), it can be conclude that biofilm has an advantage over the planktonic suggesting that biofilm act as reservoir of toxicity.
- The entire process of toxicity and bacterial biofilm treatment can only be properly understood in terms of biofilm formation therefore both label-free techniques (QCM-D and EIS technology) permits the monitorization of biofilm responses.
- Contrary to other state-of-the-art approaches based on commercial multi-well plates used today for biofilm assays (Real Time Cell Analyzer), our multi-parametric microfluidic platform could be integrated in multiple environments offering the advantage to account the effect of shear stress on the formation of bacterial biofilm, a variable that affects biofilm structure and behaviour.

CONCLUSIONES

- Se ha demostrado que la microbalanza de cuarzo con disipación (QCM-D) y la Espectroscopia de impedancia electroquímica son técnicas *"label-free"* que tienen la habilidad de monitorizar biofilms sobre sensores de oro, incrementando un poco más de percepción sobre la detección a tiempo real combinada con microfluidica.
- Los resultados de QCM-D pueden asociarse a modelos teóricos para la interpretación de parámetros físicos significativos tales como masa, grosor, densidad y viscoelasticidad, por tanto es un enfoque óptimo para abordar cuestiones sobre materiales biológicos y sus posibles interacciones para estudiar la fabricación de recubrimientos antimicrobianos.
- Los prometedores resultados de los recubrimientos antibacterianos animan a la futura exploración de la polimerización por plasma como técnica potencial para desarrollar multicapas estructuradas sobre diferentes materiales para obtener implantes antimicrobianos funcionales.
- Las condiciones de trabajo establecidas por el equipo comercial disponible (QCM-D) son útiles para aplicar en la plataforma fabricada para la utilización de Espectroscopia electroquímica de impedancia.
- La geometría del dispositivo diseñado por Fluido-dinámica computacional y Modelado por elementos finitos ha sido optimizada para la detección la proliferación de biofilms de *Staphylococcus aureus* con microelectrodos interdigitados que permiten el análisis usando las configuraciones de dos- y cuatro-electrodos.
- Los resultados comparativos de las configuraciones de dos- y cuatro-electrodos exhiben diferencias reales con la detección confirmando que el método usualmente utilizado (dos-electrodos) presenta inconvenientes significantes, tales como la baja sensibilidad del grosor de bacterias una vez la superficie es cubierta, y los efectos de enmascaramiento como los cambios de temperatura.
- El método con cuatro-electrodos permite la interpretación morfológica del espectro de impedancia e información estructural respecto al biofilm mediante el ajuste al modelo de Cole.
- El sistema presentado también ofrece la posibilidad de medir múltiples lecturas para detectar otros analitos de interés como oxígeno disuelto, K+, Na+ y pH.
- La investigación de la sensibilidad de vesículas a la liberación de toxinas por parte de un biofilm crecido bajo condiciones de flujo, ha resultado efectivo en la lisis de membranas, asegurando una liberación efectiva de carboxifluoresceina encapsulada en las vesículas.

- La medición multiparamétrica de la actividad de toxinas acoplada a lecturas de impedancia concluyen que la actividad tóxica ocurre cuando el biofilm se forma, no cuando el biofilm está formado, en contraposición del comportamiento de bacteria en forma planctónica que se vuelve tóxico en la fase estacionaria.
- Como el momento en que empieza la actividad tóxica es diferente comparando las medidas a tiempo real de ambos modos de existencia (biofilm y planctónico), se puede concluir que los biofilms tienen ventaja sobre la forma planctónica sugiriendo que el biofilm actúa como reservorio de toxicidad.
- Todo el proceso de toxicidad y tratamiento de biofilm bacteriano solamente puede ser entendido de manera apropiada en términos de formación de biofilm, por tanto ambas técnicas *label-free* (microbalanza de cuarzo y espectroscopia de impedancia) permiten la monitorización de la respuesta de biofilm a cualquier tratamiento.
- Contrariamente a otros enfoques de última generación basados en placas comerciales de múltiples pocillos utilizadas hoy en día para ensayos con biofilms, nuestra plataforma de microfluídica puede estar integrada en múltiples ambientes ofreciendo la ventaja de tener en cuenta el efecto del estrés mecánico en la formación de biofilm bacteriano, que es una variable que afecta la estructura del biofilm y su comportamiento.

ANNEXES

Annex I

Supplementary Video: Time-lapse of the biofilm captured in the EIS device. Bacterial biofilm formation was recorded using the PDMS window of the designed device to capture static images every minute during the 24 hour experiment of biofilm development.

Annex II

Matlab script used for Electrochemical Impedance Spectroscopy (EIS) analysis:

```
%close all

clc

clear all

%%

[fileNameImpedance,pathfile]          =   uigetfile('*.*','Select   CNM
measurement file:');

if isequal(fileNameImpedance,0) || isequal(pathfile,0)

   break;

end

matfile           = strcat(fileNameImpedance,'.mat');

fileNameImpedance = strcat(pathfile,fileNameImpedance);

%%

fid = fopen(fileNameImpedance);

tline = fgetl(fid);

ii=0;

while ischar(tline)

%     disp(tline);

    tline = fgetl(fid);

    ii=ii+1;

    if ii==2

        parts = textscan(tline, '%s', 'Delimiter', '\t');

        f=parts{1,1};

        for jj=2:length(f)

         fv(jj-1)=str2num(f{jj,1});

        end

    end

    if ii>=5 && ischar(tline)

        parts = textscan(tline, '%s', 'Delimiter', '\t');

        dat=parts{1,1};

        for jj=2:length(f)
```

```
         M(ii-4,jj-1)=str2num(dat{2+(jj-2)*4,1});
         P(ii-4,jj-1)=str2num(dat{3+(jj-2)*4,1});
         R(ii-4,jj-1)=str2num(dat{4+(jj-2)*4,1});
         X(ii-4,jj-1)=str2num(dat{5+(jj-2)*4,1});
        end
    end
end
fclose(fid);
figure(1);
subplot(221);semilogx(fv,M);
hXLabel=xlabel('frequency (Hz)');
hYLabel=ylabel('Impedance (Ohms)');
set( gca                       , ...
    'FontName'   , 'Helvetica' );
set([hXLabel, hYLabel], ...
    'FontName'   , 'AvantGarde');
set([hXLabel, hYLabel]  , ...
    'FontSize'   , 10          );
set(gca, ...
  'Box'         , 'off'     , ...
  'TickDir'     , 'out'     , ...
  'TickLength'  , [.02 .02] , ...
  'XMinorTick'  , 'on'      , ...
  'YMinorTick'  , 'off'      , ...
  'YGrid'       , 'on'      , ...
  'XColor'      , 'k', ...
  'YColor'      , 'k', ... %'YTick'       , 80:110, ...
  'LineWidth'   , 1         );
set(gcf, 'PaperPositionMode', 'auto');

subplot(222);semilogx(fv,P);
hXLabel=xlabel('frequency (Hz)');
hYLabel=ylabel('Phase (degrees)');
```

```
set( gca                       , ...
    'FontName'   , 'Helvetica' );
set([hXLabel, hYLabel], ...
    'FontName'   , 'AvantGarde');
set([hXLabel, hYLabel]  , ...
    'FontSize'   , 10          );
set(gca, ...
  'Box'         , 'off'     , ...
  'TickDir'     , 'out'     , ...
  'TickLength'  , [.02 .02] , ...
  'XMinorTick'  , 'on'      , ...
  'YMinorTick'  , 'off'      , ...
  'YGrid'       , 'on'      , ...
  'XColor'      , 'k', ...
  'YColor'      , 'k', ... %'YTick'       , 80:110, ...
  'LineWidth'   , 1         );
set(gcf, 'PaperPositionMode', 'auto');


subplot(223);loglog(fv,R);
hXLabel=xlabel('frequency (Hz)');
hYLabel=ylabel('Resistance (Ohms)');
set( gca                       , ...
    'FontName'   , 'Helvetica' );
set([hXLabel, hYLabel], ...
    'FontName'   , 'AvantGarde');
set([hXLabel, hYLabel]  , ...
    'FontSize'   , 10          );
set(gca, ...
  'Box'         , 'off'     , ...
  'TickDir'     , 'out'     , ...
  'TickLength'  , [.02 .02] , ...
  'XMinorTick'  , 'on'      , ...
  'YMinorTick'  , 'off'      , ...
```

```
  'YGrid'       , 'on'      , ...
  'XColor'      , 'k', ...
  'YColor'      , 'k', ... %'YTick'       , 80:110, ...
  'LineWidth'   , 1         );
set(gcf, 'PaperPositionMode', 'auto');


subplot(224);loglog(fv,X);
hXLabel=xlabel('frequency (Hz)');
hYLabel=ylabel('-Reactance (Ohms)');
set( gca                       , ...
    'FontName'   , 'Helvetica' );
set([hXLabel, hYLabel], ...
    'FontName'   , 'AvantGarde');
set([hXLabel, hYLabel]  , ...
    'FontSize'   , 10          );
set(gca, ...
  'Box'         , 'off'     , ...
  'TickDir'     , 'out'     , ...
  'TickLength'  , [.02 .02] , ...
  'XMinorTick'  , 'on'      , ...
  'YMinorTick'  , 'off'      , ...
  'YGrid'       , 'on'      , ...
  'XColor'      , 'k', ...
  'YColor'      , 'k', ... %'YTick'       , 80:110, ...
  'LineWidth'   , 1         );
set(gcf, 'PaperPositionMode', 'auto');


averages=4;
if averages==4
    for jj=1:floor(ii/4)-4
        MM(jj,:)             =    0.25*(M(jj*4-3,:)+M(jj*4-2,:)+M(jj*4-
1,:)+M(jj*4,:));
        PP(jj,:)             =    0.25*(P(jj*4-3,:)+P(jj*4-2,:)+P(jj*4-
1,:)+P(jj*4,:));
```

```
        stdM(jj,:)        =        std([M(jj*4-3,:);M(jj*4-2,:);M(jj*4-
1,:);M(jj*4,:)]);

    end

elseif averages==3

    for jj=1:floor(ii/3)-3

        MM(jj,:)   = 0.33*(M(jj*3-2,:)+M(jj*3-1,:)+M(jj*3,:));

        PP(jj,:)   = 0.33*(P(jj*3-2,:)+P(jj*3-1,:)+P(jj*3,:));

        stdM(jj,:) = std([M(jj*3-2,:);M(jj*3-1,:);M(jj*3,:)]);

    end

else

    disp('not implemented yet');

end


[numofmeas numoffreq]=size(MM);

tmeas = 10; %time between meas 10 min

t     = (0:1:numofmeas-1)*tmeas;

thour = t/60;

flow  = 16;


%%

figure(89)

semilogx(fv,(MM(floor(length(t)*1/4),:)),'ro-
','MarkerFace','r','MarkerSize',4);hold on

semilogx(fv,(MM(floor(length(t)*2/4),:)),'go-
','MarkerFace','g','MarkerSize',4)

semilogx(fv,(MM(floor(length(t)*3/4),:)),'ko-
','MarkerFace','k','MarkerSize',4)

semilogx(fv,(MM(floor(length(t)*4/4),:)),'co-
','MarkerFace','c','MarkerSize',4)


name2=strcat('t = ',num2str(floor((thour(end)*1/4))),'h');

name3=strcat('t = ',num2str(floor((thour(end)*2/4))),'h');

name4=strcat('t = ',num2str(floor((thour(end)*3/4))),'h');

name5=strcat('t = ',num2str(round(thour(end))),'h');

yLims=ylim;
```

```
ylim([60 yLims(2)])


hLegend=legend(name2,name3,name4,name5,'Location','Northeast');

hYLabel=ylabel('Magnitude (\Omega)');

hXLabel=xlabel('Frequency (Hz)');

set( gca                       , ...

    'FontName'   , 'Helvetica' );

set([hXLabel, hYLabel], ...

    'FontName'   , 'AvantGarde');

set([hLegend, gca]             , ...

    'FontSize'   , 8           );

set([hXLabel, hYLabel]  , ...

    'FontSize'   , 10          );

set(gca, ...

  'Box'         , 'off'     , ...

  'TickDir'     , 'out'     , ...

  'TickLength'  , [.02 .02] , ...

  'XMinorTick'  , 'on'      , ...

  'YMinorTick'  , 'off'      , ...

  'YGrid'       , 'on'      , ...

  'XColor'      , 'k', ...

  'YColor'      , 'k', ... %'YTick'       , 80:110, ...

  'LineWidth'   , 1         );

set(gcf, 'PaperPositionMode', 'auto');

%%

figure(90)

semilogx(fv,(PP(floor(length(t)*1/4),:)),'ro-
','MarkerFace','r','MarkerSize',4);hold on

semilogx(fv,(PP(floor(length(t)*2/4),:)),'go-
','MarkerFace','g','MarkerSize',4)

semilogx(fv,(PP(floor(length(t)*3/4),:)),'ko-
','MarkerFace','k','MarkerSize',4)

semilogx(fv,(PP(floor(length(t)*4/4),:)),'co-
','MarkerFace','c','MarkerSize',4)
```

```
name2=strcat('t = ',num2str(floor((thour(end)*1/4))),'h');
name3=strcat('t = ',num2str(floor((thour(end)*2/4))),'h');
name4=strcat('t = ',num2str(floor((thour(end)*3/4))),'h');
name5=strcat('t = ',num2str(round(thour(end))),'h');
yLims=ylim;
%ylim([-90 yLims(2)])

hLegend=legend(name2,name3,name4,name5,'Location','Northeast');
hYLabel=ylabel('Phase (Deg)');
hXLabel=xlabel('Frequency (Hz)');
set( gca                       , ...
    'FontName'   , 'Helvetica' );
set([hXLabel, hYLabel], ...
    'FontName'   , 'AvantGarde');
set([hLegend, gca]             , ...
    'FontSize'   , 8           );
set([hXLabel, hYLabel]  , ...
    'FontSize'   , 10          );
set(gca, ...
  'Box'         , 'off'     , ...
  'TickDir'     , 'out'     , ...
  'TickLength'  , [.02 .02] , ...
  'XMinorTick'  , 'on'      , ...
  'YMinorTick'  , 'off'      , ...
  'YGrid'       , 'on'      , ...
  'XColor'      , 'k', ...
  'YColor'      , 'k', ... %'YTick'       , 80:110, ...
  'LineWidth'   , 1         );
set(gcf, 'PaperPositionMode', 'auto');
%%
figure(2);
plot(thour,MM(:,flow));hold on;
hYLabel=ylabel('(\Omega)');
```

```
hXLabel=xlabel('time (h)');
set( gca                       , ...
    'FontName'   , 'Helvetica' );
set([hXLabel, hYLabel], ...
    'FontName'   , 'AvantGarde');
% set([hLegend, gca]             , ...
%     'FontSize'   , 8           );
set([hXLabel, hYLabel]  , ...
    'FontSize'   , 10          );
set(gca, ...
  'Box'         , 'off'     , ...
  'TickDir'     , 'out'     , ...
  'TickLength'  , [.02 .02] , ...
  'XMinorTick'  , 'on'      , ...
  'YMinorTick'  , 'off'      , ...
  'YGrid'       , 'on'      , ...
  'XColor'      , 'k', ...
  'YColor'      , 'k', ... %'YTick'       , 80:110, ...
  'LineWidth'   , 1         );
set(gcf, 'PaperPositionMode', 'auto');

%%
norm=MM(:,flow)/max(MM(:,flow));

figure(3);
plot(thour,norm,'o','MarkerSize',4);hold on;
plot(thour,filtfilt(ones(5,1)/5,1,norm),'LineWidth',1.5);
hYLabel=ylabel('Normalized Impedance');
hXLabel=xlabel('Time (h)');
set( gca                       , ...
    'FontName'   , 'Helvetica' );
set([hXLabel, hYLabel], ...
    'FontName'   , 'AvantGarde');
```

```
% set([hLegend, gca]             , ...
%     'FontSize'   , 8           );
set([hXLabel, hYLabel]  , ...
    'FontSize'   , 10          );
set(gca, ...
  'Box'         , 'off'     , ...
  'TickDir'     , 'out'     , ...
  'TickLength'  , [.02 .02] , ...
  'XMinorTick'  , 'on'      , ...
  'YMinorTick'  , 'off'      , ...
  'YGrid'       , 'on'      , ...
  'XColor'      , 'k', ...
  'YColor'      , 'k', ... %'YTick'       , 80:110, ...
  'LineWidth'   , 1         );
set(gcf, 'PaperPositionMode', 'auto');


figure(4)
E2=(MM(:,flow)-MM(:,end))./MM(:,flow)*100;
plot(thour,E2,'r');hold on;
% hLegend=legend('E_2','Location','NorthWest');
hYLabel=ylabel('E_2(%)');
hXLabel=xlabel('time (h)');


set( gca                       , ...
    'FontName'   , 'Helvetica' );
set([hXLabel, hYLabel], ...
    'FontName'   , 'AvantGarde');
% set([hLegend, gca]             , ...
%     'FontSize'   , 8           );
set([hXLabel, hYLabel]  , ...
    'FontSize'   , 10          );
set(gca, ...
  'Box'         , 'off'     , ...
```

```
  'TickDir'     , 'out'     , ...
  'TickLength'  , [.02 .02] , ...
  'XMinorTick'  , 'on'      , ...
  'YMinorTick'  , 'off'      , ...
  'YGrid'       , 'on'      , ...
  'XColor'      , 'k', ...
  'YColor'      , 'k', ... %'YTick'       , 80:110, ...
  'LineWidth'   , 1         );
set(gcf, 'PaperPositionMode', 'auto');


[R,X]=pol2cart(PP.*ones(size(PP))*pi/180,MM);
% figure;
% plot(R',-X')


figure(5)
% plot(R(1,:),-X(1,:),'bo-','MarkerFace','b');hold on;
plot(R(floor(length(t)*1/4),:),-X(floor(length(t)*1/4),:),'ro-
','MarkerFace','r');hold on
plot(R(floor(length(t)*2/4),:),-X(floor(length(t)*2/4),:),'go-
','MarkerFace','g');
plot(R(floor(length(t)*3/4),:),-X(floor(length(t)*3/4),:),'ko-
','MarkerFace','k');
plot(R(length(t),:),-X(length(t),:),'co-','MarkerFace','c');
name1=strcat('t = ',num2str(t(1)),'h');
name2=strcat('t = ',num2str(floor((thour(end)*1/4))),'h');
name3=strcat('t = ',num2str(floor((thour(end)*2/4))),'h');
name4=strcat('t = ',num2str(floor((thour(end)*3/4))),'h');
name5=strcat('t = ',num2str(round(thour(end))),'h');
yLims=ylim;
ylim([0 yLims(2)])


hLegend=legend(name2,name3,name4,name5,'Location','NorthWest');
hYLabel=ylabel('-Reactance (\Omega)');
hXLabel=xlabel('Resistance (\Omega)');
```

```
set( gca                        , ...
    'FontName'   , 'Helvetica' );
set([hXLabel, hYLabel], ...
    'FontName'   , 'AvantGarde');
set([hLegend, gca]              , ...
    'FontSize'   , 8           );
set([hXLabel, hYLabel]  , ...
    'FontSize'   , 10          );
set(gca, ...
  'Box'         , 'off'     , ...
  'TickDir'     , 'out'     , ...
  'TickLength'  , [.02 .02] , ...
  'XMinorTick'  , 'on'      , ...
  'YMinorTick'  , 'off'      , ...
  'YGrid'       , 'on'      , ...
  'XColor'      , 'k', ...
  'YColor'      , 'k', ... %'YTick'       , 80:110, ...
  'LineWidth'   , 1         );
set(gcf, 'PaperPositionMode', 'auto');


figure(6);
plot(thour,PP(:,flow));
hYLabel=ylabel('(\Omega)');
hXLabel=xlabel('time (h)');
set( gca                        , ...
    'FontName'   , 'Helvetica' );
set([hXLabel, hYLabel], ...
    'FontName'   , 'AvantGarde');
% set([hLegend, gca]              , ...
%     'FontSize'   , 8           );
set([hXLabel, hYLabel]  , ...
    'FontSize'   , 10          );
set(gca, ...
```

```
  'Box'         , 'off'     , ...
  'TickDir'     , 'out'     , ...
  'TickLength'  , [.02 .02] , ...
  'XMinorTick'  , 'on'      , ...
  'YMinorTick'  , 'off'      , ...
  'YGrid'       , 'on'      , ...
  'XColor'      , 'k', ...
  'YColor'      , 'k', ... %'YTick'       , 80:110, ...
  'LineWidth'   , 1         );
set(gcf, 'PaperPositionMode', 'auto');


reZcal = R;
imZcal = X;
time   = t;
save(strcat(pathfile,matfile),'f','reZcal','imZcal','stdM','time');


addpath C:\Users\oscar\Dropbox\matlab
z24Deis(fv,MM,PP,thour(end))
```

Annex III

Matlab script used for Quartz Crystal Microbalance with Dissipation (QCM-D) viscoelastic analysis:

```
%----------- Leer archivo Excel ------------------

a=                          xlsread('C:\Users\oscar\Dropbox\phD\CHAPTERS
phD\3_Chapter\Figures\DF-t plots\A_Temperature\temperature.xlsx');

plot3(a(:,1), a(:,2), a(:,3),'bo-', 'LineWidth',1.5);hold on;

plot3(a(:,4), a(:,5), a(:,6),'ro-', 'LineWidth',1.5);

plot3(a(:,7), a(:,8), a(:,9),'go-', 'LineWidth',1.5);

name1=strcat('20 °C');

name2=strcat('27 °C');

name3=strcat('37 °C');

hLegend=legend(name1,name2,name3,'Location','NorthWest');

hXLabel=xlabel('Frequency shift (Hz)');

hYLabel=ylabel('Time (h)');

hZLabel=zlabel('Dissipation shift (x10^-6)');

set( gca                       , ...

    'FontName'   , 'Arial' );

set([hXLabel, hYLabel, hZLabel], ...

    'FontName'   , 'Arial');

set([hXLabel, hYLabel, hZLabel]  , ...

    'FontSize'   , 11          );

a=get(gca, 'xlabel');

set(a,'rotation',17.5)

a=get(gca, 'ylabel');

set(a,'rotation',-23.5)

set(gca, ...

  'Box'         , 'off'     , ...

  'TickDir'     , 'out'     , ...

  'TickLength'  , [.02 .02] , ...

  'XMinorTick'  , 'on'      , ...

  'YMinorTick'  , 'off'      , ...

  'YGrid'       , 'on'      , ...
```

```
  'XColor'      , 'k', ...
  'YColor'      , 'k', ... %'YTick'       , 80:110, ...
  'LineWidth'   , 2         );
set(gca, ...
  'Box'         , 'off'     , ...
  'TickDir'     , 'out'     , ...
  'TickLength'  , [.02 .02] , ...
  'YMinorTick'  , 'on'      , ...
  'ZMinorTick'  , 'off'      , ...
  'XGrid'       , 'on'      , ...
  'YColor'      , 'k', ...
  'ZColor'      , 'k', ... %'YTick'       , 80:110, ...
  'LineWidth'   , 2         );
set(gca, ...
  'Box'         , 'off'     , ...
  'TickDir'     , 'out'     , ...
  'TickLength'  , [.02 .02] , ...
  'XMinorTick'  , 'on'      , ...
  'ZMinorTick'  , 'off'      , ...
  'ZGrid'       , 'on'      , ...
  'XColor'      , 'k', ...
  'ZColor'      , 'k', ... %'YTick'       , 80:110, ...
  'LineWidth'   , 2         );
set(gcf, 'PaperPositionMode', 'auto');
```

Annex IV

Different versions of the platform.

Version	Experiment type	Technology	Equipment	Material	Task	Results
1	Dynamic	PolyJet™ Technology	Objet Eden™ line	RGD525	Evaluate the spring-load location	Fail
					Evaluate the hinge tolerance	Correct
					Evaluate the fluid escape of the inlet-outlet connectors	Correct
					Evaluate how the magnets close the 2part platform	Correct
					Evaluate the tolerance of the space sensor of 0,5mm of thickness	Fail
					Test PDMS as the O-ring seal for 1mm of space	Fail
1	Dynamic	DLP® Technology (Digital Light Processing)	EnvisionTEC	e-Shell 300 crystal clear	Evaluate the transparency of the high resolution technology	Not enough
2	Dynamic	PolyJet™ Technology	Objet Eden™ line	veroclear	Test Epidor 1mm O-ring seal for 0,8mm of space	Not enough
					Evaluate the tolerance of the space sensor of 1mm of thickness	Fail
2	Static	PolyJet™ Technology	Objet Eden™ line	veroclear	Evaluate the correct design for the spring-load	Design complication
					Compare the transparency of the last technology	Not enough
3	Static	Fused deposition modeling (FDM)	Fortus 400mc	PC	Evaluate the tolerance of the space sensor of 1mm of thickness	Correct
					Evaluate the space tolerance of the outer glass	Correct
					Test Epidor 1mm O-ring seal for 0,7mm of space	Not enough
					Evaluate the fluid escape of the entire platform	Fail
4	Static	Fused deposition modeling (FDM)	Fortus 400mc	PC	Evaluate the correct design for the double spring-load and alignment	Correct
					Evaluate the fluid escape of the entire platform	Fail
					Test Epidor 1mm O-ring seal for 0,5mm of space	Correct

Version	Experiment type	Technology	Equipment	Material	Task	Results
5	Static	Fused deposition modeling (FDM)	Fortus 400mc	PC	Evaluate the tolerance of the space sensor of 0.5mm of thickness	Correct
					Evaluate O-ring size reduction to contact the sensor	Correct
					Test Epidor 1mm O-ring seal for 0,6mm of space	Correct
					Evaluate the fluid escape of the entire platform	Fail
6	Static	Fused deposition modeling (FDM)	Fortus 400mc	PC	Evaluate bigger magnets to close the 2part platform	Correct
					Evaluate the space tolerance of the outer glass	Correct
					Evaluate the increment of the internal volume of the platform	Correct
7	Dynamic	Fused deposition modeling (FDM)	Fortus 400mc	PC	Evaluate flow passing only over the electrodes	Correct
					Evaluate the reduction of low volume in the platform	Correct
					Evaluation of an autoclave test of the magnets without corrosion	Fail
8	Static	Fused deposition modeling (FDM)	Fortus 400mc	PC	The substitution of the magnets for double hinge	Correct
					Evaluate the fluid escape of the entire platform	Fail
					Evaluation of a mechanization of the surface contact	Not enough
9	Dynamic	Fused deposition modeling (FDM)	Fortus 400mc	PC	Evaluate a high flow passing over the sensor	Correct
					Evaluate the fluid escape of the entire platform at with low flow	Fail
10	Static	Fused deposition modeling (FDM)	Fortus 400mc	PC	Evaluate the substitution of double hinge for 4 screw closure	Correct
11	Dynamic	Fused deposition modeling (FDM)	Fortus 400mc	PC	Evaluate the flow with new closure and PDMS window	Not enough
12	Dynamic	Fused deposition modeling (FDM)	Fortus 400mc	PC	Evaluate the flow from the bottom and new connectors	Fail
13	Dynamic	Fused deposition modeling (FDM)	Fortus 400mc	PC	Evaluate the fluid scape with connectors surrounded with PDMS	Not enough
14	Dynamic	Fused deposition modeling (FDM)	Fortus 400mc	PC	Evaluate the fluid scape with a PDMS for base sensor and O-ring	Correct
15	Dynamic	Fused deposition modeling (FDM)	Fortus 400mc	PC	Evaluate the reduction of material for cost reduction	Correct

Annex V

Top Part designed for rapid prototyping fabrication:

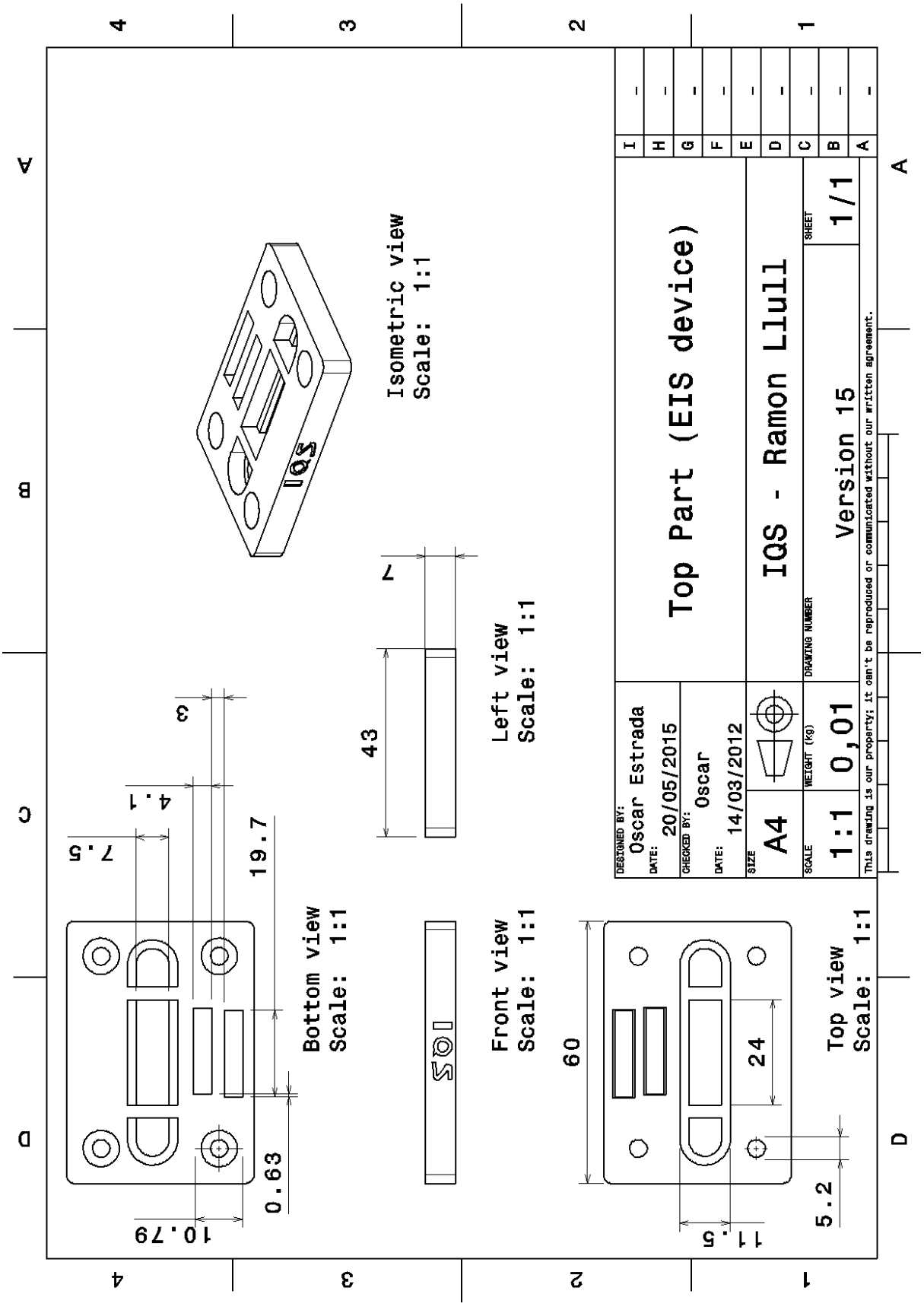

Bottom Part designed for rapid prototyping fabrication:

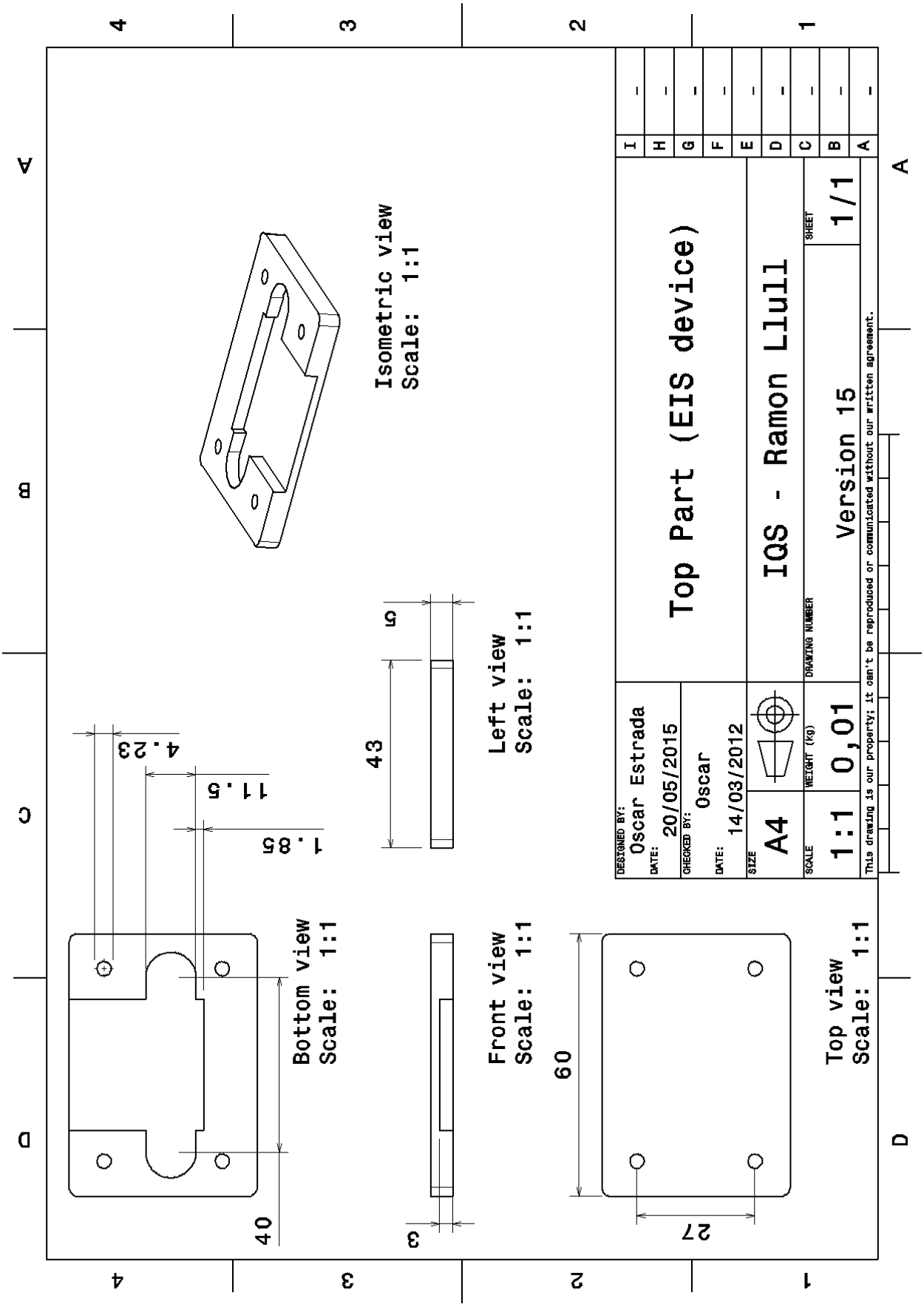

Annex VI

The data presented in this Thesis has been published or is under process of publication. The state of publication is the following:

Chapter 4 and Chapter 5:

O. Estrada-Leypón, a. Moya, a. Guimerà, G. Gabriel, M. Agut, B. Sánchez, S. Borrós. Simultaneous monitoring of Staphylococcus aureus growth in a multi-parametric microfluidic platform using microscopy and impedance spectroscopy, *Bioelectrochemistry*. 105 (2015) 56–64. doi:10.1016/j.bioelechem.2015.05.006.

Chapter 6:

O. Estrada-Leypón, M. Laabei, W. D. Jamieson, A. Moya, R. Villa, A. T. A. Jenkins, S. Borrós. Correlation between biofilm evolution and secreted virulence factors of Staphylococcus aureus using a customized microfluidic platform.

Chapter 3 and Chapter 7:

O. Estrada-Leypón, A. Mas, J. Gilbert, A. Moya, A. Guimerà, G. Gabriel, M. Agut, S. Borrós. Microfluidic devices for real-time studies of bacterial biofilms quantified with label-free technologies tuned with antibacterial coatings.

Bioelectrochemistry 105 (2015) 56–64

Contents lists available at ScienceDirect

Bioelectrochemistry

journal homepage: www.elsevier.com/locate/bioelechem

Simultaneous monitoring of *Staphylococcus aureus* growth in a multi-parametric microfluidic platform using microscopy and impedance spectroscopy

O. Estrada-Leypon [a], A. Moya [b,c], A. Guimera [b,c], G. Gabriel [b,c], M. Agut [e], B. Sanchez [d], S. Borros [a,*]

[a] Grup d'Enginyeria de Materials (GEMAT), Institut Químic de Sarrià, Universitat Ramon Llull, Spain
[b] Instituto de Microelectrónica de Barcelona (IMB-CNM, CSIC), Bellaterra, Spain
[c] Centro de Investigación Biomédica en Red, Bioingeniería, Biomateriales y Nanomedicina (CIBER-BBN), Zaragoza, Spain
[d] Department of Neurology, Division of Neuromuscular Diseases, Beth Israel Deaconess Medical Center, 330 Brookline Avenue, Harvard Medical School, Boston, MA 02215-5491, USA
[e] Grup d'Enginyeria Molecular (GEM), Institut Químic de Sarrià, Universitat Ramon Llull, Spain

ARTICLE INFO

Article history:
Received 13 November 2014
Received in revised form 22 April 2015
Accepted 4 May 2015
Available online 13 May 2015

Keywords:
Biofilm
Microfluidic device
Bacitracin
Impedance spectroscopy
Interdigitated microelectrodes

ABSTRACT

We describe the design, construction, and characterization of a scalable microfluidic platform that allows continuous monitoring of biofilm proliferation under shear stress conditions. Compared to other previous end-point assay studies, our platform offers the advantages of integration into multiple environments allowing simultaneous optical microscopy and impedance spectroscopy measurements. In this work we report a multi-parametric sensor that can monitor the growth and activity of a biofilm. This was possible by combining two interdigitated microelectrodes (IDuEs), and punctual electrodes to measure dissolved oxygen, K+, Na+ and pH. The IDuE has been optimized to permit sensitive and reliable impedance monitoring of *Staphylococcus aureus* V329 growth with two- and four-electrode measurements. We distinguished structural and morphological changes on intact cellular specimens using four-electrode data modeling. We also detected antibiotic mediated effects using impedance. Results were confirmed by scanning electrode microscopy and fluorescence microscopy after live/dead cell staining. The bacitracin mediated effects detected with impedance prove that the approach described can be used for guiding the development of novel anti-biofilm agents to better address bacterial infection.

1. Introduction

Bacterial attachment and the development of microbial communities commonly known as biofilms cause equipment damage and product contamination and are prominent sources of infection [1]. For example, in the clinical setting, the infection on implants and/or indwelling medical devices such as catheters or heart stents requires a complete removal of the device from the patient very often [2]. In this regard, the attention towards the development of novel lab on a chip platforms to address bacterial infection has increased in the past years [3–5]. These platforms are very attractive because they allow the continuous flow of nutrients. Such conditions are more realistic regarding pathogenesis. Moreover, lab on a chip platforms offer the possibility to study biofilm formation under controlled conditions. Biofilm formation has been described in the literature as a three-step process [6]. It starts with an initial attachment of the bacteria to the material surface by the action of physical forces followed by the formation and maturation of a strong bacterial layer by secreting extracellular polymeric substances (EPS) that provides the biofilm a high resistance to antibiotics [7,8].

To study this biofilm formation methods of continuous label-free monitoring techniques such as surface plasmon resonance [9,10] and quartz crystal microbalance [11] have been developed in the lasts years also gaining a lot of attention in microbiology. The quartz crystal microbalance is able to calculate the amount of biomass attached on the surface applying mathematical approximations. Although both techniques have shown promising results, they are not designed for in-field analysis as they require skilled personnel and the use of equipment that is expensive, non-portable, and cumbersome to assemble. Optical microscopy is a cheap and simple alternative method for characterizing biofilms but, at the same time, it is an end-point assay that involves labeling and destruction of bacteria. Therefore, it is pertinent to develop tools that allow non-disruptive, continuous and label-free monitoring of the dynamic processes and mechanisms of biofilm formation under real conditions [12].

A widely used alternative method for microorganism growth detection is based on electrical impedance spectroscopy measurements [13]. Numerous *in vitro* studies can be found in the literature based on the

* Corresponding author at: Via Augusta 390, 08017 Barcelona, Spain.
E-mail address: salvador.borros@iqs.url.edu (S. Borros).

http://dx.doi.org/10.1016/j.bioelechem.2015.05.006
1567-5394/

relative impedance changes induced after cell adhesion onto the electrodes [14,15], some of them using commercial interdigitated microelectrodes (IDuE) [16,17]. Despite offering a large sensitive area in a limited space, most of commercial IDuE do not offer the possibility of studying cell growth under flow conditions, a variable that is known to affect biofilm structure and behavior [18], or to measure additional cell culture parameters to control other cell cultures analytes of interest [19]. Furthermore, not many studies have been published on biofilm growth monitoring in a microfluidic channel using IDuEs [20–23], a technology that deserves further study and refinement.

To address some of the technological limitations faced by the conventional electrodes and current devices for bacterial biofilm growth primarily based on cultivation within multi-well platforms, we have designed and fabricated our own multi-parametric sensor and low-cost microfluidic platform. The system is designed to be used in multiple environments and to allow simultaneous and continuous monitoring of biofilm proliferation under shear stress using optical microscopy and multiple read-outs. The chip used in this study contains two IDuEs (rectangular and circular) and punctual electrodes to measure dissolved oxygen (DO) [24], K+, Na+ and pH. Two- and four-electrode configuration impedance measurements can be performed indistinctly on the same IDuE. In this work we optimize the rectangular IDuE geometry with a finite element model (FEM) to reduce the measurement spatial resolution while maintaining a large electrode area. The culture area of the proposed platform is fabricated using transparent material including the electrode substrate to enable the comparison with microscopy evaluation techniques. Real-time monitoring of the important pathogen, *Staphylococcus aureus*, biofilm formation during 24-h experiments using the optimized IDuE was compared to a circular IDuE electrode similar to that from Roche Applied Science (Basel, Switzerland). Susceptibility to the antimicrobial peptide bacitracin was also investigated. The results were confirmed by scanning electrode microscopy and fluorescence microscopy after live/dead cell staining of the bacteria in the measured biofilm.

2. Materials and methods

2.1. Multi-parametric sensor

This section details the overall design of the multi-parametric sensor. In this work, we have focused only on the performance of the impedance characteristics. To optimize the physical dimensions and geometry of the IDuE (Fig. 1A), we simulated a 2D cross-section FEM model of the electrode geometry with a mesh of 20,000 elements (Fig. 1B) with COMSOL Multiphysics® 4.4 (Burlington, MA, USA). The impedance sensitivity, which depends on the electrode dimensions, was calculated according to [25]

$$S = \frac{\vec{J}_1 \vec{J}_2}{I^2}, \quad (1)$$

where S is the sensitivity to the conductivity changes as a function of the position, J_1 is the current density vector when the current is injected between I+ and I− electrodes, and J_2 is the current density vector when the same current is injected between the voltage sensing electrodes V+ and V−.

The results in Fig. 1B reveal that the area where the IDuE sensitivity is higher corresponds to gap area between the IDuE groups denoted in the figure as W_{INT}. The FEM results (Supplementary Fig. 1) reveal that the optimal geometry is a trade-off between minimizing W_{INT} while also keeping minimal W_D and n_D, and maximal L_D. In all, the dimensions of the IDuE are $W_{INT} = 21$ μm the interdigitated group space, $W_D = 21$ μm the digit width, $n_D = 32$ the number of digit pairs and $L_D = 7.11$ mm the digit length (detail shown in Fig. 1C). The chip dimensions are 23 mm × 18 mm.

The chip also incorporates additional sensors (Fig. 1D) described elsewhere [24,26] for measuring different biofilm parameters of interest. The punctual electrodes allow to make electrochemical measurements of DO, K+, Na+ and pH. The amperometric measurement of DO is achieved using a working electrode (WE), a reference electrode (RE) and a counter electrode (CE) [24]. The measurement of Na+ and K+ ions is performed with a potentiometric ion-selective technique using the WE for each ion measurement and the RE [27]. Finally, the pH sensor consists of a punctual electrode with an iridium oxide layer using the WE and the RE [26].

The chip was fabricated in the clean room facilities at the Barcelona Microelectronics Institute, Spain, through standard photolithography techniques [28–30]. Three different metal layers (titanium, nickel and gold) were deposited by sputtering over a 500 μm thick Pyrex wafer. First, a 15 nm titanium layer was placed just to improve the adhesion of subsequent metals. Then, a 15 nm nickel layer was deposited on top to the Ti layer to provide a diffusional barrier and to prevent the formation of intermetallic titanium–gold compounds. Finally, the active metal layer was obtained by depositing 150 nm of gold. Thereupon, the electrodes and the metal tracks were patterned using selective wet etching baths, according to a standard lithographic process. At the end, a double layer of 400 nm of silicon oxide and 400 nm of silicon nitride (Si3N4) was deposited by plasma enhanced vapor deposition. This double layer was used for passivation and defining the electrode active area and the connection pads. After the clean room process, a disk saw was used to dice the wafer into individual chips (8 per wafer). Finally, each chip was characterized by cyclic voltammetry using saline solution (0.9% sodium chloride) to verify that there was no shortcut between the IDuE fingers.

2.2. Microfluidic device design and fabrication

Initially, the design of the flow chamber was based on the general microfluidic description reported in [31]. Although the general trend in the field is to reduce both the channel and the chamber size [32], in our approach, the minimal dimensions were constrained by the requirement to allow visual inspection and time-lapse recording of the experiment with a microscope. The final size of the platform is 60 mm × 43 mm (Fig. 2), sufficient to accommodate the microscope objective. Since it has been reported that the biofilm attaches to (non-)biological biocompatible surfaces [33], the device is made of a combination of polycarbonate and polydimethylsiloxane (PDMS).

Polycarbonate is used for the construction of the upper and lower lids (Fig. 2A). The top lid holds the connectors, the screws, and the spring-loads for the electrical connections to the sensor. The bottom part is a solid support containing the PDMS support for the sensor and the threaded holes to close the device in a single piece (Fig. 2B). The platform was designed using Catia V5R19 and built with 3D printing technology with fused deposition modeling (FDM) technology. The microfluidic channel and the sensor support were made of PDMS because of its characteristics: biocompatibility [34], gas permeability to supplement oxygen while the nutrients were pumped through the channel, mechanical flexibility to avoid chip fracture and, finally, optical transparency [35] to allow microscopy imaging over the sensing area. The parts fabricated with PDMS (Fig. 2C) were patterned using a replica molding technique applying a master structure made of the negative piece printed in 3D with FDM technology as well. Once the device is closed, the bacterial culture is only in contact with PDMS and the biosensor (Fig. 2D).

The use of the spring-load connectors provided a good electrical contact with the pads and simplified the process of replacing the chip when necessary. It also made possible to reuse the sensor by autoclaving. Besides, the biofilm formed could be imaged easily with a confocal microscope because the sensor, as an independent part, fitted perfectly with the cover slip to perform an end-point assay.

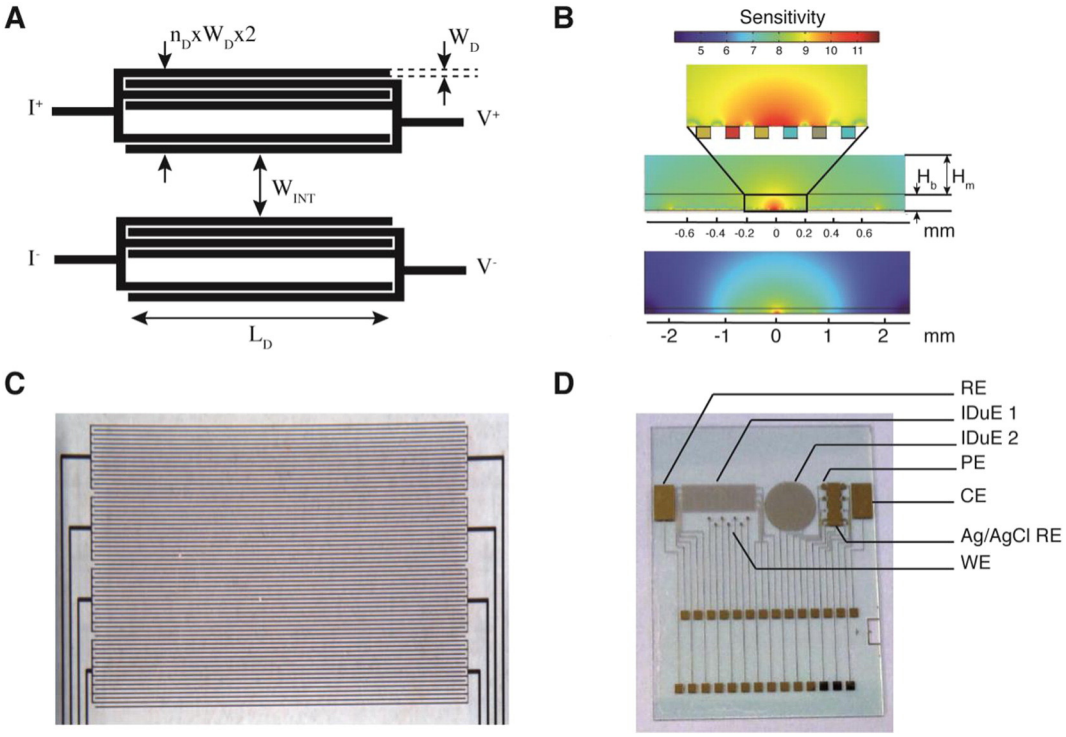

Fig. 1. (A) Schematic design of the optimized interdigitated microelectrode (IDuE). The IDuE fingers are connected to the outer and inner current and voltage electrodes denoted in the figure as I+ and I− and V+ and V− respectively. (B) Sensitivity map obtained from a 2D cross-section finite element model (FEM) considering the height of the biofilm and the flow channel, H_b and H_m respectively. Abbreviations: W_{INT}, interdigitated group space; W_D, digit width; n_D, number of digit pairs and L_D, digit length. (C) Zoom of the rectangular IDuE fabricated on a Pyrex substrate. (D) Chip module containing the different sensors. The chip contains two IDuEs, rectangular (IDuE 1) and circular (IDuE 2). The electrodes for the measurement of dissolved oxygen are the reference electrode (RE), the working electrode (WE) and the counter electrode (CE). The punctual electrodes (PE) for the potentiometric measures were prepared to be selective of Na+ and K+. For the pH measurement, an additional iridium oxide layer is electrodeposited on the electrode selected. For robustness purposes, the PE are replicated. The reference electrode for potentiometric measures of Na+, K+ and pH is the silver/silver chloride electrode (Ag/AgCl RE).

2.3. Biofilm culture

The bacteria were prepared from glycerol stock cultures stored at −80 °C and streaked onto tryptic soy agar (TSA) plates [36] because the strain *S. aureus* V329 is Gram positive [37]. The agar plate was placed in an incubator at 37 °C for 16 h to grow the colonies. A single colony was then transferred from the plate to a falcon tube containing 10 mL of tryptic soy broth (TSB) media agitated for 16 h at 37 °C. Following, the suspension was diluted to have a final absorbance of 0.084 at 600 nm wavelength. This dilution was used to feed the microfluidic device in the stage 2 of the flow experiment to generate the biofilm (refer to Section 2.6).

2.4. Impedance system

A commercialized stepped-sine impedance analyzer 4192A from Hewlett-Packard was used to perform impedance spectroscopy measurements. The impedance meter was connected to a custom multiplexed front end. The system was controlled by customized LabVIEW (National Instruments, Austin, TX, USA) based software using a 82357B USB/GPIB interface, allowing to switch between two- and four-electrode impedance configuration measurements automatically. The impedance (magnitude and phase) was acquired performing a frequency sweep between 100 Hz and 1 MHz (10 frequency points per decade). Each measurement included an average of 3 sweeps and required a total acquisition time of about 1 min. The technical details regarding the performance of the front-end can be found elsewhere [38]. Impedance measurements were calibrated using baseline solution measurement to compensate the frequency response of cable and electronics.

2.5. Optical microscopy

The bacterial biofilm was observed non-invasively during the 24 h course of the experiments with reflected light microscopy (Leica 2500DM) using a differential interference contrast technique. Images were taken every minute to obtain a time-lapse evolution of the biofilm adhesion and proliferation (data available in the Supplementary material).

2.6. Experiment design

During the course of the experiments, the two independent channels of the peristaltic pump (Reglo ICC, Ismatec, Glattbrugg, Switzerland) were working simultaneously. Both channels were connected with PharMed® Ismaprene tubes (0.89 mm internal diameter) to the microfluidic platform. A third channel was used to introduce fresh TSB medium into a second microfluidic platform to have negative control of biofilm formation. Both devices were connected to the impedance analyzer multiplexed front end and the impedance measurements were repeated every 10 min. The experiment consisted of three stages:

1. Conditioning. Constant feeding of TSB medium to stabilize the system forming the conditioning layer over the electrode and to prevent the formation of bubbles. Duration 2 h, flow rate 50 μL/min.
2. Seeding. Introduction of the bacteria into the system. Duration 2 h, flow rate 50 μL/min.
3. Biofilm growth. Constant feeding of sterile TSB media to establish the biofilm over the biosensor. Duration 22 h, flow rate 50 μL/min.

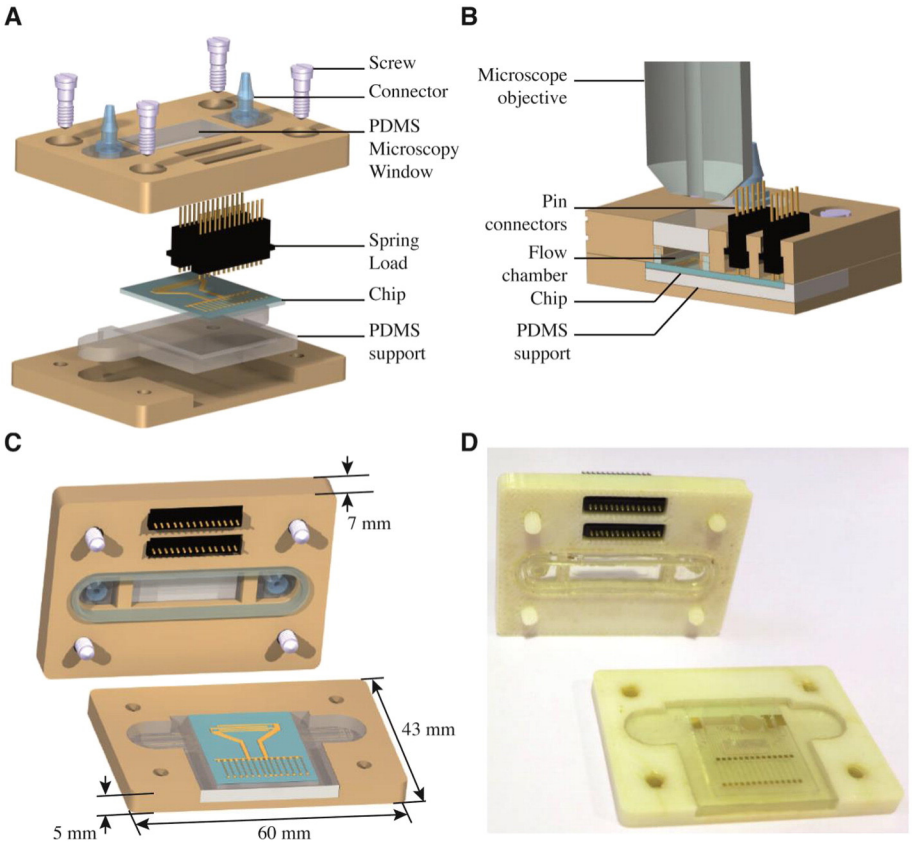

Fig. 2. (A) Computed aided design and components of the designed microfluidic device. (B) Cross-section of the device under the microscope. (C) Open view of the microfluidic platform. (D) Zenithal view of the platform fabricated with a rapid prototyping technique.

2.7. Equivalent electrical circuit and fitting

Impedance data measured with the four-electrode configuration method was fitted to the empirical complex nonlinear model described by the Cole in [39],

$$Z(f) = R_\infty + \frac{R_0 - R_\infty}{1 + \left(j\frac{f}{f_c}\right)^{\alpha}}. \quad (2)$$

in Matlab (Natick, MA, USA) using the Marquardt–Levenberg iterative weighted complex nonlinear least square algorithm [40]. The maximum iterations and the fitting tolerance were set to 1e6 and 1e−12 respectively. From the optimal curve-fit parameters, the Jacobian was calculated numerically. The covariance matrix was estimated from the Jacobian using a diagonal matrix containing as weights the impedance data std. The asymptotic standard error for the optimal model parameters was finally obtained from the square root of the diagonal elements of the covariance matrix.

The central relaxation frequency f_c corresponds to the frequency with the highest absolute value of the impedance imaginary part. The α parameter explains the dispersion in the cellular membrane capacitances measured and is thus related to the dispersion of the shape and size distribution. The case when $\alpha = 1$ the ideal case when cells are perfectly homogenous with a spherical shape as proposed by Fricke and Morse [41]. The resistances R_0 and R_∞ are the resistances when $f \to 0$ and $f \to \infty$ respectively [42].

2.8. Live/dead viability assay

The end-point assay was realized immediately after the completion of the 24 h experiment opening the microfluidic device and staining the IDuE with fluorescence. We used a confocal laser scanning microscope (LSM510 META, Zeiss) controlled by AIM software (version 3.2, Carl Zeiss MicroImaging GmbH, Jena, Germany). The microscope is equipped with two lasers (480 nm syto9 and 490 nm propidium iodide wavelengths) that are used to determine the presence of biofilm alive with Live/Dead Baclight™ Bacterial Viability Kit L13152 from Invitrogen. The staining was carried out for 15 min and the sensor was washed seven times before it was placed on a coverslip of 60 mm × 24 mm upside down to image the sample from the bottom. Biofilm image was acquired 15 min after the end of the 24 h experiment.

2.9. Scanning electron microscopy as end-point assay

Biofilms were prepared for scanning electron microscopy (SEM) as described previously [43]. Briefly, the air-dried biofilms were fixed with 2 mL of 2.5% glutaraldehyde in 0.1 mol/L sodium phosphate buffer, rinsed once in the same buffer and then in deionized water followed by overnight drying. The biosensor was attached to aluminum mounts and coated with gold using a Polaron Emitech SC7640 sputter coater (New Haven, UK). Images were obtained with a JEOL JSM-5310 scanning electron microscope (JEOL Ltd., Tokyo, Japan) at 3000× magnification.

3. Experimental results and discussion

3.1. Microscope characterization images

To evaluate the feasibility of the microfluidic platform to monitor biofilm formation on the IDuE, we performed real-time image recording and impedance measurements simultaneously. Fig. 3 shows time-lapse microscopy images indicating the two main steps of biofilm conditioning and formation [44]. In the initial absorption phase (Fig. 3B–C), the IDuE surface is initially covered by the conditioning film [45,46], a

mixture of small molecules (water and salt ions) followed by a single layer of small organic molecules or proteins that are present in the medium. Then, the second stage (Fig. 3C–D), is characterized by the initially reversible adsorption of microorganisms to the conditioning film, which arrives by Brownian motion, gravitation, diffusion or intrinsic motility [44]. At the same time, bacteria also adhere to each other forming microbial aggregates before adsorbing the conditioning film (Fig. 3E). Since the bacteria adhere to the conditioning film and not to the IDuE surface, the strength of the initial biofilm will depend on the structure of the conditioning film and/or the flow conditions of the system. The beginning of the third stage starts when the initial biofilm has enough strength to support the constant flow of fresh TSB media for a long period of time (Fig. 3G–H). At a certain point during the third stage, the initial reversible adsorption becomes irreversible, mainly through the secretion of EPS by the adsorbed bacteria in the second stage. The final result is the biofilm structure (Fig. 4), a community of cells which together are medically important as they are highly resistant to both the cells of the immune system and antibiotics and provide a reservoir for future infection [7]. The thickness of the dehydrated biofilm was estimated at 100 μm approximately using SEM.

3.2. Live/dead cell staining

Although most of the bacteria were still alive after 24 h (Supplementary Fig. 2), the number of cells on the electrode was less than expected considering the thickness shown in Fig. 4B. Even if we could have quantified the number of cells by means of colony-forming unit or spectrophotometry, we preferred no to do so to prevent altering the course of the experiment. The disagreement in the estimated biofilm thickness between the SEM experiment and the live and dead experiment was caused by the dry cleaning cycles performed on the stained sample. On the other hand, this result serves to prove the point that biofilm is capable of withstanding high shear forces due to the washing process as compared to the low shear stress of media flow and SEM preparation.

3.3. Impedance monitoring of bacterial biofilm in growth media

Monitoring biofilm formation combining label-free biosensors and impedance spectroscopy measurements on the surface of electrodes is an alternative approach that has gained increasing interest, previously described using IDuEs [47,48] which combine both impedimetric and amperometric measurements [49]. In particular, much of the existing studies are based on two- or three-electrode measurements [50,51,52–54] because of their simplicity and ability to detect and track the biofilm formation by the changes occurring at the surface electrode. These features are of great interest by themselves but introduce a source of indetermination if the interest is to obtain a quantitative measurement of the biofilm growing in the layers above the electrode surface. On top of that, the fact that the two-electrode configuration includes the impedance and polarization of the counter and the working electrodes can jeopardize the data analysis if the contribution of each electrode is not the same. Furthermore, when the electrode surface is fully covered by bacteria or EPS, the inherent sensibility of this technique is significantly reduced as compared to the four-electrode configuration technique [38]. With the four-electrode method [55], the effect of the electrode–electrolyte is excluded from the impedance measurement offering an increased sensitivity to monitor cell concentration and the possibility to extract morphological and structural information from the impedance (refer to Section 3.5). Despite the aforementioned advantages, we are not aware of any previous work where four-electrode measurements were performed in a microfluidic device to monitor biofilm.

Fig. 5A shows the time course of the impedance magnitude at 10 kHz where it is more sensitive to biofilm formation [56]. Impedance is normalized to its maximum value for comparison purposes (Supplementary Fig. 3). The unexpected increase at 2 h is attributed to the transient phase before stabilization and the fact that the medium containing the bacterial suspension was not pre-warmed. Similar to the results shown in [47], the time to be detected by impedance changes due to biofilm growth is about 5 h. In the initial phase where the concentration of biofilm is low, we can see the sensibility of the two-electrode technique to detect that biofilm proliferation is decreased. Fig. 5A also shows that the two-electrode circular IDuE has lower dynamic range to detect cell growth than the rectangular IDuE, and saturates to its maximum value after 10 h. The ability to detect growth changes can be further improved with the four-electrode method. The detected change is 15%, approximately 5% higher than that of the two-electrode method measuring under the same experimental conditions. The level of impedance changes detected is similar to that of the 10% change detected for the same range of frequencies at 12 h obtained by Zikmund et al. [57] where the growth of *Escherichia coli* was monitored. Despite the differences in the dimensions and geometry between pathogens, *E. coli* is a rod-shaped bacterium and measures approximately 0.5 μm in width by 2 μm in length while *S. aureus* has a spherical shape and a size of 0.5–1 μm, we detected the same relative change at 10 h after infection (2 h after starting the experiment). Compared to the 5% impedance change detected in [47], we think this difference may be due to the electrode optimization through FEM simulations. On the other hand, the four-electrode method allows the morphological impedance spectrum and structural information regarding the biofilm to be interpreted (Fig. 7).

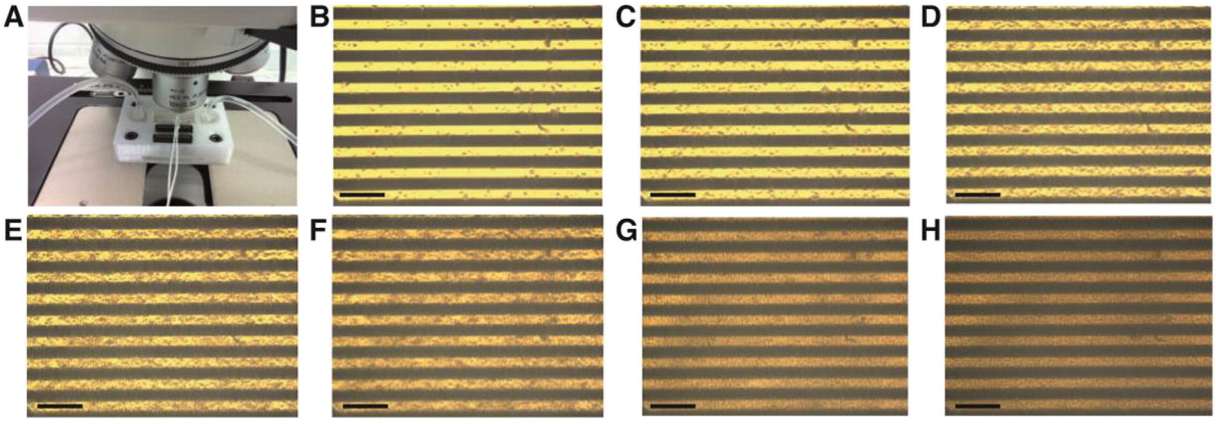

Fig. 3. (A) Time-lapse optical microscope (Leica DM2500) at the initial timing just before the bacterial infection; (B), 0 h; (C), 3 h; (D), 5 h; (E), 8 h; (F), 13 h; (G), 16 h; and (H), 21 h. The time-lapse recording was performed with a 1 min interval for 24 h for editing a video at 25 fps (data available in the Supplementary material). Scale bar: 200 μm.

3.4. Bacitracin mediated effects on impedance

In Fig. 5B we targeted *S. aureus* bacteria with bacitracin, an antibiotic frequently used for antimicrobial therapy [58]. Bacitracin is a polypeptide antibiotic that inhibits the dephosphorylation of the lipid carrier bactoprenol, an important lipid molecule which transports peptidoglycan precursors across the cell membrane and is therefore essential in the synthesis of growing peptidoglycan, by forming a complex lipid–antibiotic, which is very strong and specific to this phospholipid. The inhibition of the complex lipid carrier in the cell wall biosynthesis ceases bacterial growth. Apart from disrupting bacterial wall biosynthesis, bacitracin provokes modifications in the permeability of the plasma membrane as the lipid is an integral component of the membrane [59,60]. Unlike other antibacterial compounds that only affect earlier phases in the biofilm formation such as mupirocin [61], bacitracin influences biofilm at any stage of the process. The effects that bacitracin has on biofilms are illustrated in Fig. 5B using the multi-parametric platform presented in this paper. During normal proliferation conditions the impedance changes are detected until 15 h of inoculation (Fig. 5A), with bacitracin the relative changes in impedance observed during the first 10 h are not significant as they are in the same order of the standard deviation. The fact that there is no significant change from baseline to the end of the experiment indicated the inhibition effect of bacitracin effect on biofilm formation.

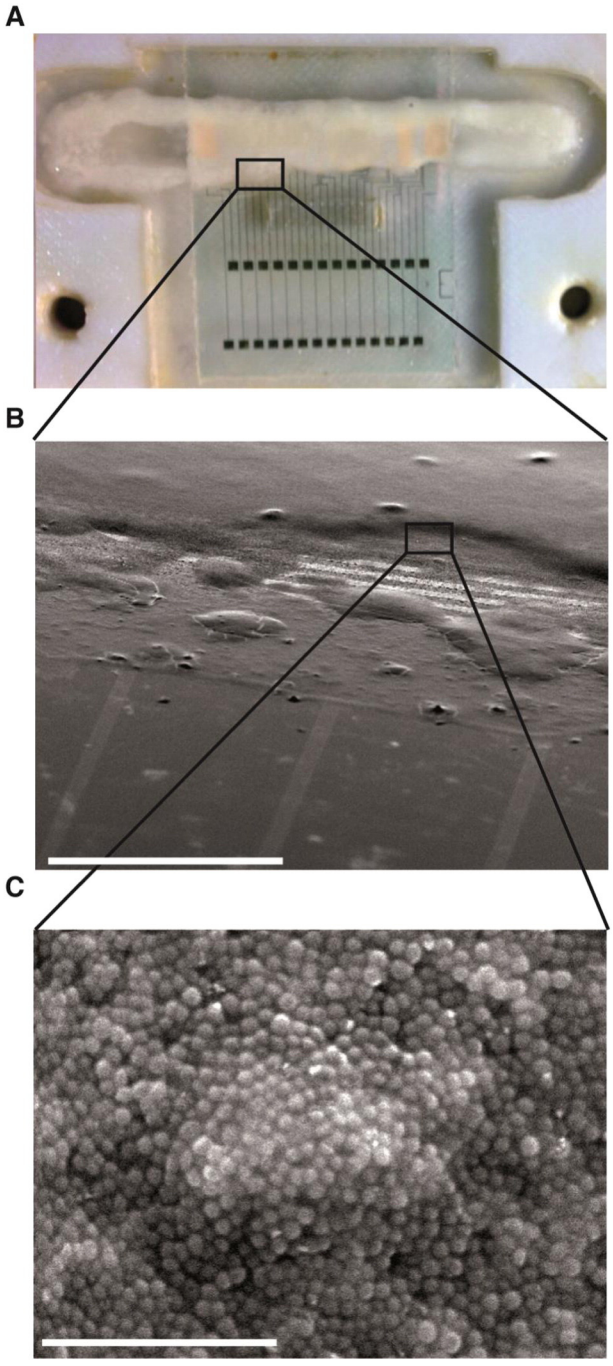

Fig. 4. (A) Presence of biofilm in the flow chamber after the end of the 24 h experiment. (B) Scanning electron microscopy images showing the biofilm growth on top of the interdigitated microelectrode. (C) Detail of *Staphylococcal* bacteria attached on the IDuE surface. Scale bars: (B), 700 μm; (C), 10 μm.

3.5. Structural and morphological biofilm changes

Fig. 6A shows the fitting four-electrode impedance data to the Cole model for different time instants. It is noted that as the experiment proceeds, the impedance arc moves on the horizontal axis due to an increased resistance caused by cell proliferation consistent with [62]. The details of the time evolution of the parameters R_0 and R_∞ are

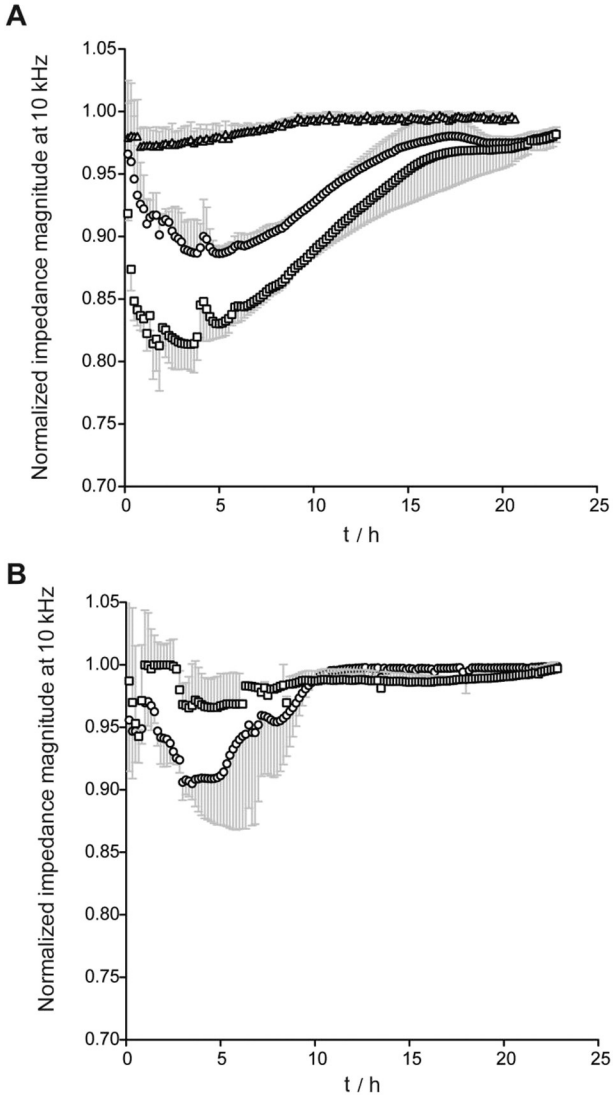

Fig. 5. Time course of the normalized impedance magnitude (mean ± std., $n = 3$) detected with the rectangular and circular interdigitated microelectrodes (IDuEs), IDuE 1 and IDuE 2 respectively. (A) Normal conditions using IDuE 1 performing 2 electrode configuration (circles) and 4 electrode configuration (squares). Data acquired with IDuE 2 performing 2 electrode configuration (triangles). (B) Presence of bacitracin using IDuE 1 performing 2 electrode configuration (squares) and 4 electrode configuration (circles).

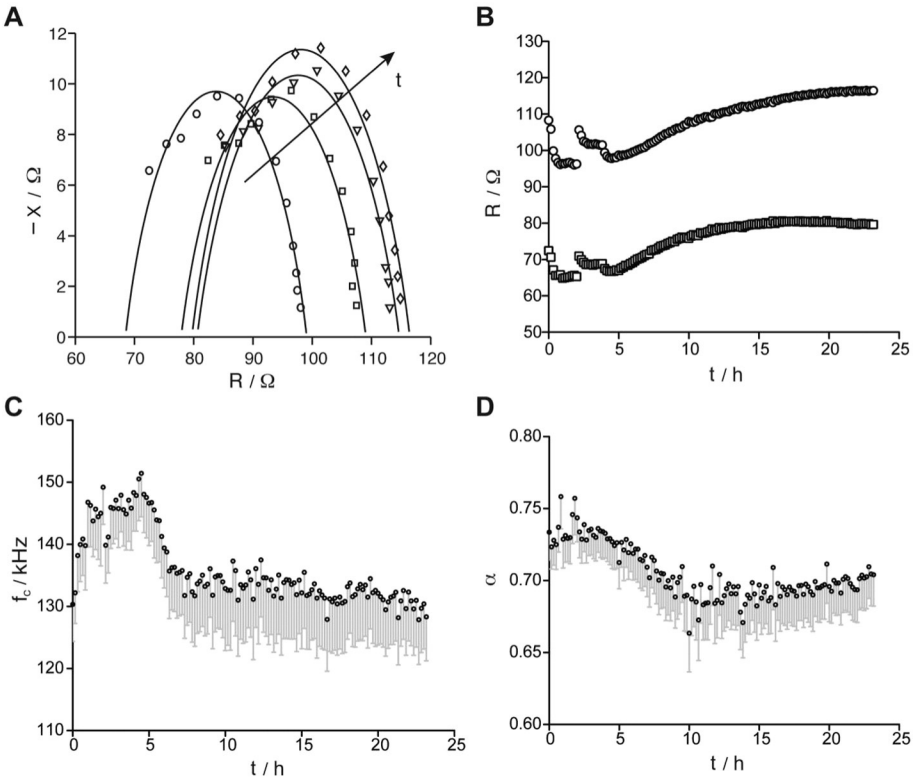

Fig. 6. Representation of the complex plane of the impedance measured with the four-electrode method. (A) The solid lines correspond to the Cole fitting at different times of 5 h (circles), 11 h (squares), 17 h (triangles), and 23 h (diamonds). (B) Time course of the impedance model parameters (mean ± std.); R_0 (circles) and R_∞ (squares) represent the impedance resistances when $f \to 0$ and $f \to \infty$, (C) f_c is the center frequency of the impedance relaxation and (D) α the empirical parameter.

illustrated in Fig. 6B. The increase in R_0 and R_∞ at 2 h is due to the same reasons mentioned in Section 3.3. Immediately after, both parameters R_0 and R_∞ started to increase during the first 15 h. Thereafter, while R_0 continued to increase slightly over time, R_∞ experienced a slight decrease starting at 20 h. We believe that this decrease in R_∞ might due to the metabolic activity of the biofilm, which changes the intracellular ionic concentration of the medium affecting the high frequencies as reported in [20].

As for the value of the center frequency shown in Fig. 6C, the high value at the beginning of the experiment (approximately 150 kHz) and the monotonously decreasing evolution from 5 h indicates possible structural changes occurring during formation of the biofilm. The initial high value of the center frequency in the early hours correlates with a lower cell dimension corresponding to a few scattered cells on top of the electrode surface. We think that the increase in dimension when cells are clustered forming colonies leads to a reduction in the center frequency (about 130 kHz) at 20 h. Of note, the frequency range in which morphological changes can be detected is in the range of 100 kHz to 200 kHz, where the electrode impedance contribution measured with the two-electrode method might hinder the detection of such changes (Supplementary Fig. 3) [63–65].

Our previous observation in the change in biofilm structure is also supported analyzing the time dependence of the α parameter in Fig. 6D. At the beginning of the experiment, the value of α is closer to one due to the homogeneity of the cells present on the electrode. The few sparse cells present on the electrode surface still maintain their spherical shape intact. The lower α value could explain why cells group together to create colonies [18]. At first, clusters of cells and colonies were of a variety of sizes and therefore more heterogeneous than the initial phase. As the dimensions of the colonies are more homogenous, the alpha value increases towards 1. In all, our limited results indicate that it is possible to use the Cole model parameters as surrogate measures of biofilm activity, however, further work in this direction is needed.

3.6. Biofilm estimator E

To prevent the interpretation of the four-electrode impedance measurements from being influenced by ion concentration changes due to the biofilm metabolic activity [20] or temperature variation effects, we propose the use of a ratiometric biofilm estimator E following the same reasoning as in [38,66]. The estimator allows for obtaining a quantitative measurement of biofilm considering cells above the electrode surface. The estimator is based on the relative variation of the Cole resistances R_0 and R_∞ and it is proportional to the biofilm volume fraction. We use the full expression for the calculation of the propagation of uncertainty σ_E based on the parameters covariance matrix calculated in the fitting procedure, wherein

$$E(\%) = 100 \cdot \left(1 - \frac{R_\infty}{R_0}\right)$$
$$\sigma_E(\%) = 100 \cdot \sqrt{\left(\frac{1}{R_0}\right)^2 \sigma_{R_\infty}^2 + \left(\frac{R_\infty}{R_0^2}\right)\sigma_{R_\infty}^2 - 2\left(\frac{R_\infty}{R_0^3}\right)\mathrm{Cov}(R_0, R_\infty)}. \quad (3)$$

Fig. 7 shows the E biofilm density estimator time course. It can be seen that during the first 5 h, the estimated biofilm density decreased 5% until 7–10 h, after which it increased progressively during the consecutive 15 h. The fact that the estimator is far from being saturated at 24 h value suggests that it is possible to quantify biofilm with the four-electrode method performing an experiment that lasts more than 24 h.

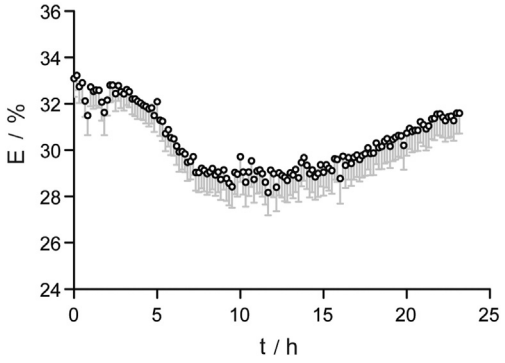

Fig. 7. Time course of the Cole-based biofilm estimator *E* (mean ± std.). Impedance data are shown in Fig. 6.

4. Conclusions

By simulating the geometry of the interdigitated microelectrode (IDuE) with a finite element model, we have been able to optimize the sensitivity of our sensor for the detection of *S. aureus* biofilm proliferation. The suitability of the microfluidic platform design was validated performing selective label-free monitoring of *S. aureus* under constant flow conditions simultaneously combining microscopy and impedance measurements with the two- and four-electrode methods. Contrary to other state-of-the-art approaches based on commercial multi-well plates used today for biofilm assays, our multi-parametric microfluidic platform can be integrated in multiple environments and offers the advantage of accounting for the effect of shear stress on the formation of bacterial biofilm, a variable that affects biofilm structure and behavior [18]. Furthermore, the system presented also offers the possibility of measuring multiple read-out configurations to detect other analytes of interest such as dissolved oxygen, K+, Na+ and pH.

Both impedance and microscopy images conveyed the same results and were in good agreement with the timings and relative changes published in the literature [49]. The novel four-electrode based measurements confirmed an improvement in detecting biofilm formation compared to the two-electrode technique as shown by the 5% increased sensitivity, in part because the effect of the electrode–electrolyte was excluded from the measurement and the IDuE was optimized. Perhaps more importantly, we could detect and track biofilm morphological and structural changes by fitting impedance to the Cole model. Unlike the two-electrode method approach based on equivalent electrical circuits, the four-electrode technique along with the Cole-based fitting approach allowed to obtain a quantitative estimate of biofilm estimator free of temperature variations and changes in ionic concentrations. The detected changes by the estimator confirm that it is possible to detect biofilm growth by performing experiments that lasts more than 24 h.

Finally, the susceptibility of biofilm to bacitracin was corroborated by a flat impedance response from baseline during the course of the experiment. The bacitracin mediated effects on impedance prove that the approach described in this work can contribute in guiding the development of new anti-biofilm agents to better address bacterial infection, for example, when antibiotics are attached on the surface of the electrodes using plasma treatment, a technology which is on the verge of development.

Acknowledgments

The authors are grateful to Dr. Jacobo Paredes for his comments on the paper. This work has been supported by the Spanish Ministry of Economia y Competitividad (MICINN) under the grant TEC2009-14779-C02-02 and the fellowship number BES-2010-033566. The authors are thankful for the help and assistance from the Grup d'Enginyeria de Materials (GEMAT) from the University Ramon Llull (URL) and the Bio model facility.

Appendix A. Supplementary data

Supplementary data to this article can be found online at http://dx.doi.org/10.1016/j.bioelechem.2015.05.006.

References

[1] L. Yang, Y. Liu, H. Wu, Z. Song, N. Høiby, S. Molin, et al., Combating biofilms, FEMS Immunol. Med. Microbiol. 65 (2012) 146–157, http://dx.doi.org/10.1111/j.1574-695X.2011.00858.x.
[2] J.J. Richards, C. Melander, Controlling bacterial biofilms, Chembiochem 10 (2009) 2287–2294, http://dx.doi.org/10.1002/cbic.200900317.
[3] J.-H. Lee, J.B. Kaplan, W.Y. Lee, Microfluidic devices for studying growth and detachment of *Staphylococcus epidermidis* biofilms, Biomed. Microdevices 10 (2008) 489–498, http://dx.doi.org/10.1007/s10544-007-9157-0.
[4] J. Kim, M. Hegde, H. Kim, K. Wood, A. Jayaraman, A microfluidic device for high throughput bacterial biofilm studies, Lab Chip 12 (2012) 1157–1163, http://dx.doi.org/10.1039/c2lc20800h.
[5] J.L. Song, K.H. Au, K.T. Huynh, A.I. Packman, Biofilm responses to smooth flow fields and chemical gradients in novel microfluidic flow cells, Biotechnol. Bioeng. 111 (2014) 597–607, http://dx.doi.org/10.1002/bit.25107.
[6] Y.H. An, R.J. Friedman, Handbook of Bacterial Adhesion, Humana Press, New Jersey, 2000.http://dx.doi.org/10.1385/1592592244.
[7] J.L. del Pozo, R. Patel, The challenge of treating biofilm-associated bacterial infections, Clin. Pharmacol. Ther. 82 (2007) 204–209, http://dx.doi.org/10.1038/sj.clpt.6100247.
[8] J. Chandra, D.M. Kuhn, P.K. Mukherjee, L.L. Hoyer, T. Mccormick, A. Mahmoud, et al., Biofilm formation by the fungal pathogen *Candida albicans*: development, architecture, and drug resistance, J. Bacteriol. 183 (2001) 5385–5394, http://dx.doi.org/10.1128/JB.183.18.5385.
[9] A.T.A. Jenkins, R. Ffrench-Constant, A. Buckling, D.J. Clarke, K. Jarvis, Study of the attachment of *Pseudomonas aeruginosa* on gold and modified gold surfaces using surface plasmon resonance, Biotechnol. Prog. 20 (2004) 1233–1236, http://dx.doi.org/10.1021/bp034367u.
[10] T.N. Tun, P.J. Cameron, A.T. Jenkins, Sensing of pathogenic bacteria based on their interaction with supported bilayer membranes studied by impedance spectroscopy and surface plasmon resonance. Biosens. Bioelectron. 28 (2011) 227–231, http://dx.doi.org/10.1016/j.bios.2011.07.023.
[11] A.L. Schofield, T.R. Rudd, D.S. Martin, D.G. Fernig, C. Edwards, Real-time monitoring of the development and stability of biofilms of *Streptococcus mutans* using the quartz crystal microbalance with dissipation monitoring, Biosens. Bioelectron. 23 (2007) 407–413, http://dx.doi.org/10.1016/j.bios.2007.05.001.
[12] P.S. Stewart, J.W. Costerton, Antibiotic resistance of bacteria in biofilms, Lancet 358 (2001) 135–138.
[13] P. Cady, S.W. Dufour, P. Lawless, B. Nunke, S.J. Kraeger, Impedimetric screening for bacteriuria, J. Clin. Microbiol. 7 (1978) 273–278.
[14] S.B. Martins, M.J. Selby, Evaluation of a rapid method for the quantitative estimation of coliforms in meat by impedimetric procedures, Appl. Environ. Microbiol. 39 (1980) 518–524.
[15] T. Kim, J. Kang, J.-H. Lee, J. Yoon, Influence of attached bacteria and biofilm on double-layer capacitance during biofilm monitoring by electrochemical impedance spectroscopy, Water Res. 45 (2011) 4615–4622, http://dx.doi.org/10.1016/j.watres.2011.06.010.
[16] E. Urcan, U. Haertel, M. Styllou, R. Hickel, H. Scherthan, F.X. Reichl, Real-time xCELLigence impedance analysis of the cytotoxicity of dental composite components on human gingival fibroblasts, Dent. Mater. 26 (2010) 51–58, http://dx.doi.org/10.1016/j.dental.2009.08.007.
[17] S. Rahim, A. Üren, A real-time electrical impedance based technique to measure invasion of endothelial cell monolayer by cancer cells, J. Vis. Exp. (2011)http://dx.doi.org/10.3791/2792.
[18] P. Stoodley, Z. Lewandowski, J.D. Boyle, H.M. Lappin-Scott, Oscillation characteristics of biofilm streamers in turbulent flowing water as related to drag and pressure drop, Biotechnol. Bioeng. 57 (1998) 536–544.
[19] V. Thiagarajan, K.L. Swope, M.C. Flickinger, Immobilized cells — basics and applications, Proceedings of an International Symposium Organized Under Auspices of The Working Party on Applied Biocatalysis of the European Federation of Biotechnology Noordwijkerhout, Elsevier, 1996http://dx.doi.org/10.1016/S0921-0423(96)80041-4.
[20] M. Varshney, Y. Li, Double interdigitated array microelectrode-based impedance biosensor for detection of viable *Escherichia coli* O157:H7 in growth medium, Talanta 74 (2008) 518–525, http://dx.doi.org/10.1016/j.talanta.2007.06.027.
[21] L. Yang, Electrical impedance spectroscopy for detection of bacterial cells in suspensions using interdigitated microelectrodes, Talanta 74 (2008) 1621–1629, http://dx.doi.org/10.1016/j.talanta.2007.10.018.
[22] R. Gomez, R. Bashir, A. Sarikaya, M.R. Ladisch, J. Sturgis, J.P. Robinson, et al., Microfluidic biochip for impedance spectroscopy of biological species, Biomed. Microdevices 3 (2001) 201–209, http://dx.doi.org/10.1023/A:1011403112850.
[23] R. Gomez-Sjoberg, D.T. Morisette, R. Bashir, Impedance microbiology-on-a-chip: microfluidic bioprocessor for rapid detection of bacterial metabolism, J.

Microelectromechanical Syst. 14 (2005) 829–838, http://dx.doi.org/10.1109/JMEMS.2005.845444.
[24] A. Moya, X. Guimera, F.J. del Campo, E. Prats-Alfonso, A.D. Dorado, M. Baeza, et al., Profiling of oxygen in biofilms using individually addressable disk microelectrodes on a microfabricated needle, Microchim. Acta (2014) (accepted fro publication).
[25] S. G, Ø.G. Martinsen, Sources of error in tetrapolar impedance measurements on biomaterials and other ionic conductors, J. Phys. D. Appl. Phys. 40 (2006), http://dx.doi.org/10.1088/0022-3727/40/1/S02.
[26] E. Prats-Alfonso, L. Abad, N. Casañ-Pastor, J. Gonzalo-Ruiz, E. Baldrich, Iridium oxide pH sensor for biomedical applications. Case urea–urease in real urine samples. Biosens. Bioelectron. 39 (2013) 163–169, http://dx.doi.org/10.1016/j.bios.2012.07.022.
[27] A. Moya, N. Zine, X. Illa, E. Prats-Alfonso, G. Gabriel, A. Errachid, et al., Flexible polyimide platform based on the integration of potentiometric multi-sensor for biomedical applications, Procedia Eng. 87 (2014) 276–279, http://dx.doi.org/10.1016/j.proeng.2014.11.661.
[28] G. Gabriel, I. Erill, J. Caro, R. Gómez, D. Riera, R. Villa, et al., Manufacturing and full characterization of silicon carbide-based multi-sensor micro-probes for biomedical applications, Microelectronics J. 38 (2007) 406–415, http://dx.doi.org/10.1016/j.mejo.2006.11.008.
[29] A. Guimera, G. Gabriel, M. Plata-Cordero, L. Montero, M.J. Maldonado, R. Villa, A non-invasive method for an in vivo assessment of corneal epithelium permeability through tetrapolar impedance measurements, Biosens. Bioelectron. 31 (2012) 55–61, http://dx.doi.org/10.1016/j.bios.2011.09.039.
[30] D. Bonilla, M. Mallén, R. de la Rica, C. Fernández-Sánchez, A. Baldi, Electrical readout of protein microarrays on regular glass slides, Anal. Chem. 83 (2011) 1726–1731, http://dx.doi.org/10.1021/ac102938z.
[31] G.M. Whitesides, The origins and the future of microfluidics, Nature 442 (2006) 368–373, http://dx.doi.org/10.1038/nature05058.
[32] M. Zhan, L. Chingozha, H. Lu, Enabling systems biology approaches through microfabricated systems, Anal. Chem. 85 (2013) 8882–8894, http://dx.doi.org/10.1021/ac401472y.
[33] L. Hall-Stoodley, J.W. Costerton, P. Stoodley, Bacterial biofilms: from the natural environment to infectious diseases, Nat. Rev. Microbiol. 2 (2004) 95–108, http://dx.doi.org/10.1038/nrmicro821.
[34] P. Sethu, L.L. Moldawer, M.N. Mindrinos, P.O. Scumpia, C.L. Tannahill, J. Wilhelmy, et al., Microfluidic isolation of leukocytes from whole blood for phenotype and gene expression analysis, Anal. Chem. 78 (2006) 5453–5461, http://dx.doi.org/10.1021/ac060140c.
[35] S.D. Minteer, Microfluidic techniques, Humana Press Inc., Totowa, New Jersey 07512, 2006.
[36] M.A. Tormo, C. Ubeda, M. Martí, E. Maiques, C. Cucarella, J. Valle, et al., Phase-variable expression of the biofilm-associated protein (Bap) in *Staphylococcus aureus*, Microbiology 153 (2007) 1702–1710, http://dx.doi.org/10.1099/mic.0.2006/005744-0.
[37] A. Toledo-arana, N. Merino, M. Vergara-irigaray, M. De, R. Penade, *Staphylococcus aureus* develops an alternative, ica-independent biofilm in the absence of the arlRS two-component system, Am. Soc. Microbiol. 187 (2005) 5318–5329, http://dx.doi.org/10.1128/JB.187.15.5318.
[38] E. Sarro, M. Lecina, A. Fontova, C. Sola, F. Godia, J.J. Cairo, et al., Electrical impedance spectroscopy measurements using a four-electrode configuration improve on-line monitoring of cell concentration in adherent animal cell cultures, Biosens. Bioelectron. 31 (2012) 257–263, http://dx.doi.org/10.1016/j.bios.2011.10.028.
[39] K.S. Cole, Permeability and impermeability of cell membranes for ions, Cold Spring Harb. Symp. Quant. Biol. 8 (1940) 110–122, http://dx.doi.org/10.1101/SQB.1940.008.01.013.
[40] D.W. Marquardt, An algorithm for least-squares estimation of nonlinear parameters, J. Soc. Ind. Appl. Math. 11 (1963) 431–441, http://dx.doi.org/10.1137/0111030.
[41] H. Fricke, S. Morse, The electric resistance and capacity of blood for frequencies between 800 and 4(1/2) million cycles, J. Gen. Physiol. 9 (1925) 153–167.
[42] O.G. Martinsen, S. Grimnes, Bioimpedance and Bioelectricity Basics, Second ed. Academic Press, 2008.
[43] P. Sule, T. Wadhawan, N.J. Carr, S.M. Horne, A.J. Wolfe, B.M. Prüss, A combination of assays reveals biomass differences in biofilms formed by *Escherichia coli* mutants, Lett. Appl. Microbiol. 49 (2009) 299–304, http://dx.doi.org/10.1111/j.1472-765X.2009.02659.x.
[44] Y.H. An, R.J. Friedman, Handbook of Bacterial Adhesion, Humana Press, New Jersey, 2000.http://dx.doi.org/10.1385/1592592244.
[45] R.J. Palmer, K. Kazmerzak, M.C. Hansen, Mutualism versus independence: strategies of mixed-species oral biofilms in vitro using saliva as the sole nutrient source, Infect. Immun. 69 (2001) 5794–5804, http://dx.doi.org/10.1128/IAI.69.9.5794.
[46] R. Murga, J.M. Miller, Biofilm formation by Gram-negative bacteria on central venous catheter connectors: effect of conditioning films in a laboratory model, J. Clin. Microbiol. 39 (2001) 2294–2297, http://dx.doi.org/10.1128/JCM.39.6.2294.
[47] J. Paredes, S. Becerro, F. Arizti, A. Aguinaga, J.L. Del Pozo, S. Arana, Interdigitated microelectrode biosensor for bacterial biofilm growth monitoring by impedance spectroscopy technique in 96-well microtiter plates, Sensors Actuators B Chem. 178 (2013) 663–670, http://dx.doi.org/10.1016/j.snb.2013.01.027.
[48] J. Paredes, S. Becerro, S. Arana, Label-free interdigitated microelectrode based biosensors for bacterial biofilm growth monitoring using Petri dishes, J. Microbiol. Methods 100 (2014) 77–83, http://dx.doi.org/10.1016/j.mimet.2014.02.022.
[49] L. Pires, K. Sachsenheimer, T. Kleintschek, A. Waldbaur, T. Schwartz, B.E. Rapp, On-line monitoring of biofilm growth and activity using a combined multi-channel impedimetric and amperometric sensor, Biosens. Bioelectron. 47 (2013) 157–163, http://dx.doi.org/10.1016/j.bios.2013.03.015.
[50] R. Ehret, W. Baumann, M. Brischwein, A. Schwinde, K. Stegbauer, B. Wolf, Monitoring of cellular behaviour by impedance measurements on interdigitated electrode structures, Biosens. Bioelectron. 12 (1997) 29–41, http://dx.doi.org/10.1016/0956-5663(96)89087-7.
[51] M. Faure, A. Pallandre, S. Chebil, I. Le Potier, M. Taverna, B. Tribollet, et al., Improved electrochemical detection of a transthyretin synthetic peptide in the nanomolar range with a two-electrode system integrated in a glass/PDMS microchip, Lab Chip 14 (2014) 2800–2805, http://dx.doi.org/10.1039/c4lc00240g.
[52] M. Varshney, Y. Li, Interdigitated array microelectrodes based impedance biosensors for detection of bacterial cells, Biosens. Bioelectron. 24 (2009) 2951–2960, http://dx.doi.org/10.1016/j.bios.2008.10.001.
[53] S.M. Radke, E.C. Alocilja, A high density microelectrode array biosensor for detection of *E. coli* O157:H7. Biosens. Bioelectron. 20 (2005) 1662–1667, http://dx.doi.org/10.1016/j.bios.2004.07.021.
[54] J. Paredes, S. Becerro, F. Arizti, A. Aguinaga, J.L. Del Pozo, S. Arana, Real time monitoring of the impedance characteristics of staphylococcal bacterial biofilm cultures with a modified CDC reactor system, Biosens. Bioelectron. 38 (2012) 226–232, http://dx.doi.org/10.1016/j.bios.2012.05.027.
[55] H.P. Schwan, Four-electrode null techniques for impedance measurement with high resolution, Rev. Sci. Instrum. 39 (1968) 481, http://dx.doi.org/10.1063/1.1683413.
[56] L. Yang, Y. Li, C.L. Griffis, M.G. Johnson, Interdigitated microelectrode (IME) impedance sensor for the detection of viable *Salmonella typhimurium*, Biosens. Bioelectron. 19 (2004) 1139–1147, http://dx.doi.org/10.1016/j.bios.2003.10.009.
[57] A. Zikmund, P. Ripka, L. Krasny, T. Judl, D. Jahoda, Biofilm detection by the impedance method, 2010 3rd Int. Conf. Biomed. Eng. Informatics, IEEE 2010, pp. 1432–1434, http://dx.doi.org/10.1109/BMEI.2010.5639411.
[58] M. Amato, S. Pershing, M.W. Do, S. Tanaka, Trends in ophthalmic manifestations of methicillin-resistant *Staphylococcus aureus* (MRSA) in a northern California pediatric population, J. AAPOS. 17 (2009) 243–247, http://dx.doi.org/10.1016/j.jaapos.2012.12.151.
[59] D.R. Storm, Mechanism of bacitracin action: a specific lipid–peptide interaction, Ann. New York Acad. Sci. 387–398 (1967).
[60] K.J. Stone, L. Jack, Complexation pyrophosphate, Proc. Natl. Acad. Sci. U. S. A. 68 (1971) 3223–3227.
[61] E.D. Roche, P.J. Renick, S.P. Tetens, D.L. Carson, A model for evaluating topical antimicrobial efficacy against methicillin-resistant *Staphylococcus aureus* biofilms in superficial murine wounds, Antimicrob. Agents Chemother. 56 (2012) 4508–4510, http://dx.doi.org/10.1128/AAC.00467-12.
[62] R. Bragós, E. Sarró, A. Fontova, A. Soley, J. Cairó, A. Bayés-Genís, et al., Four versus two-electrode measurement strategies for cell growing and differentiation monitoring using electrical impedance spectroscopy, Annu. Int. Conf. IEEE Eng. Med. Biol. — Proc. 2006, pp. 2106–2109, http://dx.doi.org/10.1109/IEMBS.2006.260287.
[63] S.M. Hunt, E.M. Werner, B. Huang, A. Hamilton, P.S. Stewart, S.M. Hunt, et al., Hypothesis for the role of nutrient starvation in biofilm detachment, Appl. Environ. Microbiol. 70 (2004) 7418–7425, http://dx.doi.org/10.1128/AEM.70.12.7418.
[64] R. Wang, B.A. Khan, G.Y.C. Cheung, T.H.L. Bach, M. Jameson-Lee, K.F. Kong, et al., *Staphylococcus epidermidis* surfactant peptides promote biofilm maturation and dissemination of biofilm-associated infection in mice, J. Clin. Invest. 121 (2011) 238–248, http://dx.doi.org/10.1172/JCI42520.
[65] E.J. Stewart, A.E. Satorius, J.G. Younger, M.J. Solomon, Role of environmental and antibiotic stress on *Staphylococcus epidermidis* biofilm microstructure, Langmuir 29 (2013) 7017–7024, http://dx.doi.org/10.1021/la401322k.
[66] A. Soley, M. Lecina, X. Gámez, J.J. Cairó, P. Riu, X. Rosell, et al., On-line monitoring of yeast cell growth by impedance spectroscopy, J. Biotechnol. 118 (2005) 398–405, http://dx.doi.org/10.1016/j.jbiotec.2005.05.022.